



**HAL**  
open science

# Solid-phase synthesis of molecularly imprinted polymer nanoparticles for protein recognition

Jingjing Xu

► **To cite this version:**

Jingjing Xu. Solid-phase synthesis of molecularly imprinted polymer nanoparticles for protein recognition. Biotechnology. Université de Technologie de Compiègne, 2017. English. NNT : 2017COMP2349 . tel-01593087

**HAL Id: tel-01593087**

**<https://theses.hal.science/tel-01593087>**

Submitted on 25 Sep 2017

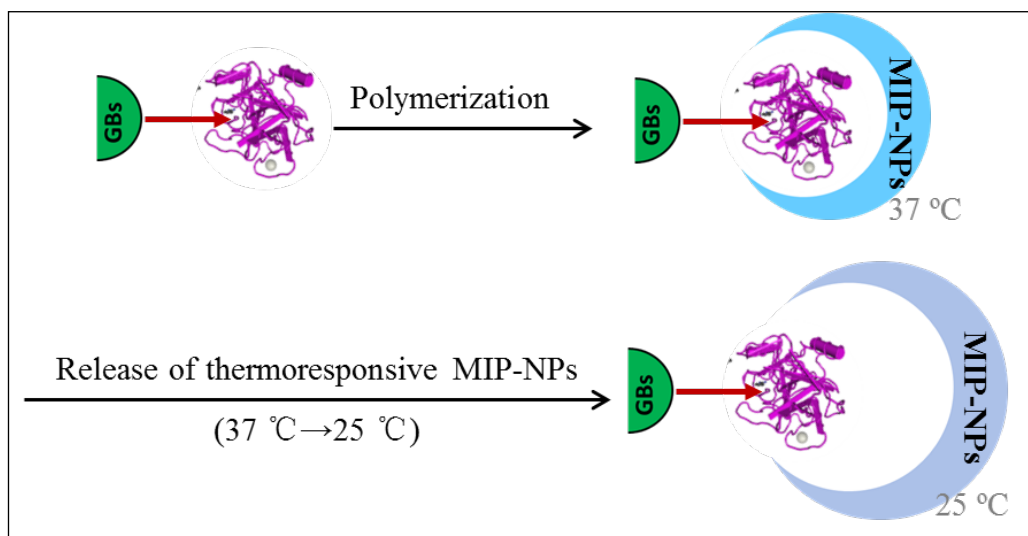
**HAL** is a multi-disciplinary open access archive for the deposit and dissemination of scientific research documents, whether they are published or not. The documents may come from teaching and research institutions in France or abroad, or from public or private research centers.

L'archive ouverte pluridisciplinaire **HAL**, est destinée au dépôt et à la diffusion de documents scientifiques de niveau recherche, publiés ou non, émanant des établissements d'enseignement et de recherche français ou étrangers, des laboratoires publics ou privés.

Par Jingjing XU

*Solid-phase synthesis of molecularly imprinted polymer nanoparticles for protein recognition*

Thèse présentée  
pour l'obtention du grade  
de Docteur de l'UTC



Soutenue le 21 avril 2017

**Spécialité** : Biotechnology : Unité de recherche Génie  
Enzymatique et Cellulaire - GEC (FRE-3580)

D2349



## **DOCTORAL THESIS**

submitted for graduation as

**DOCTEUR de l'Université de Technologie de Compiègne**

Speciality : Biotechnology

by **Jingjing XU**

## **Solid-phase synthesis of molecularly imprinted polymer nanoparticles for protein recognition**

Thesis supervised by Prof. Karsten HAUPT and Dr. Bernadette TSE SUM BUI.

Disputation on 21<sup>th</sup> April 2017, in front of the jury composed of:

- Alessandra Maria Bossi, Pr. University of Verona, Verona, Italie Reviewer
- Peter Lieberzeit, Pr. University of Vienne, Austria Reviewer
- Patrice Debré, Pr. Hôpital Pitié Salpêtrière, France Examiner
- Bérangère Bihan Avalle, Pr. Université de Technologie de Compiègne, France Examiner
- Bernadette Tse Sum Bui, Dr. Université de Technologie de Compiègne, France Supervisor
- Karsten Haupt, Pr. Université de Technologie de Compiègne, France Supervisor

## Table of content

---

<b>Acknowledgements</b>	1
<b>Abbreviations</b>	2 - 3
<b>Abstract in English</b>	4
<b>Résumé en Français</b>	5
<b>General introduction</b>	6 - 7
<b>Chapter 1.</b> Recent advances in the molecular imprinting of proteins – a literature review	8 - 67
<b>Chapter 2.</b> Solid-phase synthesis of molecularly imprinted polymer nanoparticles as antibody mimics for protein recognition	68 - 126
<b>Summary</b>	68
<b>Publication 1.</b> Toward a universal method for preparing molecularly imprinted polymer nanoparticles with antibody-like affinity for proteins	71
<b>Publication 2.</b> Guide to the preparation of molecularly imprinted polymer nanoparticles for protein recognition, by solid-phase synthesis	85
<b>Chapter 3.</b> Application of a molecularly imprinted polymer as plastic antibody in bioassays	127 - 179
<b>Summary</b>	127
<b>Manuscript 1.</b> Fluorescent core-shell MIP nanoparticle as a plastic antibody for the pseudo-immunoassay of trypsin in human serum	131
<b>Manuscript 2.</b> Rapid detection of trypsin with a molecularly imprinted polymer as a selective fluorescence nanoprobe	158
<b>Chapter 4.</b> Conformational epitope imprinting by solid-phase synthesis	180 - 208
<b>Summary</b>	180

## Table of content

---

<b>Manuscript 3.</b> Antibody-like molecularly imprinted polymer nanoparticles for the recognition of an HIV-gp41 epitope peptide	183
<b>General conclusion and perspectives</b>	209 - 210
<b>Annex</b>	211 - 220
<b>Annex 1.</b> Poster for 8 <sup>th</sup> international conference on molecular imprinting (MIP 2014)	211
<b>Annex 2.</b> Publication 3: Water compatible silica sol–gel    molecularly imprinted polymer as a potential delivery system for the controlled release of salicylic acid.	212
<b>Annex 3.</b> Achievements	220

## Acknowledgments

---

First of all, I gratefully acknowledge Prof. Alessandra Maria Bossi and Prof. Peter Lieberzeit to revise this thesis, and Prof. Patrice Debré and Prof. Bérangère Bihan Avalle for being the examiners of this work.

My biggest acknowledgements go to my supervisors Dr. Bernadette Tse Sum Bui and Prof. Karsten Haupt for your guidance, support and encouragement for this work during these three years and a half.

Karsten, thank you very much for offering me the opportunity to work with so many people on various subjects about MIP in this laboratory. I am very grateful for your expertise, advices, and creative ideas that show me the right direction toward achieving the goal of all the projects.

Bernadette, a warm thank for you, for your constant support and numerous advices. Your great contribution not only helps a lot to build up this thesis, but also has created a young researcher, who pursues to learn more about the truth and to contribute to the research area. Personally, I am very grateful for your accompany and sharing during these beautiful years, and a deep thank to you for giving me the chance to meet a better myself.

I sincerely thank our external collaborator, Prof. Patrice Debré and all the members of his group, Dr. Vincent Vieillard, Dr. Karim Dorgham, Olivier Lucar. Thanks for your deep interest in our collaboration, for the knowledge you have shared to advance our project, and for the work you have done.

To finish, I give my acknowledgments to all the members in this laboratory GEC, my dearest friends Sofia, Maria, Nadja, Billal, my lovely Paulina, and my previous supervisor LiBin, Xuan-Anh, and Serena. Thanks for your accompany that makes my life more beautiful and enjoyable. A special thank to my boyfriend, my fiancé, for your love, for your comprehension, it is more than words. In the end, a warm thankful heart will be sent to my family in China, who are waiting for me to reunite all this time.

## Abbreviations

---

2, 4-D: 2,4-dichlorophenoxyacetic acid	MAA: methacrylic acid
AAM: acrylamide	MABA: 4-[2-( <i>N</i> -methacrylamido)ethylaminomethyl] benzoic acid
ACPA: 4, 4'-azobis-(4-cyanopentanoic acid)	MAH: <i>N</i> -methacryloyl-L-histidine methyl ester
AFM: atomic force microscope	MB: methylene blue
AFP: $\alpha$ -fetoprotein	MBA or Bis: <i>N,N'</i> -methylenebis(acrylamide)
ALP: alkaline phosphatase	MEO <sub>2</sub> MA: di(ethylene glycol) methyl ether methacrylate
APBA: 3-aminophenylboronic acid	MIP: molecularly imprinted polymer
APS: ammonium persulfate	MITC: <i>p</i> -isothiocyanatophenyl $\alpha$ -D-mannopyranoside
APTES: (3-aminopropyl)triethoxysilane	MPS: 3-(trimethoxysilyl)propyl methacrylate
ATP: adenosine triphosphate	NHMA: <i>N</i> -hydroxymethylacrylamide
ATRP: atom transfer radical polymerization	NIPAm: <i>N</i> -isopropylacrylamide
BLAST: basic local alignment search tool	OVDAC: octadecyl- <i>p</i> -vinylbenzyltrimethylammonium chloride
BSA or HSA or PSA: bovine or human or porcine serum albumin	PCR: polymerase chain reaction
CRP: controlled/living radical polymerization	PEG: poly(ethylene glycol)
CTA: chain transfer agent	PERS: plasmon-enhanced Raman scattering
DCAA: diethylthiocarbamoylsulfanyl acetic acid	PISA: plasmonic immunosandwich assay
DNase: deoxyribonuclease	PET: polyethylene terephthalate
DSF: differential scanning fluorimetry	RAFT: reversible addition-fragmentation chain transfer
ECL: electrochemiluminescence	RNase: ribonuclease

## Abbreviations

---

EDMA: ethylene glycol dimethacrylate	SDS: sodium dodecyl sulfate
ELISA: enzyme-linked immunosorbent assay	SEM: scanning electron microscope
FIP: fingerprint-imprinted polymers	SPR: surface plasmon resonance
FITC: fluorescein isothiocyanate	tBMA: <i>tert</i> -butylmethacrylate
FMA: fluorescein O-methacrylate	TEM: transmission electron microscope
FRP: free radical polymerization	TEMED: <i>N,N,N',N'</i> -tetramethylethylenediamine
HRP: horseradish peroxidase	TMB: 3,3',5,5'-tetramethylbenzidine
IDA: iminodiacetic acid	TRF: transferrin
IgG: immunoglobulin G	VAZO 56: 2, 2'-azobis(2-amidinopropane) dihydrochloride
IMAC: immobilized-metal affinity chromatography	VAZO 68: 4, 4'-azobis(4-cyanovaleric acid)
KPS: potassium persulfate	VP: vinylpyridine
LOD: limit of detection	VPBA: 4-vinylphenylboronic acid
LOQ: limit of quantification	TEOS: tetraethoxysilane

# Solid-phase synthesis of molecularly imprinted polymer nanoparticles for protein recognition

---

*Keywords: molecularly imprinted polymer, solid-phase synthesis, protein recognition, protein protection, immunoassay, biosensing, peptide epitope*

This thesis describes the synthesis, by a solid-phase synthesis approach, of nanoparticles of molecularly imprinted polymers (MIPs) for the recognition of proteins. Molecularly imprinted polymers are biomimetic receptors synthesized by a nanomolding process of the polymer around single molecules. They therefore possess specific recognition cavities for their target molecule. The technique of molecular imprinting for small target molecules is well established, while protein imprinting remains a challenge due to the flexibility and complexity of their native structure and functional sites, but also because of their low stability under unusual conditions. Therefore, a solid-phase synthesis approach has been developed where the protein is immobilized on a support before the synthesis of water-soluble MIP nanogel particles by radical polymerization. The MIPs obtained have affinities comparable to those of antibodies, and low cross-reactivities. They have advantages such as better stability, lower cost, and can potentially be regenerated and reused, thus becoming promising alternatives to real antibodies. We have synthesized MIPs against serine proteases such as trypsin, and kallikrein, but also against a peptide epitope of the HIV gp41 protein. Thermosensitive MIP nanogels were synthesized in a thermostated column-type reactor or a petri dish, by thermally or photo-initiated radical polymerization. Their thermosensitivity allows the MIPs to be released from the immobilized protein by a simple temperature change. They are water-soluble as a function of temperature and have a diameter of less than 100 nm. Their affinity for their target is strong, with a  $K_d$  in the nano or picomolar range. These 'synthetic antibodies' have been applied in binding assays with quartz crystal microbalance, but also as 'synthetic chaperones'. Preliminary studies of the protection of proteins from thermal denaturation or from denaturation by an unfavorable pH have been carried out. The use of an iniferter to initiate the living photopolymerization of MIP made it possible to synthesize nanogels of core-shell type. By introducing fluorescent markers into MIPs, immunoassay applications in biological fluids have been demonstrated, indicating the great potential of these MIPs in clinical diagnostics. In conclusion, we have developed a novel approach to the synthesis of soluble MIP nanoparticles having high affinity for a protein, usable in place of antibodies in real world applications such as the detection of biomarker proteins in complex samples, and potentially as an active principle *in vivo*.

# Synthèse en phase solide de nanoparticules de polymères à empreintes moléculaires pour la reconnaissance de protéines

---

*Mots-clés: polymère à empreinte moléculaire, synthèse en phase solide, protéines, anticorps synthétique, immunodosage, biocapteur, épitope peptidique*

Cette thèse décrit la synthèse de nanoparticules de polymères à empreintes moléculaires (MIP, de l'anglais *molecularly imprinted polymer*) pour la reconnaissance de protéines, par une approche de synthèse en phase solide. Les polymères à empreintes moléculaires sont des récepteurs biomimétiques synthétisés sur mesure par un processus de nanomoulage du polymère autour de la molécule unique. Ils possèdent ainsi des cavités de reconnaissance spécifiques pour leur molécule cible. La technique de l'impression moléculaire pour les petites molécules cibles est bien établie, alors que l'impression de protéines reste encore un défi en raison de la flexibilité et complexité de leur structure native et de leurs nombreux sites fonctionnels, mais aussi en raison de leur faible stabilité dans des conditions inhabituelles. Par conséquent, une approche de synthèse en phase solide a été développée ici où la protéine est immobilisée sur un support avant la synthèse de nanoparticules hydrosolubles de MIP par polymérisation radicalaire. Les MIPs obtenus ont des affinités comparables à celles des anticorps, et des réactivités croisées faibles. Ils possèdent des avantages tels qu'une stabilité meilleure, un coût plus faible et peuvent potentiellement être régénérés et réutilisés, devenant ainsi des alternatives prometteuses aux anticorps naturels.

Nous avons fabriqué des MIPs contre des protéases à sérine, telles la trypsine et la kallikréine, mais aussi contre un épitope peptidique de la protéine gp41 du VIH. Des nanogels de MIP thermosensibles ont été synthétisés dans un réacteur sous la forme d'une colonne thermostatée ou une boîte de Pétri, par polymérisation radicalaire initiée par voie thermique ou photochimique. Un simple changement de la température permet de libérer les MIPs de la protéine immobilisée. Ces MIPs sont hydrosolubles en fonction de la température et ont un diamètre inférieur à 100 nm. Leur affinité pour leur cible est élevée, avec un  $K_d$  du nano ou picomolaire. Ces 'anticorps synthétiques' ont été appliqués dans des tests d'adsorption sur microbalance à cristal de quartz, mais également comme 'chaperons synthétiques'. Des études préliminaires de la protection des protéines d'une dénaturation thermique ou par un pH défavorable ont été effectuées. L'utilisation d'un iniferté pour initier la photopolymérisation vivante du MIP a permis de synthétiser des nanogels de type core-shell. En introduisant des marqueurs fluorescents dans les MIPs, les tests d'immunoessai dans des fluides biologiques ont été démontrés, ce qui indique le grand potentiel de ces MIPs dans le diagnostic clinique.

En conclusion, nous avons développé une nouvelle approche de synthèse de nanoparticules de MIP hydrosoluble ayant une haute affinité pour une protéine, utilisables à la place des anticorps dans des applications dans le monde réel tel que la détection de protéines biomarqueurs dans des échantillons complexes, et potentiellement comme principe actif *in vivo*.

## General introduction

The work presented in this Ph.D thesis was funded by the China Scholarship Council (CSC). The work was carried out from September 2013 to February 2017 in the Laboratory of Enzyme and Cell Engineering at the University of Technology of Compiègne.

The aim of this thesis was to develop high-affinity molecularly imprinted polymeric nanoparticles (MIP-NPs) for the recognition of proteins, by a recently emerged solid-phase synthesis approach. These synthetic antibody mimics, also referred to as 'plastic antibodies', can potentially be used in any application where specific molecular recognition for a target molecule is required. Considering the growing demand in the biomedical diagnostics market, the development of antibody substitutes is of particular interest for this area.

The MIP-NPs were synthesized as thermoresponsive hydrogels, with a diameter below 100 nm, are water-soluble and feature tailor-made homogeneous binding sites and antibody-like affinity and selectivity. Thus these MIP-NPs show high potential for diagnostic assays but appear also promising for therapeutic applications.

This Ph.D thesis is composed of four chapters: one literature review chapter and three results chapters. The chapters are presented in the form of articles.

Chapter I provides a general overview of the current progress made in the molecular imprinting of proteins, focusing on a variety of applications that have recently appeared, such as protein crystallization, protective/chaperone agent, ELISA test and as *in vivo* therapeutics.

Chapter II comprises two published papers. Paper 1, published in *Biomacromolecules*, is entitled "Toward a universal method for preparing molecularly imprinted polymer nanoparticles with antibody-like affinity for proteins". It describes the technique used in this Ph.D thesis, the solid-phase synthesis approach. This allows to synthesize nanosized water-soluble MIPs, with antibody-like affinity and low cross-reactivity. Paper 2, entitled "Guide to the preparation of molecularly imprinted polymer nanoparticles for protein recognition, by solid-phase synthesis", is a book chapter destined for *Methods in Enzymology*.

The content describes specific and detailed guidelines to perform the solid-phase synthesis method step by step. In addition to the description of the synthesis method, the application of MIPs as synthetic chaperones to protect proteins from denaturation is investigated.

Chapter III presents the synthesis of water-soluble MIP-NPs by the solid-phase approach, via iniferter-induced living photopolymerization. This allows obtaining core-shell nanoparticles and post-functionalization of these particles, to fine-tune their surface chemistry or to allow their attachment to surfaces, or their labeling with fluorophores. This chapter contains two manuscripts of publications ready to be submitted. In the first manuscript, fluorescent core-shell MIPs were synthesized by post-derivatization, with the aim of applying them as direct substitutes of biological antibodies in immunoassays. This fluorescent core-shell MIP is applied to the detection of trypsin in human serum in a direct pseudo-ELISA format. The second manuscript describes the development of MIP nanoprobe with direct incorporation of a fluorescent monomer, which renders them appropriate for the rapid detection of trypsin in human urine.

Chapter IV describes the solid-phase synthesis of MIPs against a protein epitope, an internal peptide sequence. This involves the design of a cyclic peptide mimicking an epitope of glycoprotein 41 of HIV and selection of functional monomers. The resulting MIP exhibits high affinity and selectivity, comparable to those of natural antibodies, and is capable to detect changes in the amino acid sequence of the peptide. Owing to its high affinity and selectivity for the HIV protein in an *in vitro* assay, it has potential to work in an *in vivo* assay. The latter work is carried out in collaboration with Prof. Patrice Debré at Pitié Salpêtrière hospital in Paris.

# Chapter 1

**Recent advances in molecular imprinting of proteins**

– A literature review

## Summary

I. Molecular imprinting technique.....	10
I-1. Molecularly imprinted polymers – antibody mimics .....	10
I-2. Challenges in protein imprinting.....	14
II. Protein imprinting .....	15
II-1. Water-based systems .....	15
II-2. Polymerization mechanism .....	17
II-2-1. Free radical polymerization .....	17
II-2-2. Controlled/Living radical polymerization .....	18
II-3. Spatial strategy.....	24
II-3-1. Surface imprinting.....	25
II-3-2. Epitope imprinting .....	30
II-3-3. Solid-phase synthesis .....	33
II-4. Different formats of protein-imprinted polymers .....	35
II-5. Rational design of polymers .....	36
III. Applications of protein-imprinted polymers .....	38
III-1. Separation.....	38
III-2. Diagnostics .....	41
III-2-1. Biosensor.....	41
III-2-2. ELISA .....	45
III-3. In vivo applications.....	48

III-4. Emerging applications.....	52
III-4-1. Protein crystallization .....	52
III-4-2. Synthetic chaperone or inhibitor.....	53
III-5. Conclusions and perspectives.....	56
References.....	57

## **I. Molecular imprinting technique**

### **I-1. Molecularly imprinted polymers – antibody mimics**

It has been a long-term goal for scientists to mimic natural receptors like antibodies and enzymes. One strategy to obtain tailor-made synthetic biomimetic receptors such as molecularly imprinted polymers (MIPs), is to use the molecular imprinting technique [Haupt, 2003]. Molecular imprinting is based on the co-polymerization of functional and cross-linking monomers in the presence of a molecular template. The template can be the target molecule or a derivative thereof. The functional monomers initially form a complex with the template and after polymerization, the monomer-template assembly is held in position by the highly cross-linked three-dimensional rigid structure. Subsequent removal of the imprint molecule leaves cavities with a size, shape and chemical functionality complementary to the template. In this way, a molecular memory is introduced into the polymer that is now capable of selectively binding the target with affinities comparable to natural receptors (Fig. 1) [Haupt, 2003].

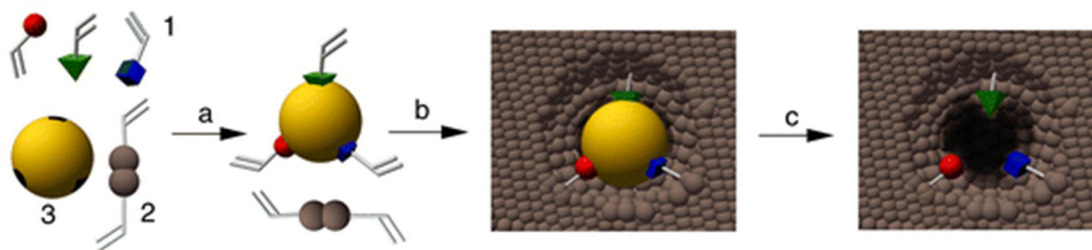


**Figure 1.** Schematic representation of non-covalent molecular imprinting. 1: Functional monomers, 2: cross-linker, 3: template molecule; a: assembly of the pre-polymerization complex, b: polymerization, c: extraction of the template liberating the binding site. Reprinted from [Haupt, 2003].

Three types of molecular imprinting approach exist:

- non-covalent or self-assembly, as described above.
- covalent, where monomers are covalently coupled to the template, generating a polymerizable imprint molecule derivative. For successful covalent imprinting, the choice of the covalent linkage connecting the functional monomer with the template is crucial, but the number of covalent bonds that fulfill the requirements of stability and reversibility is small. This is the reason why MIPs are more frequently prepared using the non-covalent approach which is more flexible concerning the choice of functional monomers. Covalent bonds include boronic acid esters [Wulff & Haarer, 1991], Schiff bases [Wulff et al., 1986], ketals [Shea & Sasaki, 1991] and sulfide bonds [Wulff & Schulze, 1978] (Fig. 2)

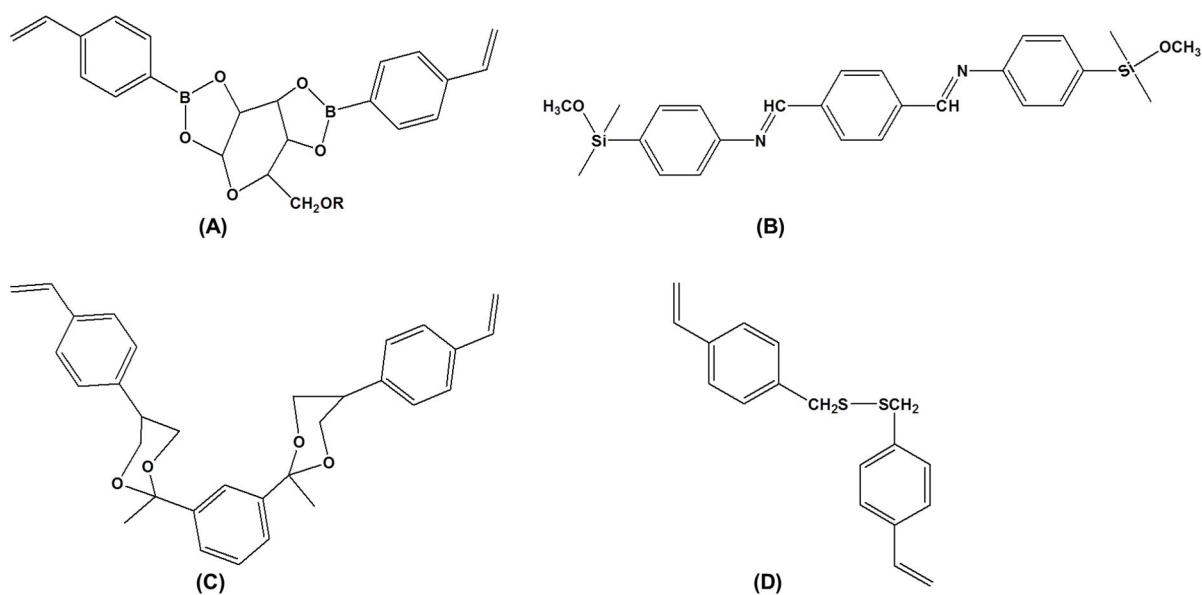


**Figure 2.** Covalent conjugates of template and functional monomer via (A) boronic acid ester, (B) Schiff bases, (C) ketals, and (D) sulfide bonds.

- semi-covalent, which is a mixture of both covalent and non-covalent methods. A covalent linkage between template and functional monomer is generated during synthesis and rebinding takes place by non-covalent interaction [Whitcombe et al., 1995]. A representative example is shown in Fig. 3.

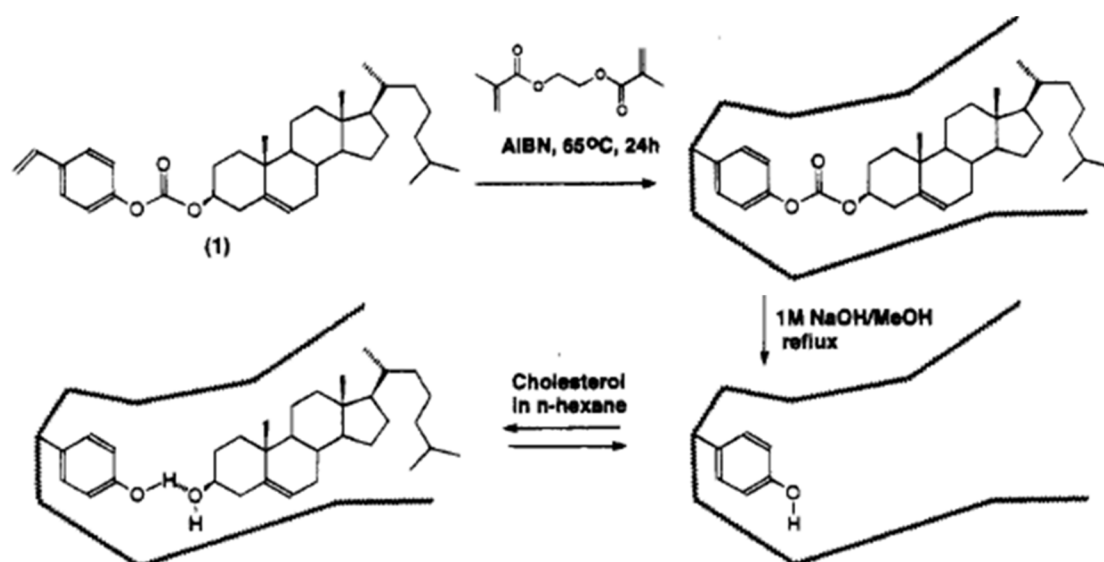


**Figure 3.** Semi-covalent approach: cholesterol-imprinted polymer synthesis using cholesterol (4-vinyl)phenyl carbonate. Reprinted from [Whitcombe et al., 1995].

Currently, non-covalent imprinting is the most versatile and the most widely used approach, due to its simple operation and rapid binding and dissociation properties, which is similar to interactions occurring between biomolecules in nature.

Molecular imprinting can be applied to a wide range of target molecules, from small molecules (MW < 1500 Da, such as sugars, hormones, antibiotics, mycotoxins, drugs, endocrine disrupting chemicals, nucleotides, amino acids, peptides, etc.) to biomacromolecules (proteins, DNA) and even larger entities (proteins, DNAs, bacteria, and viruses). The majority of molecular imprinting processes involving non-covalent synthesis is performed in aprotic and low polarity organic solvents so as to favour hydrogen bonding and electrostatic interactions between the template and the functional monomer [Haupt et al., 2012]. These conditions are optimum to obtain MIPs with high binding specificity and selectivity for small target molecules in organic solvents. The resulting MIPs were considered as stable alternatives to antibodies. Moreover, MIPs present other advantages such as low cost, ease of obtention, high batch-to-batch reproducibility, mechanical and chemical robustness and no killing of animal is needed. Table 1 shows a few comparisons of MIPs and natural antibodies.

**Table 1.** Comparison of antibodies and MIPs [Bowen et al., 2013].

	Antibodies	MIPs
Affinity	$10^{-7} - 10^{-11}$ M	$10^{-3} - 10^{-10}$ M
Application	Physiological conditions	Organic or aqueous media
Capacity	$\sim 6 \mu\text{mol.g}^{-1}$	$\sim 0.1 - 10 \mu\text{mol.g}^{-1}$
Cost	£100's for $\mu\text{g}$ quantities	£10's for g quantities
Production	Animal host, months	2 – 3 days
Reusability	Not usually	100's of times
Stability	Narrow temperature and pH range	Wide temperature and pH range
Storage time	Limited	Stable over period of years

Though the imprinting of small molecules is now considered almost routine, the imprinting of proteins still faces a lot of challenges [Takeuchi et al., 2008, Bossi et al., 2007]. This drawback comes from its incompatibility with organic solvents and to other shortcomings that will be discussed in the next sections.

## **I-2. Challenges in protein imprinting**

The challenges include incompatibility of traditional MIPs with aqueous media, native configuration maintenance of proteins, low binding capacity and slow mass transfer due to their large structure, heterogeneous binding sites caused by a multitude of functional sites, permanent entrapment of the protein, etc [Chen et al., 2011; Li et al., 2014].

In order to overcome these challenges, much research progress on other types of polymerization (controlled/living polymerization) and formats as well as on materials innovation for proteins imprinting was accomplished during the last decades. Furthermore, research efforts have sought to impart MIPs with additional capabilities like biocompatibility, stimuli-responsivity, etc. Due to all the progresses, the study on protein imprinting has shown a rapid increasing trend, as from 2005 [Menger et al., 2016] (Fig. 4). Proteins that are imprinted are no longer the traditional proteins used as models such as albumin, lysosyme, cytochrome c or haemoglobin [Verheyen et al., 2011], but they are useful proteins such as cancer or disease biomarkers. They are mostly hydrolytic enzymes (trypsin, kallikrein, RNase A, pepsin, amylase) and glycoproteins (horseradish peroxidase, RNase B,  $\alpha$ -fetoprotein) [Ma et al., 2016; Shen et al., 2016].

Note that in the special issue on molecular imprinting for proteins, edited on the occasion of Prof. Toshifumi Takeuchi's 60<sup>th</sup> birthday, you can find interesting examples of the recent work being carried out on protein MIPs, in the leading MIP groups around the world [*Molecular Imprinting*. Retrieved 13 Mar. 2017, from <http://www.degruyter.com/view/j/molim>].

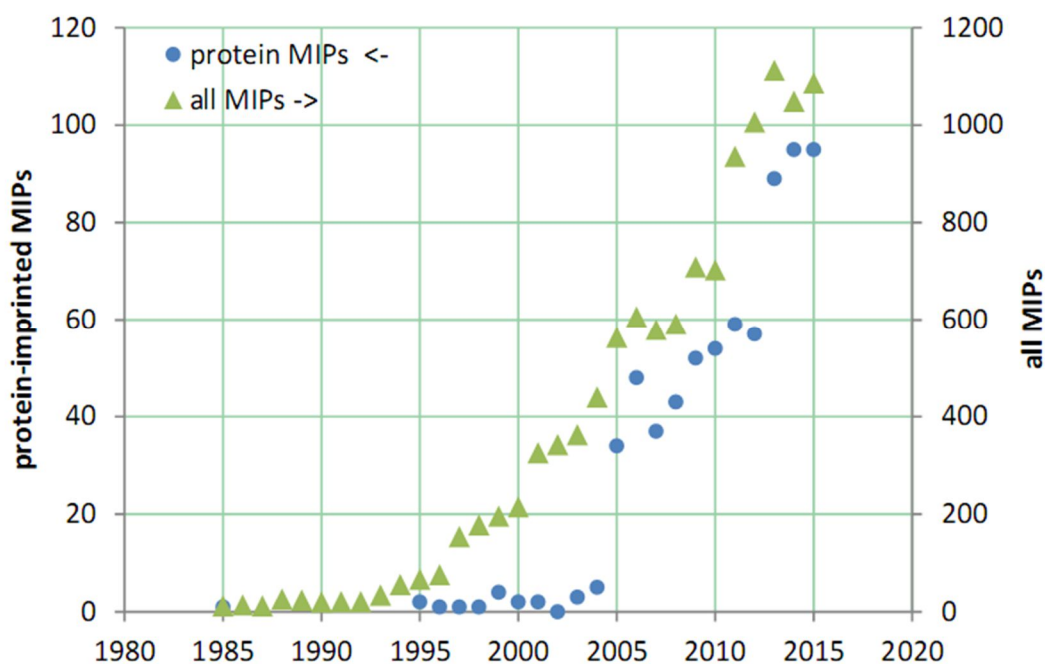


**Figure 4.** Number of publications on protein-imprinted (circles) and all molecularly imprinted (triangles, right axis) polymers, until the end of 2015. (Generated by means of MIP database and reprinted from [Menger et al., 2016]).

## II. Protein imprinting

### II-1. Water-based systems

In the protein imprinting process, the use of aqueous medium provides a favorable environment to proteins. Most molecularly imprinted polymers for proteins were designed to be water compatible, and they have predominately been based on cross-linked polyacrylamide. Fig. 5 and Fig. 6 represent the most commonly-used organic functional monomers and cross-linkers commercially available for the preparation of protein imprinted polymers.

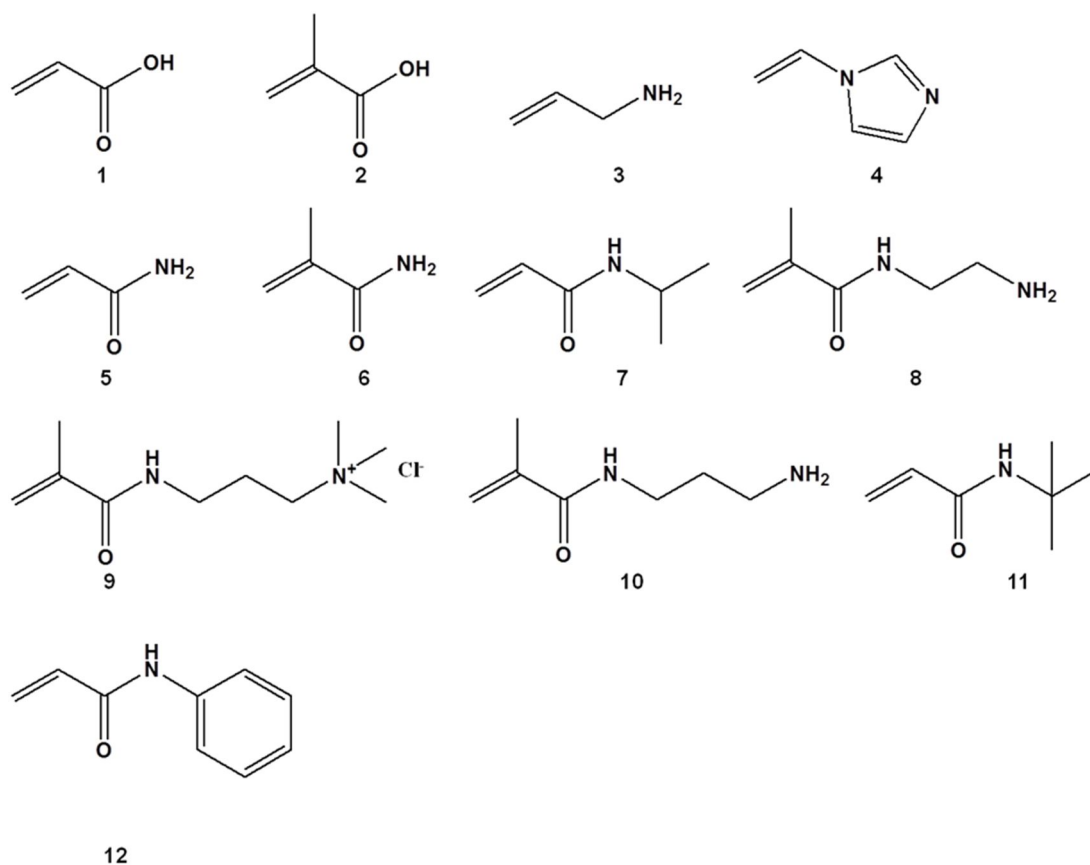


**Figure 5.** Common functional monomers used in protein imprinting. 1. Acrylic acid; 2. Methacrylic acid; 3. Allylamine; 4. 1-vinyl imidazole; 5. Acrylamide; 6. Methacrylamide; 7. *N*-isopropylacrylamide; 8. Aminoethylacrylamide; 9. (3-acrylamidopropyl) trimethyl ammonium chloride; 10. *N*-(3-Aminopropyl)methacrylamide; 11. *N*-tert-butyl acrylamide; 12. *N*-phenylacrylamide.

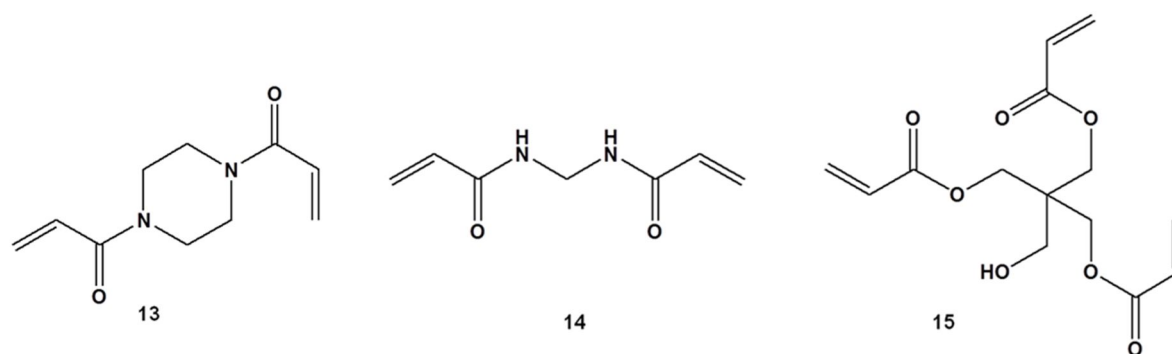


**Figure 6.** Chemical structures of commonly used cross-linking monomers. 13. Piperazine diacrylamide; 14. *N,N'*-methylene bis(acrylamide); 15. Pentaerythritol triacrylate.

## II-2. Polymerization mechanism

### II-2-1. Free radical polymerization

Most of the time, the imprinted polymer network is formed by using conventional free radical polymerization (FRP), due to its high tolerance for a wide range of functional monomers and its great adaptability to all kinds of reaction conditions. Inspired by the protocol for polyacrylamide gel preparation in protein electrophoresis, early developments for the imprinting of proteins were performed in polyacrylamide gels [Hjerten et al., 1997], using ammonium persulfate (APS) or potassium persulfate (KPS) accompanied by the catalyst *N,N,N',N'*-tetramethylethylenediamine (TEMED). Nowadays, this combination is still widely used for protein imprinting based on FRP. Aqueous soluble azoinitiators VAZO 56 and VAZO 68, have also been used (Fig. 7).

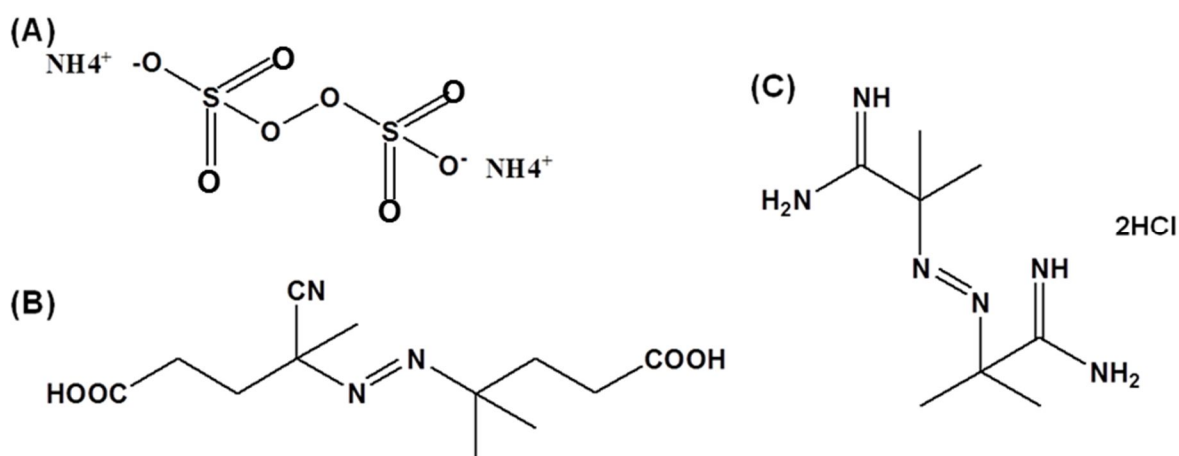


**Figure 7.** Chemical structures of FRP initiators: (A) APS; (B) VAZO 68 and (C) VAZO 56.

Typically, the FRP process is performed in three steps [Haupt et al., 2012]:

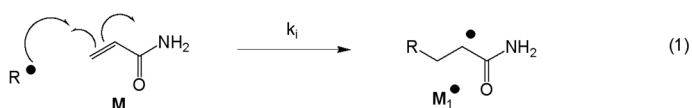
1) Initiation: First, an initiator molecule decomposes under heating or UV or visible irradiation, to generate free radicals  $R^\bullet$ . Then the formed radical attacks the double bond of a monomer, resulting in the formation of an intermediate radical  $M_1^\bullet$ .

2) Propagation: The macromolecular chain is formed by successive additions of monomers on

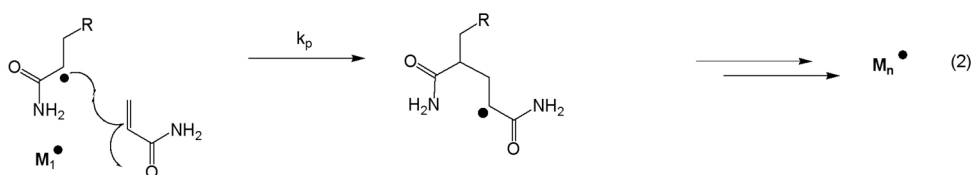
the growing macroradical  $M_n^\bullet$ . The result is a mixture of polymer chains with high molecular weights.

3) Termination: (A) recombination of two macroradicals to form a macrochain; (B) disproportionation yielding a double bond and a C–H bond at the chain terminus.

**Initiation**



**Propagation**



**Termination**

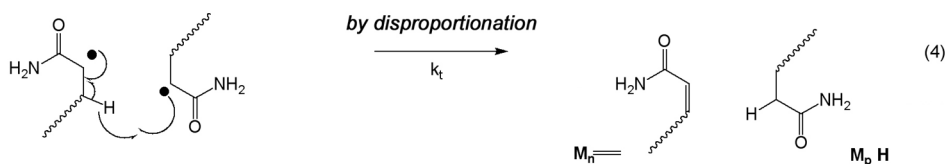
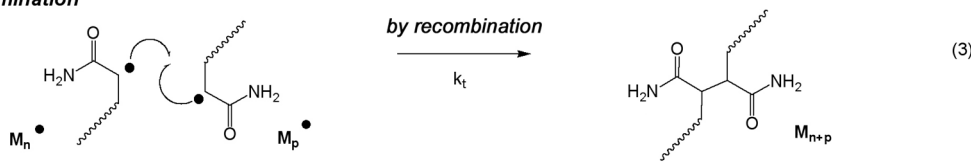


**Figure 8.** Schematic representation of free radical polymerization. Reprinted from [Haupt et al., 2012].

### II-2-2. Controlled/Living radical polymerization

In conventional free radical polymerization processes, it is difficult to control the chain propagation and termination, and this leads to heterogeneous structures and low binding specificity and selectivity when used for MIPs. Therefore, it is of importance to develop MIPs with homogeneous structures and well-defined properties, so as to improve their binding performance. In this respect, controlled/living radical polymerization (CRP) has drawn a great attention due to negligible chain termination and a more constant rate for chain growth, leading to a more homogeneous MIP internal structure with narrow distribution of molecular

weights.

Nowadays, a few protein-imprinted polymers with homogeneous structures have been prepared via CRP techniques. Up to now, three main types of CRPs were used for protein imprinting, including iniferter-induced radical polymerization, atom transfer radical polymerization (ATRP) and reversible addition-fragmentation chain transfer (RAFT) polymerization [Zhang, 2014]. Their mode of action is respectively presented in Fig. 9 and one application example of their use, either in solution or in its immobilized state for protein imprinting is described.

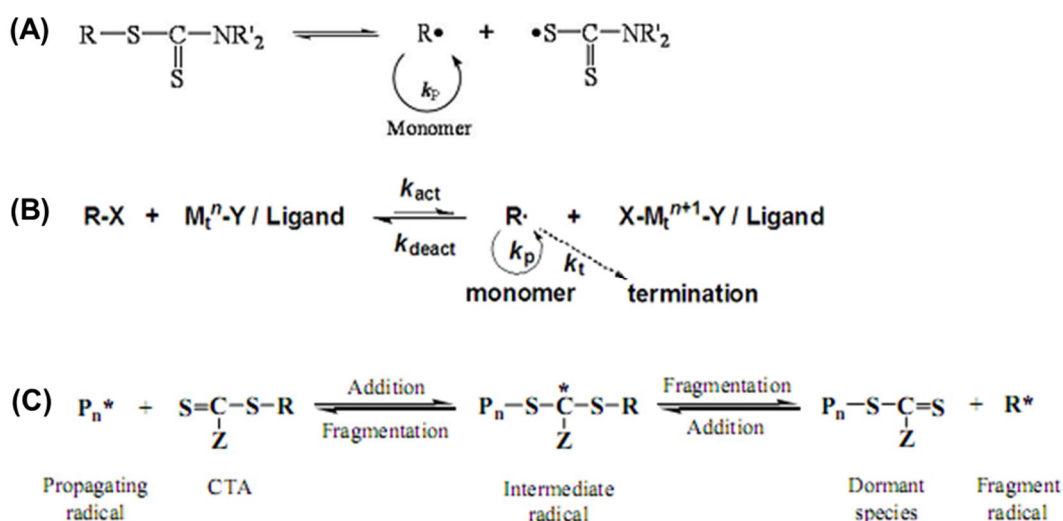


**Figure 9.** Mechanism of controlled/living radical polymerization: (A) Iniferter-induced radical polymerization; (B) Atom transfer radical polymerization (ATRP); (C) Reversible addition-fragmentation chain transfer (RAFT) polymerization. Reprinted from [Zhang et al., 2014].

*Iniferter polymerization.* Iniferters stand for initiator-transfer agent-terminator because they behave sequentially as initiator, transfer agent and terminator during the polymerization process. Iniferters are compounds usually containing a dithiocarbamate moiety which undergoes reversible photodissociation into a propagating alkyl radical and a dormant dithiocarbamyl (Fig. 10A). Many MIPs for small templates (< 1500 kDa), soluble in organic solvents have been synthesized using this approach [Beyazit et al., 2016]. However, examples of iniferter-induced polymerization for protein imprinting are scarce due to the poor solubility

of existing iniferters in aqueous media. In 2006, a water-soluble iniferter was reported by [Tsuji & Kawaguchi, 2006]. This iniferter was shown to initiate photopolymerization at room temperature and quasi-living polymerization was observed during the preparation of particles of poly(glycerolmethacrylate)core-pNIPAm shell (Fig. 10B) [Sato et al., 2008].

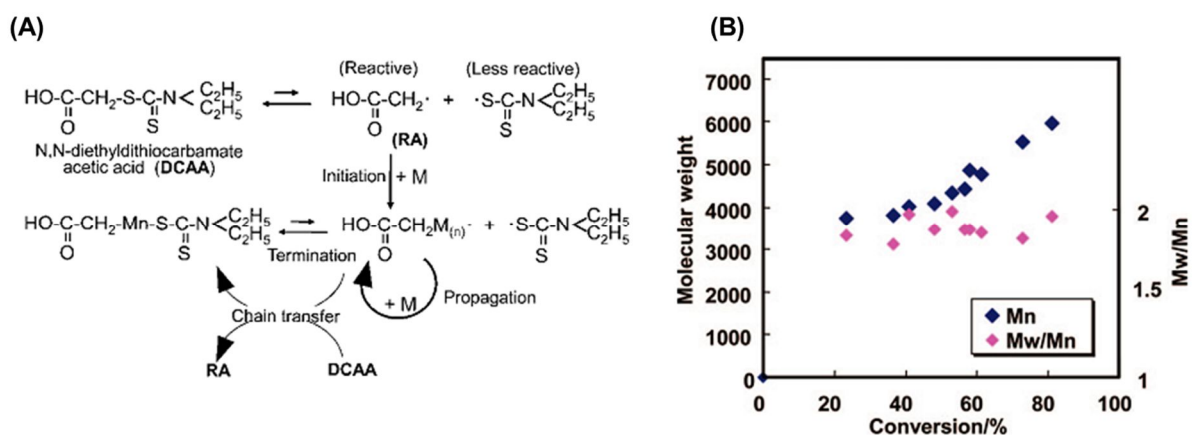


**Figure 10.** (A) Mechanism for living polymerization using DCAA and (B) Molecular weight increase with conversion, proving the living character of DCAA [Sato et al., 2008].

DCAA was later applied for imprinting of MIP for lysozyme using a two-step post-imprinting strategy, as shown in Fig. 11 [Sunayama et al., 2014]. The polymerization mixture was composed of acrylamide-based monomers and a new functional monomer 4-[2-(N-methacrylamido)ethylaminomethyl] benzoic acid (MABA), which contains benzoic acid for interaction with the target protein and a secondary amine for post-imprinting modifications. After the extraction of lysozyme to create specific binding cavities, lysozyme was again added to protect the high-binding cavities. *p*-isothiocyanatophenyl  $\alpha$ -D-mannopyranoside (MITC) was then introduced to block the exposed amine groups. Afterward, lysozyme was removed again, and amine in the high affinity cavities was conjugated with fluorescein isothiocyanate (FITC), thus binding performance could be measured by monitoring the change of fluorescence intensity of FITC.

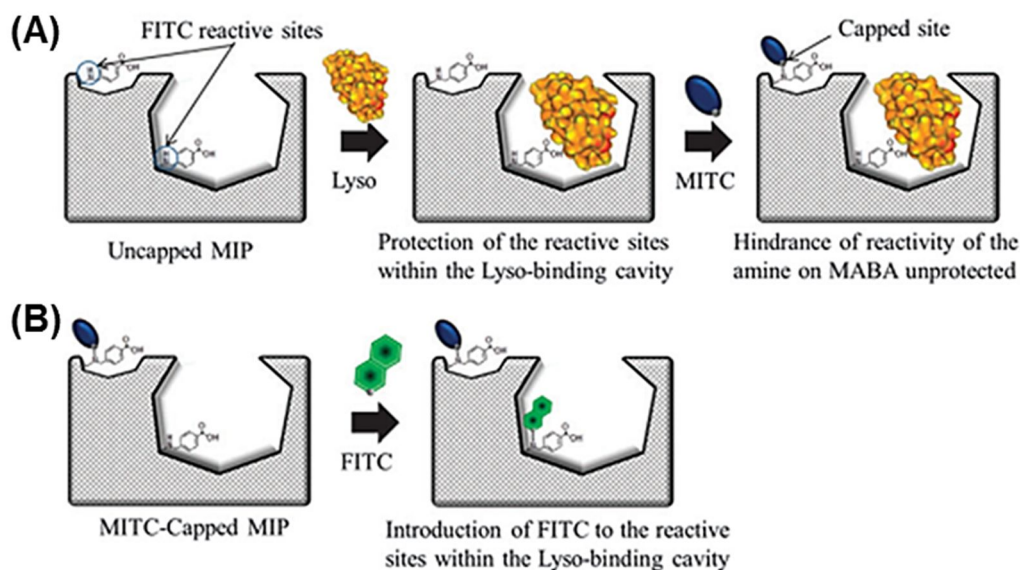


**Figure 11.** Schematic representation of the two-step post-imprinting modification process: (A) capping treatment by MITC; (B) introduction of FITC. Reprinted from [Sunayama et al., 2014].

*ATRP polymerization.* In ATRP, controlled conditions are achieved through a redox process involving a transition metal complex ( $M_t^n$ ) and an organic halide (R-X) (Fig. 9B). The oxidative addition of a halide to the metal centre results in the formation of an oxidized ( $M_t^{n+1}$ ) complex and a radical species ( $R^*$ ), which propagates until a halide back-transfer from the oxidized metal ( $M_t^{n+1}$ ) stops the chain growth by converting the system to its dormant state. Normally, an ATRP system uses catalysts of the type  $CuCl/CuCl_2/Bpy$ .

Recently, Ulbricht and co-workers reported the development of MIP hydrogels, imprinted with lysozyme via a two-step grafting procedure by an ATRP initiator immobilized on polyethylene terephthalate (PET) membrane surface [Yin & Ulbricht, 2013]. An alkyl bromide as ATRP initiator, was immobilized on the membrane surface, through oxidative PET hydrolysis and subsequent coupling (Fig. 12A). Thereafter, surface-immobilized scaffold poly(methacrylic acid) (PMAA) was prepared by hydrolysis of grafted poly(tert-butylmethacrylate) (PtBMA), which has been synthesized via ATRP of tBMA with C-Br at the polymer chain end (Fig. 12B). Lysozyme was bound to the scaffold to form a stable PMAA-lysozyme complex for imprinting. Polyacrylamide (PAAM) based hydrogel

layer was generated via UV-initiated grafting/crosslinking copolymerization using mixtures of acrylamide and methylenebisacrylamide. Subsequently, the template was eluted from the hydrogel layer to yield a porous membrane adsorber with imprinting cavities (Fig. 12C). The selectivity of this surface imprinted MIP membrane via ATRP toward lysozyme, compared with cytochrome c, was increased by optimization of the scaffold chain length, UV grafting/crosslinking time and the chemical crosslinking degree. Thus, the feasibility for development protein imprinted hydrogel membrane through surface-imprinted ATRP was demonstrated.

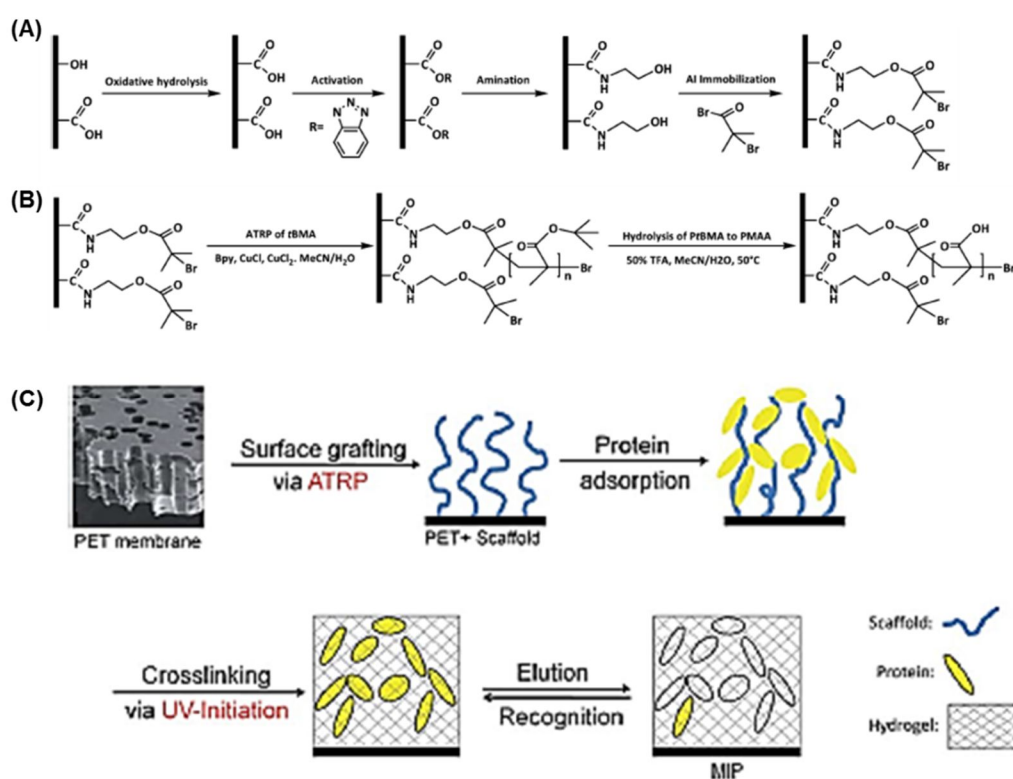


**Figure 12.** (A). Immobilization of ATRP initiator on polyethylene terephthalate (PET) membrane; (B) Generation of scaffold of PMAA through surface-initiated (SI)-ATRP on PET surface; (C) General procedure of protein imprinting via two step grafting using SI-ATRP and UV-initiated grafting/crosslinking copolymerization on the PET membrane surface. Reprinted from [Yin & Ulbricht, 2013].

*RAFT polymerization.* This method involves reversible addition-fragmentation sequences in which the transfer of a dithioester moiety between active and dormant chains serves to maintain the living character of the polymerization. Initiation of polymerization is by a

classical FRP initiator. Growing chains ( $P_n^*$ ) are added up successively to the chain transfer agent (CTA). Addition of this macroradical on CTA gives rise to an unstable radical which fragments into a new radical  $R^*$  which can polymerize a new polymer chain (Fig. 9C). For RAFT, the polymerization is mainly performed in organic phase, which makes it difficult to be employed for protein imprinting. So, efforts have been made to solve this problem, and progress has already been made to develop RAFT in aqueous solution. Compared with ATRP, no biological-unfriendly metal catalyst is needed for conducting RAFT, thus the latter is more promising for biomacromolecule imprinting. However, most of the time, RAFT reaction lasts a long time like 24 – 48 h and takes place at high temperatures from 40 – 70 °C, which limits its application to a great extent [Yang et al., 2011]. Still, for some stable proteins like lysozyme, this new technology is of great potential.

Recently, Li et al., 2014, has developed a novel surface protein imprinted core-shell particles based on RAFT strategy for lysozyme recognition. As shown in Fig. 13, 4-cyano-4-(phenylcarbonothioylthio) pentanoic acid as a RAFT initiator and lysozyme as template protein, were first adsorbed on silica beads. Then polymerization was performed with methacrylic acid and 2-hydroxyethyl methacrylate as functional monomers, and *N,N'*-methylenebis(acrylamide) as cross-linker, mixed with silica beads at 40 °C for 48 h. Finally, the surface-imprinted particles for lysozyme recognition was obtained after the removal of template and destroying the dithioester groups with hexylamide. With controllable polymer chain length, this MIP particles showed improved specificity (IF = 3.7) and selectivity (in a four-proteins mixture and egg white sample) toward lysozyme, and the adsorption equilibration could be reached in 1 h.

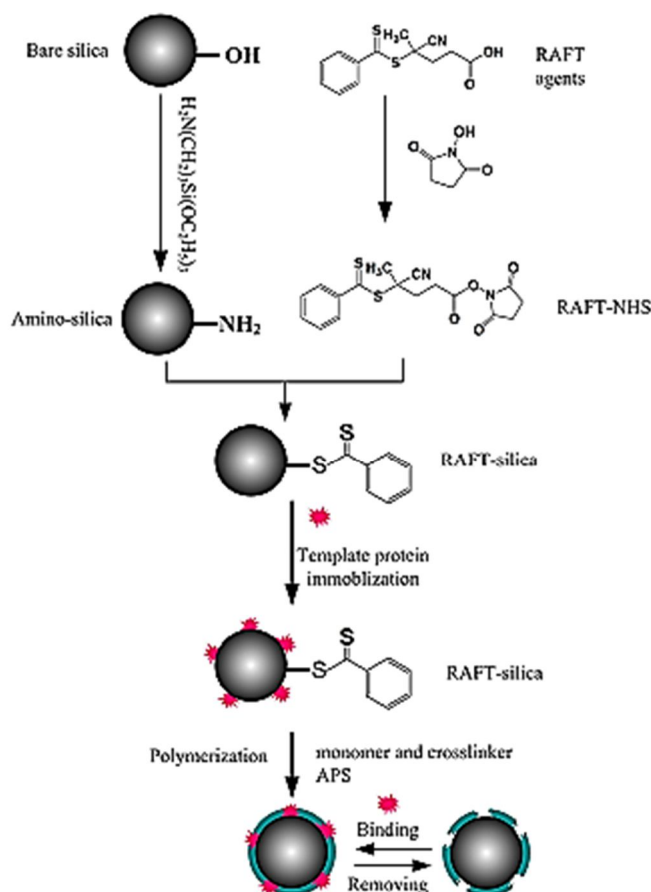


**Figure 13.** Illustration of surface lysosyme imprinted core-shell particles synthesis by RAFT strategy. Reprinted from [Li et al., 2014].

### II-3. Spatial strategy

The current protein imprinted polymers can be classified as 3D and 2D formats. Concerning the first protein-MIPs which were in 3D or bulk format, one major drawback is the elimination of the template after polymerization. For instance, a systematic study was carried out by Cutivet et al., 2009, who tried different methods for the removal of trypsin from polyacrylamide-based MIPs, namely, electromigration, 2 M and 10 M urea, digestion by proteinase K (100  $\mu\text{g}/\text{mL}$ ), 5% SDS in 10% acetic acid, autolysis at 40  $^{\circ}\text{C}$ . Fig. 14 shows the SDS-PAGE analysis of the MIP after the above treatments for template removal. Only electromigration and proteinase K treatment resulted in the quantitative removal of trypsin from the MIP ; using SDS/acetic acid, the most widely used technique for template removal, was less effective. Moreover, the SDS-acetic acid has to be eliminated carefully in a following

step, specially the SDS which imparts a negative charge on the MIP and can cause artefact binding.

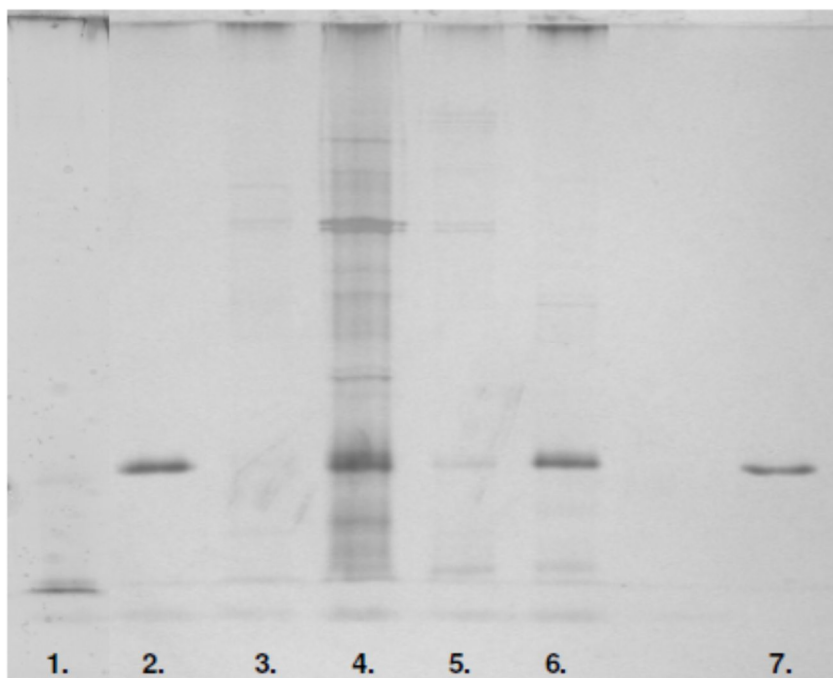


**Figure 14.** SDS-PAGE analysis of a copolymer of methacrylamide and ethylene bisacrylamide, 60% cross-linking, 1.5  $\mu\text{m}$  mean particle size, after template removal. Type of washing : 1. electromigration; 2. incubation in urea 2 M; 3. digestion by proteinase K; 4. Incubation in urea 10 M; 5. incubation in SDS/AcOH ; 6. autolysis at 40  $^{\circ}\text{C}$ ; 7. reference trypsin 100 ng. Reprinted from [Cutivet et al., 2009]

Because of these shortcomings, 2D protein imprinting which gained popularity due to the fast mass transfer property, has been adopted by many researchers in the field. Since whole proteins are difficult to imprint, epitope imprinting approach is often a solution and intensive effort has been devoted to its development. For example, the combination of surface imprinting and epitope approach often seems to be preferentially adopted.

### **II-3-1. Surface imprinting**

Ratner and co-workers were among the first to create imprints of proteins in a surface bound polymer film [Shi et al., 1999]. They showed that an atomically flat mica surface imprinted

with bovine serum albumin (BSA) preferentially adsorbed the template protein from a binary mixture with IgG. Since then, with the development of MIP materials science, more and more surface imprinted polymers were synthesized. Owing to the fact that surface-imprinted nanomaterials always show extremely high surface-to-volume ratio, which facilitate template transfer, thus both binding capacity and kinetics are improved. Moreover, this kind of nanostructures can provide additional features through the integration of other functions. So, the synthesized MIPs can be applied for affinity separation, sensing, and specific capture and release. The materials used for surface polymerization are usually of high dispersion stability and excellent biocompatibility. The widely used surfaces mostly concern two categories:  $\text{Fe}_3\text{O}_4$  nanoparticles and  $\text{SiO}_2$  surface.

**$\text{Fe}_3\text{O}_4$  nanoparticles** are usually synthesized in aqueous solutions by the coprecipitation of  $\text{Fe}^{2+}$  and  $\text{Fe}^{3+}$  in the presence of a base [Rutnakornpituk et al., 2009]. Using this procedure, the obtained  $\text{Fe}_3\text{O}_4$  nanoparticles possess super hydrophilic surface, but high aggregation properties. Addressing this disadvantage, a variety of modification of  $\text{Fe}_3\text{O}_4$  nanoparticles was performed, such as carboxyl group functionalization, chitosan covering,  $\text{SiO}_2$  coating, graphene oxide decoration, etc. Core-shell MIPs using  $\text{Fe}_3\text{O}_4$  nanoparticles as substrate has gained wide attraction, due to their low toxicity, high adsorption capacity and kinetics, as well as good reusability. Therefore, this kind of MIPs is widely used in protein purification and proteomic research. In particular, they possess the high convenience of being easily separated from the surrounding media, by applying a simple magnet.

One interesting example of MIP synthesis on  $\text{Fe}_3\text{O}_4$  nanoparticles was reported by Bie et al., 2015. They developed a boronate-affinity glycan-oriented surface imprinting strategy for the preparation of lectin-like MIPs that can recognize an intact glycoprotein and its characteristic fragments. As illustrated in Fig. 15, a target glycoprotein was digested by glycosidase into multiple glycans, which were purified by ultrafiltration. Then, the glycans, acting as templates, were immobilized onto boronic acid magnetic nanoparticles. Afterward, a thin layer of polymer was formed to cover the templates. After washing with acidic solution to remove the templates, the obtained MIPs can recognize not only the intact glycoprotein, but also its

digested glycopeptides and glycans. Using RNase B as a glycoprotein template, the obtained MIP exhibited a specific binding toward RNase B with an IF value of 8.4, and a very selective binding performance compared with other proteins like RNase A, transferrin and HRP.

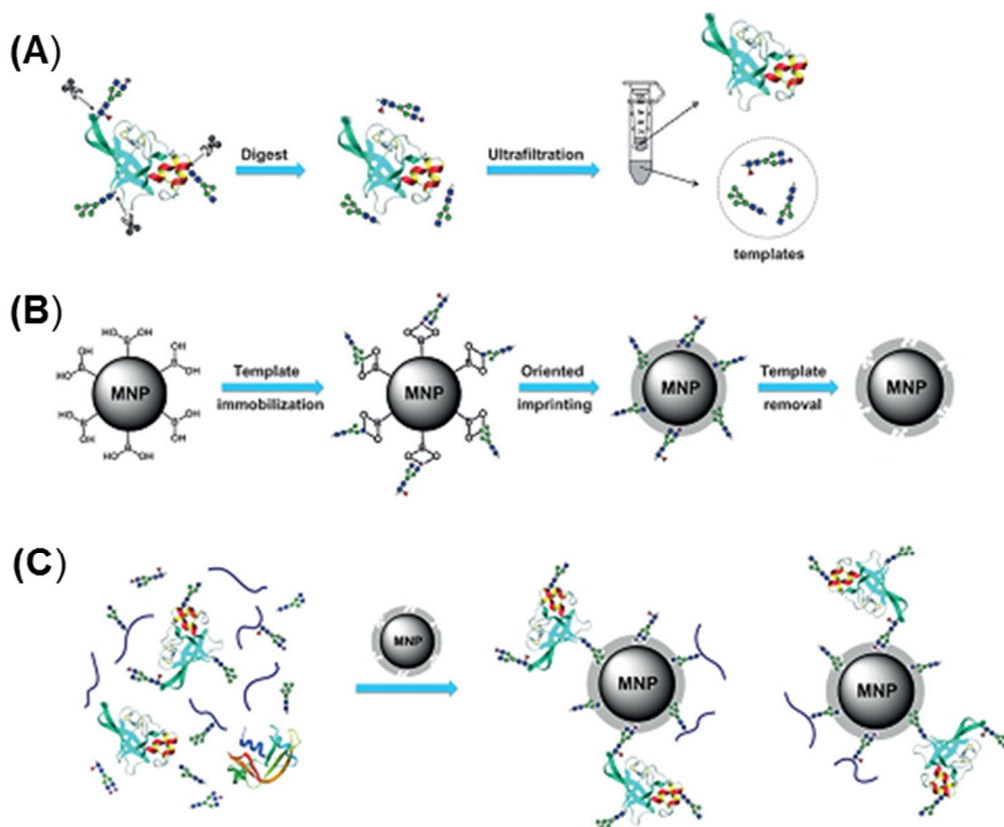


**Figure 15.** General view of surface imprinting for digested glycans of glycoprotein: (A) Preparation of glycan templates by digestion of glycoproteins; (B) Surface imprinting of immobilized glycan templates on boronic acid-functionalized magnetic nanoparticles; (C) Recognition of glycan templates and glycoprotein. Reprinted from [Bie et al., 2015].

**SiO<sub>2</sub> surface** is very hydrophilic, so materials synthesized on glass slides or silica nanoparticles are very homogeneous in aqueous solution without aggregation problems. In order to use SiO<sub>2</sub> surface, some functionalization steps are necessary for protein immobilization prior to MIPs synthesis, such as boronic acid functionalization for oriented glycoprotein immobilization, IDA-Cu<sup>2+</sup> introduction to immobilize surface-His containing proteins, etc.

Recently, 3-(trimethoxysilyl)propyl methacrylate (MPS) modified SiO<sub>2</sub> nanoparticles

(denoted as SiO<sub>2</sub>-MPS) became quite popular [Li et al., 2015]. As illustrated in Fig. 16, SiO<sub>2</sub>-MPS nanoparticles were first coated with a cross-linked polymer layer, composed of *N,N'*-methylenebis(acrylamide) (MBA) and acrylamide (AAm). With lysozyme as template protein chelated with Cu<sup>2+</sup> containing monomer, and SiO<sub>2</sub>@poly(MBA-co-AAm) as core, functional monomers and cross-linker were added for precipitation polymerization, at 37 °C. In the procedure of surface imprinting of lysozyme via aqueous precipitation polymerization, functional monomer including di(ethylene glycol) methyl ether methacrylate (MEO<sub>2</sub>MA), AAm, and Cu<sup>2+</sup> chelating monomer were used. According to their study, the best binding performance occurred at 37 °C with highest imprinting factor (up to 22.7) and selectivity. The rebinding reached equilibrium within 10 min with a high affinity (K<sub>d</sub> = 336 nM). Furthermore, their MIP nanoparticles could be regenerated and reused for three cycles.

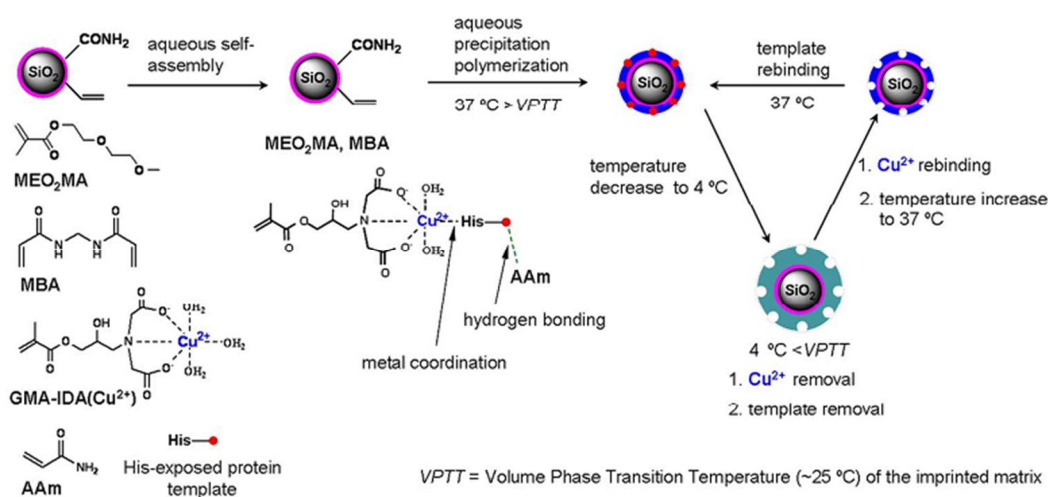
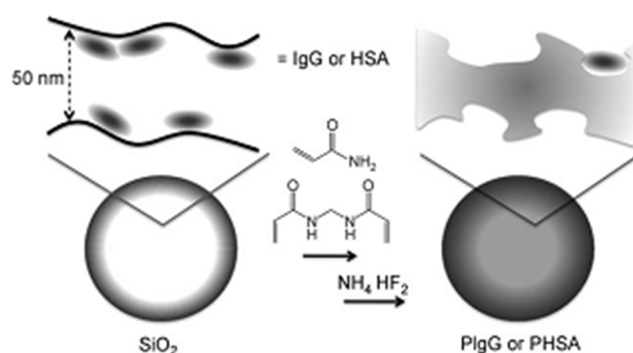


Figure 16. Schematic representation of surface imprinting of lysozyme via aqueous precipitation polymerization. Reprinted from [Li et al., 2015].

In 2000, Mosbach and co-workers were the first to propose a new surface imprinting strategy, called hierarchical imprinting [Yilmaz et al., 2000]. Through polymerization in porous silica, as sacrificial solid support, regular-sized MIPs particles were prepared, and showed superiority of high binding capacity, good selectivity and fast mass transfer (Fig. 17) [Nematollahzadeh et al., 2011; Li et al., 2013]. Similarly, Haupt and coworkers prepared protein-imprinted polymer nanofilaments (specific for myoglobin) in using nanomolding in a

a sacrificial porous alumina membrane [Linares et al. 2009].



**Figure 17.** Hierarchical protein imprinting strategy starting from wide-pore silica particles with adsorbed protein (IgG and HSA in this example). Pores were first filled with prepolymerization mixture, afterward binding sites at the pore walls of silica beads were obtained by subsequent removal of template proteins by ammonium hydrogen difluoride etching and washing. Reprinted from [Nematollahzadeh et al., 2011].

In 2014, Zhang and co-workers developed hierarchical imprinting technique to prepare protein imprinted materials for the selective depletion of HSA from human serum [Lui et al., 2014]. The synthesis procedure is presented in Fig.18. Using porcine serum albumin (PSA) as template, MIPs obtained by hierarchical imprinting were compared with those obtained by traditional bulk imprinting. It was found that hierarchically imprinted polymers exhibited higher binding capacity of 12 mg/g of PSA (9.4 mg/g for bulk polymers), and equilibration was reached in less than 20 min (600 min for bulk polymers). Although the selectivity of both MIPs were high, the binding capacity reproducibility of hierarchically imprinted polymers was much better than that of bulk polymers.

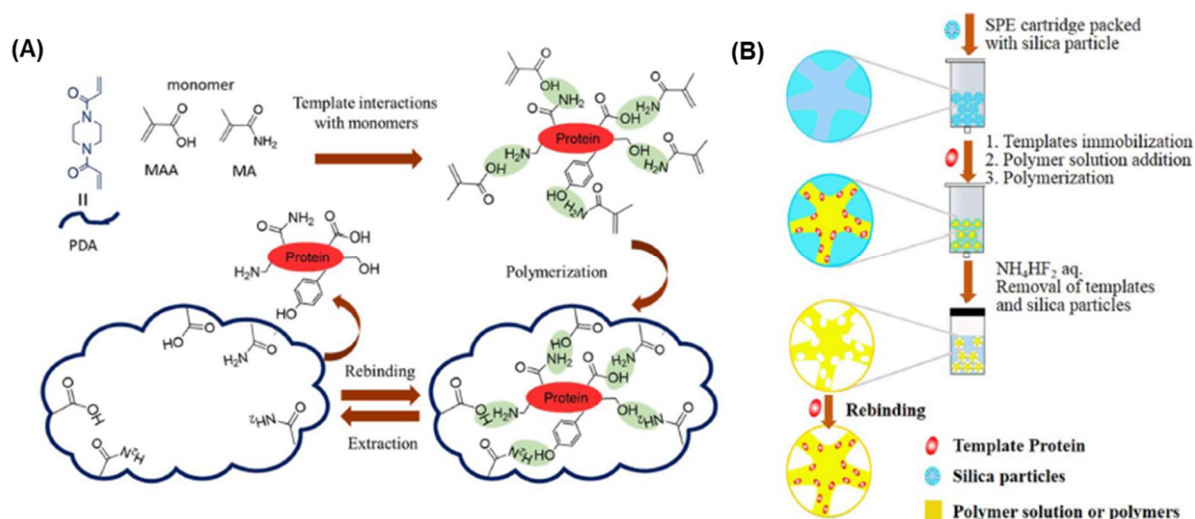


**Figure 18.** (A) Schematic illustration of interactions between monomers and template protein; (B) synthesis of protein imprinted polymers by hierarchical imprinting. Reprinted from [Lui et al., 2014].

### II-3-2. Epitope imprinting

Whole proteins are difficult to imprint due to their complex structure and numerous functionalities and their risk of denaturation. Therefore, decreasing the complexity of protein structure is perceived as a promising strategy. Since antibodies against a protein recognize their target via certain sequential or conformational epitopes, it has been suggested to use an epitope approach also with MIPs [Rachkov & Minoura, 2001]. Efficient epitope imprinting, leading to selective MIPs for binding the whole protein, requires a minimum of 9 amino acids [Nishino et al., 2006]. This sequence length was chosen, as short epitopes focus on developing capture agents for the primary structure of the peptide rather than the more complex secondary and tertiary structures of a target protein. Since it has been reported that epitope-imprinted polymers can not only distinguish the peptide with only one amino acid mutation, but also recognize the whole protein even in real samples [Yang et al., 2014], epitope imprinting seems to have a bright future.

Bossi and coworkers reported an approach to the rational selection of epitope peptides for protein imprinting [Bossi et al., 2012]. In the epitope imprinting approach, the selected epitope peptide templates are short and exposed peptide sequences on the surface of the protein, which are identified by analysis of crystallographic structures of proteins in the Protein Databank. However, the more conserved epitopes of diagnostic interest, which lead to pathogens, are located in the core of the protein. So, in their work, they presented a rational approach to the selection of key epitopes to prepare fingerprint-imprinted polymers (FIP) for NT-proBNP detection. The procedure is presented in Fig. 19. The sequence of NT-proBNP was cleaved *in silico* with different enzymes. All the hydrophilic primary peptides, both exposed or internal ones, with appropriate length of 7 – 12 amino acids, were then selected. The alignment of the 7 – 12 mers with all the protein sequences stored in UniProt Knowledge base was performed by Basic Local Alignment Search Tool (BLAST), so as to choose the distinctive and unique peptides of the target protein. The selected peptides were then synthesized and used as templates for molecular imprinting. Their final results demonstrated the successful selection of epitope peptides. The obtained MIP gave a high imprinting factor of 10 and a great rebinding ability of 40% template in complex sample.

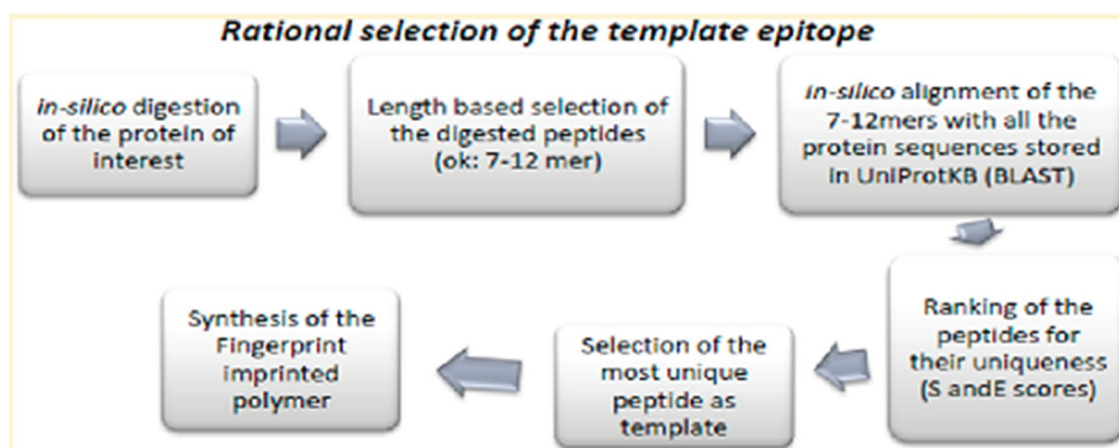


**Figure 19.** Procedure for the rational selection of template epitope for the preparation of fingerprint-imprinted polymers. Reprinted from [Bossi et al., 2012].

If the right epitope is selected, epitope imprinting approach has several advantages, like

abundant choice of templates, a variety of reaction conditions and defined orientation to binding the target proteins [Yang et al., 2014]. Usually, the obtained MIP has  $K_d$  in nM range for the imprinted peptides and  $K_d$  in  $\mu$ M range for the corresponding proteins [Yang et al., 2013]. Recently, a combination of surface imprinting and epitope approach is proposed for special applications such as protein purification [Qin et al., 2016], development of sensors [Yang et al., 2014], etc.

For the simultaneous capture of various proteins to achieve precise diagnosis and high-throughput analysis, many efforts have been made to develop a multiepitope-imprinted polymer. Recently, Yang et al., 2016, have developed a universal method to prepare multiepitope templates imprinted particles through phase inversion-based poly(ethersulfone) (PES) self-assembly polymerization, as shown in Fig. 20A. In their work, N-terminal epitope peptides of three high-abundance proteins in human plasma: albumin, immunoglobulin G (IgG), and transferrin (TRF), were used as templates. Fig. 20B shows that the MIPs could recognize selectively the target proteins, HSA (P1), IgG (P2), and TRF (P3), simultaneously, in 100-fold diluted human plasma, with obviously greater binding amounts than the NIPs. For the other high abundance proteins, such as KRT1 keratin type II cytoskeletal 1 (P4), macroglobulin (P5), fibrinogen- $\alpha$  (P6), and  $\alpha$ -2-glycoprotein (P7), the binding amounts on the MIPs were similar to those on the NIPs, due to the nonspecific adsorption. These findings open a new era of MIP to achieve simultaneous recognition of various proteins.

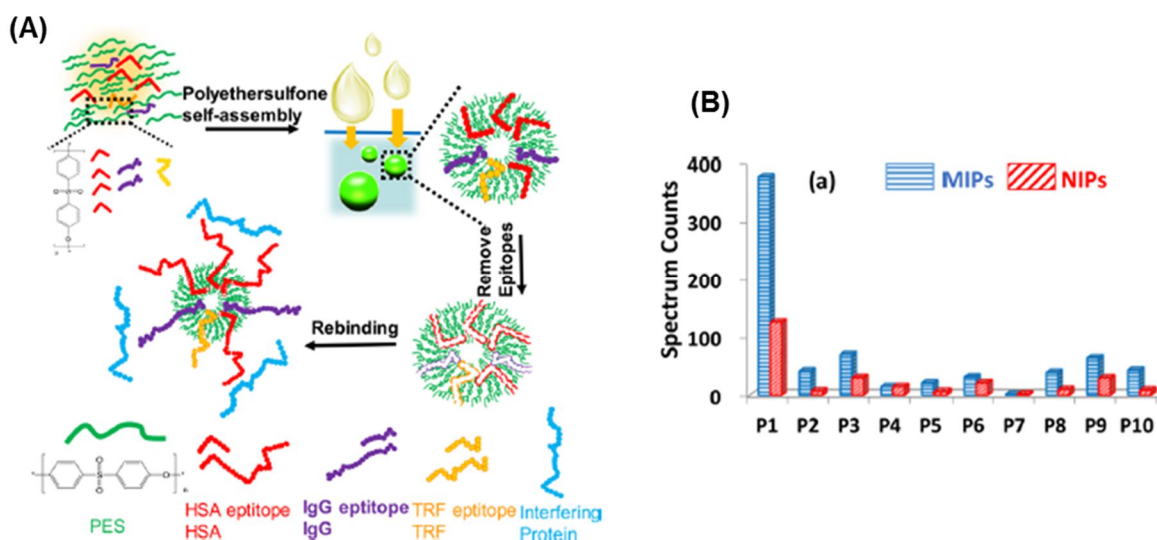


**Figure 20.** (A) Preparation of multi-epitope templates imprinted polymers via PES self-assembly and the simultaneous capture of various target proteins; (B) Binding amounts of 10 highly abundant proteins by MIPs and NIPs in human plasma samples. P1 : albumin; P2 : transferrin; P3 : IgG; P4 :KRT1 keratin type II cytoskeletal 1; P5 : macroglobulin; P6 : fibrinogen-alpha; P7 : alpha-2-glycoprotein; P8 : alpha-1-antitrypsin; P9 :complement C3; P10 :apolipoprotein A-IV. Reprinted from [Yang et al., 2016].

### II-3-3. Solid-phase synthesis

The solid-phase synthesis approach was first introduced by Piletsky's group for the synthesis of MIPs for small templates [Poma et al., 2013]. With this method, the MIP particles are obtained in a soluble form, in either organic or aqueous solvent. They use an automated reactor for solid-phase synthesis under computer control. The template is immobilized on a functionalized solid phase, and then MIPs are synthesized around the immobilized protein. After washing at low temperature (15 °C) to remove the low affinity polymers and unreacted monomers, the high affinity MIPs are eluted by applying high temperatures (60 °C) (Fig. 21).

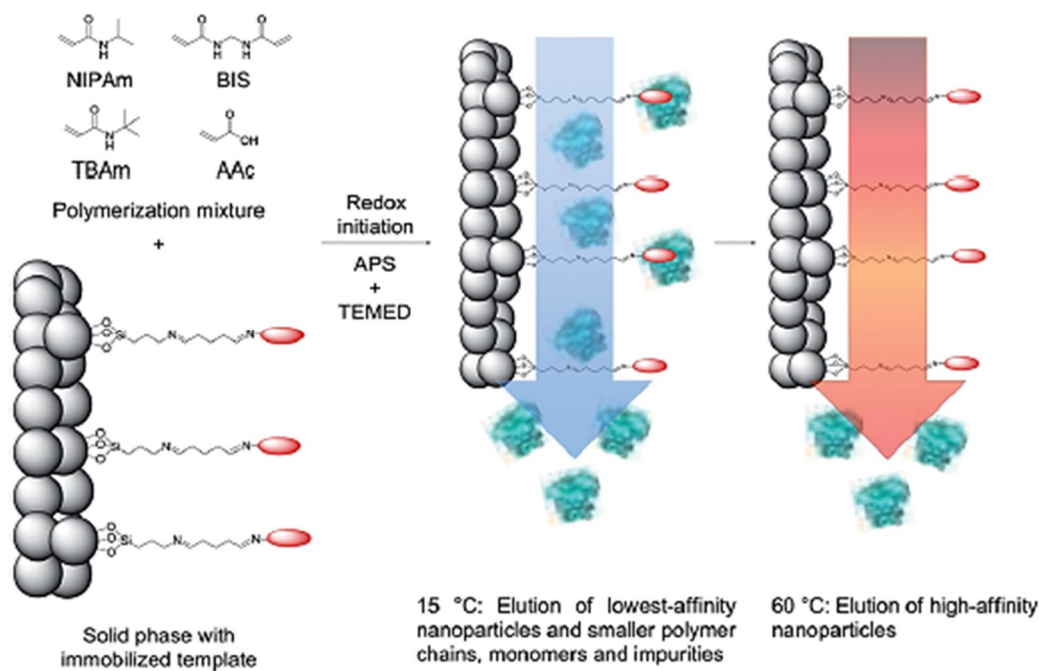


**Figure 21.** Schematic representation of the solid-phase synthesis using a general ligand for protein immobilization and high temperature elution of MIP. Reprinted from [Poma et al., 2013].

Till now, several template proteins such as trypsin, pepsin A,  $\alpha$ -amylase, HRP and cytochrome c have been imprinted using this approach. Generally, they use covalent coupling protocols for the immobilization of the proteins, like (3-aminopropyl)trimethoxysilane and glutaraldehyde. Although, this type of general protocol provides more choice of target proteins that can be imprinted [Cáceres, et al., 2016], the variation of protein orientation may bring heterogeneous binding cavities, thus more non-specificity and less oriented functionality of the obtained MIP [Guerreiro et al., 2014]. Furthermore, the final elution of MIP is always performed at high temperature, a condition not compatible with protein conformation integrity if the reactor has to be recycled.

On the other hand, Haupt's group uses an oriented immobilization of the protein via an affinity ligand [Ambrosini et al., 2013]. At the beginning, they employed a competitive inhibitor to immobilize the enzyme in a fixed orientation. Then this method was developed to become more universal by using a metal-chelate as affinity ligand, so as to immobilize all

proteins containing histidine groups on the surface and potentially His-tag engineered proteins. MIP-NPs are then synthesized on the solid support, and they are easily released, thanks to their thermoresponsive properties. By a judicious combination of functional monomers used in the polymerization mixture, the elution takes place at room temperature or below, i.e. in milder conditions as compared to 60 °C. The advantage of the method is that all binding sites have the same orientation and are located at the surface of the particle, thus improving binding site homogeneity and accessibility of the sites by the bulky protein. *This work is part of the present thesis and will be developed more in detail in the 2 publications of chapter 2.*

## II-4. Different formats of protein-imprinted polymers

By using different spatial strategy for protein imprinting, different structures and morphologies of MIPs can be obtained (Fig. 22 and Fig. 23). Since every structure owns its own benefits for a particular purpose, comparison between them is not very useful.

### 2D imprinted structures:

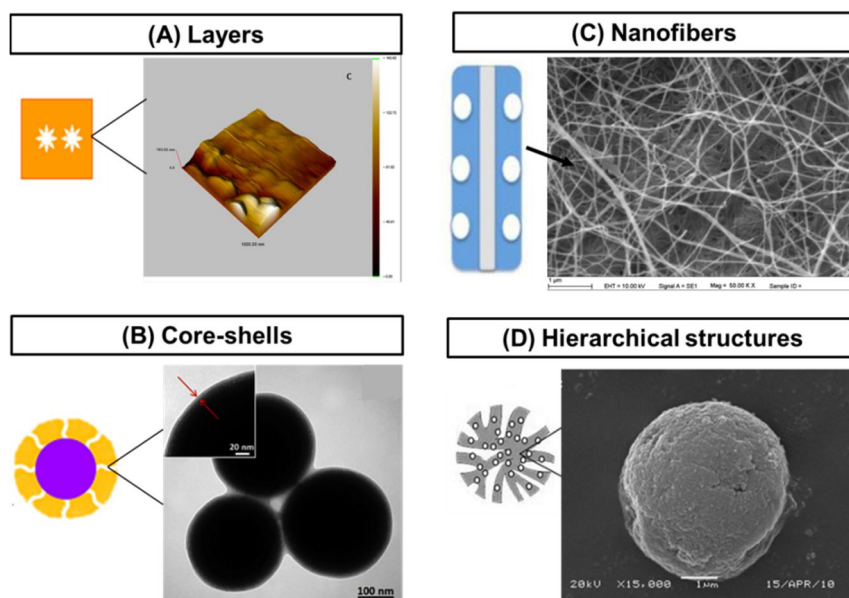


**Figure 22.** (A) Microcontact imprinted polymers on surface plasmon resonance (SPR) biosensor and AFM image, reprinted from [Ertürk et al., 2016]; (B) Surface imprinted polymers on silica nanoparticles and TEM image, reprinted from [Li et al., 2016]; (C) Surface imprinted polymers on bacterial nanofibers and SEM image, reprinted from [Tamahkar et al., 2015]; (D) Hierarchical imprinted polymers in wide-pore silica and SEM image, reprinted from [Li et al., 2013].

### 3D imprinted structures:

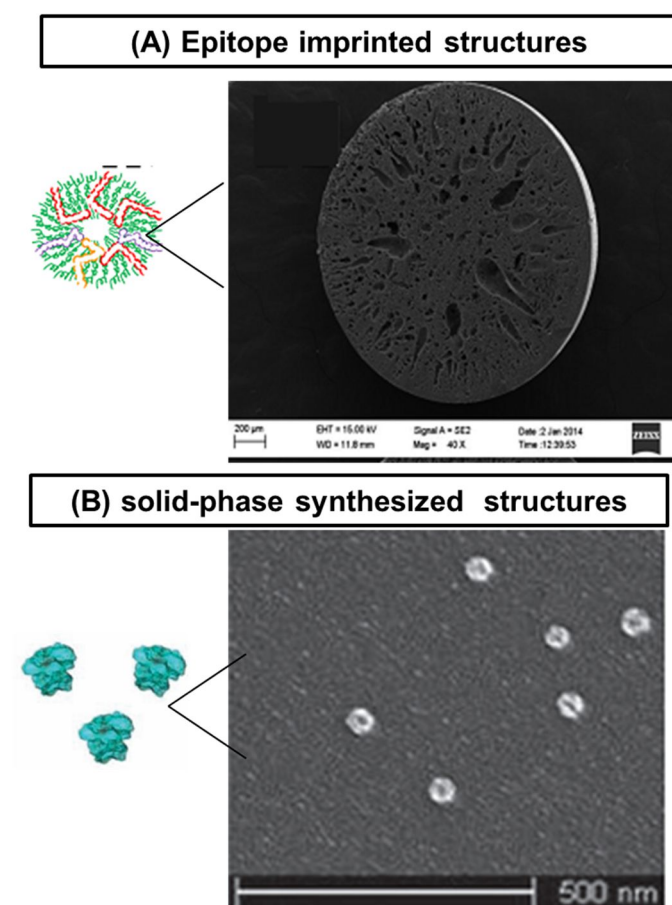


**Figure 23.** (A) Multi-epitope imprinted polymer by PES self-assembly, reprinted from [Yang et al., 2016]; (B) Solid-phase synthesized MIP nanoparticle, reprinted from [Poma et al., 2013].

## II-5. Rational design of polymers

Computational studies for the effective design of imprinted polymers have made a great progress for small targets. Owing to the complexity of biological macromolecules and their interactions, this technique has not been widely used in rational design of protein imprinted polymers. Until 2010, attempts to simulate protein imprinting were performed by Levi and Srebnik. They did an evaluation report on the pore properties, efficiency and selectivity of imprinting [Levi & Srebnik, 2009, 2010, 2011].

In general, the most important issue in protein imprinting is the stability of proteins under a

given condition. Differential scanning fluorimetry (DSF) is a technique applied to measure the thermal stability of a protein in a given set such as pH, ionic buffer strength and salt concentrations, and also the melting point of protein upon binding to a small ligand. To investigate the limit of a set, the measurement was performed by plotting fluorescence signal of labelled proteins against incremental increases of a set. Since these experiments can be done on a 96 well plate real time – PCR machine, which leads to a high throughput of screening a large amount of buffer conditions and functional monomers for MIP synthesis [Ashley et al., 2016]. As shown in Fig. 24, a variety of monomers were investigated by DSF technique for  $\beta$ -lactoglobulin MIP synthesis. Because, in the presence of strong interactions caused by some monomers, the melting point of the target protein is going to be higher. In the end, their results show qualitative binding between the protein and optimal MIP.

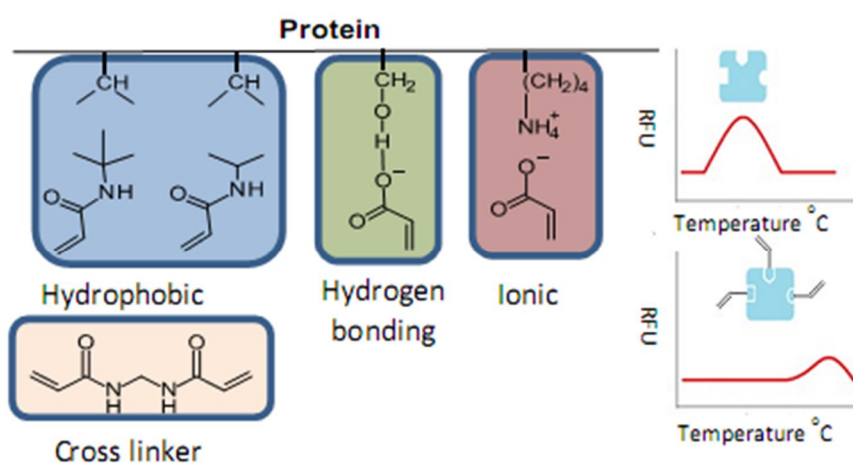


**Figure 24.** A bank of acrylic monomer ligands for protein imprinting and the melting profiles using DSF in the presence of the target protein with and without interacted monomers. Reprinted from [Ashley et al., 2016].

For surface imprinting, it is impossible to apply universal thickness for all the proteins [Li et al., 2014]. Some studies showed proof-of-concept that indeed the thickness imprinted film generated over substrate needs to be tailored for individual templates. And the optimal film thickness providing the highest binding capacities and imprinting factors was in a positive correlation with the template protein size. For example, the best thickness of imprinted polymer

film for RNase B (3.1 x 5.1 x 7.6 nm), HRP (4.0 x 6.7 x 11.7 nm), glucose oxidase (5.8 x 13.2 x 15.2 nm) were 5.7 nm, 10.2 nm, 16.3 nm respectively [Wu et al., 2015].

For solid-phase synthesis approach, low yield is a concern. To improve on this, Piletsky's group described a novel method to optimize the synthesis parameters affecting the yield of obtained MIP nanoparticles with specificity for vancomycin [Muzyka et al., 2014]. Experiment design was carried out by MODDE 9.0 software. In order to establish an analyzing model, parameters like the amount of functional monomers, UV irradiation time, temperature during polymerization, and elution temperature. In the end, the yield was increased a lot and conclusion was that irradiation time is the most important and temperature is the last important factor which influences the yield of nanoparticles for UV induced polymerization.

### **III. Applications of protein-imprinted polymers**

MIPs for protein recognition have broad applications including affinity separation, biosensing, proteomic analysis, clinical diagnosis, drug delivery, and so forth. From a commercial point of view, the development of MIP as antibody mimics has drawn a lot of attention during the last decades due to their growing demand for the diagnostic market.

#### **III-1. Separation**

From a commercial point of view, affinity separation remains the most important application; for instance in clinical diagnosis, it is of great interest to isolate and identify some special proteins, like glycoproteins which are biomarkers of diseases. A small summary of recent progress of MIP application for protein separation or extraction from complex samples is presented in Table 2.

**Table 2.** A few recent and relevant MIP applications in protein separation or extraction from complex samples.

Target proteins	Separation strategy	Material development	Reference
HRP	Magnetic	Solvothermal method to develop Fe <sub>3</sub> O <sub>4</sub> NPs with optimum thickness	Ma et al., 2016
His-tag	Epitope imprinted enhanced IMAC	SiO <sub>2</sub> @IDA/MAPS-Ni <sup>2+</sup> nanoparticles	Li et al., 2016
Transferrin	Concanavalin A-mediated sugar-lectin interaction	<i>In situ</i> surface imprinting by Con A-mediated template immobilization on Fe <sub>3</sub> O <sub>4</sub> with dopamine	Qu et al., 2016
Cytochrome c	Coordination with MAH-Cu <sup>2+</sup>	Surface-imprinted bacterial cellulose	Tamahkar et al., 2015
BSA	Solid phase extraction	MIP composed of 2-VP and EDMA	Soleimani et al., 2012

Currently, immobilized metal ion affinity chromatography (IMAC) has been considered as one of the most effective approach to separate surface histidine-containing proteins or His-engineered recombinant proteins, by coordination interaction between histidine and transition metal, usually Cu<sup>2+</sup> and Ni<sup>2+</sup> respectively [Porath, 1988; Block et al., 2009]. However, proteins with inherent cysteine or metal center can also be co-purified non-specifically on IMAC, which results in contamination of samples [Young et al., 2012]. So, to overcome this problem, imprinting enhanced IMAC (EI-IMAC) was recently developed by the combination of MIP materials with metal ion immobilized solid phase. Zhang's group

introduced a universal method for the purification of His-tag engineered protein by epitope imprinting [Li et al., 2016]. They endowed the IMAC surface with a His-tag (6 His) imprinted polymer matrix, thus the His-tag of His-tagged proteins could enter the imprinted sites and be trapped by metal ion on the surface of IMAC, while other proteins were excluded, as illustrated in Fig. 25A. The EI-IMAC could reach 100% adsorption equilibrium within 15 min, and the adsorption capacity of MIP-IMAC: 25.7 mg/g, is 7.1 times higher than NIP-IMAC. To evaluate the selectivity of the MIP-IMAC toward His-tagged protein, it was applied to a crude cell lysis containing ~18% His-tagged green fluorescent protein (GFP). The purification procedure is shown in Fig. 25B. EI-IMAC was more efficient in separating the His-tagged GFP from other impurities than traditional IMAC (Fig. 25C).

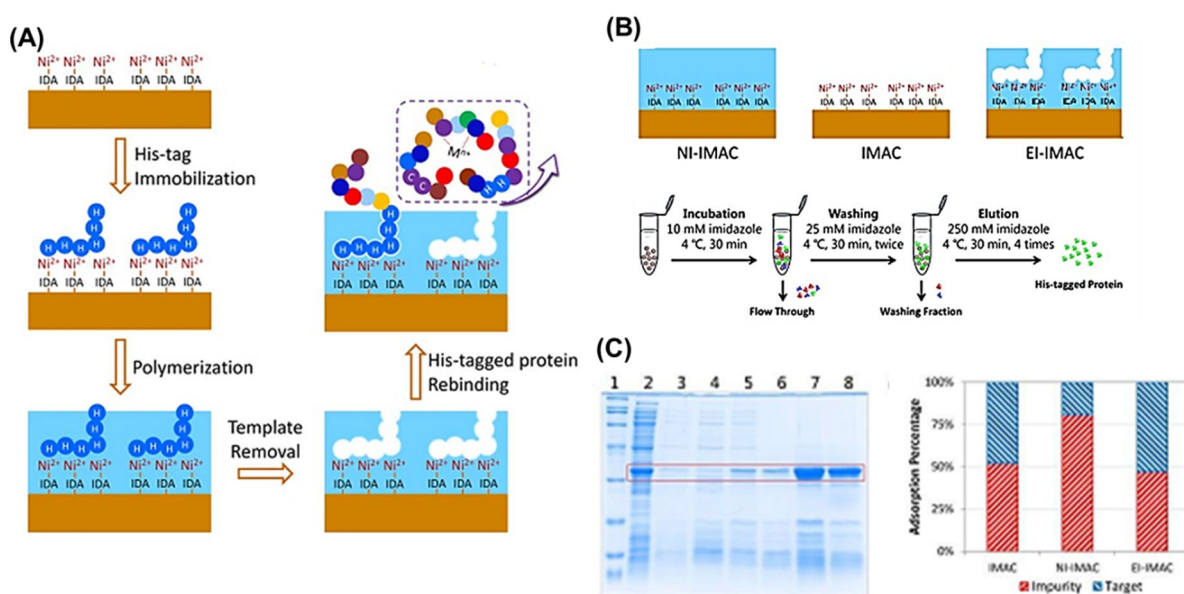


**Figure 25.** (A) Schematic illustration of preparation of His-tag imprinted IMAC materials and the separation principle on EI-IMAC; (B) Purification procedure of His-tagged protein from crude cell lysis using IMAC; (C) percentage of His-tagged protein and other impurities in the purified product using non-imprinted IMAC (NI-IMAC), IMAC and EI-IMAC, as deduced from a SDS-PAGE analysis. Reprinted from [Li et al., 2016].

## III-2. Diagnostics

### III-2-1. Biosensor

A biosensor consists of a recognition element and a transducer, as shown in Fig. 26. In a biosensor, the molecular recognition element that interacts with the analyte of interest is typically a biological element, such as enzymes, antibodies, DNA, cells, etc. The transducer converts the recognition event in a readily measurable signal. The transducers in biosensors can be electronic, chemical, micromechanical or piezoelectric [Kivirand et al., 2013; Eersels et al., 2016], and optical as well [Ton et al., 2015].

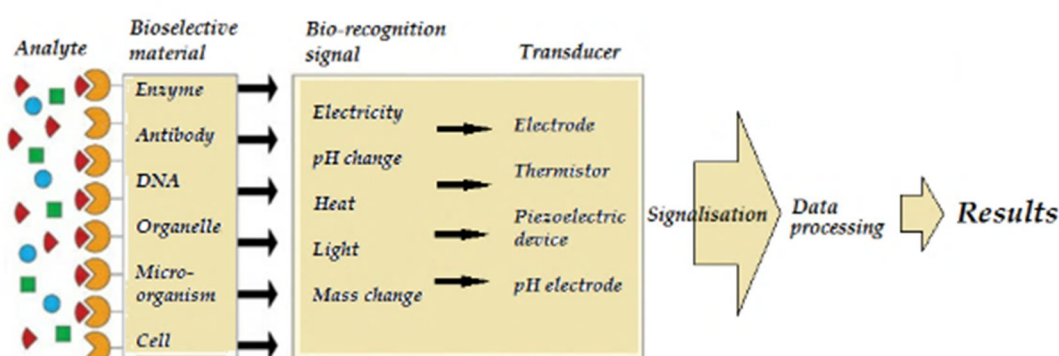


**Figure 26.** Schematic representation of a biosensor. Reprinted from [Kivirand et al., 2013].

Biological receptors bind with the analyte with high specificity and sensitivity. However, they suffer from low stability and special care must be taken during their application and storage. On the contrary, MIPs are capable of binding selectively to target molecules with a good affinity, while being chemically and thermally stable. Moreover, MIPs are relatively easy to prepare, and can be regenerated and reused. Therefore, thousands of attempts have been carried out for MIP-based biosensor fabrication during the past five years [Wackerlig & Lieberzeit, 2015]. The detection of biomacromolecules, especially proteins, is of great importance for the purpose of diagnostics, for which different kinds of sensing mechanism were employed. (Summarized in Table 3).

**Table 3.** Analytical performance of different sensing mechanism for proteins

Sensing principle	Target proteins	Linear range	Reference
Fluorescence sensor	HRP	1 – 10 $\mu$ M	Zhang et al., 2014
	Lysozyme	3 – 28 $\mu$ M	Deng et al., 2013
Electrochemiluminescence immunosensor	Hemoglobin	0.016 – 620 pM	Zhou et al., 2013
SPR or QCM sensor	Prostate specific antigen	0.2 – 100 pM	Ertürk et al., 2016
Electrochemical sensor	Hemoglobin	0.016 pM – 1.6 $\mu$ M	Luo et al., 2014

Fluorescence sensors have emerged as one of the most promising tools for proteins detection owing to their high sensitivity and fast response. Zhang et al., 2014, recently reported a novel nanosensor based on molecularly imprinted spatial structure and boronate affinity for detecting glycoproteins selectively. They coated CdTe nanocrystals (NCs) with a polymerizable surfactant octadecyl-*p*-vinylbenzyltrimethylammonium chloride (OVDAC) and copolymerized the OVDAC-coated CdTe with the monomers *N*-isopropylacrylamide (NIPAM) and 4-vinylphenylboronic acid (VPBA) in the presence of a target glycoprotein, horse radish peroxidase (HRP), as shown in Fig. 27 (A). In the imprinted polymeric network, NIPAM functioned as a thermoresponsive monomer that allows for swelling and shrinking reversibly with temperature, and the reversible interaction of VPBA with the glycoprotein was regulated by pH, as shown in Fig. 27 (B). The binding properties were determined by fluorescence quenching, and the imprinting factor of the HRP-MIP was found to be 3.83, which proved the enhanced quenching efficiency and spectral sensitivity of MIP-based nanosensor for the target glycoprotein. Selectivity and competitive experiments were carried out in the presence of different proteins, lysozyme, bovine serum albumin (BSA), transferrin, ovalbumin, or D-fructose. The results clearly demonstrated that the imprinted sensor displayed preference toward the target glycoprotein and its cross-reactivity toward the competitors was very low.

The developed MIP-based nanosensor was successfully employed for the selective detection of HRP ranging from 0 – 10  $\mu\text{M}$  in 100-fold diluted urine.

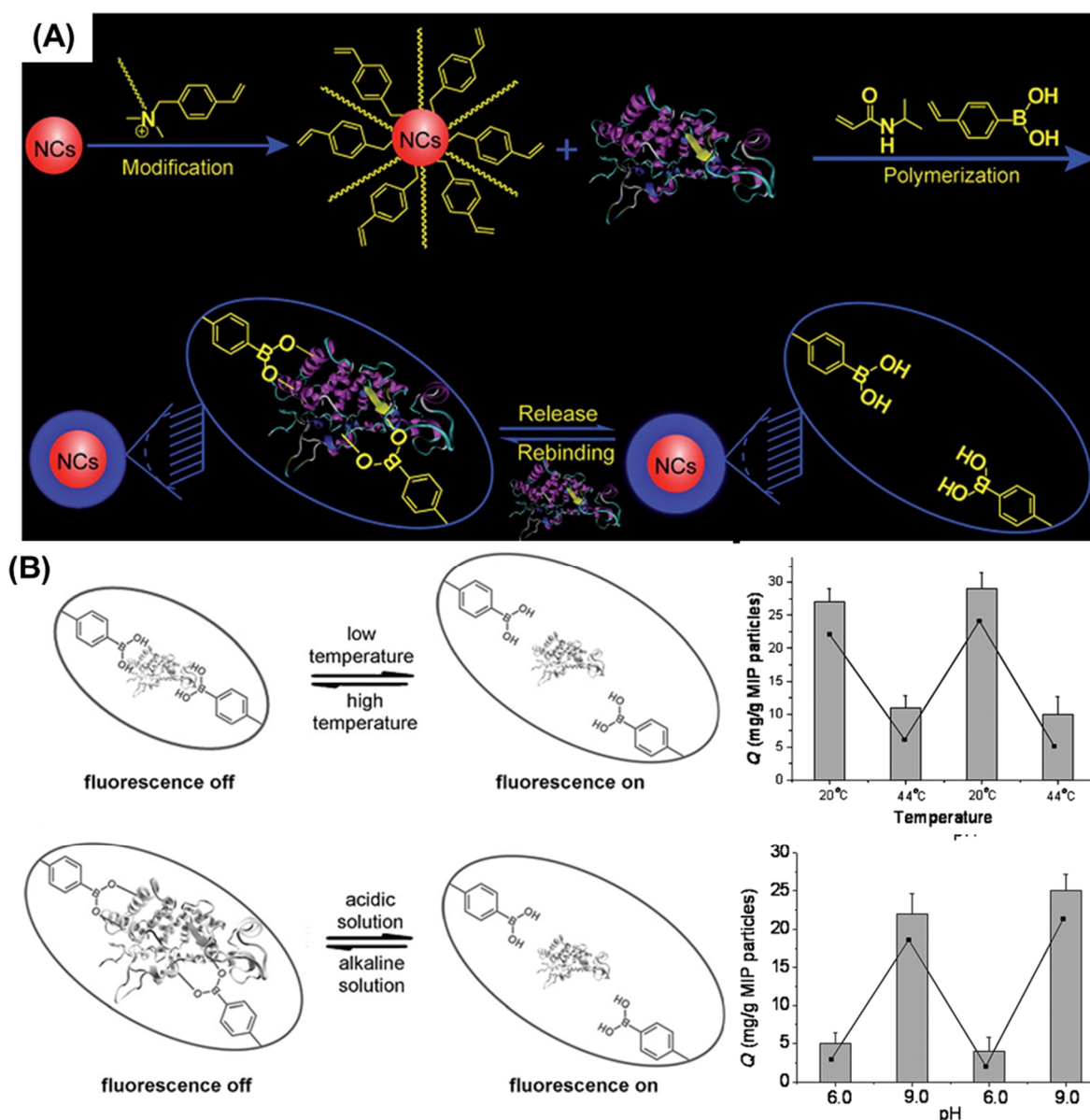


**Figure 27.** (A) Schematic procedure for the preparation of fluorescence nanosensor. A reversible covalent bond between the boronic acid and the glycoprotein's cis-diol is formed at alkaline pH and dissociates at acidic pH; (B) Proposed mechanism of the fluorescence nanosensor for the capture and release of the target glycoprotein through control of the temperature and pH. Reprinted from [Zhang et al., 2014].

This example of fluorescence sensor for protein detection has a quantification range in the  $\mu\text{M}$ , which is sometimes not sensitive enough. Ultrasensitive quantification in the pM for

ultratrace monitoring of protein for precisely diagnosing a disease is often required. Recently, a new antibody sandwich electrochemiluminescence (ECL) immunosensor based on magnetic molecularly imprinted polymers was reported [Zhou et al., 2013]. They developed a sandwich immunoreaction-based sensor by using magnetic MIP as capture antibody and a signal tag as detection antibody. The resulting sandwich complex was immobilized on an electrode surface by a magnet, which lead to the generation of an ECL signal from the signal tag upon the addition of the appropriate voltage, as shown in Fig. 28. The LOD was 0.023 pg/mL. This kind of sensor processes the following advantages: 1) reduced loss of bioactivity caused by normal protein capture antibodies; 2) magnetic separation and simplified procedures to fulfill the objective of reusability; 3) amplified detection signal caused by MIP enrichment of antigens. The specificity of the developed immunosensor shows an imprinting factor of about 2, and it selectively bound hemoglobin even in a complex mixture. Moreover, the feasibility of this immunosensor in clinical analysis was confirmed by measuring serum samples from patients and the detected results shows a recovery range from 93.2% to 105.8%, which was further validated with classical ELISA test.

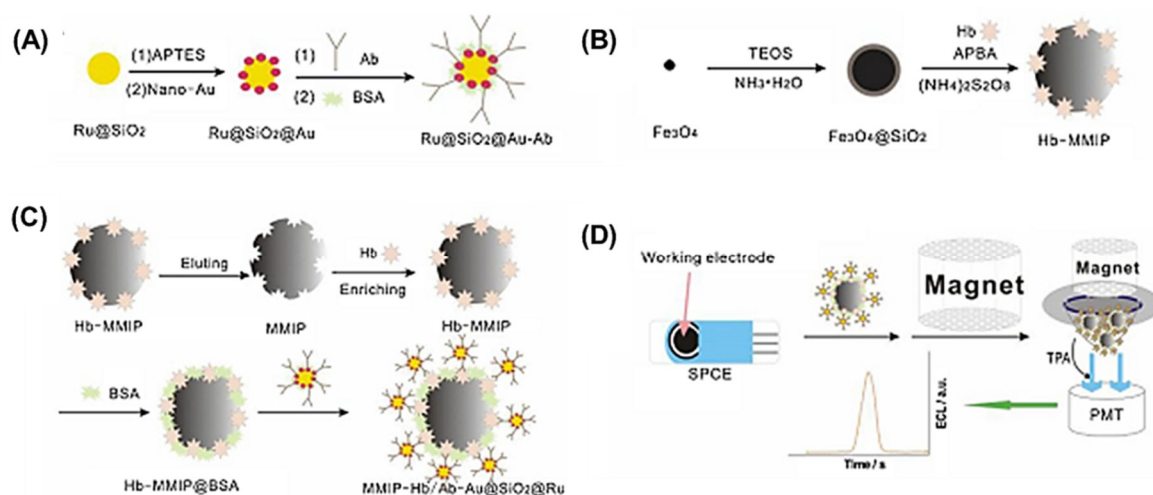


**Figure 28.** Procedure for the preparation of an electrochemiluminescence immunosensor for hemoglobin (Hb). (A) Preparation of detection antibody with a signal tag. BSA (bovine serum albumin) serves to block non-specific binding sites and APTES stands for (3-aminopropyl) triethoxysilane; (B) Preparation of magnetic MIP for hemoglobin, APBA stands for 3-aminobenzene boronic acid and TEOS for tetraethoxysilane; (C) Preparation of the sandwich immunosensor and (D) Principle for sensor detection. Reprinted from [Zhou et al., 2013].

### III-2-2. ELISA

Immunoassay is an important tool for measuring the presence or concentrations of biomacromolecules, especially some biomarker proteins, or sometimes small molecules. Immunoassay is usually rapid, sensitive and selective to the analyte of interest. So it is a widely used clinical diagnosis for the analysis of proteins. In an immunoassay, antibodies conjugated with a variety of highly sensitive detection labels are used. Usually, they are enzymes, radioactive isotopes, DNA reporters, and also fluorescence or chemiluminescence probes. So, immunoassays come in many different formats and variations. Among all, the enzyme-linked immunosorbent assay (ELISA) is probably the most commonly used method.

ELISA tests exist in three main formats (Fig. 29):

(1) direct detection, where a single antibody binds directly to the immobilized analyte; usually the antibody is labeled with an enzyme, which produces the analytical signal.

(2) indirect detection. Two antibodies are involved with a primary antibody to bind to the immobilized analyte, and an enzyme-linked second antibody to recognize the primary antibody, and produces the signal.

(3) sandwich ELISA, in which a capture antibody is immobilized, and following the absorption of analyte, a detection antibody will come to perform quantitative analysis.

If kept at 4 °C, the shelf time of an ELISA kit is about 6 months, and its sensitivity ranges from  $\mu\text{g/L}$  to  $\text{mg/L}$ . However, the use of natural antibodies always brings some shortcomings, like the issue of stability and high cost, as well as the concern of batch-to-batch viability [Lee et al., 2013].

In this regard, MIPs, as suitable substitutes for natural antibodies are employed for the replacement of natural antibodies. The concept of MIP ELISA test was first introduced by the group of Haupt [Surugiu et al., 2000]; a specific MIP for a small template, 2,4-dichlorophenoxyacetic acid (2,4-D), was synthesized by precipitation polymerization and tobacco peroxidase conjugated 2,4-D was used as competitive ligand, which allowed for

colorimetric and chemiluminescence detection. The MIP was separated by centrifugation and the detection was done on the supernatant. A detection range of 5-100  $\mu\text{g/mL}$ , using chemiluminescence and 20-1000  $\mu\text{g/mL}$ , for colorimetric detection, was attained.

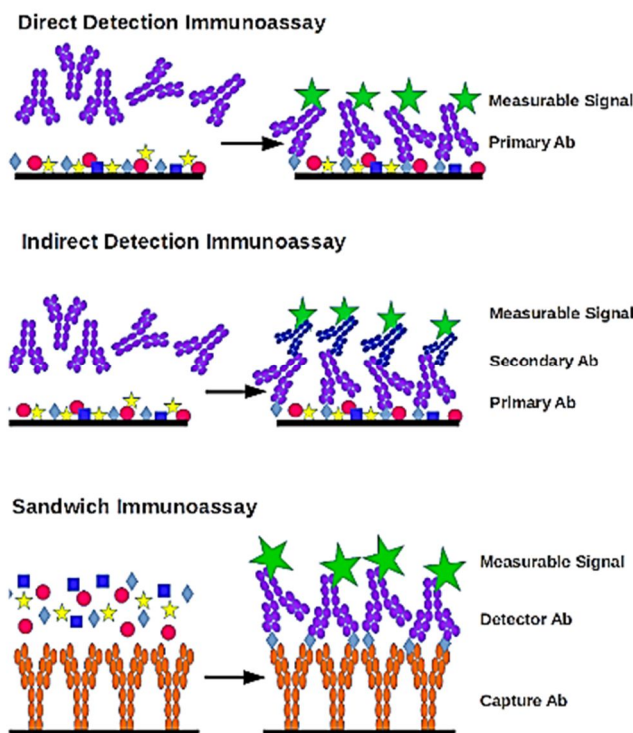


**Figure 29.** Three main types of immunoassay. Reprinted from <http://mainebiotechnology.com/fundamentals-of-immunoassays/>.

Piletsky's group reported different versions of an ELISA test, by either synthesizing MIP directly in microtiter plates [Piletsky et al., 2000] or later by coating the plate with MIP nanoparticles [Chianella et al., 2013]. In the latter case, their nanoMIP for targeting vancomycin, a peptide antibiotic, was synthesized in a computer-controlled reactor. The imprinting factor was found to be  $\sim 8$ , and the cross-reactivity toward other antibiotics was very low. Their nanoMIP-coated microplate was successfully applied for the measurement of vancomycin in blood plasma, by competitive assay with HRP-conjugated vancomycin. A low detection limit of 2.5 pM was reported. Additionally, the optimal conditions for the application of MIP in ELISA tests (conditioning, blocking and washing steps, etc) were studied, laying the foundation for MIP pseudo-ELISA test for protein detection [Cáceres et al., 2016]. The direct

pseudo-ELISA test describes nanoMIPs for HRP and cytochrome c, coated on well plates. After addition of their respective target enzymes and washing to remove non-retained enzymes, the color was developed with 3,3',5,5'-tetramethylbenzidine (TMB), the substrate for the 2 enzymes. In all the described examples, the immobilization of MIPs was achieved by passive adsorption, risking the loss of binding site orientation and the introduction of non-specific binding. One example however reports a sandwich ELISA test, using surface-orientated MIPs for detection of glycoproteins, namely  $\alpha$ -fetoprotein (AFP) [Bi & Lui, 2014]. AFP is a biomarker and routinely assayed in clinical screening for liver cancer. The template protein is immobilized on a boronic acid-modified microplate, followed by the formation of a thin film of polyaniline. After removal of template, 3D cavities are formed on the microplate surface. The detection was done with HRP-labeled anti-HRP IgG/TMB substrate (Fig. 30). Though, no cross-reactivity experiments with other proteins present in human serum were reported, a sensitive detection of 12 ng/mL of AFP in a human serum sample, which correlated well with the value by radioimmunoassay from a commercial kit, was obtained with the MIP.

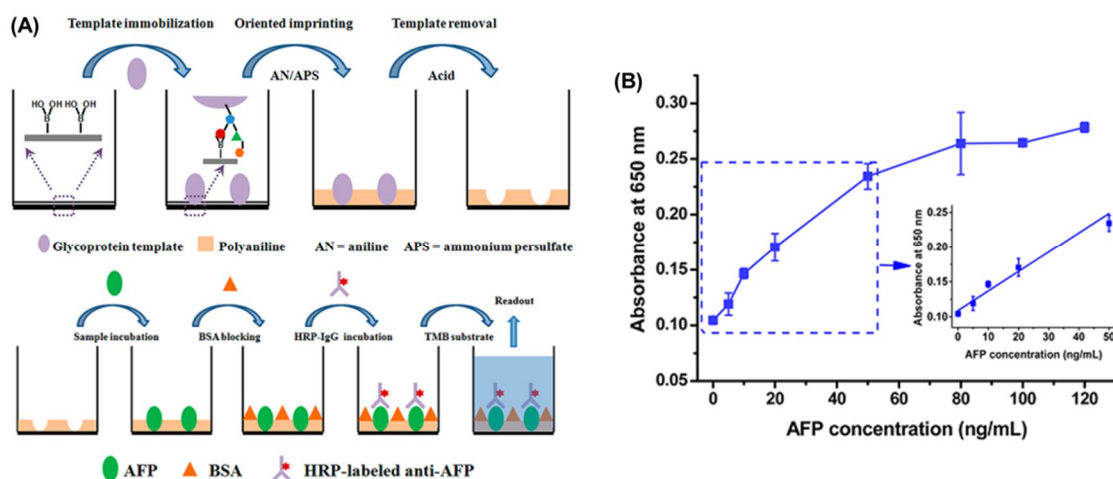


**Figure 30.** Sandwich ELISA for quantification of  $\alpha$ -fetoprotein. (A) The enzyme is immobilized by boronate affinity-based oriented surface imprinting; (B) Response curve. Inset, linear fit for the range 0-50 ng/mL. Reprinted from [Bi & Liu, 2014].

To change from most ELISA tests where MIPs are coated on the well plates by passive adsorption, a soluble MIP templated with vancomycin or ampicillin, synthesized with HRP as

functional monomer and cross-linked with glutaraldehyde, has been recently applied as recognition and signaling antibody for the detection of the antigen, immobilized on microplates. Though the yield of polymerization was very low, and the limit of quantification (LOQ) was high, in the mM range [Czulak et al, 2016], it was the first application of a MIP in an ELISA test where the MIP was not immobilized.

### III-3. In vivo applications

One of the ultimate goals is to apply MIPs for *in vivo* applications. Shea and co-workers were the first to demonstrate the *in vivo* application of MIP nanoparticles in mice model. The MIP nanoparticles proved to neutralize the toxic peptide melittin in the bloodstream of mice [Hoshino et al., 2008; Hoshino et al., 2010] (Fig. 31).

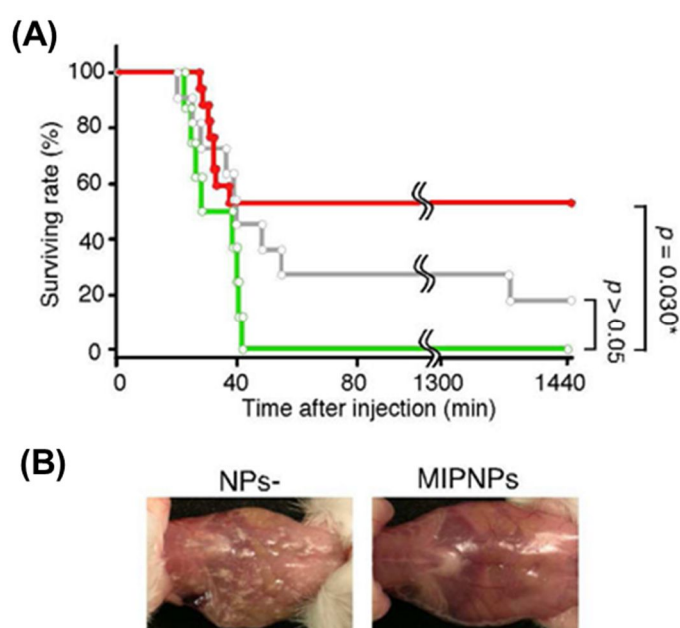


**Figure 31.** Neutralization of melittin toxicity by NPs. (A) Survival rates of mice over a 24h period after intravenous injection of 4.5 mg kg<sup>-1</sup> melittin (green); 30 mg kg<sup>-1</sup> MIPNPs (red) or NIPNPs (gray) was systemically administered via a tail vein 20 s after melittin injection. (B) Macroscopic pathology of peritoneal inflammation of mice injected with melittin (4.0 mg kg<sup>-1</sup>) followed with (left) nothing or (right) MIPNPs (30 mg kg<sup>-1</sup>). Reprinted from [Hoshino et al., 2010].

Recently, a polyacrylamide-based MIP was synthesized toward a disulfide-linked  $\alpha$ -helix-containing peptide, apamin, a conformational mimic of the N-terminal part of protein p32 [Zhang et al., 2015]. The obtained MIP with size 37 nm, could bind the target protein and recognize p32-positive cancer cells in mouse models. As shown in Fig. 32, tumor-bearing mice were treated with methylene blue (MB)-loaded MIPNPs, MB-loaded NIPNPs, free MB, and blank control. Methylene blue is a photosensitive agent used in photodynamic therapy. After post-administration, they were treated with 650-nm laser light for 10 min at 2 and 6 h, the tumor volume was recorded once every day during one week. Usually, the volume of tumor expands very fast in patients. Here the tumor volume of MIP treated mice was much smaller than that in non-treated, NIP treated and MB treated mice, which indicates a great potential of this MIP in therapeutic applications for a wide range of human diseases.

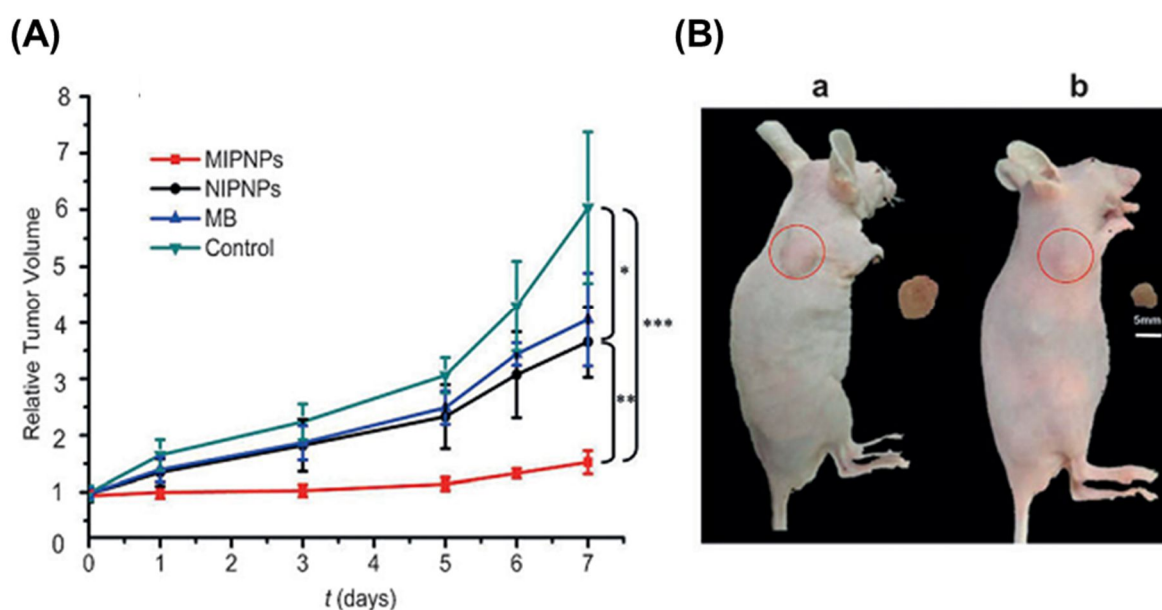


**Figure 32.** (A) In vivo antitumor effect of photodynamic treatment performed using distinct nanoparticle formulations. All injections were performed once at  $t = 0$ . Tumor volumes were measured every other day for one week; \* $P < 0.05$ , \*\* $P < 0.01$ , \*\*\* $P < 0.005$ . (B) Images of mice treated with NIPNPs (a) and MIPNPs (b). Scale bar = 5 mm. Reprinted from [Zhang et al., 2015].

Liu et al., 2015 presented the first example of engineered composite MIP nanoparticles for the selective intracellular sequestration of DNase I in living cells, without any disruption of the cell membrane. DNase I is involved in cell apoptosis and many other important cellular functions.

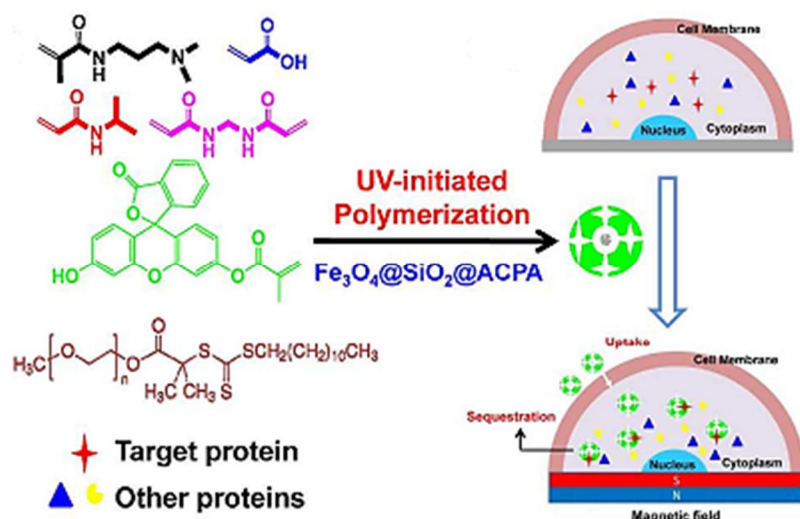


**Figure 33.** Schematic representation of the one-step synthetic approach for the PEG-modified fluorescent pNIPAM-based  $\text{Fe}_3\text{O}_4@SiO_2@MIP$  and the *in situ* sequestration of the target protein in living cells by using MIP. Reprinted from [Liu et al., 2015].

Fig. 33 shows the methodology. Briefly, a magnetic core nanoparticle composed of  $\text{Fe}_3\text{O}_4@SiO_2$ , bearing an amino group on the silica, was first prepared. 4, 4'-azobis-(4-cyanopentanoic acid) (ACPA) was then fixed on this core by covalent bonding, to initiate the polymerization. A polyacrylamide-based hydrogel MIP was synthesized around the core via a one-step *in situ* UV-induced polymerization, using a poly(ethylene glycol) (PEG)-containing macromolecular chain-transfer agent as the RAFT agent. RAFT polymerization with the PEGmacro-CTA improved the surface property of the MIP by providing good dispersion stability in buffer or water as well as a reduction in non-specific interactions and low cytotoxicity, as compared to free radical polymerization approach. Fluorescein O-methacrylate (FMA) was copolymerized into the hydrogel to facilitate the tracking of the sequestration of the target protein and cell imaging application. The magnetic MIP NPs were easily and efficiently taken up by the cells when guided by an external magnetic

field, without affecting the cell viability.

Liu et al., 2016 were the first to measure low-copy number proteins (< 1000 molecules per cell) in a single living cell by using MIP based plasmonic immunosandwich assay (PISA). This approach combines *in vivo* immunoaffinity extraction and plasmon-enhanced Raman scattering (PERS). The principle of PISA is illustrated in Fig. 34B. A gold-based MIP microprobe for alkaline phosphatase (ALP) is first prepared by using boronic-acid chemistry (Fig. 34A). The microprobe is then inserted into a cell through a micromanipulator. After extraction, the microprobe is removed, washed to eliminate unwanted species and incubated with silver-based Raman-active nanoparticles (NPs) boronate affinity for ALP. Thus, sandwich like immunocomplexes form on the extraction probe. After washing off excessive Raman nanotags, the microprobe is subjected to Raman detection. Upon irradiation with a laser beam, surface plasmon on the gold-based extraction microprobe is generated, which further enhances the SERS signal of the silver-based nanotags and thereby enables the detection of low-copy-number proteins. To facilitate wider applications, the extraction probes were extended to acupuncture needles, which allow for probing compounds with minimum invasion from living bodies. If a portable Raman spectrograph is used, the acupuncture needle version of PISA can permit point-of care and on-site assay.

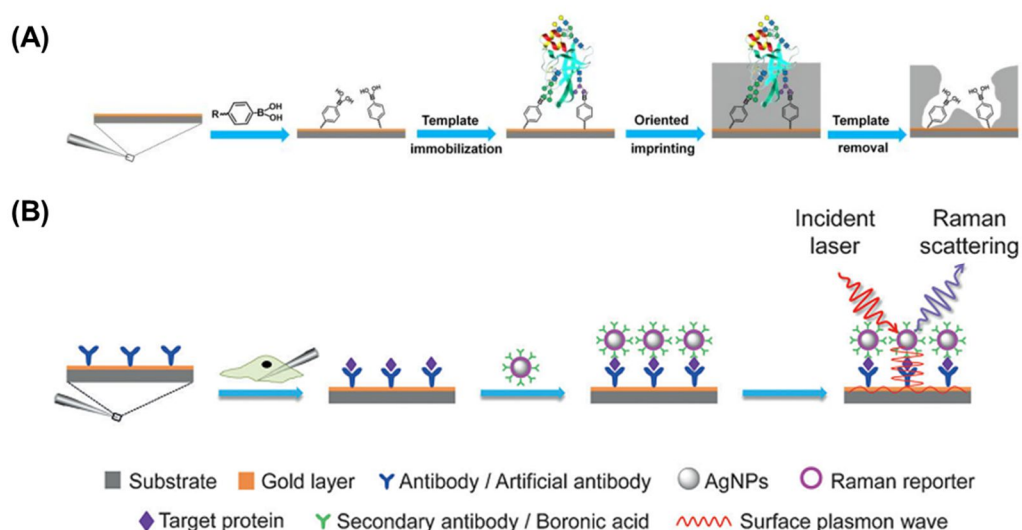


**Figure 34.** (A) Preparation of MIP-based microprobe; (B) Overview of probing protein expression in single cell by plasmonic immunosandwich assay. Reprinted from [Liu et al., 2016].

### III-4. Emerging applications

#### III-4-1. Protein crystallization

Proteins play crucial roles for the major machinery of life. Hence, the detailed 3D structure, allowing to understand the protein structure, is essential for the rational design of therapeutic treatments and structural biology. X-ray crystallography is the most powerful method for determining the 3D structure of proteins at high resolution, which is totally reliant on high quality crystals. In order to obtain good crystals, it is essential to control their nucleation stage, which is the first step in the crystallization process. Crystallization is usually induced by inserting crystal seeds (or nucleants) in the solution, which can be a variety of substances such as minerals, horse and human hair, thin films, charged surfaces, mesoporous materials etc. The problem with such materials is their poor specific affinity toward their target proteins. Recently, MIPs, have been reported to act as effective nucleants for induced crystallization of proteins. The principle is illustrated in Fig. 35 [Saridakis et al., 2013].

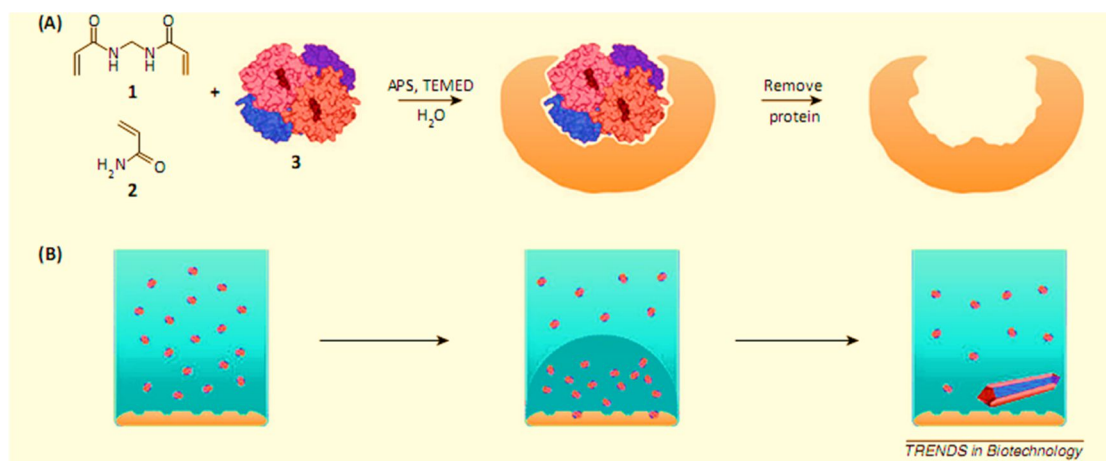


**Figure 35.** Molecularly imprinted polymers facilitate proteins crystallization. Reprinted from [Saridakis et al., 2013].

Chayen's group was the first to introduce protein crystallization performed with various MIP models and target proteins [Saridakis et al., 2011]. The ability to form crystals depends on the architecture of cavities which is complementary in size, shape and functionality toward the

target proteins. They demonstrated that the MIP cavities attracted proteins to aggregate, then the immobilized proteins would drive more proteins to come and assemble orderly.

Recently, their research demonstrated that even though the imprinting factor is close to 1, there was still a difference between MIP and NIP for the crystallization studies (normally, no crystals were formed by NIP) [Reddy et al., 2012]. For instance, in the case of trypsin as model, the trypsin MIPs lead proteins with similar sizes to crystalize but no crystals were formed for proteins with a significantly different size, which means the cavity size is an important factor for the crystallization process. On the other hand, they found the BSA MIP based on *N*-hydroxymethylacrylamide (NHMA) was super selective compared with polyacrylamide and polyNIPAm, and the crystallization based on this MIP was the best. The hydrophilicity increases in the order polyNHMA > polyacrylamide > polyNIPAm, thus they concluded that MIP selectivity was based on the hydrophilicity of the acrylamide functionalities.

In my opinion, the application of MIPs for protein crystallization is not so relevant with real imprinting or molecular recognition based interactions. There are two factors that lead to good quality crystals: 1) Cavities in size and shape that fit with target proteins; 2) hydrophilic materials composing the polymer, because this kind of materials drives the aggregation of proteins quickly. This means that whether the interaction between MIP cavities and target proteins is strong or weak, the non-specific binding is high or low, they will not affect the crystallization.

#### **III-4-2. Synthetic chaperone or inhibitor**

Proteins with flexible structures and conformations lack stability due to their intrinsic disorder. Since the 3D structure of proteins determines the functions of living organism, their misfolding is the underlying cause of many diseases [Wang et al., 2016]. Therefore, guided folding may regulate cell functions and further control disease progression. *In vivo*, the biological chaperones aid in the folding or assembly of proteins without being part of its final structure [Kim et al., 2013]. According to their function, some chaperones are foldases, because they support the folding of proteins in an ATP-dependent manner. Other chaperones

work as holdases that bind folding intermediates to prevent their aggregation [Hoffmann et al., 2004].

As synthetic chaperones, or tailor-made folding assistants, MIPs have shown a great potential. In an early study by Haruki et al., 2009, a MIP based on acrylamide/methacrylic acid/2-(dimethylamino)ethyl methacrylate/*N,N'*-methylenebisacrylamide, has proven to be efficient for refolding lysozyme after its denaturation with 8 M urea and 12 mM dithiothreitol. Compared with the refolding yield of lysozyme alone (14%) and lysozyme with non-imprinted polymers (0%), the maximum refolding yield (90%) was achieved by using 20 mg/mL MIP for 5 mg/mL lysozyme. When cytochrome c was added as a competitor at 3 molar excess to lysozyme, the refolding yield of lysozyme was unchanged. Meanwhile, the cytochrome c-imprinted MIP showed no advantage on lysozyme refolding with respect to lysozyme alone. It was explained that MIP assisted in refolding through the specific binding toward the template protein. Because MIP preferentially bound native protein rather than unfolded one, the capture of refolded protein by MIP would shift the equilibrium from unfolded toward the native form. Moreover, MIP could slightly or partially bind to unfolding protein, thereby facilitating the refolding through “induced-fitting”.

To date, the stabilization study assisted by MIP has already made some breakthrough. Liu et al., 2014, have fabricated surface-imprinted hydrogels on magnetic nanoparticles ( $\text{Fe}_3\text{O}_4$ -MIP-NPs) for DNase I, which have been demonstrated to selectively protect the protein against denaturation induced by heat, UV irradiation, ultrasonication and urea with about 75% activity remaining in all cases. The renaturation assisted by  $\text{Fe}_3\text{O}_4$ -MIP-NPs gained more than 70%, while enzyme alone regained only 15% of its original activity. However, imprinting of a whole protein may lead to the loss of folding during polymerization. Thus, more recently, Bossi and her colleagues prepared an epitope-imprinted MIP-NP for the peptide CC9ox, composed of CGGGHRSKC cyclic, corresponding to an apical portion of the  $\beta$ -hairpin hormone Heparin-25 [Cenci et al., 2016]. The MIP-NP favored the complete folding of the linear random peptide (CC9red) into CC9ox with a highly ordered structure (Fig. 36).

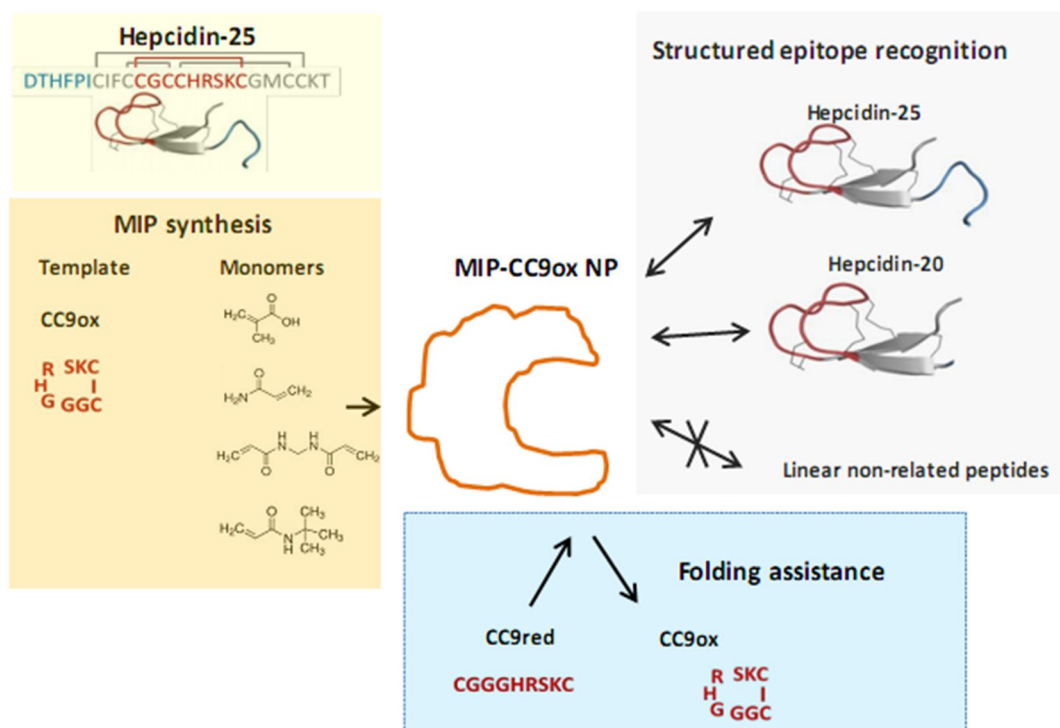


**Figure 36.** Schematic representation of Hepcidin-25 and MIP-NP; the MIP recognizes only the structured template CC9ox and contributes to the folding of CC9red into CC9ox. Reprinted from [Cenci et al., 2016].

Equally important, enzyme inhibition is one of the principles for the control of metabolic reactions and thus for the regulation of biological processes. Therefore, efficient enzyme inhibitors are potential drugs. Till now, only a few reports deal with the applications of MIP as synthetic inhibitor and this has been demonstrated on trypsin. Haupt's group was the first to demonstrate this application [Cutivet et al., 2009]. They incorporated a polymerizable benzamide functional monomer (N-methacryloyl-4-aminobenzamide) into the MIP hydrogel specific for trypsin. The MIP nanoparticles showed competitive inhibition with an inhibition constant  $K_i$  of 79 nM, a more potent inhibitor by almost three orders of magnitude compared to benzamide. Later, Piletsky's group presented a high affinity MIP for trypsin with a  $K_d$  of 0.9 nM, obtained by solid-phase synthesis, which showed mixed inhibition effect on trypsin with  $K_i = 19$  nM [Guerreiro et al., 2014].

### **III-5. Conclusions and perspectives**

In this chapter, a brief overview of the latest different techniques and formats used for molecular imprinting of proteins and the applications of protein-imprinted MIPs was presented. The large variety of new proteins, such as glycoproteins and membrane-bound proteins, often biomarkers of cancer and diseases, that are now being imprinted, as well as the efforts made to detect these minute amounts of proteins in complex samples, shows that the technique of molecular imprinting of biomacromolecules is continuously improving and that protein MIPs are promising candidates for real-life applications.

One of our major areas of interest, which is the subject of this thesis, resides in the obtention of water soluble nanosized MIPs for proteins, that will replace natural antibodies one day. The solid-phase synthesis approach, which provides a new synthetic versatile platform that can offer hydrophilic, high-affinity and selective MIPs seems to be the most promising approach to achieve this goal. The following chapters will deal more in details about this study and the applications of these MIPs for biosensing and in immunoassays.

## References

- Ambrosini, S., Beyazit, S., Haupt, K., & Tse Sum Bui, B. (2013). Solid-phase synthesis of molecularly imprinted nanoparticles for protein recognition. *Chemical Communications*, 49(60), 6746-6748.
- Ashley, J., Shukor, Y., & Tothill, I. E. (2016). The use of differential scanning fluorimetry in the rational design of plastic antibodies for protein targets. *Analyst*, 141(23), 6463-6470.
- Beyazit, S., Tse Sum Bui, B., Haupt, K., & Gonzato, C. (2016). Molecularly imprinted polymer nanomaterials and nanocomposites by controlled/living radical polymerization. *Progress in Polymer Science*, 62, 1-21.
- Bi, X., & Liu, Z. (2014). Facile preparation of glycoprotein-imprinted 96-well microplates for enzyme-linked immunosorbent assay by boronate affinity-based oriented surface imprinting. *Analytical Chemistry*, 86(1), 959-966.
- Bie, Z., Chen, Y., Ye, J., Wang, S., & Liu, Z. (2015). Boronate - affinity glycan - oriented surface imprinting: a new strategy to mimic lectins for the recognition of an intact glycoprotein and its characteristic fragments. *Angewandte Chemie International Edition*, 54(35), 10211-10215.
- Block, H., Maertens, B., Spriestersbach, A., Brinker, N., Kubicek, J., Fabis, R., et al. (2009). Immobilized-metal affinity chromatography (IMAC): a review. *Methods in Enzymology*, 463, 439-473.
- Bossi, A. M., Sharma, P. S., Montana, L., Zoccatelli, G., Laub, O., & Levi, R. (2012). Fingerprint-imprinted polymer: rational selection of peptide epitope templates for the determination of proteins by molecularly imprinted polymers. *Analytical chemistry*, 84(9), 4036-4041.
- Bossi, A., Bonini, F., Turner, A. P. F., & Piletsky, S. A. (2007). Molecularly imprinted polymers for the recognition of proteins: the state of the art. *Biosensors and Bioelectronics*, 22(6),

1131-1137.

Bowen, J. L., Manesiotis, P., & Allender, C. J. (2013). Twenty years since 'antibody mimics' by molecular imprinting were first proposed: A critical perspective. *Molecular Imprinting*, 1, 35-40.

Cáceres, C., Canfarotta, F., Chianella, I., Pereira, E., Moczko, E., Esen, C., et al. (2016). Does size matter? Study of performance of pseudo-ELISAs based on molecularly imprinted polymer nanoparticles prepared for analytes of different sizes. *Analyst*, 141(4), 1405-1412.

Cenci, L., Guella, G., Andreetto, E., Ambrosi, E., Anesi, A., & Bossi, A. M. (2016). Guided folding takes a start from the molecular imprinting of structured epitopes. *Nanoscale*, 8(34), 15665-15670.

Chen, L., Wang, X., Lu, W., Wu, X., & Li, J. (2016). Molecular imprinting: perspectives and applications. *Chemical Society Reviews*, 45(8), 2137-2211.

Chen, L., Xu, S., & Li, J. (2011). Recent advances in molecular imprinting technology: current status, challenges and highlighted applications. *Chemical Society Reviews*, 40(5), 2922-2942.

Chianella, I., Guerreiro, A., Moczko, E., Caygill, J. S., Piletska, E. V., De Vargas Sansalvador, I. M. P., et al. (2013). Direct replacement of antibodies with molecularly imprinted polymer nanoparticles in ELISA - development of a novel assay for vancomycin. *Analytical Chemistry*, 85(17), 8462-8468.

Cutivet, A., Schembri, C., Kovensky, J., & Haupt, K. (2009). Molecularly imprinted microgels as enzyme inhibitors. *Journal of the American Chemical Society*, 131(41), 14699-14702.

Czulak, J., Guerreiro, A., Metran, K., Canfarotta, F., Goddard, A., Cowan, R. H., et al. (2016). Formation of target-specific binding sites in enzymes: solid-phase molecular imprinting of HRP. *Nanoscale*, 8(21), 11060-11066.

Deng, Q., Wu, J., Zhai, X., Fang, G., & Wang, S. (2013). Highly selective fluorescent sensing of proteins based on a fluorescent molecularly imprinted nanosensor. *Sensors*, 13(10),

12994-13004.

Eersels, K., Lieberzeit, P., & Wagner, P. (2016). A review on synthetic receptors for bioparticle detection created by surface-imprinting techniques - from principles to applications. *ACS Sensors*, 1(10), 1171-1187.

Ertürk, G., Özen, H., Tümer, M. A., Mattiasson, B., & Denizli, A. (2016). Microcontact imprinting based surface plasmon resonance (SPR) biosensor for real-time and ultrasensitive detection of prostate specific antigen (PSA) from clinical samples. *Sensors and Actuators B: Chemical*, 224, 823-832.

Guerreiro, A., Poma, A., Karim, K., Moczko, E., Takarada, J., de Vargas - Sansalvador, I. P., et al. (2014). Influence of surface - imprinted nanoparticles on trypsin activity. *Advanced Healthcare Materials*, 3(9), 1426-1429.

Haruki, M., Konnai, Y., Shimada, A., & Takeuchi, H. (2007). Molecularly Imprinted Polymer - Assisted Refolding of Lysozyme. *Biotechnology Progress*, 23(5), 1254-1257.

Haupt, K. (2003). Imprinted polymers—tailor-made mimics of antibodies and receptors. *Chemical Communications*, (2), 171-178.

Haupt, K., Linares, A. V., Bompert, M., & Tse Sum Bui, B. (2012). Molecularly imprinted polymers. *Molecular Imprinting* (pp. 1-28). Springer Berlin Heidelberg.

Hjerten, S., Liao, J. L., Nakazato, K., Wang, Y., Zamaratskaia, G., & Zhang, H. X. (1997). Gels mimicking antibodies in their selective recognition of proteins. *Chromatographia*, 44(5-6), 227-234.

Hoffmann, J. H., Linke, K., Graf, P. C., Lilie, H., & Jakob, U. (2004). Identification of a redox - regulated chaperone network. *The EMBO Journal*, 23(1), 160-168.

Hoshino, Y., Kodama, T., Okahata, Y., & Shea, K. J. (2008). Peptide imprinted polymer nanoparticles: a plastic antibody. *Journal of the American Chemical Society*, 130(46), 15242-15243.

Hoshino, Y., Koide, H., Urakami, T., Kanazawa, H., Kodama, T., Oku, N., & Shea, K. J. (2010). Recognition, neutralization, and clearance of target peptides in the bloodstream of living mice by molecularly imprinted polymer nanoparticles: a plastic antibody. *Journal of the American Chemical Society*, 132(19), 6644-6645.

<http://mainebiotechnology.com/fundamentals-of-immunoassays/>.

Kim, Y. E., Hipp, M. S., Bracher, A., Hayer-Hartl, M., & Ulrich Hartl, F. (2013). Molecular chaperone functions in protein folding and proteostasis. *Annual Review of Biochemistry*, 82, 323-355.

Kivirand, K., Kagan, M. and Rincken, T. (2013). Calibrating biosensors in flow-through set-ups: studies with glucose optrodes, state of the art in biosensors - general aspects, Dr. Toonika Rincken (Ed.), InTech, DOI: 10.5772/54127. Available from: <http://www.intechopen.com/books/state-of-the-art-in-biosensors-general-aspects/calibrating-biosensors-in-flow-through-set-ups-studies-with-glucose-optrodes>

Lee, M. H., Thomas, J. L., Chen, Y. C., Chin, W. T., & Lin, H. Y. (2013). The complete replacement of antibodies by protein-imprinted poly (ethylene-co-vinyl alcohol) in sandwich fluoroimmunoassays. *Microchimica Acta*, 180(15-16), 1393-1399.

Levi, L., & Srebniak, S. (2009). Simulation of protein-imprinted polymers. 1. Imprinted pore properties. *The Journal of Physical Chemistry B*, 114(1), 107-114.

Levi, L., & Srebniak, S. (2010). Simulation of protein-imprinted polymers. 2. Imprinting efficiency. *The Journal of Physical Chemistry B*, 114(50), 16744-16751.

Levi, L., & Srebniak, S. (2011). Simulation of protein-imprinted polymers. 3. Imprinting selectivity. *The Journal of Physical Chemistry B*, 115(49), 14469-14474.

Li, Q., Yang, K., Liang, Y., Jiang, B., Liu, J., Zhang, L., et al. (2014). Surface protein imprinted core-shell particles for high selective lysozyme recognition prepared by reversible addition-fragmentation chain transfer strategy. *ACS Applied Materials & Interfaces*, 6(24), 21954-21960.

Li, Q., Yang, K., Liu, J., Zhang, L., Liang, Z., & Zhang, Y. (2013). Transferrin recognition based on a protein imprinted material prepared by hierarchical imprinting technique. *Microchimica Acta*, 180(15-16), 1379-1386.

Li, Q., Yang, K., Liu, J., Zhang, L., Liang, Z., & Zhang, Y. (2013). Transferrin recognition based on a protein imprinted material prepared by hierarchical imprinting technique. *Microchimica Acta*, 180(15-16), 1379-1386.

Li, S., Cao, S., Whitcombe, M. J., & Piletsky, S. A. (2014). Size matters: challenges in imprinting macromolecules. *Progress in Polymer Science*, 39(1), 145-163.

Li, S., Yang, K., Deng, N., Min, Y., Liu, L., Zhang, L., & Zhang, Y. (2016). Thermoresponsive epitope surface-imprinted nanoparticles for specific capture and release of target protein from human plasma. *ACS Applied Materials & Interfaces*, 8(9), 5747-5751.

Li, S., Yang, K., Zhao, B., Li, X., Liu, L., Chen, Y., et al. (2016). Epitope imprinting enhanced IMAC (EI-IMAC) for highly selective purification of His-tagged protein. *Journal of Materials Chemistry B*, 4(11), 1960-1967.

Li, W., Sun, Y., Yang, C., Yan, X., Guo, H., & Fu, G. (2015). Fabrication of surface protein-imprinted nanoparticles using a metal chelating monomer via aqueous precipitation polymerization. *ACS Applied Materials & Interfaces*, 7(49), 27188-27196.

Li, X., Zhang, B., Tian, L., Li, W., Xin, T., Zhang, H., & Zhang, Q. (2014). Effect of carboxyl density at the core-shell interface of surface-imprinted magnetic trilayer microspheres on recognition properties of proteins. *Sensors and Actuators B: Chemical*, 196, 265-271.

Linares, A.V., Vandeveld, F., Pantigny, J., Falcimaigne-Cordin, A., Haupt, K. (2009) Polymer Films composed of Surface-Bound Nano Filaments with a High Aspect Ratio Molecularly Imprinted with Small Molecules and Proteins. *Advanced Functional Materials* 19, 1-5.

Liu, J., Deng, Q., Tao, D., Yang, K., Zhang, L., Liang, Z., & Zhang, Y. (2014). Preparation of protein imprinted materials by hierarchical imprinting techniques and application in selective depletion of albumin from human serum. *Scientific reports*, 4.

Liu, J., Yin, D., Wang, S., Chen, H. Y., & Liu, Z. (2016). Probing low-copy-number proteins in a single living cell. *Angewandte Chemie International Edition*, 55(42), 13215-13218.

Liu, Y., Fang, S., Zhai, J., & Zhao, M. (2015). Construction of antibody-like nanoparticles for selective protein sequestration in living cells. *Nanoscale*, 7(16), 7162-7167.

Liu, Y., Zhai, J., Dong, J., & Zhao, M. (2014). Magnetic surface imprinted hydrogel nanoparticles for specific and reversible stabilization of proteins. *Molecular Imprinting*, 2(1).

Luo, J., Jiang, S., & Liu, X. (2014). Electrochemical sensor for bovine hemoglobin based on a novel graphene-molecular imprinted polymers composite as recognition element. *Sensors and Actuators B: Chemical*, 203, 782-789.

Ma, R. T., Ha, W., Chen, J., & Shi, Y. P. (2016). Highly dispersed magnetic molecularly imprinted nanoparticles with well-defined thin film for the selective extraction of glycoprotein. *Journal of Materials Chemistry B*, 4(15), 2620-2627.

Menger, M., Yarman, A., Erdössy, J., Yildiz, H. B., Gyurcsányi, R. E., & Scheller, F. W. (2016). MIPs and aptamers for recognition of proteins in biomimetic sensing. *Biosensors*, 6(3), 35.

*Molecular Imprinting*. Retrieved 13 Mar. 2017, from <http://www.degruyter.com/view/j/molim>

Muzyka, K., Karim, K., Guerreiro, A., Poma, A., & Piletsky, S. (2014). Optimisation of the synthesis of vancomycin-selective molecularly imprinted polymer nanoparticles using automatic photoreactor. *Nanoscale Research Letters*, 9(1), 1.

Nematollahzadeh, A., Shojaei, A., Abdekhodaie, M. J., & Sellergren, B. (2013). Molecularly imprinted polydopamine nano-layer on the pore surface of porous particles for protein capture in HPLC column. *Journal of Colloid and Interface Science*, 404, 117-126.

Nishino, H., Huang, C. S., & Shea, K. J. (2006). Selective protein capture by epitope imprinting. *Angewandte Chemie International Edition*, 45(15), 2392-2396.

Piletsky, S. A., Piletska, E. V., Chen, B., Karim, K., Weston, D., Barrett, G., et al. (2000).

Chemical grafting of molecularly imprinted homopolymers to the surface of microplates. Application of artificial adrenergic receptor in enzyme-linked assay for  $\beta$ -agonists determination. *Analytical Chemistry*, 72(18), 4381-4385.

Poma, A., Guerreiro, A., Caygill, S., Moczko, E., & Piletsky, S. (2013). Automatic reactor for solid-phase synthesis of molecularly imprinted polymeric nanoparticles (MIP NPs) in water. *RSC Advances*, 4(8), 4203-4206.

Poma, A., Guerreiro, A., Whitcombe, M. J., Piletska, E. V., Turner, A. P., & Piletsky, S. A. (2013). Solid - phase synthesis of molecularly imprinted polymer nanoparticles with a reusable template—"plastic antibodies". *Advanced Functional Materials*, 23(22), 2821-2827.

Porath, J. (1988). IMAC—Immobilized metal ion affinity based chromatography. *TrAC Trends in Analytical Chemistry*, 7(7), 254-259.

Qin, Y. P., Li, D. Y., He, X. W., Li, W. Y., & Zhang, Y. K. (2016). Preparation of high-efficiency cytochrome c-imprinted polymer on the surface of magnetic carbon nanotubes by epitope approach via metal chelation and six-membered ring. *ACS Applied Materials & Interfaces*, 8(16), 10155-10163.

Qu, X., Wang, F., Sun, Y., Tian, Y., Chen, R., Ma, X., & Liu, C. (2016). Selective extraction of bioactive glycoprotein in neutral environment through Concanavalin A mediated template immobilization and dopamine surface imprinting. *RSC Advances*, 6(89), 86455-86463.

Rachkov, A., & Minoura, N. (2001). Towards molecularly imprinted polymers selective to peptides and proteins. The epitope approach. *Biochimica et Biophysica Acta (BBA)-Protein Structure and Molecular Enzymology*, 1544(1), 255-266.

Reddy, S. M., Phan, Q. T., El-Sharif, H., Govada, L., Stevenson, D., & Chayen, N. E. (2012). Protein crystallization and biosensor applications of hydrogel-based molecularly imprinted polymers. *Biomacromolecules*, 13(12), 3959-3965.

Rutnakornpituk, M., Meerod, S., Boontha, B., & Wichai, U. (2009). Magnetic core-bilayer shell nanoparticle: a novel vehicle for entrapment of poorly water-soluble

drugs. *Polymer*, 50(15), 3508-3515.

Saridakis, E., & Chayen, N. E. (2013). Imprinted polymers assisting protein crystallization. *Trends in Biotechnology*, 31(9), 515-520.

Saridakis, E., Khurshid, S., Govada, L., Phan, Q., Hawkins, D., Crichlow, G. V., et al. (2011). Protein crystallization facilitated by molecularly imprinted polymers. *Proceedings of the National Academy of Sciences*, 108(27), 11081-11086.

Sato, T., Tsuji, S., & Kawagauchi, H. (2008). Preparation of functional nanoparticles by assembling block copolymers formed by living radical polymerization. *Industrial & Engineering Chemistry Research*, 47(17), 6358-6361.

Shea, K. J., & Sasaki, D. Y. (1991). An analysis of small-molecule binding to functionalized synthetic polymers by <sup>13</sup>C CP/MAS NMR and FT-IR spectroscopy. *Journal of the American Chemical Society*, 113(11), 4109-4120.

Shen, X., Ma, Y., Zeng, Q., Tao, J., Huang, J., & Wang, L. (2016). Molecularly imprinted electrochemical sensor for advanced diagnosis of alpha-fetoprotein. *Analytical Methods*, 8(40), 7361-7368.

Shi, H., Tsai, W. B., Garrison, M. D., Ferrari, S., & Ratner, B. D. (1999). Template-imprinted nanostructured surfaces for protein recognition. *Nature*, 398(6728), 593-597.

Soleimani, M., Ghaderi, S., Afshar, M. G., & Soleimani, S. (2012). Synthesis of molecularly imprinted polymer as a sorbent for solid phase extraction of bovine albumin from whey, milk, urine and serum. *Microchemical Journal*, 100, 1-7.

Sunayama, H., Ooya, T., & Takeuchi, T. (2014). Fluorescent protein-imprinted polymers capable of signal transduction of specific binding events prepared by a site-directed two-step post-imprinting modification. *Chemical Communications*, 50(11), 1347-1349.

Surugiu, I., Ye, L., Yilmaz, E., Dzugoev, A., Danielsson, B., Mosbach, K., & Haupt, K. (2000). An enzyme-linked molecularly imprinted sorbent assay. *Analyst*, 125(1), 13-16.

Takeuchi, T., & Hishiya, T. (2008). Molecular imprinting of proteins emerging as a tool for protein recognition. *Organic & Biomolecular Chemistry*, 6(14), 2459-2467.

Tamahkar, E., Kutsal, T., & Denizli, A. (2015). Surface imprinted bacterial cellulose nanofibers for cytochrome c purification. *Process Biochemistry*, 50(12), 2289-2297.

Ton, X. A., Acha, V., Bonomi, P., Tse Sum Bui, B., & Haupt, K. (2015). A disposable evanescent wave fiber optic sensor coated with a molecularly imprinted polymer as a selective fluorescence probe. *Biosensors and Bioelectronics*, 64, 359-366.

Tsuji, S., & Kawaguchi, H. (2006). Effect of graft chain length and structure design on temperature-sensitive hairy particles. *Macromolecules*, 39(13), 4338-4344.

Verheyen, E., Schillemans, J. P., van Wijk, M., Demeniex, M. A., Hennink, W. E., & van Nostrum, C. F. (2011). Challenges for the effective molecular imprinting of proteins. *Biomaterials*, 32(11), 3008-3020.

Wackerlig, J., & Lieberzeit, P. A. (2015). Molecularly imprinted polymer nanoparticles in chemical sensing—Synthesis, characterisation and application. *Sensors and Actuators B: Chemical*, 207, 144-157.

Whitcombe, M. J., Rodriguez, M. E., Villar, P., & Vulfson, E. N. (1995). A new method for the introduction of recognition site functionality into polymers prepared by molecular imprinting—synthesis and characterization of polymeric receptors for cholesterol. *Journal of the American Chemical Society*, 117(27), 7105-7111.

Wu, G., Li, J., Qu, X., Zhang, Y., Hong, H., & Liu, C. (2015). Template size matched film thickness for effectively in situ surface imprinting: a model study of glycoprotein imprints. *RSC Advances*, 5(58), 47010-47021.

Wulff, G., & Haarer, J. (1991). Enzyme - analogue built polymers, 29. The preparation of defined chiral cavities for the racemic resolution of free sugars. *Macromolecular Chemistry and Physics*, 192(6), 1329-1338.

Wulff, G., & Schulze, I. (1978). Directed cooperativity and site separation of mercapto groups in synthetic polymers. *Angewandte Chemie International Edition in English*, 17(7), 537-538.

Wulff, G., Heide, B., & Helfmeier, G. (1986). Enzyme-analog built polymers. 20. Molecular recognition through the exact placement of functional groups on rigid matrixes via a template approach. *Journal of the American Chemical Society*, 108(5), 1089-1091.

Yang, H. H., Lu, K. H., Lin, Y. F., Tsai, S. H., Chakraborty, S., Zhai, W. J., & Tai, D. F. (2013). Depletion of albumin and immunoglobulin G from human serum using epitope - imprinted polymers as artificial antibodies. *Journal of Biomedical Materials Research Part A*, 101(7), 1935-1942.

Yang, H., Guo, T. Y., & Zhou, D. (2011). Surface hydrophilic modification with well-defined glycopolymer for protein imprinting matrix. *International Journal of Biological Macromolecules*, 48(3), 432-438.

Yang, K., Li, S., Liu, J., Liu, L., Zhang, L., & Zhang, Y. (2016). Multi-epitope templates imprinted particles for the simultaneous capture of various target proteins. *Analytical Chemistry*, 88(11), 5621-5625.

Yang, K., Liu, J., Li, S., Li, Q., Wu, Q., Zhou, Y., et al. (2014). Epitope imprinted polyethersulfone beads by self-assembly for target protein capture from the plasma proteome. *Chemical Communications*, 50(67), 9521-9524.

Yang, Y. Q., He, X. W., Wang, Y. Z., Li, W. Y., & Zhang, Y. K. (2014). Epitope imprinted polymer coating CdTe quantum dots for specific recognition and direct fluorescent quantification of the target protein bovine serum albumin. *Biosensors and Bioelectronics*, 54, 266-272.

Yilmaz, E., Haupt, K., & Mosbach, K. (2000). The use of immobilized templates—A new approach in molecular imprinting. *Angewandte Chemie International Edition*, 39(12), 2115-2118.

Yin, D., & Ulbricht, M. (2013). Protein-selective adsorbers by molecular imprinting via a

novel two-step surface grafting method. *Journal of Materials Chemistry B*, 1(25), 3209-3219.

Young, C. L., Britton, Z. T., & Robinson, A. S. (2012). Recombinant protein expression and purification: a comprehensive review of affinity tags and microbial applications. *Biotechnology Journal*, 7(5), 620-634.

Zhang, H. (2014). Recent advances in macromolecularly imprinted polymers by controlled radical polymerization techniques. *Molecular Imprinting*, 2(1).

Zhang, W., Liu, W., Li, P., Xiao, H., Wang, H., & Tang, B. (2014). A fluorescence nanosensor for glycoproteins with activity based on the molecularly imprinted spatial structure of the target and boronate affinity. *Angewandte Chemie*, 126(46), 12697-12701.

Zhang, Y., Deng, C., Liu, S., Wu, J., Chen, Z., Li, C., & Lu, W. (2015). Active targeting of tumors through conformational epitope imprinting. *Angewandte Chemie International Edition*, 54(17), 5157-5160.

Zhou, J., Gan, N., Hu, F., Li, T., Zhou, H., Li, X., & Zheng, L. (2013). A single antibody sandwich electrochemiluminescence immunosensor based on protein magnetic molecularly imprinted polymers mimicking capture probes. *Sensors and Actuators B: Chemical*, 186, 300-307.

# Chapter 2

---

Solid-phase synthesis of molecularly imprinted polymer nanoparticles as antibody mimics for protein recognition

## Summary

Ever since Klaus Mosbach's publication in Nature in 1993 [Vlatakis et al., 1993], where for the first time, MIPs were referred to as 'antibody mimics', researchers have endeavored to fabricate MIPs that can mimic as closely as possible natural antibodies, such as their water solubility, size and monoclonality (homogeneous binding site). One of the most elegant examples tending towards this goal was developed in Kenneth Shea's group and was applied for the first time *in vivo* [Hoshino et al., 2010]. They prepared water soluble MIP-NPs against a peptide, melittin, via aqueous precipitation polymerization in the presence of a surfactant, sodium dodecyl sulfate (SDS). The resulting nanosized MIP had binding affinity ( $K_{dapp} < \text{nM}$ ) comparable to that of a natural antibody. Remarkably it could capture and remove the peptide from the bloodstream of living mice. However, the obtention of their MIPs was quite complex and time-consuming since removal of SDS took several days by dialysis and usually can never be complete, which might be a problem, due to its toxicity, for biological applications in humans. One of the solutions to overcome this drawback is to employ a solid-phase synthesis approach combined with surfactant-free precipitation polymerization in a dilute medium. Herein, we demonstrate the preparation of aqueous, stable (no aggregation at 8 °C for a period of 6 months), nanosized (70 – 109 nm) MIPs for trypsin and kallikrein (among others), with high affinity (apparent dissociation constants  $K_{dapp} = 0.02 - 2 \text{ nM}$ ). The solid-phase support consists of glass beads (GBs) functionalized with two affinity ligands of the enzymes, the competitive inhibitor *p*-aminobenzamidine (Figure A) or a  $\text{Cu}^{2+}$ -chelate (Figure B), so as to orientate the immobilization of the enzymes via their active site or via their surface histidine residues, respectively.

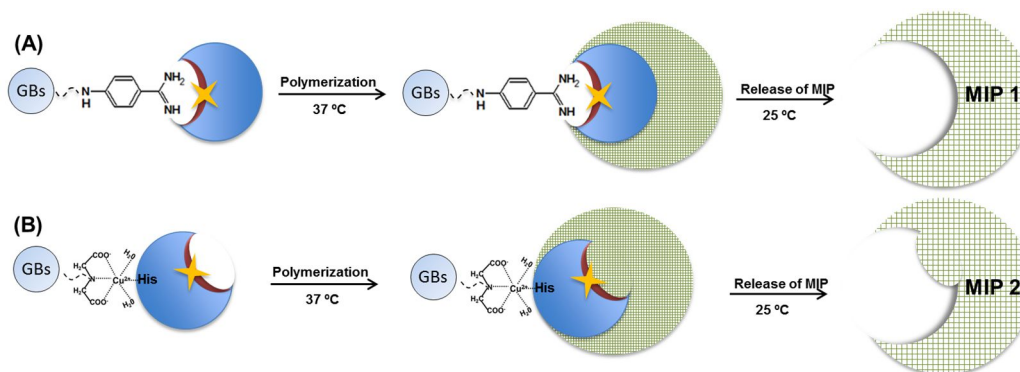


**Figure.** Synthesis of MIP-NPs. (A) *p*-aminobenzamidine is immobilized on glass-beads (GBs) to attract the enzyme via its active site, represented by a star; (B) Cu<sup>2+</sup>-chelate is immobilized on GBs to attract the enzyme via its surface histidine(s), leaving its active site free. This orientated conformation of the enzyme will in turn yield MIP-NPs interacting with different locations of the enzyme and is reflected by the different affinity constants.

Thermoresponsive MIP nanoparticles (MIP-NPs) were then synthesized around the immobilized enzyme. The MIP-NPs were released by a simple temperature change, resulting in protein-free polymers endowed with improved binding site homogeneity since all the binding sites have the same orientation. This study is presented in Publication 1. In addition, we applied these polymers, as synthetic chaperones, to protect their target proteins from high temperature and pH denaturation (Results presented in publication 2).

## References

- Hoshino, Y., Koide, H., Urakami, T., Kanazawa, H., Kodama, T., Oku, N., & Shea, K. J. (2010). Recognition, neutralization, and clearance of target peptides in the bloodstream of living mice by molecularly imprinted polymer nanoparticles: a plastic antibody. *Journal of the American Chemical Society*, 132(19), 6644-6645.
- Vlatakis, G., Andersson, L. I., Müller, R., & Mosbach, K. (1993). Drug assay using antibody mimics made by molecular imprinting. *Nature*, 361(6413), 645-647.

## Publication 1

### **Toward a universal method for preparing molecularly imprinted polymer nanoparticles with antibody-like affinity for proteins**

Jingjing Xu,<sup>†</sup> Serena Ambrosini,<sup>†</sup> Emel Tamahkar,<sup>§</sup> Claire Rossi,<sup>†</sup> Karsten Haupt,<sup>\*,†</sup> and Bernadette Tse Sum Bui<sup>\*,†</sup>

<sup>†</sup> Sorbonne Universités, Université de Technologie de Compiègne, CNRS Enzyme and Cell Engineering Laboratory, Rue Roger Couitolenc, CS 60319, 60203 Compiègne Cedex, France

<sup>§</sup> Hitit University, Faculty of Engineering, Department of Chemical Engineering, 19030 Çorum, Turkey

*Corresponding Authors*

*\*E-mail: [jeanne.tse-sum-bui@utc.fr](mailto:jeanne.tse-sum-bui@utc.fr); Fax: (+) 33 3 44203910; Tel: (+) 33 3 44234402*

*\*E-mail: [karsten.haupt@utc.fr](mailto:karsten.haupt@utc.fr)*

# Toward a Universal Method for Preparing Molecularly Imprinted Polymer Nanoparticles with Antibody-like Affinity for Proteins

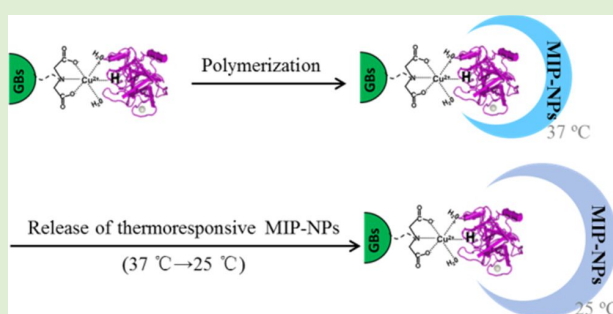
Jingjing Xu,<sup>†</sup> Serena Ambrosini,<sup>†</sup> Emel Tamahkar,<sup>§</sup> Claire Rossi,<sup>†</sup> Karsten Haupt,<sup>\*,†</sup> and Bernadette Tse Sum Bui<sup>\*,†</sup>

<sup>†</sup>Sorbonne Universités, Université de Technologie de Compiègne, CNRS Enzyme and Cell Engineering Laboratory, Rue Roger Coultolenc, CS 60319, 60203 Compiègne Cedex, France

<sup>§</sup>Hittit University, Faculty of Engineering, Department of Chemical Engineering, 19030 Çorum, Turkey

## Supporting Information

**ABSTRACT:** We describe a potentially universal, simple and cheap method to prepare water-compatible molecularly imprinted polymer nanoparticles (MIP-NPs) as synthetic antibodies against proteins. The strategy is based on a solid phase synthesis approach where glass beads (GBs) are functionalized with a metal chelate, acting as a general affinity ligand to attract surface-bound histidines present on proteins. This configuration enables an oriented immobilization of the proteins, upon which thermoresponsive MIP-NPs are synthesized. The GBs play the role of both a reactor and a separation column since, after synthesis, the MIP-NPs are released from the support by a simple temperature change, resulting in protein-free polymers. The resulting MIP-NPs are endowed with improved binding site homogeneity, since the binding sites have the same orientation. Moreover, they are stable (no aggregation) in a buffer solution for prolonged storage time and exhibit apparent dissociation constants in the nanomolar range, with little or no cross-reactivity toward other proteins.



## INTRODUCTION

The world's diagnostics market, worth \$46 billion in 2011 and expected to reach ~\$74 billion in 2018,<sup>1</sup> relies mainly on highly specific antibodies targeted toward a large variety of chemical and biological molecules. Despite their relevance, they suffer from poor thermal and pH stability, short storage lifetime, high cost, and, particularly, their production from animals is of concern.<sup>2</sup> A viable alternative would be the use of water-compatible nanosized molecularly imprinted polymers (MIPs), endowed with high affinity ( $K_d \sim$  nM) for their target molecules.<sup>3–7</sup> MIPs, commonly dubbed “plastic antibodies” are synthesized by the copolymerization of functional monomers and cross-linker around a template molecule.<sup>2–8</sup> The template molecule can be the target analyte or a derivative thereof. Removal of the template leaves cavities complementary in shape, size, and functional groups orientation in the polymer network, which are able to rebind the template molecule with high affinities and selectivities. MIPs have considerable advantages over antibodies as they possess a higher chemical, physical, and thermal stability, ease of obtention, and low cost. While molecular imprinting of small molecules is now considered a routine, the imprinting of proteins still remains a challenge.<sup>9–12</sup> This is mainly due to their complex structure in their native conformation that has to be preserved during the polymerization process. Furthermore, the generation of selective imprinted cavities is extremely difficult due to the multitude of functional sites and their large size hampers their

extraction so that permanent entrapment of template is often encountered.

However, as we previously demonstrated with the template trypsin,<sup>13</sup> if the template can be preoriented in a fixed position by using an anchoring monomer containing its affinity ligand, for instance, the competitive inhibitor *p*-aminobenzamidine (PAB), the polymerization can be confined to the close proximity of the recognition site of the protein.<sup>14,15</sup> Subsequently, we have used PAB to orientate the immobilization of the trypsin template on GBs as solid support before imprinting.<sup>16</sup> Instead of directly attaching the protein to the support by a covalent bond,<sup>17</sup> this oriented approach will generate MIP nanoparticles (NPs) with binding sites having the same orientation, located at the surface of the particle. Thus, the MIP-NPs will not only have binding sites easily accessible for the protein, but will also be associated with an improved binding site homogeneity. A thermoresponsive monomer, *N*-isopropylacrylamide (NIPAm), was included in the polymerization mixture so that the synthesized MIPs could be released from the solid phase by a simple temperature change, resulting in template-free polymers (Figure 1).

In this work, in order to make the solid-phase synthesis approach more generic and versatile, metal chelates were used

**Received:** October 29, 2015

**Revised:** December 3, 2015

**Published:** December 7, 2015

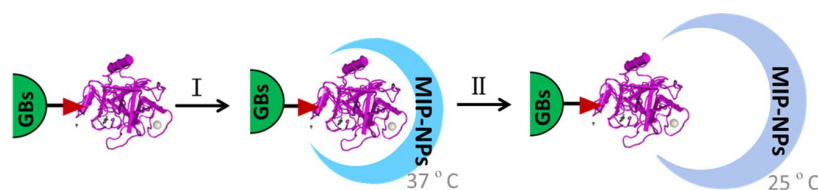


**Figure 1.** Schematic representation of the solid-phase synthesis of MIP-NPs. I: Polymerization; II: Release of thermoresponsive MIP-NPs (temperature change from 37 °C to room temperature, 25 °C).

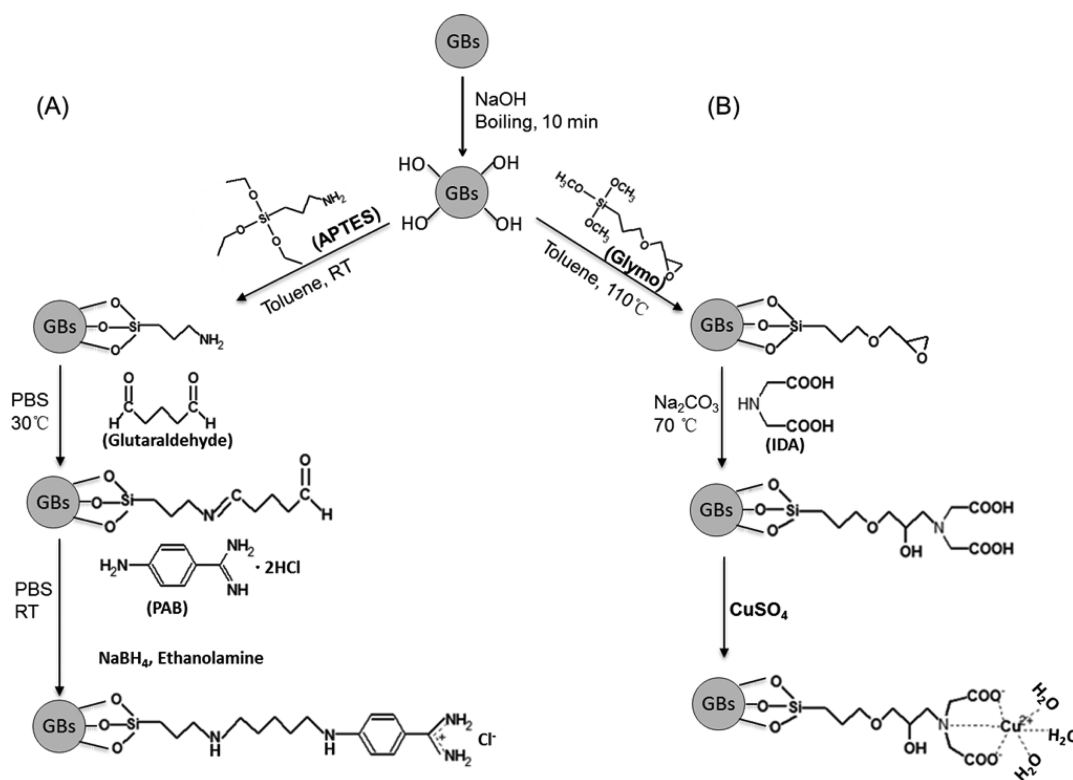


**Figure 2.** Immobilization of the affinity ligands (A) *p*-aminobenzamidine (PAB) and (B) IDA-Cu<sup>2+</sup> on glass beads (GBs).

as affinity ligands to fix the orientation of the proteins.<sup>18,19</sup> Immobilized metal chelates are routinely employed in academia and industries as small and large-scale affinity chromatographic sorbents for the isolation of proteins containing histidines on their surface or bearing a His tag (for recombinant proteins).<sup>20,21</sup> Thus, using a metal chelate as a general affinity ligand will enable the immobilization of almost any protein with histidine groups on its surface or recombinant proteins bearing a His-Tag. To validate our concept, trypsin, kallikrein and ribonuclease A (RNase A) were chosen. These proteins have been described in the literature to be retained on an immobilized metal ion affinity chromatography (IMAC) column.<sup>22–24</sup> Proteins were adsorbed on Cu<sup>2+</sup> immobilized on GBs via a chelating agent, iminodiacetic acid (IDA) (Figure 2B). Additionally, kallikrein and trypsin were immobilized on PAB (Figure 2A), in order to compare between the MIP-NPs obtained using the two different affinity ligands. Trypsin has already been described previously to demonstrate our solid-phase strategy,<sup>16</sup> here we confirm the versatility of immobilized PAB for imprinting another serine protease, kallikrein.<sup>25</sup> Recently, kallikreins and kallikrein-related peptidases have come into clinical highlights because they are involved in a

broad array of pathophysiological processes such as cardiovascular disorders, diabetes and skin diseases. In particular, they are correlated with cancer initiation and progression and are biomarkers for prostate and ovary cancer diagnosis.<sup>26–28</sup> Water-compatible MIP-NPs selective for these target proteins were synthesized on the GBs that play the role of a reactor and an affinity purification column simultaneously. The physicochemical properties and binding characteristics of the MIP-NPs were examined. MIP-NPs exhibit strong affinities for their respective template proteins comparable to those of natural antibodies, with partial or no cross-reactivities toward other proteins.

## EXPERIMENTAL SECTION

**Materials.** All chemicals and solvents were of analytical grade and purchased from VWR International (Fontenay sous Bois, France) or Sigma-Aldrich (St Quentin Fallavier, France), unless otherwise stated. The proteins: trypsin from bovine pancreas (specific activity: > 10 000 units/mg protein), kallikrein from porcine pancreas (specific activity: 40 units/mg protein), thrombin from bovine plasma, RNase from bovine pancreas, cytochrome c from horse heart, myoglobin from equine skeletal muscle, and human hemoglobin were purchased from Sigma-Aldrich. Glass beads (GBs) of diameter 0.1 mm, were obtained from Roth Sochiel E.U.R.L (Lauterbourg, France). Buffers were

prepared with Milli-Q water, purified using a Milli-Q system (Millipore, Molsheim, France).

**Functionalization of GBs.** Before functionalization, GBs were activated by boiling in 4 M NaOH (typically 100 g of GBs in 100 mL of NaOH), for 10 min. The activated GBs were then washed with water and acetone and then dried in an oven at 50 °C.

**IDA-Cu<sup>2+</sup> Functionalized GBs.** First, (3-glycidyloxypropyl)-trimethoxysilane (Glymo) was introduced on the GBs, as reported.<sup>29</sup> Briefly, 50 g of activated GBs were added to a mixture of 100 mL anhydrous toluene and 100 mL Glymo in a round-bottom flask and refluxed at 110 °C for 17 h. The Glymo-coupled glass beads (Glymo-GBs) were collected and washed three times with toluene and acetone. After drying in an oven at 50 °C, the Glymo-GBs were immersed into 500 mL of a 0.75 M IDA solution (containing 0.34 M NaCl and 2.0 M Na<sub>2</sub>CO<sub>3</sub>, pH 11.0) and stirred at 70 °C for 17 h. The final GBs were obtained after washing five times with water.

**p-Aminobenzamidine-Functionalized GBs.** GBs were functionalized as previously described.<sup>16,30</sup> Briefly, 100 g of activated GBs were incubated in 2% (v/v) (3-aminopropyl)triethoxysilane (APTES) in toluene, with shaking overnight at room temperature. After silanization, the GBs were rinsed with toluene, acetone, and dried. The silanized GBs were incubated in a 5% (v/v) glutaraldehyde solution in 0.1 M sodium phosphate buffer +0.15 M NaCl, pH 7.4 (PBS buffer). After shaking at 30 °C for 12 h, the GBs were washed with water. The glutaraldehyde-activated glass beads were dispersed in a 0.1 M PAB solution in PBS buffer and incubated at room temperature for 5 h. Then the PAB-GBs were washed with PBS buffer and immersed in 1 mg/mL solution of NaBH<sub>4</sub> in PBS buffer for 30 min at room temperature. The unreacted carbonyl groups were blocked by incubation in 40 mM ethanolamine for 30 min. Finally, the obtained PAB-GBs were washed with PBS buffer and water and stored at 8 °C in 1 M NaCl containing 20% ethanol until use.

The structural integrity of the GBs after activation and different derivatization processes was verified by scanning electron microscopy (SEM) analysis (Supporting Information Figure S1).

**Characterization of Functionalized GBs.** IDA-Cu<sup>2+</sup>-Functionalized GBs. Evidence that metal chelates are formed when CuSO<sub>4</sub> is added to IDA-GBs was investigated by incubating 1 g of IDA-GBs with 5 mL of CuSO<sub>4</sub> solution at various concentrations (5–100 mM) overnight, then washed with 5 mL water five times to remove unbound Cu<sup>2+</sup> (Figure S2B). Bound Cu<sup>2+</sup> was desorbed by adding 5 mL of 50 mM ethylene diamine tetraacetic acid (EDTA) solution for 1 h. The amount of Cu<sup>2+</sup>-EDTA complex was determined by measuring the absorbance at 733 nm.<sup>31</sup> The calibration curve (Figure S2A), prepared by mixing 50 mM EDTA to CuSO<sub>4</sub> (1–15 mM) solutions in a final volume of 1 mL, was used for quantification.

To determine the amount of protein bound on Cu<sup>2+</sup>-chelate, 1 g of IDA-GBs was incubated with 5 mL of 50 mM CuSO<sub>4</sub> solution (saturating concentration, Figure S2B) overnight, washed with 5 mL of water five times followed by 5 mL of 25 mM sodium phosphate buffer pH 7.0, (buffer A), three times. The Cu<sup>2+</sup>-IDA-GBs were then incubated with 1 mL of 1 mg/mL protein for 1 h. The amount of unbound protein was determined on the supernatant by the method of Bradford, using bovine serum albumin (BSA) as the standard (Figure S3). Bound protein was calculated by subtracting the amount of the unbound protein from the total amount of protein added to the mixture.

**p-Aminobenzamidine-Functionalized GBs.** After silanization, the amino groups available on the silanized glass bead surface were determined using a colorimetric assay with the anionic dye Orange II.<sup>16</sup> The affinity of PAB-GBs for trypsin and kallikrein was evaluated by incubating 150 mg of PAB-GBs in 1 mL trypsin or kallikrein solution (0.5 mg/mL) in buffer A, at room temperature for 30 min. This amount of trypsin is in excess with respect to the amount of amino groups determined on the surface of the glass beads. After removing the supernatant, the functionalized glass beads were washed with buffer A to remove the unbound trypsin, and incubated in 1 mL of 10 mM HCl + 0.5 M NaCl solution for 10 min to desorb bound trypsin. In the case of kallikrein, 8 μL of 1 M Tris-HCl buffer, pH 9.0 was added after incubation to prevent its denaturation under acidic

conditions. The supernatant was collected and subjected to enzyme activity assay with *N*<sub>α</sub>-*p*-tosyl-L-arginine methyl ester hydrochloride (TAME) or *N*<sub>ε</sub>-benzoyl-L-arginine ethyl ester hydrochloride (BAEE) to quantify the bound trypsin and kallikrein, respectively. The calibration curve in Figure S4 was used for quantification.

**Enzymatic Activity Assays.** Trypsin and kallikrein enzymatic activity measurements were done spectrophotometrically on a CARY60 UV–vis spectrophotometer (Agilent Technologies). Molecular weights of trypsin and kallikrein taken to prepare the stock solutions were 23.8 kDa and 25.6 kDa, respectively.

A stock solution of trypsin (1 μM) was prepared in 1 mM HCl + 10 mM CaCl<sub>2</sub> and stored in ice. Trypsin activity assay was carried out at 25 °C with TAME as the substrate. In a quartz cuvette was added 50 mM Tris-HCl pH 8.0 and 50 μL of 10 mM TAME (final concentration: 500 μM). The reaction was initiated by the addition of 10 to 100 μL trypsin (final concentration: 10 to 100 nM). The final reaction mixture was 1 mL. After mixing, the hydrolysis of TAME was monitored by the change in absorbance at 247 nm for 1.5 min. A calibration curve for trypsin is shown in Figure S4A.

A stock solution of kallikrein (2 μM) was prepared in water. Kallikrein activity assay was carried out at 25 °C with BAEE as substrate in a reaction mixture (1 mL) containing 50 mM Tris-HCl pH 8.7, 50 μL of 10 mM BAEE (final concentration: 500 μM), the reaction being initiated by the addition of 10 to 100 μL kallikrein (final concentration: 20 to 200 nM). After mixing, the hydrolysis of BAEE was monitored by the change in absorbance at 253 nm for 5 min. A calibration curve for kallikrein activity is shown in Figure S4B.

**Solid-Phase Synthesis of MIP-NPs for Proteins.** The solid-phase synthesis of MIP-NPs was carried out in a glass column equipped with a thermostated jacket (XK 26/40, GE Healthcare, Fontenay sous Bois, France), connected to a circulation thermostated water-bath (Bioblock Scientific polystat 5, Fischer Scientific, France). The solvents were pumped through the column using a peristaltic pump at a flow rate of 2.5 mL/min (1.2 mL/min during protein loading).

**IDA-Cu<sup>2+</sup>-Functionalized GBs.** The column was packed with 50 g functionalized IDA-GBs, corresponding to a bed height of 5.5 cm and washed with 100 mL water. Then 250 mL of 50 mM CuSO<sub>4</sub> was loaded on the column, and unbound Cu<sup>2+</sup> was removed by passing 150 mL water and 150 mL of buffer A. The column was further equilibrated with buffer A prior to the loading of protein. Afterward, 50 mL of a solution of the target protein (1 mg/mL) was percolated through the column. The flow-through was collected and passed through the column again for 1 h. Excess protein was removed by passing 250 mL buffer A.

The polymerization mixture was prepared by mixing NIPAm (246.2 mg) and EbAm (19.2 mg) (95/5 molar ratio) in 53 mL of buffer A so that the total monomer concentration is 0.5% (w/w). The solution was purged with nitrogen for 30 min. Afterward, the initiation couple composed of potassium persulfate (KPS) (18.5 mg in 500 μL buffer A) and *N,N,N',N'*-tetramethylethylenediamine (TEMED) (1.35 μL) (the amount of KPS was 3% mol/mol with respect to polymerizable double bonds) were added to the reaction mixture. The latter was percolated through the reactor, and the temperature was set at 37 °C for 15 h (overnight). The column was then washed with 250 mL (5 × 50 mL) of buffer A at 37 °C, and the MIP-NPs were eluted with 15 mL portions (6 times) of buffer A at room temperature (~25 °C).

**p-Aminobenzamidine-Functionalized GBs.** Ninety-five grams of GBs, corresponding to a bed height of 10 cm, were packed in the column, washed with 100 mL water, and equilibrated in 200 mL of buffer A. Then 25 mL of a solution of trypsin or kallikrein (0.5 mg/mL) was percolated through the column. The flow-through was collected and passed through the column again for 1 h. Excess protein was removed by passing 300 mL buffer A. The MIP was synthesized and recovered as described for the metal-chelate GBs.

All eluted fractions were subjected to enzymatic activity assay and Bradford assay so as to check for eventual leakage of the protein template. The eluted fractions from the metal-chelate column was additionally checked for the presence of Cu<sup>2+</sup> by using the calibration curve in Figure S2A.

Table 1. Characteristics of MIP-NPs

entry <sup>a</sup>	MIP-NPs	yield (mg/g GBs)	size (nm)	polydispersity index	dissociation constant ( $K_{dapp}$ )
1	trypsin	0.32 ± 0.02	119 ± 5	0.278	1.9 × 10 <sup>-11</sup>
2	kallikrein	0.36 ± 0.04	97 ± 3	0.319	4.9 × 10 <sup>-11</sup>
3	trypsin	0.45 ± 0.03	70 ± 6	0.284	2.1 × 10 <sup>-9</sup>
4	kallikrein	0.65 ± 0.03	106 ± 5	0.395	2.6 × 10 <sup>-10</sup>
5	RNase	0.58 ± 0.02	78 ± 6	0.289	7.5 × 10 <sup>-10</sup>

<sup>a</sup>MIPs obtained on PAB (entries 1 and 2) and metal-chelate (entries 3–5), as affinity ligands.

DLS analysis was performed on all eluted fractions, and MIPs having similar sizes and dispersities were pooled. In order to determine the amount of MIP-NPs produced, 2 mL of the pooled fraction was centrifuged at 40 000g for 1 h at 37 °C so as to precipitate the polymer NPs. After discarding the supernatant, the precipitate was resuspended in water and lyophilized. The dry MIP-NPs were weighed; this allows one to determine the concentration of the MIP-NPs (mg/mL) and the yield of polymerization, calculated as milligrams of MIP-NPs per gram of GBs.

**Particle Size Determination.** The hydrodynamic size of the MIP-NPs was measured directly on the eluate fractions from the column by dynamic light scattering (DLS) at 25 °C (unless specified), using a Zeta-sizer NanoZS (Malvern Instruments Ltd., Worcestershire, UK). MIPs having similar sizes and dispersities were pooled to constitute our stock of working MIP-NPs.

For scanning electron microscopy imaging, an aliquot of the pooled fraction was dialyzed overnight against Milli Q water. SEM imaging was carried out on a Quanta FEG 250 scanning electron microscope (Eindhoven, Netherlands). Polymer particles were sputter coated with gold prior to the SEM measurement.

**Binding Experiments of MIP-NPs by Piezoelectric Microgravimetry.** A quartz crystal microbalance (QCM) was employed to evaluate the recognition properties of the MIP-NPs. All measurements were performed with a Q-Sense E1 instrument (Biolin Scientific, Sweden) in a flow-through mode using a peristaltic pump (flow rate: 50 μL/min). The functionalization of the QCM crystal (with IDA-Cu<sup>2+</sup> or PAB and further immobilization of the protein) was carried out at 25 °C, whereas the binding experiments with the MIP-NPs were performed at 37 °C (unless specified).

Silicon dioxide-coated crystals (QSX 303) (Lot Quantum Design, France) were cleaned by soaking them in a solution of NH<sub>4</sub>OH (28%)/H<sub>2</sub>O<sub>2</sub> (35%)/H<sub>2</sub>O, 1/1/6 (v/v/v) for 10 min at 70 °C. They were then rinsed with water, dried under nitrogen, and further cleaned for 10 min under UV/ozone irradiation (ProCleaner 220, BioForce Nanoscience, USA). The surface was then washed with water and dried under nitrogen.

**PAB-Functionalized QCM Sensor.** PAB was covalently coupled to the QCM crystal using a similar protocol as adopted for the GBs. Briefly, the cleaned QCM crystal was incubated in a solution of 2% (v/v) APTES in toluene at room temperature overnight. After rinsing with toluene followed by acetone and drying under nitrogen, the QCM chip was immersed in a solution of 5% glutaraldehyde in PBS buffer at 30 °C overnight. The activated QCM sensor was washed with PBS buffer, water, dried under nitrogen and stored at 8 °C until use. The above steps were conducted in a beaker, whereas the immobilization of PAB was carried out online in the QCM system.

**Glymo-IDA-Functionalized QCM Sensor.** The functionalization was performed following a similar protocol as used for the glass beads. Briefly, the cleaned QCM crystal was incubated in a solution of Glymo in toluene at room temperature overnight. After rinsing with toluene and acetone and drying under nitrogen, the QCM chip was immersed in a solution of IDA at 70 °C for 4 h. The QCM sensor was washed with 10% acetic acid, water, and methanol, dried under nitrogen, and stored at 8 °C until use. The above steps were conducted in a beaker, whereas the immobilization of Cu<sup>2+</sup> was carried out online in the QCM system.

Proteins at 1 mg/mL in buffer A were loaded on the functionalized QCM sensor until the baseline was reached. Unbound protein was removed by washing the cell with buffer A until the baseline was stable.

The polymer–protein interactions were investigated at 37 °C. Increasing concentrations of MIP-NPs (0.6–250 μg/mL) in buffer A were sequentially injected into the cell. A washing step with buffer A was conducted between every injection until the baseline was stable. To avoid bubble formation, the samples and the washing buffer were thermostated at 37 °C during the injection. Apparent molarities of the NPs were calculated using eq 1 below:<sup>3,32</sup>

$$[\text{NPs}] = (6/\pi N_A d^3 \rho) X \quad (1)$$

where  $N_A$  is Avogadro's constant,  $d$  is the hydrodynamic diameter (cm) of the particles found by DLS,  $\rho$  is the density of the particles (g/cm<sup>3</sup>), and  $X$  is the polymer weight concentration (g/L). The polymer density was taken to be 0.36 ± 0.03 g/cm<sup>3</sup> ( $\rho$  values for NIPAm-based polymers in the collapsed state).<sup>33</sup> Calculated apparent dissociation constants ( $K_{dapp}$ ) (M) (Table 1) were obtained by nonlinear fitting of the data to a single-site Langmuir-type binding isotherm.

## RESULTS AND DISCUSSION

**Preparation of the Column Reactor.** The solid-phase synthesis approach is represented in Figure 2. The immobilization of *p*-aminobenzamidine (Route A) was done as described in our precedent communication.<sup>16</sup> Activated GBs were silanized with APTES, followed by coupling with glutaraldehyde and attachment of PAB. Before packing the column, the properties of the silanized GBs and the PAB-functionalized GBs were evaluated in terms of their amino group content (0.2 ± 0.01 μmol per g of GBs) and binding capacity for trypsin and kallikrein, respectively. The amount of bound trypsin and kallikrein was 1.9 ± 0.2 nmol and 1.4 ± 0.3 nmol per gram of GBs, respectively. PAB-GBs were then packed in a column, equipped with two adapters for regulation of the bed volume and a thermostated jacket. This column, as compared to the previous one,<sup>16</sup> enables the scaling-up of MIP production with a better control of the temperature. Trypsin or kallikrein was then loaded on the column with a peristaltic pump.

For immobilization of the metal-chelate (Route B), activated GBs were silanized with Glymo, followed by coupling with the chelating agent, IDA.<sup>29</sup> Before packing the column, the performance of IDA-GBs and IDA-Cu<sup>2+</sup>-GBs was evaluated in terms of their binding capacity for Cu<sup>2+</sup> and the target proteins, respectively. Figure S2B shows that 1 g of IDA-GBs is saturated by 50 mM CuSO<sub>4</sub>. Cu<sup>2+</sup> interacts with IDA via coordinate bonding, and protein adsorption occurs by coordinate bonding of the imidazole nitrogen of histidine side chains with the metal ion. The amount of trypsin, kallikrein, and RNase bound per gram of IDA-Cu<sup>2+</sup> GBs was 15.9 ± 0.8, 14.2 ± 1.2, 16.5 ± 0.5 nmol respectively, indicating the higher binding capacity of these GBs as compared to PAB-functionalized GBs. The IDA-GBs were then packed in a column, and a solution of 50 mM CuSO<sub>4</sub> was pumped through. After washing the excess Cu<sup>2+</sup> with water and equilibration with buffer A, the template proteins trypsin or kallikrein or RNase A, were loaded on the column. Buffer A, at pH 7.0, used during

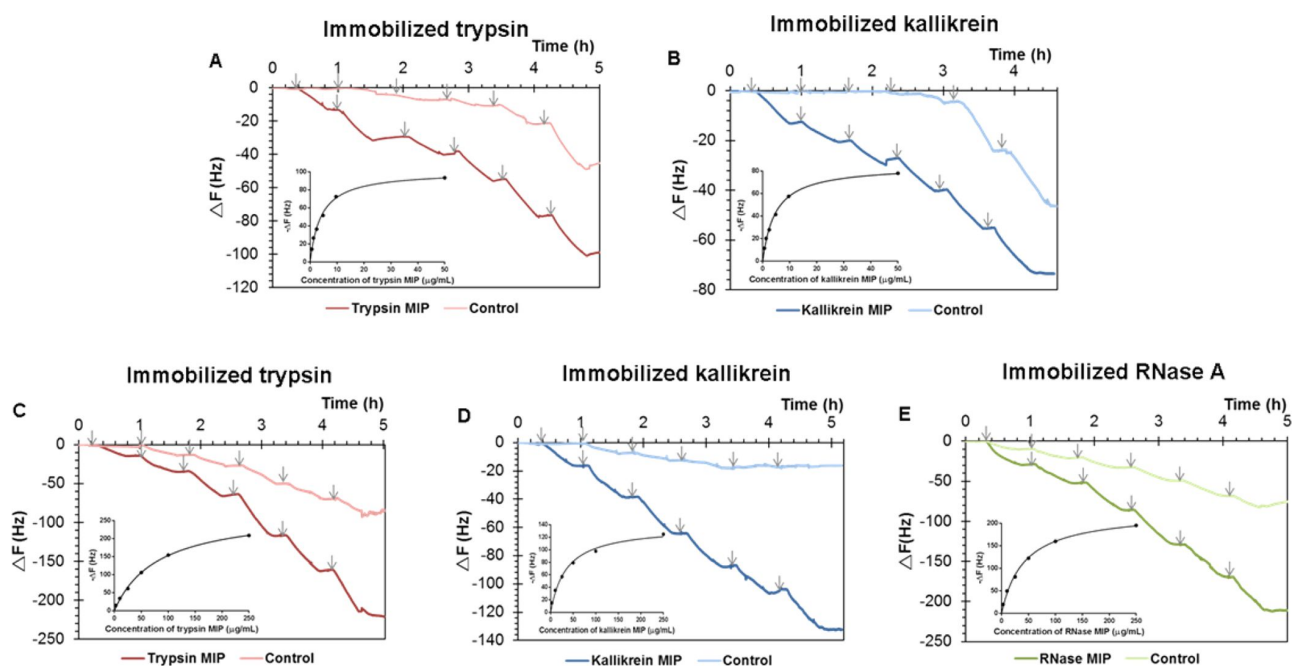


**Figure 3.** Time course of the frequency change ( $\Delta F$ ), on PAB-derivatized QCM sensor of (A) immobilized trypsin and (B) immobilized kallikrein, following injection of trypsin and kallikrein MIP-NPs; on  $\text{Cu}^{2+}$  chelate-derivatized sensor of immobilized (C) trypsin with trypsin MIP-NPs and (D) kallikrein with kallikrein MIP-NPs; (E) RNase with RNase MIP-NPs, in 25 mM sodium phosphate buffer pH 7.0 at 37 °C. Injections at the time point are indicated by the arrows, and the concentrations were 0.6, 1.2, 2.4, 4.8, 9.6, and 50  $\mu\text{g/mL}$  on PAB-derivatized QCM sensor and 2.5, 10, 25, 50, 100, 250  $\mu\text{g/mL}$  on  $\text{Cu}^{2+}$  chelate-derivatized sensor. Control means injection of the MIP on PAB or IDA- $\text{Cu}^{2+}$  functionalized GBs alone. Measurements were performed three times (RSD  $\pm$  5%) independently using two batches of MIPs. Inset: Corresponding binding isotherms of the MIPs for their respective templates.

the whole procedure, ensures that the imidazole group remains nonprotonated for interaction.

#### Solid-Phase Synthesis of Imprinted Nanoparticles.

After the formation of the affinity ligand-protein complex, polymerization was conducted around the immobilized protein. The same polymerization mixture was used for all MIP syntheses. The polymerization solution was composed of NIPAm and  $N,N'$ -ethylenebis(acrylamide) (EbAm) (95/5 molar ratio, total monomer concentration 0.5% w/w) and the initiator system (potassium persulfate/ $N,N,N',N'$ -tetramethylene diamine (TEMED)) in buffer A. NIPAm was used as the major component in this polymer recipe in order to obtain thermoresponsive MIP-NPs.<sup>34</sup> pNIPAm is known to undergo a volume-phase transition at its lower critical solution temperature (LCST) of 32 °C. The imprinted polymer was synthesized at 37 °C, and the growing polymeric nanoparticles, which are in the collapsed state at this temperature, encapsulate the immobilized protein during polymerization. It should be noted that an optimized molar ratio of NIPAm/EbAm (95/5) was employed because we observed that a higher amount of cross-linker (10 or 20%) produced polymers with no thermoresponsivity, as no significant change in size was observed by DLS analysis.

After polymerization, the column reactor was washed with buffer A at 37 °C to remove unreacted reagents and particles that polymerized distantly from the immobilized template. The reactor was then washed with the same buffer at room temperature (25 °C), allowing the MIP-NPs to swell and be eluted. The strategy is schematically represented in Figure 1. The yield of polymerization for all MIP-NPs is shown in Table 1.  $\text{Cu}^{2+}$  was not detected in the MIP-NPs (limit of

quantification (LOQ): 1  $\mu\text{mol/mL}$ ) (calibration curve of Figure S2A).

A major concern after polymerization is the complete removal of template so as to avoid bleeding of trace proteins interfering with future applications. To verify that there was no leakage of the template protein from the column, as previously demonstrated for a smaller column,<sup>16</sup> fractions collected from the elution step at room temperature (containing the MIP particles) were analyzed by enzymatic activity assay (LOQ is 10 nM for trypsin and 20 nM for kallikrein) (Figure S4) and by Bradford assay (LOQ = 0.1 mg/mL) (Figure S3). The former is a more sensitive assay, as it can detect proteins in the nM range but it detects only active proteins. Bradford assay detects in the  $\mu\text{M}$  range but was additionally used so as to detect all proteins. No active or denatured protein was detected in any fraction.

**Physicochemical Characterization of MIP-NPs.** The size and morphology of the MIP-NPs were analyzed by DLS (Table 1) and scanning electron microscopy (Figure S5, inset) respectively. Diameters of the various MIP-NPs span between 70 nm for the smallest and 119 nm for the largest, measured at 25 °C. The MIP-NPs appear as a transparent solution (Figure S5, inset), and no aggregation was observed for a period of six months when stored in a refrigerator.

The thermoresponsivity of the polymers was confirmed on one example, the trypsin MIP-NPs obtained on GBs-PAB. DLS measurements at temperatures in the vicinity of the expected phase transition temperature show the reduction of the hydrodynamic diameter of trypsin MIP-NPs from  $115 \pm 13$  nm at 32 °C to  $74 \pm 5$  nm at 33 °C (Figure S6).

**Evaluation of the Binding Characteristics of MIP-NPs by Piezoelectric Microgravimetry.** The recognition properties of all MIP-NPs were investigated using a quartz crystal microbalance (QCM).

**PAB as Affinity Ligand.** PAB was attached to the silicon dioxide surface of quartz crystals using a similar protocol as the one described for the GBs. After immobilization of trypsin on the QCM sensor, trypsin MIP-NPs (0.6 to 50  $\mu\text{g}/\text{mL}$ ) were sequentially injected into the cell at 37  $^{\circ}\text{C}$ , the temperature at which the MIP was synthesized. The change in frequency ( $\Delta F$ ) of the oscillating quartz crystal sensor, which represents the interaction of the MIP-NPs with the immobilized protein, was measured (Figure 3A, red line). This binding represents the sum of the specific binding to the template protein and the nonspecific adsorption to other parts of the GBs. To investigate the contribution of nonspecific interaction, MIP-NPs were injected on a PAB-functionalized QCM chip alone. Nonspecific interactions proved to be low (Figure 3A, pink line). Conventionally, to assess the specificity of a MIP, its binding behavior toward its template is compared in parallel with that of a nonimprinted polymer (NIP), a control polymer prepared without immobilized trypsin. In this solid-phase synthesis method, due to the large size of the protein, a NIP was not appropriate, as there would be too much difference in morphology and therefore would not be a good control.

The same analysis was performed on immobilized kallikrein (Figure 3B, dark blue line) and immobilized PAB (Figure 3B, pale blue line) with kallikrein MIP-NPs. Figures 3A,B show that trypsin and kallikrein MIP-NPs were specific as they bind their respective template proteins to a higher extent as compared to the control experiments.

As expected, no binding was observed when the MIP-NPs were injected at 25  $^{\circ}\text{C}$ . Indeed when trypsin MIP-NPs were injected on immobilized trypsin, no binding was observed at 25  $^{\circ}\text{C}$  (Figure S7). This is in agreement with the synthesis strategy that we adopted: during the synthesis at 37  $^{\circ}\text{C}$ , the MIP-NPs are in the collapsed state and bind to the protein and at 25  $^{\circ}\text{C}$ , which is below the LCST, the imprinted cavities are swollen, and therefore the MIP-NPs are liberated from the protein.

**IDA-Cu<sup>2+</sup> as Affinity Ligand.** IDA-Cu<sup>2+</sup> was attached to the silicon dioxide surface of quartz crystals using a protocol similar to that described for the GBs. Trypsin, kallikrein, and RNaseA were separately immobilized on the QCM sensor, and the corresponding MIP NPs (2.5 to 250  $\mu\text{g}/\text{mL}$ ) were then sequentially injected into the cell at 37  $^{\circ}\text{C}$  (Figure 3C-E, dark-colored lines). To assess nonspecific contribution, trypsin MIP, kallikrein MIP, and RNase MIP were injected on IDA-Cu<sup>2+</sup>-functionalized GBs alone (Figure 3C-E, pale-colored lines). In the three cases, binding of MIPs to their respective templates was high, indicating the creation of specific imprinted sites.

Overall, these results imply that the MIP-NPs synthesized by the solid-phase approach are specific toward their corresponding templates. Calculated apparent dissociation constants ( $K_{\text{dapp}}$ ), based on eq 1 as described in the Experimental Section for all MIP-NPs, were obtained by nonlinear fitting of the data to a single-site Langmuir-type binding isotherm and are shown as an inset in Figure 3 and in Table 1. The MIP-NPs, with their high affinity binding comparable to antibody-antigen interaction, seem to be quite promising as alternatives to natural antibodies.

**Selectivity studies of MIP-NPs.** The selectivity of MIP-NPs was studied in the presence of related and unrelated proteins, by QCM.

**PAB as Affinity Ligand.** Trypsin, kallikrein, and thrombin, three serine proteases known to be inhibited by PAB,<sup>25</sup> were separately immobilized on QCM sensors. Trypsin and kallikrein MIP-NPs (0.6 to 50  $\mu\text{g}/\text{mL}$ ) were sequentially injected at 37  $^{\circ}\text{C}$ . The change in frequency ( $\Delta F$ ) of the oscillating quartz crystal sensor was measured and clearly indicates the selectivity of the two imprinted materials, since a much higher frequency change is observed when the MIP-NPs were injected on their respective protein template (Figure 4A,B). However, to be strictly comparable, the amount of proteins immobilized on the sensor should be determined. The Sauerbrey equation, where a  $\Delta F$  of 1 Hz corresponds to an adsorption of 17.7  $\text{ng}/\text{cm}^2$  (for a 5 MHz quartz crystal),<sup>35</sup> was employed. From the  $\Delta F$  recorded after injection of the proteins (Figure S8) and the molecular weight of the proteins (Table 2), the maximum amount of proteins ( $\text{pmol}/\text{cm}^2$ ) bound to the sensor (Figure S9) was deduced. Similarly, the saturation amount of MIP-NPs bound to the sensor ( $\text{ng}/\text{cm}^2$ ) was calculated from the  $\Delta F$  recorded after the injection of 50  $\mu\text{g}/\text{mL}$ , followed by washing with buffer until a stable baseline is reached. Hence, the maximum amount of polymer bound to immobilized proteins ( $Q_{\text{max}}$ ) ( $\text{ng}/\text{pmol}$ ) was calculated, enabling a normalization of all the data for an absolute comparison of the binding between each polymer and each protein. The results are presented as bar-charts (Figure 4, right). It is interesting to note that both MIPs do not bind to thrombin. Sequence alignment, with the CLUSTAL OMEGA program, of trypsin and kallikrein showed 35% identity, whereas trypsin with thrombin and kallikrein with thrombin have only 14% and 12% identity, respectively.

**IDA-Cu<sup>2+</sup> as Affinity Ligand.** Proteins with different isoelectric points (pI) and molecular weights (MW), which, according to the literature, could be retained on an IMAC column and were stable at 37  $^{\circ}\text{C}$ , like cytochrome c,<sup>36</sup> myoglobin<sup>24</sup> and hemoglobin<sup>37</sup> (Table 2), as well as the template proteins trypsin, kallikrein and RNase A, were individually immobilized on the QCM sensor. Trypsin MIP-NPs (Figure 4C), kallikrein MIP-NPs (Figure 4D), and RNase MIP-NPs (Figure 4E) were sequentially injected at 37  $^{\circ}\text{C}$ . In all cases, a higher  $\Delta F$  was observed when the MIP NPs were injected on their respective protein template. The normalization of the binding of the polymers with the immobilized protein was done using the same reasoning as described above, except that the saturating amount of MIP-NPs bound to the sensor ( $\text{ng}/\text{cm}^2$ ) was calculated from the  $\Delta F$  recorded after the injection of 250  $\mu\text{g}/\text{mL}$ . Remarkably, no cross-reactivity was observed with the heme proteins, cytochrome c, myoglobin, and hemoglobin; trypsin MIP has some cross-reactivity with kallikrein/RNase A (Figure 4C) and RNase A MIP with trypsin/kallikrein (Figure 4E). Kallikrein MIP (Figure 4D) was less selective than the other MIPs.

The MIP was composed of only uncharged monomers, NIPAm<sup>38</sup> and EbAm, to avoid eventual nonspecific electrostatic interactions from charged functional monomers with the PAB and IDA-Cu<sup>2+</sup>, both being positively charged under the working conditions (Figure 2). Therefore, binding of the immobilized proteins with the MIP-NPs occurred mainly through hydrogen and hydrophobic interaction. Noncharged multiple weak interactions have been reported to be optimum for conferring selectivity to neutral acrylamide/*N,N'*-methylenebis-(acrylamide)-based polymers, whereas the presence of electrostatic interactions still remains controversial and does not systematically lead to better imprinting.<sup>10,39</sup> The selectivity

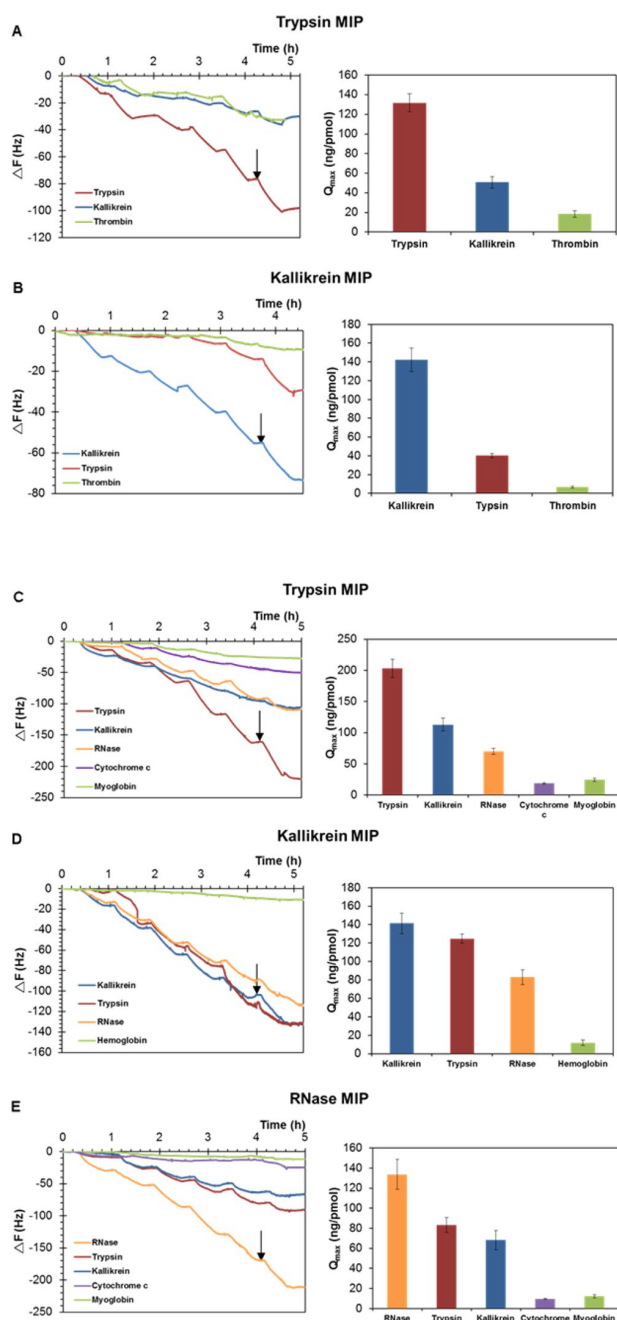


**Figure 4.** Time course of the frequency change ( $\Delta F$ ) on immobilized proteins as marked on the figures, after injection of (A,C) trypsin MIP-NPs, (B,D) kallikrein MIP-NPs, and (E) RNase A MIP-NPs. The QCM crystal was derivatized with PAB for panels A and B, and with IDA-Cu<sup>2+</sup> for panels C–E. Injections were done in 25 mM sodium phosphate buffer pH 7.0, 37 °C, with concentrations from 0.6–50  $\mu\text{g}/\text{mL}$  in the case of PAB and 2.5–250  $\mu\text{g}/\text{mL}$  for Cu<sup>2+</sup> chelate-derivatized sensor. The arrow represents the last MIP injection. Measurements were performed in duplicate with two different batches of MIP-NPs. The corresponding selectivity profile of each MIP, after data normalization, is represented on the right.

profile that we observed here was independent of the charge or the molecular weight of the proteins (Table 2). For instance, trypsin and cytochrome c have similar isoelectric points, but trypsin MIP has no affinity for cytochrome c, even though it has

**Table 2.** Properties of Proteins Immobilized on IDA-Cu<sup>2+</sup>

protein	MW <sup>b</sup> (kDa)	accession number (Uniprot)	3D structure in PDBe	surface histidine <sup>a</sup>	pI <sup>d</sup>
trypsin <i>bovine pancreas</i>	23.8	P00760	1s0q	2	10.3
kallikrein <i>porcine pancreas</i>	25.6	P00752	2kai	5	4.2
ribonuclease A <i>bovine pancreas</i>	13.7	P61823	1bel	2	9.6
cytochrome c <i>horse heart</i>	11.7	P00004	1hrc	2	10.3
myoglobin <i>equine skeletal muscle</i>	17.0	P68082	1npg <sup>c</sup>	6	6.8/7.4
hemoglobin <i>human</i>	62.4	nd	nd	nd	6.8

<sup>a</sup>Derived from Swiss-PdbViewer program by selecting 10% surface accessibility of the protein indicated in the 3D structure entry. <sup>b</sup>From Protein Data Bank Europe (PDBe) or SIGMA. <sup>c</sup>Of equine heart. <sup>d</sup>SIGMA and ref 40; nd: not determined.

a smaller size (Figure 4C). RNase A and cytochrome c have almost similar molecular weights and pIs but RNase A MIP has no affinity for cytochrome c (Figure 4E).

To increase selectivity on immobilized metal chelate, one possibility would be to employ other metal ions. The strength of protein adsorption for IMAC metal ions increases in the following order: Co<sup>2+</sup> < Zn<sup>2+</sup> < Ni<sup>2+</sup> < Cu<sup>2+</sup>.<sup>20</sup> From Table 2, trypsin and RNase A possess at least 2 surface His; either both His are engaged simultaneously in binding with Cu<sup>2+</sup> or only one His is involved. Thus, different protein conformations could be offered for imprinting, because Cu<sup>2+</sup> due to its high binding strength is less discriminative toward the different “types” of His residues. As for kallikrein, since there are five His present on the surface, more protein conformations could be proposed for imprinting, which might explain the lower selectivity of the kallikrein MIP (Figure 4D). The use of other metal ions could restrict the binding to a single or another protein conformation, which might lead to more selective MIPs.

## CONCLUSIONS

We have described a novel, general, and versatile method for the solid phase synthesis of water-compatible molecularly imprinted polymer nanoparticles for proteins. Metal chelate was used as a general affinity ligand to immobilize proteins via their accessible surface histidines. This configuration leads to an oriented immobilization of the protein, resulting in the formation of uniformly oriented homogeneous binding sites on the MIP surface. Moreover, tedious washing steps for template extraction are no longer required. RNase A, trypsin and kallikrein were chosen as model systems. RNase A and homologous proteins are implicated in oncology, suggesting that RNase A MIP-NPs can potentially contribute, as a controlled drug delivery system, to an optimal ribonuclease-based cancer therapy.<sup>41,42</sup> We<sup>13</sup> and others<sup>32</sup> have previously shown that trypsin MIP was a more potent inhibitor of trypsin, than its well-known inhibitor PAB. RNase MIPs as inhibitors would certainly constitute a cheap and thermally stable inactivator to help prevent RNA degradation by RNase for routine biological experiments. Concerning trypsin and kallikrein, it was interesting to study the MIPs obtained using

two different affinity ligands that target different locations on the proteins. With immobilized PAB, the active site region of the enzyme is engaged, and in the case of immobilized  $\text{Cu}^{2+}$ , the surface His are involved, possibly leaving the active site cleft free. Protein digestion by immobilized trypsin via an immobilized  $\text{Cu}^{2+}$  reactor has been reported, suggesting that the catalytic active site region is accessible.<sup>43</sup> Accordingly, MIP-NPs with different  $K_{\text{dapp}}$  values were obtained; those synthesized with PAB as the affinity ligand have higher binding affinities and were also more selective than those synthesized on IDA- $\text{Cu}^{2+}$  (Table 1 and Figure 4). We were specially interested in the obtention of MIPs targeting kallikrein for their future development in in vitro diagnostics because kallikrein and kallikrein-like proteases are cancer biomarkers that are involved in many cancer-related processes, including cell growth regulation, angiogenesis, invasion, and metastasis.<sup>26–28</sup> Particularly promising were the kallikrein MIP nanoparticles obtained on immobilized PAB as they were stable in buffer (no aggregation) during 6-month storage at 4 °C, possessed a  $K_{\text{dapp}}$  of 49 pM (Table 1), and were selective toward kallikrein, as little or no binding occurred with the other serine proteases, trypsin and thrombin (Figure 4B).

Future work will focus on improving the selectivity of the MIPs obtained on metal chelate, by changing the metal ions,<sup>20,24,36</sup> changing the composition of the polymerization mixture<sup>3,10,17,44</sup> or optimizing the buffer conditions.<sup>45</sup> We believe that our solid-phase synthesis approach using immobilized metal-chelate can be used as a universal method for the future development of water-compatible MIP-NPs for proteins with antibody-like properties.

## ■ ASSOCIATED CONTENT

### 📄 Supporting Information

The Supporting Information is available free of charge on the ACS Publications website at DOI: 10.1021/acs.biomac.5b01454.

Binding capacity of functionalized GBs for proteins, enzymatic assays, size distribution analysis, SEM images, and determination of amounts of proteins immobilized on QCM chips (PDF)

## ■ AUTHOR INFORMATION

### Corresponding Authors

\*E-mail: [jeanne.tse-sum-bui@utc.fr](mailto:jeanne.tse-sum-bui@utc.fr); Fax: (+) 33 3 44203910; Tel: (+) 33 3 44234402

\*E-mail: [karsten.haupt@utc.fr](mailto:karsten.haupt@utc.fr)

### Notes

The authors declare no competing financial interest.

## ■ ACKNOWLEDGMENTS

This work was supported by the European Commission (Marie Curie Actions, projects IRMED, MCIAPP-2009-251307). J.X. thanks the China Scholarship Council (CSC) and E.T. thanks the Turkish Higher Education Council for financial support. The authors acknowledge financial support from the Region of Picardy (cofunding of equipment under CPER 2007-2013). We thank Dr. Jacqueline Maximilien for her help with the QCM and Frederic Nadaud for the SEM images.

## ■ REFERENCES

(1) Transparency Market Research. In Vitro Diagnostics Market (Clinical Chemistry, Immunoassay, Diabetes Testing, Blood Testing,

Molecular Diagnostics) - Global Industry Analysis, Size, Share, Growth and Forecast, 2012–2018. Online. 2013 July. Available from URL: <http://www.prnewswire.com/news-releases/in-vitro-diagnostics-market-is-expected-to-reach-usd-742-billion-globally-in-2018-transparency-market-research-217756061.html>.

(2) Lavignac, N.; Allender, C. J.; Brain, K. R. *Anal. Chim. Acta* **2004**, *510*, 139–145.

(3) Hoshino, Y.; Kodama, T.; Okahata, Y.; Shea, K. J. *J. Am. Chem. Soc.* **2008**, *130*, 15242–15243.

(4) Poma, A.; Turner, A. P. F.; Piletsky, S. A. *Trends Biotechnol.* **2010**, *28*, 629–637.

(5) Poma, A.; Guerreiro, A.; Whitcombe, M. J.; Piletska, E. V.; Turner, A. P. F.; Piletsky, S. A. *Adv. Funct. Mater.* **2013**, *23*, 2821–2827.

(6) Zhao, M.; Chen, X.; Zhang, H.; Yan, H.; Zhang, H. *Biomacromolecules* **2014**, *15*, 1663–1675.

(7) Cakir, P.; Cutivet, A.; Resmini, M.; Tse Sum Bui, B.; Haupt, K. *Adv. Mater.* **2013**, *25*, 1048–1051.

(8) Ye, L. *Adv. Biochem. Eng. Biotechnol.* **2015**, *150*, 1–24.

(9) Takeuchi, T.; Hishiya, T. *Org. Biomol. Chem.* **2008**, *6*, 2459–2467.

(10) Verheyen, E.; Schillemans, J. P.; van Wijk, M.; Demeniex, M. A.; Hennink, W. E.; van Nostrum, C. F. *Biomaterials* **2011**, *32*, 3008–3020.

(11) Bossi, A. M.; Sharma, P. S.; Montana, L.; Zoccatelli, G.; Laub, O.; Levi, R. *Anal. Chem.* **2012**, *84*, 4036–4041.

(12) Li, S.; Cao, S.; Whitcombe, M. J.; Piletsky, S. A. *Prog. Polym. Sci.* **2014**, *39*, 145–163.

(13) Cutivet, A.; Schembri, C.; Kovensky, J.; Haupt, K. *J. Am. Chem. Soc.* **2009**, *131*, 14699–14702.

(14) Zhang, H.; Jiang, J.; Zhang, H.; Zhang, Y.; Sun, P. *ACS Macro Lett.* **2013**, *2*, 566–570.

(15) Beyazit, S.; Ambrosini, S.; Marchyk, N.; Palo, E.; Kale, V.; Soukka, T.; Tse Sum Bui, B.; Haupt, K. *Angew. Chem.* **2014**, *126*, 9065–9069.

(16) Ambrosini, S.; Beyazit, S.; Haupt, K.; Tse Sum Bui, B. *Chem. Commun.* **2013**, *49*, 6746–6748.

(17) Poma, A.; Guerreiro, A.; Caygill, S.; Moczko, E.; Piletsky, S. *RSC Adv.* **2014**, *4*, 4203–4206.

(18) Qin, L.; He, X. W.; Zhang, W.; Li, W. Y.; Zhang, Y. K. *Anal. Chem.* **2009**, *81*, 7206–7216.

(19) Liu, J.; Yang, K.; Deng, Q.; Li, Q.; Zhang, L.; Liang, Z.; Zhang, Y. K. *Chem. Commun.* **2011**, *47*, 3969–3971.

(20) Winzerling, J. J.; Berna, P.; Porath, J. *Methods* **1992**, *4*, 4–13.

(21) Block, H.; Maertens, B.; Priestersbach, A.; Brinker, N.; Kubicek, J.; Fabis, R.; Labahn, J.; Schäfer, F. *Methods Enzymol.* **2009**, *463*, 439–473.

(22) Boden, V.; Rangeard, M. H.; Mrabet, N.; Vijayalakshmi, M. A. *J. Mol. Recognit.* **1998**, *11*, 32–39.

(23) Haupt, K.; Roy, F.; Vijayalakshmi, M. A. *Anal. Biochem.* **1996**, *234*, 149–154.

(24) Sulkowski, E. *Trends Biotechnol.* **1985**, *3*, 1–7.

(25) Casale, E.; Collyer, C.; Ascenzi, P.; Balliano, G.; Milla, P.; Viola, F.; Fasano, M.; Menegatti, R.; Bolognesi, M. *Biophys. Chem.* **1995**, *54*, 75–81.

(26) Borgeño, C. A.; Diamandis, E. P. *Nat. Rev. Cancer* **2004**, *4*, 876–890.

(27) Swedberg, J. E.; de Veer, S. J.; Harris, J. M. *Biol. Chem.* **2010**, *391*, 357–374.

(28) Schmitt, M.; Renné, T.; Scorilas, A. *Thromb. Haemostasis* **2013**, *110*, 396–398.

(29) Lei, W.; Xue, M.; Zhong, X.; Meng, Z. H.; Zhang, W. B.; Zhang, L. Y. *J. Liq. Chromatogr. Relat. Technol.* **2013**, *36*, 2196–2207.

(30) Yang, C.; Xing, J.; Guan, Y.; Liu, H. *Appl. Microbiol. Biotechnol.* **2006**, *72*, 616–622.

(31) Bermejo-Barrera, A.; Bermejo-Barrera, P.; Martinez, F. B. *Analyst* **1985**, *110*, 1313–1315.

(32) Guerreiro, A.; Poma, A.; Karim, K.; Moczko, E.; Takarada, J.; de Vargas-Sansalvador, I. P.; Turner, N.; Piletska, E.; de Magalhaes, C. S.;

Glazova, N.; Serkova, A.; Omelianova, A.; Piletsky, S. *Adv. Healthcare Mater.* **2014**, *3*, 1426–1429.

(33) Meeves, M.; Ricka, J.; de Silva, M.; Nyffenegger, R.; Binkert, T. *Macromolecules* **1991**, *24*, 5811–5816.

(34) Marchyk, N.; Maximilien, J.; Beyazit, S.; Haupt, K.; Tse Sum Bui, B. *Nanoscale* **2014**, *6*, 2872–2878.

(35) Höök, F.; Rodahl, M.; Brzezinski, P.; Kasemo, B. *Langmuir* **1998**, *14*, 729–734.

(36) Hemdan, E. S.; Zhao, Y. J.; Sulkowski, E.; Porath, J. *Proc. Natl. Acad. Sci. U. S. A.* **1989**, *86*, 1811–1815.

(37) Durfee, S. L.; Mathews, A. J.; Matthews, M. A. H.; Milne, E. E.; Neway, J. O.; Plomer, J. J.; Ryland, J. R.; Traylor, D. W. European Patent EP0792293A1, 1997.

(38) Pelton, R. J. *Colloid Interface Sci.* **2010**, *348*, 673–674.

(39) Hjerten, S.; Liao, J.-L.; Nakazato, K.; Wang, Y.; Zamaratskaia, G.; Zhang, H.-X. *Chromatographia* **1997**, *44*, 227–234.

(40) Raspi, G. J. *Chromatogr., Biomed. Appl.* **1996**, *684*, 265–287.

(41) Marshall, G. R.; Feng, J. A.; Kuster, D. J. *Biopolymers* **2008**, *90*, 259–277.

(42) Haigis, M. C.; Kurten, E. L.; Raines, R. T. *Nucleic Acids Res.* **2003**, *31*, 1024–1032.

(43) Ma, J.; Hou, C.; Liang, Y.; Wang, T.; Liang, Z.; Zhang, L.; Zhang, Y. K. *Proteomics* **2011**, *11*, 991–995.

(44) Reddy, S. M.; Phan, Q. T.; El-Sharif, H. F.; Govada, L.; Stevenson, D.; Chayen, N. E. *Biomacromolecules* **2012**, *13*, 3959–3965.

(45) El-Sharif, H. F.; Phan, Q. T.; Reddy, S. M. *Anal. Chim. Acta* **2014**, *809*, 155–161.

## Supplementary Information

### Toward a universal method for preparing molecularly imprinted polymer nanoparticles with antibody-like affinity for proteins

Jingjing Xu,<sup>#</sup> Serena Ambrosini,<sup>#</sup> Emel Tamahkar,<sup>S</sup> Claire Rossi,<sup>#</sup> Karsten Haupt,<sup>\*#</sup> and Bernadette Tse Sum Bui<sup>\*#</sup>

#### Morphology of glass beads after different treatments

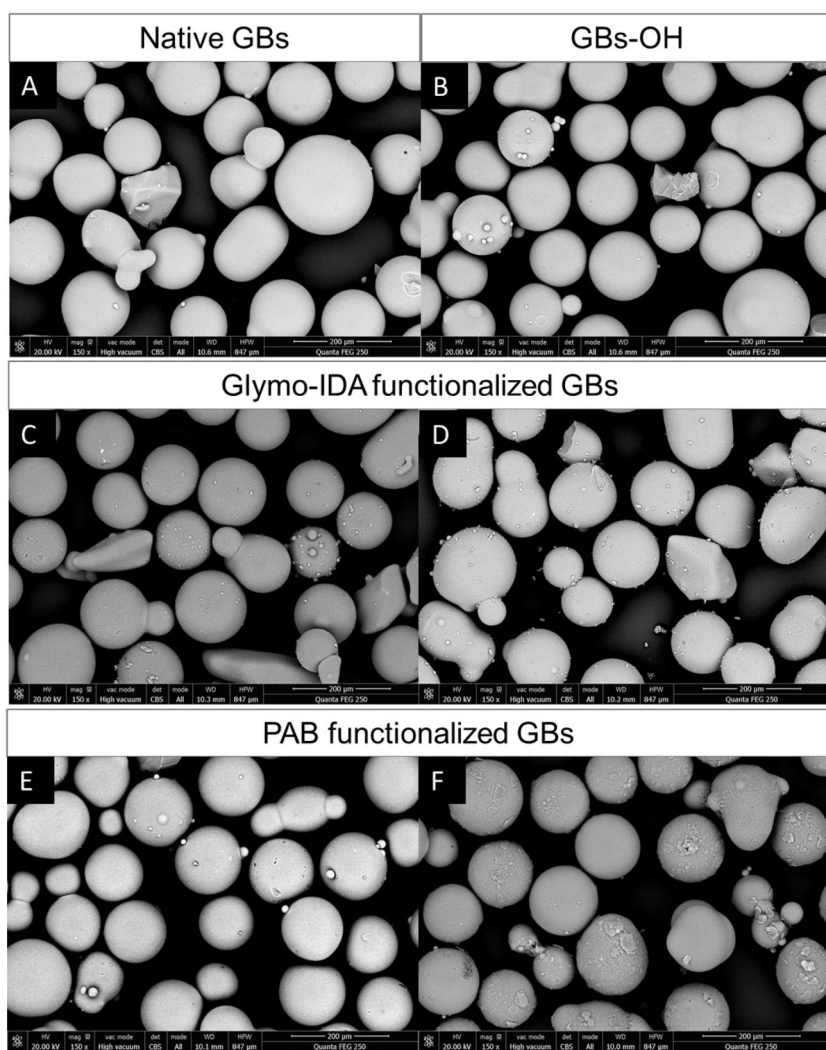


**Fig. S1.** SEM image of glass-beads in their (A) native state; after (B) boiling in 4 M NaOH; (C) refluxing with Glymo in toluene at 110 °C; (D) stirring with IDA at 70 °C; (E) shaking with APTES in toluene; (F) shaking with glutaraldehyde and PAB.

### Evidence of metal-chelates on IDA-GBs

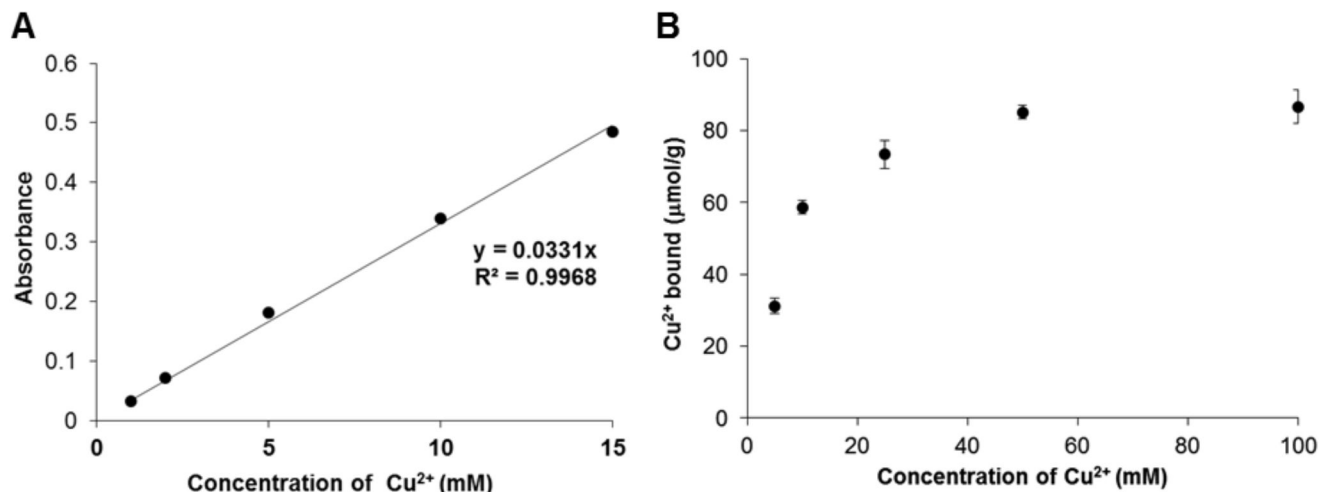


**Fig. S2.** (A) Representative calibration curve of Cu<sup>2+</sup>-EDTA complex, measured at 733 nm; (B) Evidence that Cu<sup>2+</sup> is bound on IDA-GBs. Saturation is reached with 50 mM CuSO<sub>4</sub> for 1 g of GBs.

### Protein determination by Bradford and enzymatic assays

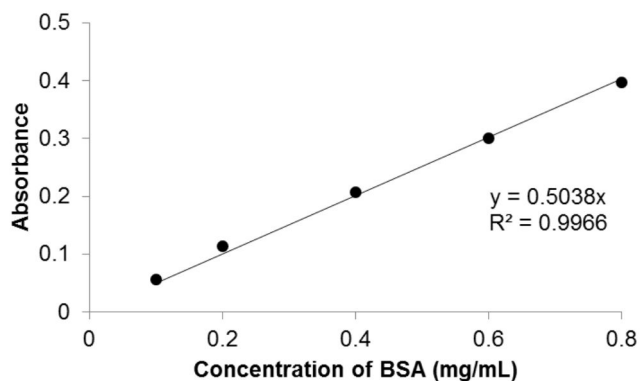


**Fig. S3.** Protein determination by the method of Bradford. Absorbance at 595 nm. BSA was used as standard.

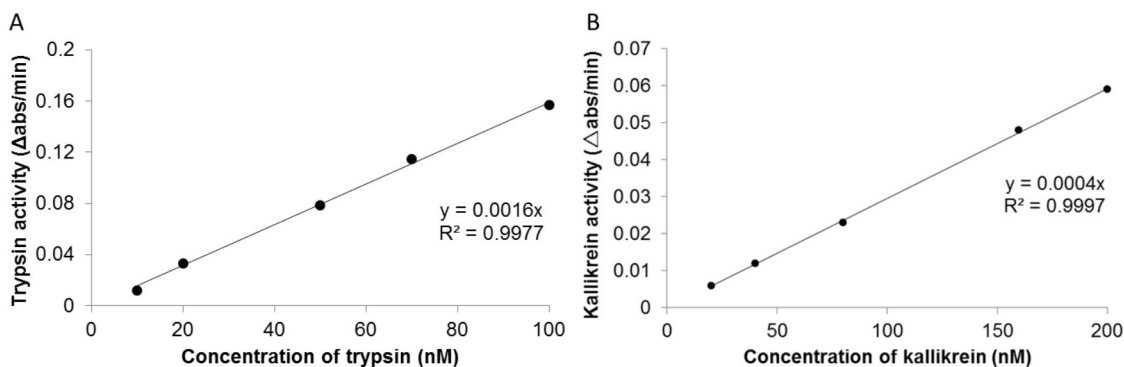


**Fig. S4.** Representative calibration curve of (A) trypsin between 10 and 100 nM in 50 mM Tris-HCl pH 8.0; (B) kallikrein between 20 and 200 nM in 50 mM Tris-HCl pH 8.7. Data are the mean from three independent measurements for each concentration.

## Physicochemical characterization of MIP-NPs

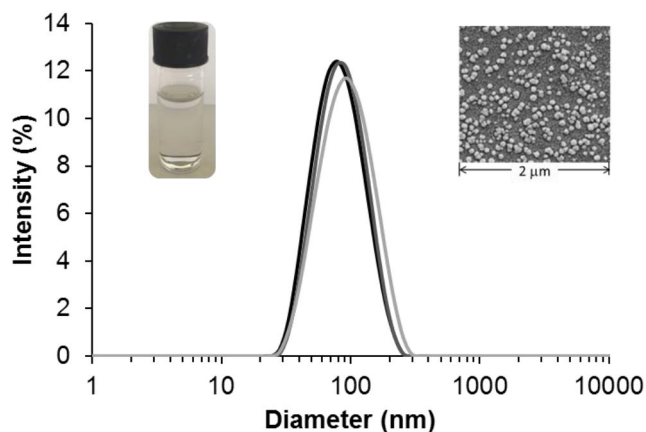


**Fig. S5.** Representative dynamic light scattering analysis, SEM image (inset) and photo (inset) of MIP-NPs, as a stable solution at 25 °C. Size distribution (n=3) of MIP-NPs obtained on PAB immobilized trypsin, as example.

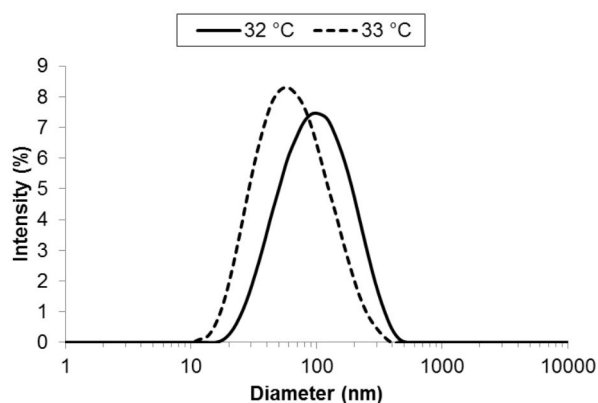


**Figure S6.** Thermoresponsivity of the MIP-NPs in 25 mM sodium phosphate buffer pH 7.0. DLS showing the decrease in size (n =3) of trypsin MIP-NPs from 32 °C (solid line) to 33 °C (dotted line).

## Evaluation of the recognition properties of MIP-NPs using a quartz crystal microbalance

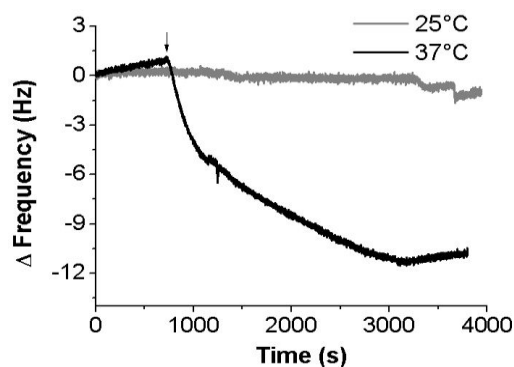


**Fig. S7.** Injection of trypsin MIP-NPs on trypsin immobilized on a PAB-QCM sensor at 25 °C and 37 °C. No binding was observed at 25 °C.

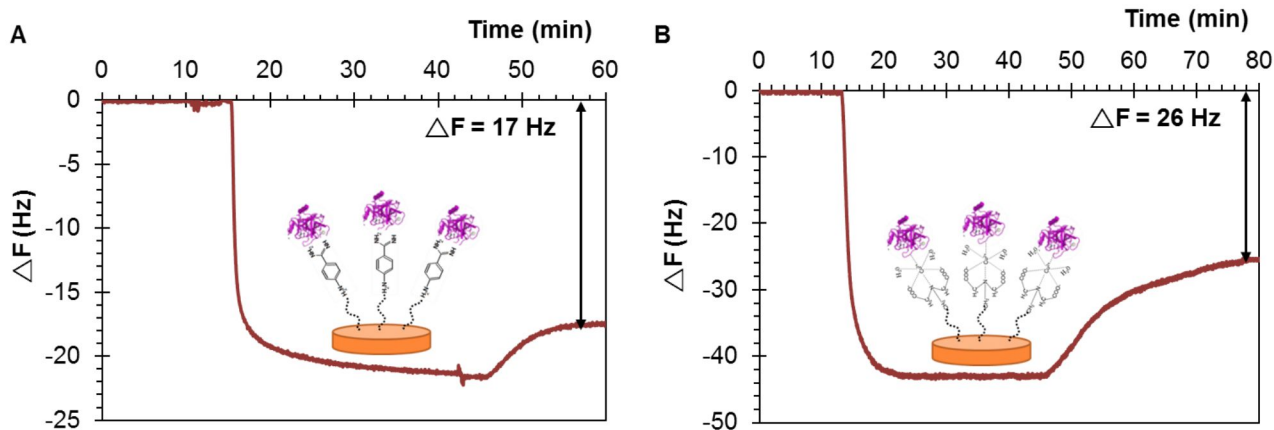


**Fig. S8.** Representative time course of the frequency change ( $\Delta F$ ) at 25 °C during immobilization of trypsin on (A) PAB and (B) IDA-Cu<sup>2+</sup>. Trypsin at a concentration of 1 mg/mL in 25 mM sodium phosphate buffer pH 7.0 was injected, followed by washing with buffer until the baseline is reached. The arrow indicates the  $\Delta F$  taken to determine the amount of trypsin immobilized on the chip.

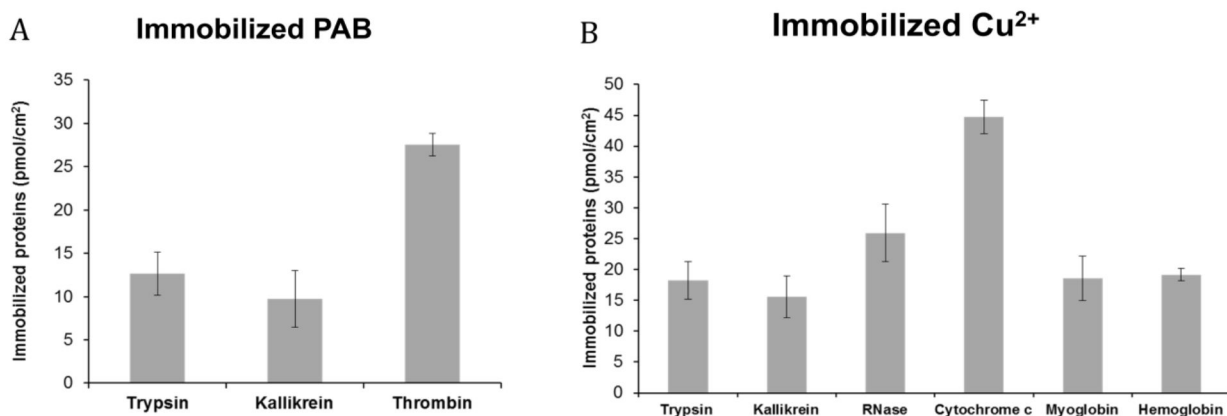


**Fig. S9.** Proteins immobilized on functionalized QCM chips. Values were determined by applying the Sauerbrey equation. Data for  $\Delta F$  are the mean of 4 independent injections and obtained as indicated in Fig. S8; molecular weight of proteins used for the calculation, as indicated in Table 2.

## **Publication 2**

### **Guide to the Preparation of Molecularly Imprinted Polymer Nanoparticles for Protein Recognition, by Solid-Phase Synthesis**

J. Xu, P. X. Medina-Rangel, K. Haupt\*, B. Tse Sum Bui\*

*Sorbonne Universités, Université de Technologie de Compiègne, CNRS Enzyme and Cell  
Engineering Laboratory, Rue Roger Couitolenc, CS 60319, 60203 Compiègne Cedex, France*

*Corresponding authors: [jeanne.tse-sum-bui@utc.fr](mailto:jeanne.tse-sum-bui@utc.fr) (B. Tse Sum Bui); [karsten.haupt@utc.fr](mailto:karsten.haupt@utc.fr)  
(K. Haupt)*

**Book title: NanoArmoring of Enzymes: Rational Design of Polymer-Wrapped Enzymes**

**Chapter title: Guide to the Preparation of Molecularly Imprinted Polymer Nanoparticles for Protein Recognition, by Solid-Phase Synthesis**

**J. Xu, P. X. Medina-Rangel, K. Haupt\*, B. Tse Sum Bui\***

*Sorbonne Universités, Université de Technologie de Compiègne, CNRS Enzyme and Cell Engineering Laboratory, Rue Roger Couitolenc, CS 60319, 60203 Compiègne Cedex, France*

Corresponding authors: [jeanne.tse-sum-bui@utc.fr](mailto:jeanne.tse-sum-bui@utc.fr) (B. Tse Sum Bui); [karsten.haupt@utc.fr](mailto:karsten.haupt@utc.fr) (K. Haupt)

## **Contents**

### **1. Introduction**

### **2. Protocols**

#### **2.1 Activation of glass-beads**

#### **2.2 Functionalization of glass-beads**

#### **2.3 Enzyme immobilization and synthesis of molecularly imprinted polymer (MIP) nanoparticles**

### **3. Physicochemical characterization of MIP nanoparticles**

### **4. Evaluation of the binding characteristics of MIP nanoparticles using a quartz crystal microbalance**

### **5. MIP nanoparticles protect enzyme from thermal and pH denaturation**

6. Concluding remarks

7. Notes

Acknowledgments

References

### **Abstract**

Molecularly imprinted polymers (MIPs) are synthetic antibody mimics possessing specific cavities designed for a target molecule. Nowadays, molecular imprinting of proteins still remains a challenge as the generation of selective imprinted cavities is extremely difficult, due to their flexible structure and the presence of a multitude of functional sites. To overcome this difficulty, we propose a solid-phase synthesis strategy to prepare MIPs specific for any protein that can be immobilized in an oriented way on a solid phase. Trypsin and kallikrein were used as model proteins. The solid-phase support consist of glass beads functionalized with two affinity ligands of the enzymes, the competitive inhibitor *p*-aminobenzamidine or a Cu<sup>2+</sup>-chelate, so as to orientate the immobilization of the enzymes via their active site or via their surface histidine residues, respectively. Thermoresponsive molecularly imprinted polymer nanoparticles (MIP-NPs) were then synthesized around the immobilized enzyme. The MIP-NPs were released by a simple temperature change, resulting in protein-free polymers endowed with improved binding site homogeneity since the binding sites have the same orientation. The MIP-NPs exhibit apparent dissociation constants between 0.02–2 nM towards their proteins, comparable to those of natural antibodies. Moreover, these water-

compatible polymers, targeting different domains of the enzyme can also function as protective agents, hence preventing their target proteins from denaturation by heat and pH.

**Keywords:** MIPs, solid-phase synthesis, protein imprinting, trypsin, kallikrein, plastic antibodies, synthetic receptors, metal-chelate

## 1. INTRODUCTION

Synthetic receptors for specific recognition of proteins are attractive in various fields including sensors, immunoassays, proteomics and clinical diagnostics. One class of such receptors are molecularly imprinted polymers (MIPs) which are tailor-made materials able to recognize and bind target molecules with affinities and specificities comparable to those of natural receptors such as antibodies. MIPs are produced by a templating process at the molecular level by copolymerization of functional and cross-linking monomers, followed by the subsequent removal of the template after polymerization (Fig. 1) (Haupt, Linares, Bompart & Tse Sum Bui, 2012; Ye, 2015; Beyazit, Tse Sum Bui, Haupt & Gonzato, 2016).

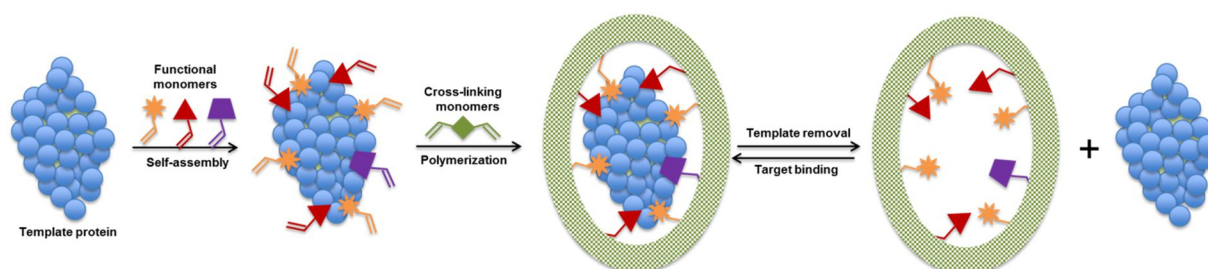


**Figure 1** Synthesis of a molecularly imprinted polymer for a protein

Advantageously, they possess a higher chemical, physical and thermal stability than biological receptors, are easily obtained and cost-effective, and can be easily engineered and adapted to standard industrial fabrication processes. However, the generation of MIPs for proteins still remains a challenge, mainly due to their complex structure in their native conformation that has to be preserved during the polymerization process (Takeuchi & Hishiya, 2008; Li, Cao, Whitcombe & Piletsky, 2014). Furthermore, the generation of selective imprinted cavities is extremely difficult due to the multitude of functional sites, and their large size hampers their extraction so that permanent physical entrapment of template protein in the polymer is often encountered. However, as previously demonstrated with trypsin, if the polymerization of the MIP around the protein is orientated with an anchoring monomer derived from its competitive inhibitor *p*-aminobenzamidine (PAB), then rather selective MIPs can be obtained (Cutivet, Schembri, Kovensky & Haupt, 2009). Indeed, the resulting MIP bound trypsin preferentially to other proteins of similar size and isoelectric points. Still, the problem related to the removal of the bulky template after polymerization remains (Verheyen, Schillemans, van Wijk, Demeniex, Hennink & van Nostrum, 2011). One solution to this problem and to produce selective MIPs at the same time is to employ a solid-phase synthesis approach where the protein is orientedly immobilized on a solid support before imprinting (Ambrosini, Beyazit, Haupt & Tse Sum Bui, 2013; Canfarotta, Poma, Guerreiro & Piletsky, 2016; Xu, Ambrosini, Tamahkar, Rossi, Haupt & Tse Sum Bui, 2016). Preferentially, the protein should be immobilized through an affinity ligand, instead of directly attaching it to the

support (Poma, Guerreiro, Caygill, Moczko & Piletsky, 2014), which would enable an oriented immobilization.

Herein, we describe this method on the example of two serine proteases, trypsin and kallikrein. Two different affinity ligands are used to immobilize the proteins in an oriented manner: *p*-aminobenzamidine (PAB), a competitive inhibitor of the enzymes, and a Cu<sup>2+</sup>-chelate which has affinity for histidines present at the surface of the protein (Fig. 2). MIP-NPs are then synthesized around the immobilized enzyme. *N*-isopropylacrylamide (NIPAM) is used as the major component in the polymerization mixture to obtain thermoresponsive MIPs. pNIPAM is well-known to undergo a volume-phase transition at its lower critical solution temperature at 32 °C (Schild, 1992; Marchyk, Maximilien, Beyazit, Haupt & Tse Sum Bui, 2014). The polymer is synthesized at 37 °C, that is, in the collapsed state, and consequently, upon cooling the polymer to below 32 °C, the MIP swells causing its release from the protein, resulting at the same time in an easy and complete template removal from the MIP (Fig. 2). Using this strategy, all binding sites should have the same orientation and be located at the surface of the particle, thus improving binding site homogeneity and accessibility by the bulky protein. Indeed, our results show that the resulting MIPs are water-soluble, have a uniform size in the nanometer range (Fig. 5) and exhibit high affinity and specificity for their corresponding targets with apparent dissociation constants in the nM range comparable to antigen-antibody interactions (Fig. 6) (Xu et al, 2016).

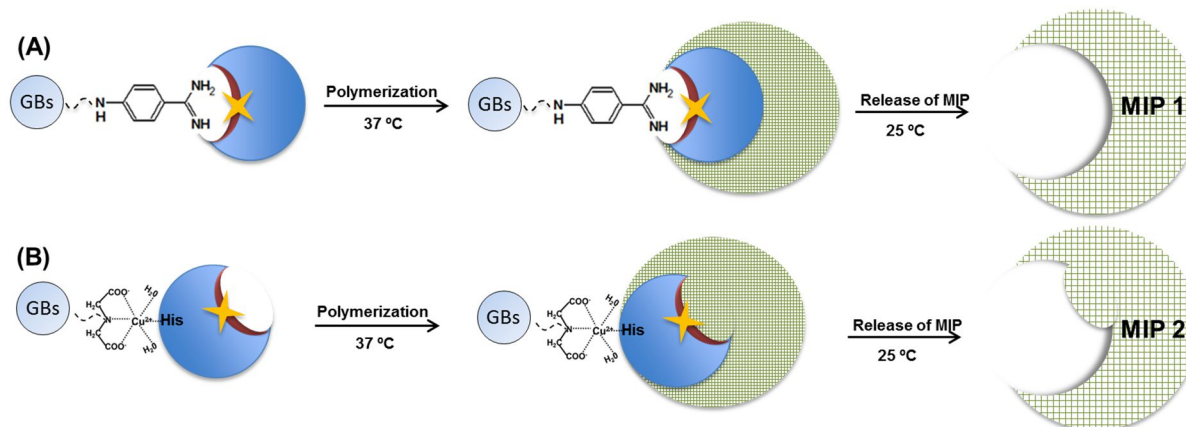


**Figure 2** Preparation of MIP-NPs wrapping different domains of the enzyme. (A) *p*-aminobenzamidine is immobilized on glass-beads (GBs) to attract the enzyme via its active site, represented by a star; (B) Cu<sup>2+</sup>-chelate is immobilized on GBs to attract the enzyme via its surface histidine, leaving its active site free. This orientated conformation of the enzyme will in turn yield MIP-NPs interacting with different locations of the enzyme.

Moreover, the different orientations of the enzymes on the solid-phase give rise to MIP-NPs that bind different locations on the enzymes. From Fig. 2A, we can see that the resulting MIPs immobilized via PAB, which we will hereafter call MIP1, should wrap but not inhibit their target enzymes. MIP1 has a binding site orientation such that when it binds the target enzyme, access of the substrate to the enzyme's active site is not blocked. On the other hand, the MIPs obtained using immobilization via the immobilized metal-chelate, hereafter referred to as MIP2, should wrap the enzymes but could also perturb the enzyme's active site (Fig. 2B).

Due to this oriented selective binding of MIP1 and MIP2, we further tested them as stabilizing agents for protecting the enzymes from thermal and pH denaturation. Trypsin is the most frequently used protease in proteomics experiments and also in numerous biotechnological processes, where high temperature processing is often required (Li, Xiong, Yang, Peng, Peng & Zhao, 2012; Vandermarliere, Mueller & Martens, 2013), but it is not

stable at high temperatures and also rapid autolysis occurs under basic pHs (Šebela et al, 2006). Therefore maintaining stability of this enzyme would be useful in several domains of biotechnological research. Our results show that MIP1<sub>Trypsin</sub> is able to protect trypsin from thermal denaturation at 45 °C and pH 7.8 but not MIP2<sub>Trypsin</sub>, which tends to inactivate the enzyme (Fig. 7A), in accord with our hypothesis.

In contrast to trypsin, kallikrein is thermally stable up to 60 °C and even retains considerable activity (70%) at 80 °C but it is denatured at low pHs (Raspi, 1996; Zuber & Sache, 1972; Chao, Shen, Gao, Xia, Bledsoe & Chao, 2010). Kallikrein MIPs are herein tested as protective agents against low pH denaturation. Our results show that MIP1<sub>Kallikrein</sub> slows down the denaturation of kallikrein at pH 4, almost suppressing it, whereas MIP2<sub>Kallikrein</sub> is less efficient (Fig. 7B). The development of such polymeric stabilizers for kallikrein would be useful, for instance to protect kallikrein from low pH environment like in the stomach, when kallikrein is administered as an oral drug for treating hypertension and other diseases (Overlack, Stumpe, Kolloch, Ressel & Krueck, 1981; Chao et al, 2010).

This solid-phase synthesis strategy can certainly be generalized to prepare MIP-NPs of other proteins. These soluble artificial antibodies can be very attractive and useful for a broad range of applications in the field of biotechnological and biomedical processes where enzyme stabilization is required (Guerreiro et al, 2014; Liu, Zhai, Dong & Zhao, 2015) or in medicine as therapeutic agents (Hoshino, Kodama, Okahata & Shea, 2008).

## 2. PROTOCOLS

The solid-phase synthesis of MIP-NPs is composed of 3 main parts:

- Activation of the GBs
- Functionalization with the affinity ligands (PAB and IDA-Cu<sup>2+</sup>)
- Immobilization of the enzyme and synthesis of the MIP-NPs

### Safety and Precautions

Wear personal protective equipment such as laboratory coat, safety glasses, disposable gloves and perform experiments under the fume cupboard when manipulating toxic and hazardous chemicals. Dispose of the resulting waste (solid and liquid) in the dedicated containers.

### General equipment

- Milli-Q purification water system (Millipore, France)
- Laboratory heating/drying oven (Mettler GmbH + Co. KG, Germany)
- Advanced Hot Plate Stirrer (VWR, France)
- Stovall Belly Dancer Laboratory Shaker (Stovall Life Science Inc, USA)
- Analytical electronic balance EX324, Explorer® (OHAUS Europe GmbH, Switzerland)
- Quanta FEG 250 scanning electron microscope (FEI Europe, Netherlands)
- Cary 60 UV-Vis spectrophotometer (Agilent Technologies, France)
- Zeta-sizer NanoZS (Malvern Instruments Ltd., UK) for dynamic light scattering (DLS) analysis

- JEM-2100F transmission electron microscope (JEOL Ltd., Japan) and 300 mesh carbon-coated copper grid from AGAR Scientific (Stansted, UK).
- Allegra 64R centrifuge (Beckman Coulter, France)
- Freeze dryer Alpha 1-4 LD plus (SciQuip LTD, UK)
- Magnetic agitator (ROTH Sochiel E.U.R.L., France)
- pH meter (Mettler-Toledo SAS, France)
- FluoroLog-3 spectrofluorimeter (Horiba Jobin Yvon, France)

## **2.1 Activation of glass-beads**

### **Equipment**

- 1L Erlenmeyer flask (VWR, 89085-018)
- Silicone oil TECHNICAL for oil baths (VWR, France, 24610.363)
- Glass funnel (VWR, LENZ5.3180.33)
- Filter paper (VWR, grade 413, 516-0820)
- Tea strainer (local supermarket)
- pH paper (ROTH Sochiel E.U.R.L, C728.1)

### **Reagents**

- Glass beads, diameter 0.1 mm (Roth Sochiel E.U.R.L., N029.1)
- Milli-Q water
- Sodium hydroxide (VWR, 28245.298)

*Prepare 4 M sodium hydroxide in water*

- Acetone AR (Biosolve Chimie, France, 01030505)

## **Method**

1. Activate the GBs by boiling in 4 M NaOH (typically 100 g GBs in 100 mL NaOH) for 10 min in a 1L Erlenmeyer flask placed in an oil-bath thermostated at 100 °C, so as to introduce – OH groups on their surface.
2. Decant the activated GBs on a funnel fitted with a filter paper and wash with 8 x 250 mL water to ensure that all the NaOH is removed (pH of water 6.5), followed by 250 mL acetone.
3. Dry in an oven at 50 °C for 6 h. Sieve with a tea strainer to remove aggregated GBs.

*The activated GBs can be stored at 8 °C for 6 months without any alteration.*

## **2.2 Functionalization of glass-beads**

### **Equipment**

- Glass Petri dish, diameter of 200 mm (VWR, 391-0477)
- 500 mL round-bottom flask (VWR, 201-1383)
- Reflux condenser (VWR, 89053-824)
- Oil bath

### **Reagents**

- Activated GBs as prepared in section 2.1

- Toluene anhydrous (99.8%) (Sigma-Aldrich, France, 244511)

- (3-Aminopropyl)triethoxysilane (APTES) (Sigma-Aldrich, A3648)

*Prepare 2% (v/v) of APTES in anhydrous toluene*

- Sodium phosphate dibasic heptahydrate, ACS (VWR, BDH9296)

- Sodium phosphate monobasic monohydrate, ACS (VWR, BDH9298)

- Sodium chloride, ACS (VWR, BDH9286)

*Prepare 100 mM sodium phosphate buffer + 150 mM NaCl, pH 7.4 (buffer A)*

- Glutaraldehyde (50% in water, Sigma-Aldrich, 340855)

*Prepare 5% (v/v) glutaraldehyde solution in buffer A*

- 4-Aminobenzamidine dihydrochloride (Sigma-Aldrich, 06880)

*Prepare 100 mM p-aminobenzamidine (PAB) in buffer A*

- Sodium borohydride (Sigma-Aldrich, 452882)

*Prepare 100 mg NaBH<sub>4</sub> in 100 mL buffer A*

- Ethanolamine 99.5% (Sigma-Aldrich, 411000)

*Prepare 41 mM ethanolamine solution in buffer A (0.25 mL ethanolamine 99.5% in 100 mL buffer A)*

- Ethanol (VWR, 1.00983.1000)

*Prepare 1 M NaCl in water:ethanol (4:1)*

- (3-glycidyloxypropyl)-trimethoxysilane (Glymo) (Sigma-Aldrich, 440167)
- Sodium carbonate (VWR, 27771.29)
- Iminodiacetic acid (IDA) (Sigma-Aldrich, 220000)

*Prepare 0.75 M IDA, 0.34 M NaCl and 2 M Na<sub>2</sub>CO<sub>3</sub> in water. The final pH is ~11*

## **Method**

### **A) Functionalization with *p*-aminobenzamidine**

The functionalization with PAB was performed as previously described (Ambrosini et al, 2013; Xu et al, 2016). A schematic representation of the procedure is shown in Fig. 3A.

- 1.** Place 100 g of activated GBs in a Petri dish and add 100 mL APTES (2%) in toluene, with gentle shaking on a Stovall Belly Dancer Laboratory Shaker overnight at room temperature.
- 2.** After silanization, wash the GBs on a funnel fitted with a filter paper with 2 x 250 mL toluene, 2 x 250 mL acetone, and dry in an oven at 50 °C for 3 h. Sieve with a tea strainer to remove aggregated GBs.
- 3.** Place the GBs on a Petri dish and add 100 mL of buffer A containing glutaraldehyde 5% (v/v), with shaking overnight on the Belly Dancer shaker, at 30 °C. Wash on filter paper with 7 x 250 mL water and 1 x 250 mL buffer A.
- 4.** Transfer the glutaraldehyde-functionalized GBs to a Petri dish and add 100 mL of buffer A containing 100 mM PAB; incubate with shaking on the Belly Dancer shaker at room temperature for 5 h. Wash the PAB-functionalized GBs on filter paper with 1 L buffer A.

5. Place the GBs in a Petri dish and add 100 mL buffer A containing 100 mg NaBH<sub>4</sub> (1 mg/mL) with shaking on the Belly Dancer shaker for 30 min at room temperature, to reduce the Schiff base. Wash the GBs on a filter paper with 1 L buffer A.

6. Transfer the GBs to a Petri dish and add 100 mL of buffer A containing 41 mM ethanolamine with shaking on the Belly Dancer shaker for 30 min so as to block the unreacted carbonyl groups.

7. Wash the GBs on filter paper with 2 x 250 mL buffer A, followed by 4 x 250 mL water (*see note 1*) for the determination of the amount of PAB bound to the GBs). Use immediately or store at 8 °C in a mixture of water:ethanol (4:1) containing 1 M NaCl.

*The GBs can be kept as such for 6 months without alteration.*

## **B) Functionalization with IDA-Cu<sup>2+</sup>**

Fig. 3B shows the procedure of derivatization of glass beads with IDA-Cu<sup>2+</sup>. Activated GBs are silanized with (3-glycidyloxypropyl)-trimethoxysilane (Glymo), as previously described (Lei, Xue, Zhong, Meng, Zhang & Zhang, 2013), with some modifications.

1. Incubate 50 g of activated GBs with a mixture of 200 mL of Glymo:toluene (1:1) in a 500 mL round-bottom flask equipped with a condenser and heat under reflux at 110 °C for 17 h.

2. After silanization, wash the GBs on a funnel fitted with a filter paper with 2 x 250 mL toluene, 2 x 250 mL acetone, and dry in an oven at 50 °C for 3 h. Sieve with a tea strainer to remove aggregated GBs.

3. Transfer the GBs to an Erlenmeyer flask of 1 L and add 500 mL of a mixture of 0.75 M IDA, 0.34 M NaCl and 2.0 M Na<sub>2</sub>CO<sub>3</sub> with gentle stirring using a magnetic agitator at 70 °C for 17 h. Wash on a filter paper with 8 x 250 mL water and dry the GBs on a Petri dish in an oven at 37 °C overnight. Sieve with a tea strainer to remove aggregated GBs.

*The IDA-functionalized GBs can be stored at 8 °C for 4 months without alteration.*

Before proceeding further, the integrity of the GBs after the different treatments was verified by scanning electron microscopy (SEM) (Fig. 4).

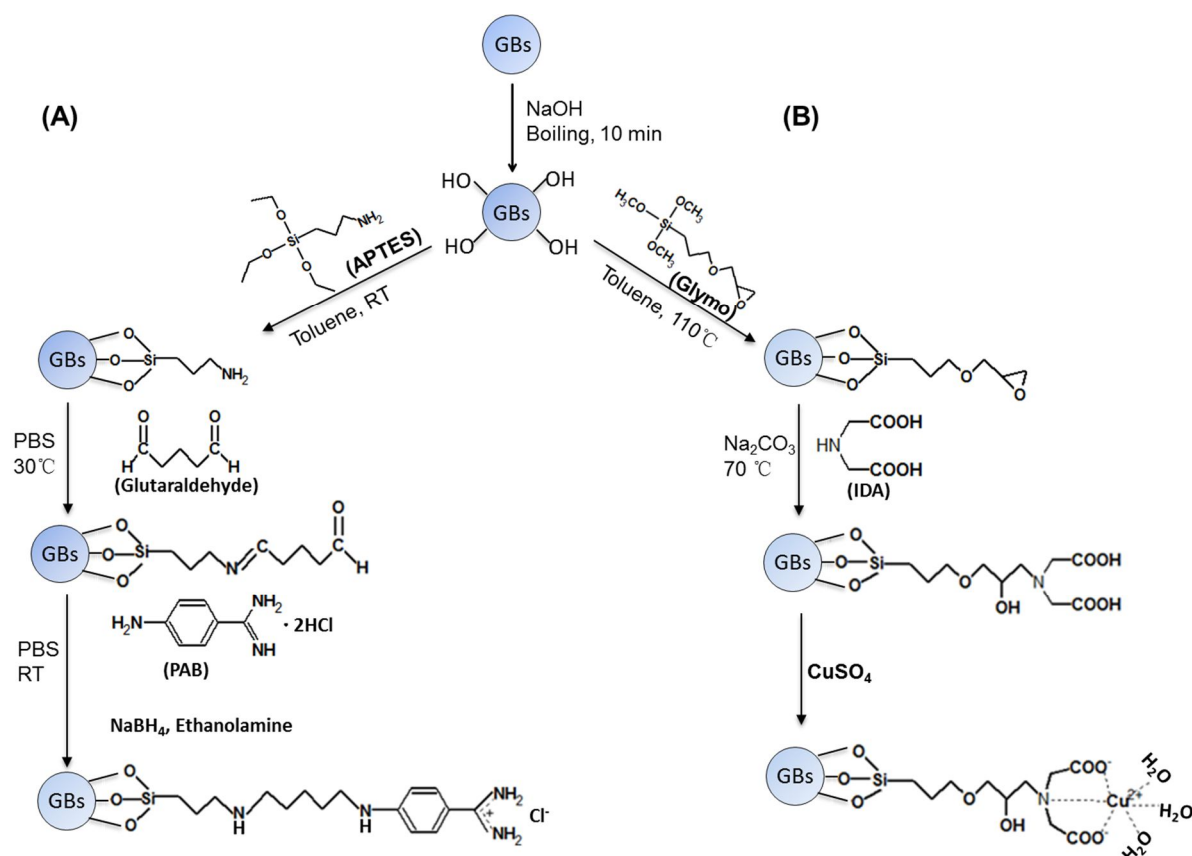


**Figure 3** Immobilization of (A) *p*-aminobenzamidine (PAB) and (B) IDA-Cu<sup>2+</sup>, on GBs.

*“Reprinted with permission from Xu, J., Ambrosini, S., Tamahkar, E., Rossi, C., Haupt, K., & Tse Sum Bui, B. (2016). Toward a universal method for preparing molecularly imprinted*

*polymer nanoparticles with antibody-like affinity for proteins. Biomacromolecules, 17(1), 345-353; Copyright 2016. American Chemical Society”*

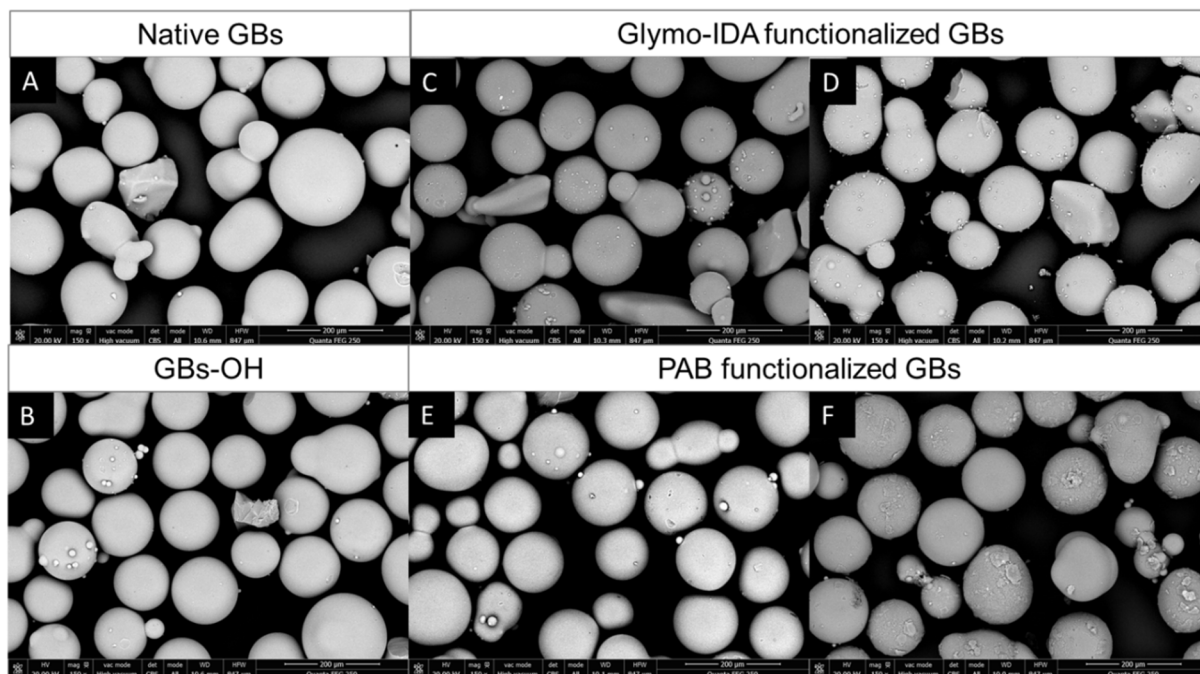


**Figure 4.** SEM image of glass-beads in their (A) native state; after (B) boiling in 4 M NaOH; (C) refluxing with Glymo in toluene at 110 °C; (D) stirring with IDA at 70 °C; (E) shaking with APTES in toluene; (F) shaking with glutaraldehyde and PAB.

### 2.3 Enzyme immobilization and synthesis of MIP-NPs

#### Equipment

- Glass column with a thermostated jacket (XK26/40, GE Healthcare, France) with adapters (XK26, GE Healthcare, France)
- Circulating thermostated water-bath (Bioblock Scientific Polystat 5, Fischer Scientific, France)
- Peristaltic pump (ISMATEC Rotary Piston Pumps, REGLO-CPF Analog, Germany)

- Nitrogen gas (Air Liquide, France)
- Glass beakers (VWR, 10754-948)
- Quartz cuvettes (Hellma Analytics, 100-5-20)

## **Reagents**

- 25 mM sodium phosphate buffer pH 7 (buffer B)
- *N*-isopropylacrylamide (NIPAM) (Sigma-Aldrich, 415324)
- *N,N'*-ethylenebis(acrylamide) (EbAm) (Sigma-Aldrich, 358878)
- Potassium persulfate (KPS) (Sigma-Aldrich, 379824)
- *N,N,N',N'*-tetramethylethylenediamine (TEMED) (Sigma-Aldrich, T9281)
- Trypsin from bovine pancreas (Sigma-Aldrich, T8003)

*Prepare 0.5 or 1 mg/mL trypsin in buffer B*

- Kallikrein from porcine pancreas (Sigma-Aldrich, K3627)

*Prepare 0.5 or 1 mg/mL kallikrein in buffer B*

- Bradford reagent (Sigma-Aldrich, B6916)
- Copper (II) sulfate (Sigma-Aldrich, 451657)

*Prepare 50 mM CuSO<sub>4</sub> in H<sub>2</sub>O*

- Ethylenediaminetetraacetic acid (EDTA) (Sigma-Aldrich, 431788)

*Prepare 100 mM EDTA in H<sub>2</sub>O*

## **Method**

A glass column with a thermostated jacket whose bed height can be adjusted with adapters was used. The temperature of the column was regulated by circulating water from a thermostated water-bath. The solvents were pumped into the column using a peristaltic pump at a flow-rate of 2.5 mL/min, unless stated otherwise.

### **A. Immobilization on PAB-functionalized GBs**

1. Suspend 95 g of functionalized GBs in 20 mL water and pour into the glass column closed at the bottom with an adapter. Add more water to pack the column; this corresponds to a bed height of 10 cm. Insert the top adapter to close the column.
2. Connect the column to the peristaltic pump and pump 100 mL water at a high flow rate of 3.7 mL/min so as to expel the air bubbles trapped in between the GBs.
3. Equilibrate the GBs with 200 mL buffer B.
4. Inject 25 mL of a trypsin or kallikrein solution (0.5 mg/mL) at a flow-rate of 1.2 mL/min; the flow-through is collected and passed through the column again for 1 h.
5. Wash the unbound protein by passing 300 mL buffer B.

*The amount of bound trypsin and kallikrein is  $1.9 \pm 0.2$  nmol and  $1.4 \pm 0.3$  nmol per g of GBs respectively (Xu et al, 2016).*

- 6.** Meanwhile, prepare the polymerization mixture. Mix (246.2 mg, 2.18 mmol) NIPAM and (19.2 mg, 0.114 mmol) EbAm (95:5 molar ratio) in 53 mL buffer B. Purge the solution with a flow of nitrogen gas for 30 min. Add the initiator composed of KPS (18.5 mg in 500  $\mu$ L buffer A) and TEMED (1.35  $\mu$ L).
- 7.** Pump the polymerization mixture through the column and switch on the circulating water-bath to set and maintain the temperature of the column to 37 °C for 15 h (overnight).
- 8.** To remove the low-affinity polymers and unreacted monomers, wash the column by volumes of 50 mL buffer B (warmed beforehand to 37 °C). Normally 5 volumes of 50 mL buffer B is needed. Check by dynamic light scattering that the last fraction does not contain any particles before proceeding to the next step.
- 9.** Leave the column to cool to room temperature. Elute the MIP-NPs by passing 5 mL volumes of buffer B. Normally 10 fractions are collected. Analyze the fractions by DLS.
- 10.** Perform enzymatic activity (*See note 2*) and Bradford assay on all the eluted fractions so as to check for the eventual leakage of the enzymes.
- 11.** To verify if the immobilized enzyme is not denatured during the polymerization procedure, at the end of the experiment, wash the column with a mixture of 10 mM HCl + 0.5 M NaCl (3 x 50 mL) to desorb the protein and determine its activity by enzymatic assay. The enzyme should be active (Ambrosini et al, 2013).

## **B. Immobilization on IDA-Cu<sup>2+</sup> functionalized GBs**

- 1.** Suspend 50 g of functionalized GBs in 20 mL water and pour into the glass column closed at the bottom with an adapter. Add more water to pack the column; this corresponds to a bed height of 5.5 cm. Insert the top adapter to close the column.
- 2.** Connect the column to the peristaltic pump and pump 100 mL water at a high flow rate of 3.7 mL/min so as to expel the air bubbles trapped in between the GBs.
- 3.** Saturate the GBs with Cu<sup>2+</sup> by passing 250 mL of 50 mM CuSO<sub>4</sub> solution; excess Cu<sup>2+</sup> is removed by passing 150 mL water. The GBs are tainted with a uniform blue color.
- 4.** Equilibrate the column with 150 mL buffer B.
- 5.** Inject 50 mL of trypsin or kallikrein (1 mg/mL) through the column at a flow-rate of 1.2 mL/min; the flow-through is collected and passed through the column again for 1 h.
- 6.** Wash the unbound enzyme with 250 mL buffer B.  
  
*The amount of bound trypsin and kallikrein is  $15.9 \pm 0.8$  nmol and  $14.2 \pm 1.2$  nmol per g of GBs respectively (Xu et al, 2016).*
- 7.** Synthesize and recover the MIP-NPs as described above for the PAB functionalized GBs (Steps 6-9).
- 8.** Perform enzymatic activity (*See note 2*) and Bradford assay on all the eluted fractions so as to check for the eventual leakage of the enzymes.

9. Determine any presence of  $\text{Cu}^{2+}$  in all the eluted fractions by measuring the absorbance at 733 nm of a complex  $\text{Cu}^{2+}$ -EDTA (Xu et al, 2016).

### 3. PHYSICOCHEMICAL CHARACTERIZATION OF MIP-NPs

#### Equipment

- Disposable plastic cuvettes (VWR, 97000-590)
- 50 mL Oak Ridge, Nalgene centrifuge tubes (VWR, 525-2244)
- Dialysis membrane of 6-8 kDa cut-off (ROTH Sochiel E.U.R.L., 4570.1)

#### Method

1. Perform DLS analysis on all eluted fractions; MIPs having similar sizes and dispersities are pooled to constitute the stock of MIP-NPs (Fig. 5, Table 1).

*The MIP-NPs are very stable at 8 °C as no aggregation is observed for a period of six months (as verified by DLS analysis).*

2. In order to determine the concentration of the stock solution, pipet 2 mL of MIP-NPs in a centrifuge tube and centrifuge at 40,000g for 1 h at 37 °C. Discard the supernatant by inverting the tube. Resuspend the precipitate in 2 mL of water and transfer to a 5-mL Eppendorf tube weighed beforehand. Rinse twice successively with 1 mL water and transfer to the 5-mL tube for lyophilization overnight. Weigh the dry MIP-NPs.

*Tip: the centrifuge machine must be preheated at 37 °C before centrifuging the MIP. The*

*supernatant must be discarded rapidly so as to avoid loss of MIP caused by temperature change.*

Typically, concentrations of MIP-NPs for proteins immobilized via PAB (MIP1<sub>trypsin</sub> and MIP1<sub>kallikrein</sub>) of ~0.6 mg/mL and via IDA-Cu<sup>2+</sup> (MIP2<sub>trypsin</sub> and MIP2<sub>kallikrein</sub>) of ~1.2 mg/mL are obtained. Knowing the mass of GBs and the total volume of stock MIP-NPs, the yield of MIP synthesis can be calculated, as milligrams of MIP-NPs per gram of GBs (Table 1).

3. Determine the morphology of the stock MIP-NPs by transmission electron microscopy (TEM) imaging. For this, dialyse 2 mL of the stock MIP-NPs overnight in 1 L of water using a dialysis membrane of 6-8 kDa cut-off.

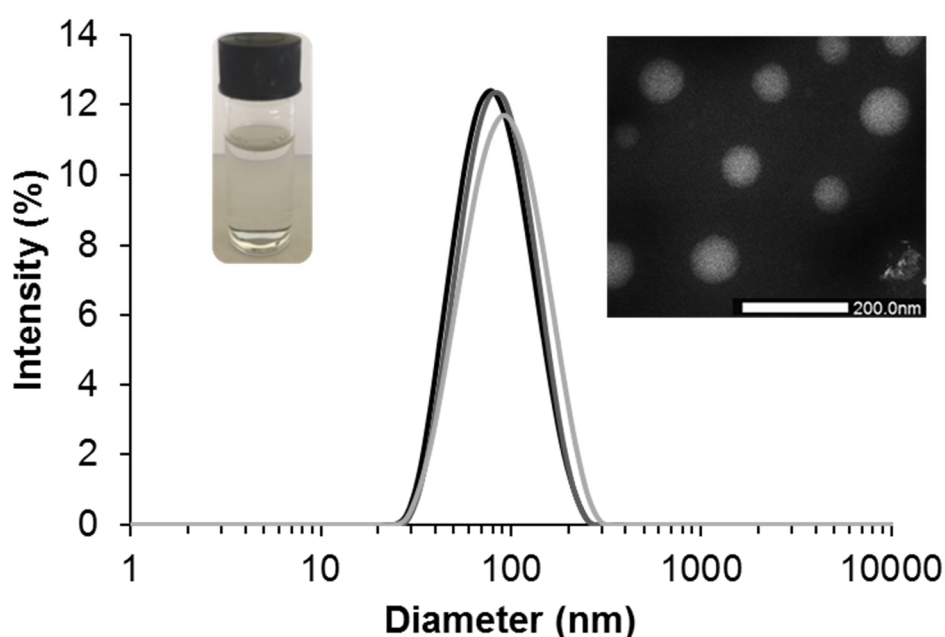


**Figure 5** Physicochemical characteristics of trypsin-imprinted MIP-NPs obtained on PAB functionalized GBs. From left to right: 1 mg/mL MIP-NPs in water appears as a transparent solution at 25 °C; Size distribution as measured by DLS (n=3); TEM image.

**Table 1** Physicochemical characteristics of MIP-NPs

MIPs <sup>a</sup>	Diameter (nm)	Polydispersity index	Yield
	n = 3		(mg/g GBs)
MIP1 <sub>Trypsin</sub>	119 ± 5	0.278	0.32 ± 0.02
MIP1 <sub>Kallikrein</sub>	97 ± 3	0.319	0.36 ± 0.04
MIP2 <sub>Trypsin</sub>	70 ± 6	0.284	0.45 ± 0.03
MIP2 <sub>Kallikrein</sub>	106 ± 5	0.395	0.65 ± 0.03

<sup>a</sup> MIP1 are obtained with the template enzymes immobilized on PAB, and MIP2 on IDA-Cu<sup>2+</sup>.

#### **4. EVALUATION OF THE BINDING CHARACTERISTICS OF MIP-NPs USING A QUARTZ CRYSTAL MICROBALANCE**

##### **Equipment**

- Silicon dioxide coated crystals (QSX 303) (Lot Quantum Design, France)
- UV/ozone cleaner (ProCleaner<sup>TM</sup> 220, BioForce Nanosciences, USA)
- Q-Sense E1 instrument and Q-sensor holder (Biolin Scientific, Sweden)
- Peristaltic pump (ISMATEC Rotary Piston Pumps, REGLO-CPF Analog, Germany)

##### **Reagents**

- Ammonium hydroxide, ACS, 28% (VWR, L13168.AU)
- Hydrogen peroxide 35% (Sigma-Aldrich, 1.08556.9025)

*Prepare NH<sub>4</sub>OH (28%)/H<sub>2</sub>O<sub>2</sub> (35%)/H<sub>2</sub>O (1/1/6, v/v/v)*

- Anhydrous toluene, APTES, acetone, 5% glutaraldehyde, 100 mM PAB, Glymo, IDA, CuSO<sub>4</sub>, buffer A, buffer B, trypsin (2 mg trypsin in 2 mL buffer B), kallikrein (2 mg kallikrein in 2 mL buffer B) as described in the previous sections

- 0.6, 1.2, 2.4, 4.8, 9.6 and 50 µg/mL MIP 1<sub>trypsin</sub> prepared in buffer B, diluted from the stock (0.6 mg/mL)

- 0.6, 1.2, 2.4, 4.8, 9.6 and 50 µg/mL MIP 1<sub>kallikrein</sub> prepared in buffer B, diluted from the stock (0.6 mg/mL)

- 2.5, 10, 25, 50, 100 and 250 µg/mL MIP 2<sub>trypsin</sub> prepared in buffer B, 5 mL each, diluted from the stock (1.2 mg/mL)

- 2.5, 10, 25, 50, 100 and 250 µg/mL MIP 2<sub>kallikrein</sub> prepared in buffer B, 5 mL each, diluted from the stock (1.2 mg/mL)

## **Method**

A quartz crystal microbalance (QCM) sensor was employed to evaluate the binding affinity and capacity of the MIP-NPs. All measurements were performed with a Q-Sense E1 in a flow-through mode using a peristaltic pump (flow rate: 50 µL/min). The functionalization of the QCM crystal (with IDA-Cu<sup>2+</sup> or PAB and further immobilization of the protein) was carried out at 25 °C, whereas the binding experiments with the MIP-NPs were performed at 37 °C. All manipulations of the QCM crystals were done with tweezers.

### **A. Cleaning and activation of QCM crystals**

1. Place 4 silicon dioxide coated sensor crystals in a Q-sensor holder and immerse in a glass beaker containing 80 mL of  $\text{NH}_4\text{OH}$  (28%)/ $\text{H}_2\text{O}_2$  (35%)/ $\text{H}_2\text{O}$  (1/1/6, v/v/v).
2. Put the beaker in a water-bath at 70 °C for 10 min.
3. Rinse each crystal with 5 x 5 mL water, dry under nitrogen gas.
4. Place the QCM crystals under UV/ozone irradiation (ProCleaner™ 220) for 10 min for further cleaning.
5. Rinse each crystal with 5 x 5 mL water, dry under nitrogen gas.

### **B. Functionalization with PAB, enzyme immobilization and binding with $\text{MIP1}_{\text{Trypsin}}$ and $\text{MIP1}_{\text{Kallikrein}}$**

1. Place the 4 QCM crystals in a 50 mL glass beaker containing 5 mL toluene and 5 mL APTES; incubate with gentle shaking on a Belly dancer Shaker overnight at room temperature.
2. Rinse each crystal with 5 x 5 mL toluene followed by 5 x 5 mL acetone; dry them under nitrogen gas.
3. Place the QCM chips into 10 mL of buffer A containing 5% glutaraldehyde in the beaker, incubate them on a Belly dancer Shaker overnight at room temperature.
4. Rinse each crystal with 10 x 5 mL buffer A, dry under nitrogen gas.

*Glutaraldehyde functionalized crystals can be stored at 8 °C for one week without alteration.*

**5.** Place the crystal in the flow-module of the Q-Sense Instrument and pass buffer A until a stable baseline is reached.

*Here, start monitoring the change in frequency ( $\Delta F$ ).*

**6.** Pass buffer A containing 100 mM PAB until saturation is observed.

**7.** After functionalization with PAB, wash the module with buffer B until the baseline is stable for more than 15 min.

**8.** Pump 2 mL of trypsin or kallikrein (1 mg/mL) through the sensor until saturation is observed, and then wash with buffer B for 15-30 min until the signal is stable.

**9.** Meanwhile, prepare 5 mL aliquots of MIP1<sub>Trypsin</sub> and MIP1<sub>Kallikrein</sub> at concentrations of 0.6, 1.2, 2.4, 4.8, 9.6 and 50 µg/mL and place in a water-bath at 37 °C.

**10.** Set the temperature control of the QCM apparatus to 37 °C. When the temperature is stable, wash with buffer B at 37 °C until the baseline is stable for more than 15 min.

**11.** Inject each concentration of MIP1<sub>Trypsin</sub> or MIP1<sub>Kallikrein</sub> at 37 °C for 30 min until saturation is observed. Between each concentration, wash with buffer B for 15-30 min until the signal is stable.

**12.** Inject MIP1<sub>Trypsin</sub> or MIP1<sub>Kallikrein</sub> 1 (0.6 to 50 µg/mL) sequentially on PAB functionalized GBs alone so as to investigate the contribution of non-specific interactions. Non-specific

interactions (Fig. 6(A-B, light-colored lines) proved to be low.

These results show that trypsin and kallikrein-imprinted MIP-NPs were specific as they bind their respective template proteins to a higher extent than the other parts of the GBs.

### **C. Functionalization with IDA-Cu<sup>2+</sup>, enzyme immobilization and binding with MIP<sub>2</sub><sub>Trypsin</sub> and MIP<sub>2</sub><sub>Kallikrein</sub>**

1. Place the 4 QCM chips in a 50 mL glass beaker containing 5 mL toluene and 5 mL Glymo; incubate on a Belly dancer shaker overnight at room temperature.

2. Rinse each crystal with 5 x 5 mL toluene followed by 5 x 5 mL acetone; dry them under nitrogen gas.

3. Place the QCM chips in a glass beaker containing 10 mL of 0.75 M iminodiacetic acid (IDA), 0.34 M NaCl and 2.0 M Na<sub>2</sub>CO<sub>3</sub> in water; put the beaker in an oven maintained at 70 °C for 4 h.

4. Rinse each crystal with 10 x 5 mL water, dry under nitrogen gas.

*IDA functionalized chips can be stored at 8 °C for 2 weeks without alteration.*

*Here, start monitoring the change in frequency ( $\Delta F$ ).*

5. Place the crystal in the flow-module of the QCM apparatus, and pass 50 mM CuSO<sub>4</sub> solution until saturation is observed, then wash with water for ~30 min until the signal is stable.

6. After charging with  $\text{Cu}^{2+}$ , wash the system with buffer B until the baseline is stable for more than 15 min.
7. Pump 2 mL of trypsin or kallikrein (1 mg/mL) onto the IDA- $\text{Cu}^{2+}$  functionalized QCM sensor (saturation is observed), and then wash with buffer B for 15-30 min until the signal is stable.
8. Meanwhile, prepare 5 mL aliquots of  $\text{MIP2}_{\text{Trypsin}}$  or  $\text{MIP2}_{\text{Kallikrein}}$  at concentrations of 2.5, 10, 25, 50, 100, 250  $\mu\text{g/mL}$  and place in a water-bath at 37 °C.
9. Set the temperature control of the QCM apparatus to 37 °C. When the temperature is stable, wash with buffer B at 37 °C until the baseline is stable for more than 15 min.
10. Inject each concentration of  $\text{MIP2}_{\text{Trypsin}}$  or  $\text{MIP2}_{\text{Kallikrein}}$  at 37 °C for 30 min until saturation is observed. Between each concentration, wash with buffer B for 15-30 min until the signal is stable.
11. Inject  $\text{MIP2}_{\text{Trypsin}}$  or  $\text{MIP2}_{\text{Kallikrein}}$  2 (2.5 to 250  $\mu\text{g/mL}$ ) sequentially on IDA- $\text{Cu}^{2+}$  functionalized GBs alone (Fig. 6 (C-D, pale-colored lines)), so as to investigate the contribution of non-specific interaction. In both cases, binding of MIPs to their respective templates was high, indicating the creation of imprinted sites.

Overall, these results imply that the MIP-NPs synthesized by the solid-phase approach are specific towards their corresponding templates. Calculated apparent dissociation constants ( $K_{\text{dapp}}$ ) for all MIP-NPs (*see note 3*) were obtained by nonlinear fitting of the data to a single-

site Langmuir-type binding isotherm and are shown in Fig. 6.

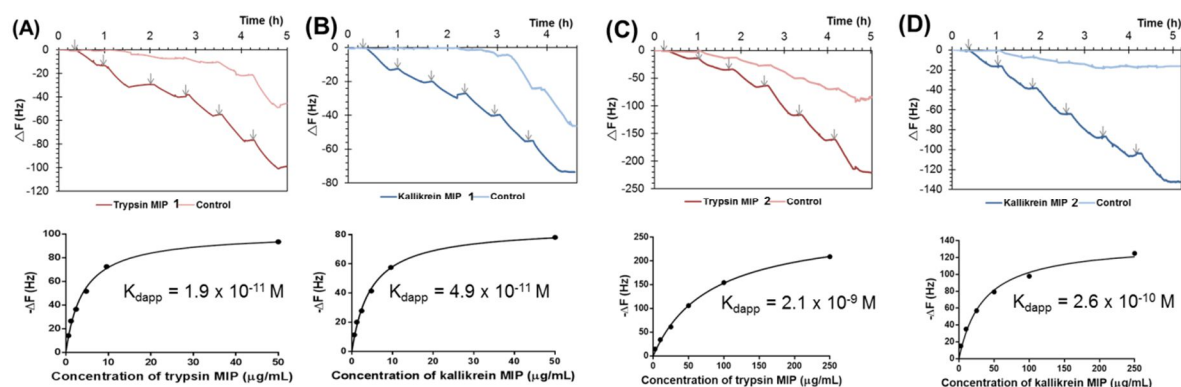


**Figure 6** Time course of the frequency change ( $\Delta F$ ), on PAB-derivatized QCM sensor of (A) immobilized trypsin and (B) immobilized kallikrein, following injection of MIP<sub>1</sub><sub>Trypsin</sub> and MIP<sub>1</sub><sub>Kallikrein</sub> respectively; on Cu<sup>2+</sup> chelate-derivatized sensor of immobilized (C) trypsin with MIP<sub>2</sub><sub>Trypsin</sub> and (D) kallikrein with MIP<sub>2</sub><sub>Kallikrein</sub>, in 25 mM sodium phosphate buffer pH 7, at 37 °C. Injections at the time point are indicated by the arrows and the concentrations were 0.6, 1.2, 2.4, 4.8, 9.6 and 50  $\mu\text{g/mL}$  on PAB-derivatized QCM sensor and 2.5, 10, 25, 50, 100, 250  $\mu\text{g/mL}$  on Cu<sup>2+</sup> chelate-derivatized sensor. Control means injection of the MIP on immobilized ligand only. Measurements were performed three times independently with two batches of MIPs. Corresponding binding isotherms of the MIPs for their respective targets are shown below. “Adapted with permission from Xu, J., Ambrosini, S., Tamahkar, E., Rossi, C., Haupt, K., & Tse Sum Bui, B. (2016). Toward a universal method for preparing molecularly imprinted polymer nanoparticles with antibody-like affinity for proteins. *Biomacromolecules*, 17(1), 345-353; Copyright 2016. American Chemical Society”

## 5. MIP-NPs PROTECT ENZYME FROM THERMAL AND pH DENATURATION

### Equipment

- Gilson Pipetman P1000, P100, P20
- 50 mL Oak Ridge, Nalgene centrifuge tubes (VWR, 525-2244)
- 4 mL glass tubes (VWR, 548-0051)
- Water-bath (Bioblock Scientific Polystat 5, Fischer Scientific, France)
- Digital thermometer (VWR, TD10 type T)

### A. Protection of trypsin by MIP1<sub>Trypsin</sub> against thermal inactivation at 45 °C

### Reagents

- Hydrochloric acid, 37% (VWR, 20252.290)
- Calcium chloride (Sigma-Aldrich, C5670)

*Prepare a solution of 1 mM HCl + 10 mM CaCl<sub>2</sub> in water, the pH is ~5*

-Trypsin

*Prepare 50 μM trypsin in 1 mM HCl + 10 mM CaCl<sub>2</sub>*

- Tris base (Sigma-Aldrich, T1378)

*Prepare 50 mM Tris-HCl pH 8. Use Tris base and adjust the pH with 1 M HCl*

- *N*<sub>α</sub>-*p*-tosyl-*L*-arginine methyl ester hydrochloride (TAME) (Sigma-Aldrich, T4626)

*Prepare 10 mM TAME in 50 mM Tris-HCl pH 8*

- 50 mM sodium phosphate buffer pH 8

- MIP1<sub>Trypsin</sub> (11 mg/mL, obtained by centrifuging 10 mL of MIP1<sub>Trypsin</sub> in a centrifuge tube at 40,000g at 37 °C, then dissolving the precipitate with the required volume of buffer B at room temperature).

- MIP2<sub>Trypsin</sub> (11 mg/mL in buffer B).

## **Method**

Thermal inactivation of trypsin was done at 45 °C. This temperature was chosen because it is the maximum temperature at which the MIP stays soluble. MIP2<sub>Trypsin</sub> and buffer B alone (no polymer) were used as controls.

1. To 3 separate glass tubes of 4 mL, pipet 900 μL of 50 mM sodium phosphate buffer pH 8 and place in a water bath at 45 °C.

*Tip: Use a water bath instead of a dry block heater since the former produces a more homogeneous heating*

2. In three 4 mL glass tubes containing separately 90 μL of MIP1<sub>Trypsin</sub> (11 mg/mL) or MIP2<sub>Trypsin</sub> (11 mg/mL) (final concentration: 1 mg/mL, final volume: 1 mL) or buffer B alone, add 10 μL of a stock solution of 50 μM trypsin (final concentration: 500 nM). Incubate in a

water-bath at 37 °C for 30 min. Transfer the contents to tubes **1** (final pH 7.8, verified with a pH meter) and incubate at 45 °C.

**3.** Withdraw 100 µL from each tube every hour, starting from t=0 to t=6h; determine residual trypsin activity by assay with TAME at 25 °C (*see note 2*).

### **B. Protection of kallikrein by MIP1<sub>Kallikrein</sub> against pH inactivation**

#### **Reagents**

- Stock solution of 50 µM kallikrein in water
- MIP1<sub>Kallikrein</sub> (10 mg/mL in buffer B).
- MIP2<sub>Kallikrein</sub> (10 mg/mL in buffer B).
- Sodium acetate (Sigma-Aldrich, S2889)
- Acetic Acid, >99.7%, ACS (VWR, BDH3092-500MLP)

*Prepare 100 mM sodium acetate buffer pH 4*

- N<sub>α</sub>-benzoyl-L-arginine ethyl ester hydrochloride (BAEE) (Sigma-Aldrich, B4500)

*Prepare 10 mM BAEE in 50 mM Tris-HCl pH 8.7*

#### **Method**

**1.** In 3 glass tubes of 4 mL containing separately 100 µL of MIP 1<sub>kallikrein</sub> (10 mg/mL) or MIP2<sub>Kallikrein</sub> (10 mg/mL) (final concentration: 1 mg/mL, final volume: 1 mL) or buffer B

alone, add 10  $\mu\text{L}$  of a stock solution of 50  $\mu\text{M}$  kallikrein (final concentration: 500 nM). Adjust the volume to 500  $\mu\text{L}$  with buffer B. Incubate in a water-bath at 37  $^{\circ}\text{C}$  for 1 h. The temperature was additionally verified with a digital thermometer (accuracy: 0.1  $^{\circ}\text{C}$  in the used temperature range).

2. Add 500  $\mu\text{L}$  of 100 mM sodium acetate buffer pH 4 to the 3 tubes (the pH stays 4, as verified by pH paper).

3. Withdraw 100  $\mu\text{L}$  from each tube every hour, starting from  $t=0$  to  $t=4\text{h}$ ; determine residual kallikrein activity by assay with BAEE at 25  $^{\circ}\text{C}$  (*see note 2*).

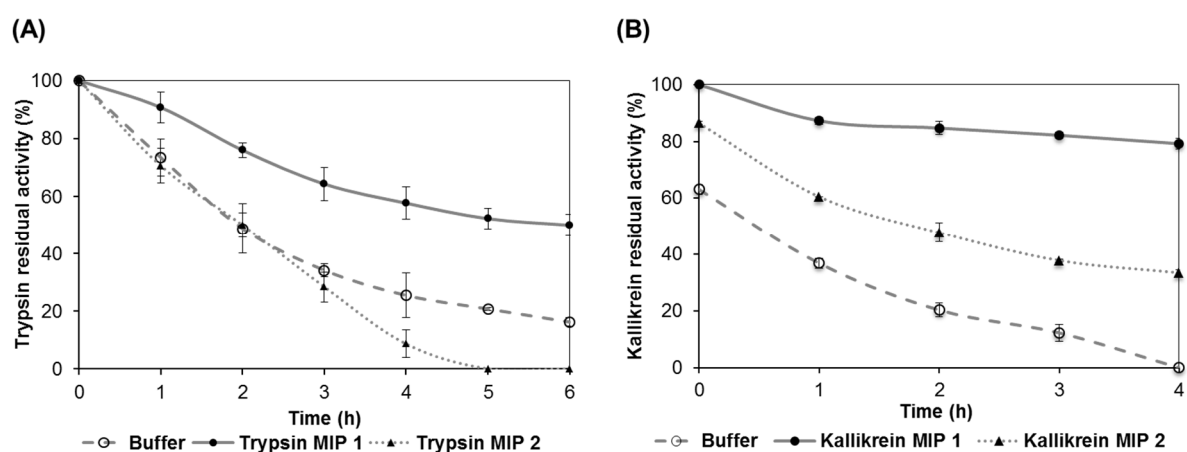


**Figure 7** Residual activity of (A) trypsin incubated without polymer (dashed line) or with 1 mg/mL MIP1<sub>Trypsin</sub> (full line) or MIP2<sub>Trypsin</sub> (dotted line) in 50 mM sodium phosphate buffer pH 7.8 at 45  $^{\circ}\text{C}$ ; (B) kallikrein incubated without polymer (dashed line) or with 1 mg/mL MIP1<sub>Kallikrein</sub> (full line) or MIP2<sub>Kallikrein</sub> (dotted line) in 100 mM sodium acetate buffer pH 4 at 37  $^{\circ}\text{C}$ . Data are means from three independent experiments with three different batches of polymers. The error bars represent standard deviations.

## 6. CONCLUDING REMARKS

The synthesis of soluble nanosized molecularly imprinted polymers for proteins, based on a solid-phase approach was described. Glass beads (GBs) were functionalized with affinity ligands for specific recognition and binding of the target proteins. This configuration enabled an oriented immobilization of the proteins, upon which thermoresponsive MIP-NPs were synthesized. The GBs play the role of both a reactor and a separation column since, after synthesis, the MIP-NPs were released from the support by a simple temperature change, resulting in protein-free polymers. This solid-phase synthesis approach is versatile and can be generalized to the synthesis of MIP-NPs for any serine protease inhibited by PAB or any enzyme bearing surface histidine residues and potentially, engineered proteins bearing a His-tag. In the latter case,  $\text{Ni}^{2+}$  associated with another chelating group could be envisaged. More generally, this approach can be applied to obtain MIPs as synthetic antibody mimics specific for any protein that can be immobilized in an oriented way on a solid phase.

## 7. NOTES

### 1. Determination of PAB immobilized on glutaraldehyde functionalized GBs

#### Reagents and Materials

- Glutaraldehyde-functionalized GBs (section 2.2A)
- 100 mM PAB dissolved in buffer A
- Fluorescence cuvettes (Hellma analytics, 111-061-40)

## Method

PAB was quantified by measuring its fluorescence ( $\lambda_{\text{ex}}$ : 285 nm,  $\lambda_{\text{em}}$ : 365 nm, slit: 4 nm) at 25 °C on a spectrofluorimeter. A calibration curve of PAB ranging from 1-10  $\mu\text{M}$  was constructed (Fig. 8). 1 g of glutaraldehyde functionalized GBs was incubated with 1 mL of 100 mM PAB in buffer A. The amount of unbound PAB was determined on the supernatant, which was diluted with buffer A, so that the values fall within the calibration curve. Bound PAB was calculated by subtracting the amount of the unbound ligand from the total amount of ligand added to the GBs. The amount of PAB immobilized on the GBs was found to be  $22.6 \pm 2.3$  nmol/g of GBs.

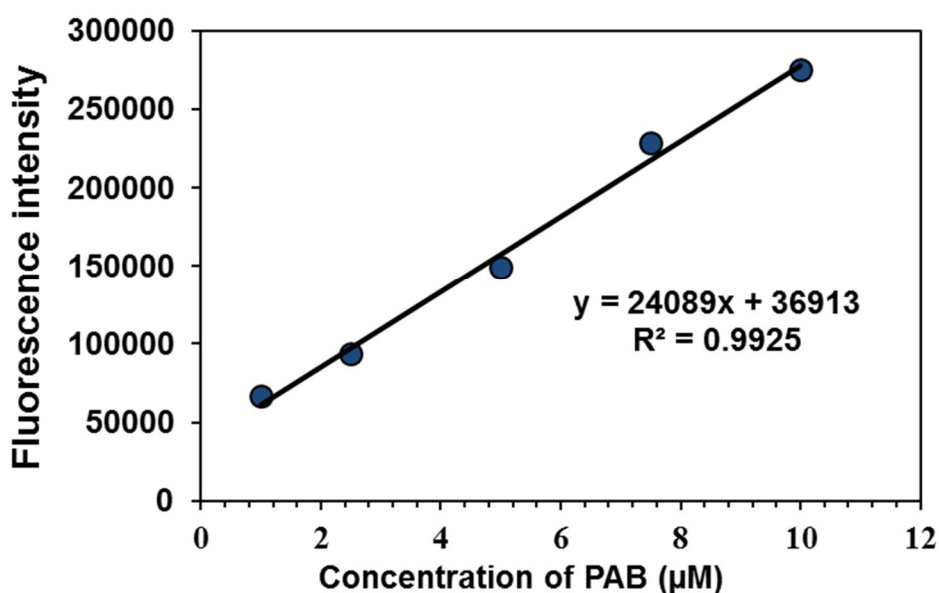


**Figure 8** Calibration curve of PAB in 100 mM sodium phosphate buffer + 150 mM NaCl pH 7.4 ( $\lambda_{\text{ex}}$ : 285 nm,  $\lambda_{\text{em}}$ : 365 nm, slit: 4 nm. Data represent the mean of two independent experiments.

## 2. Enzymatic activity assays

### Reagents

- 1  $\mu$ M trypsin stock solution prepared in 1 mM HCl + 10 mM CaCl<sub>2</sub>, pH ~ 5, kept in ice  
(diluted from 50  $\mu$ M trypsin prepared in 1 mM HCl + 10 mM CaCl<sub>2</sub>, pH ~ 5)
- 50 mM Tris-HCl pH 8
- 10 mM TAME prepared in 50 mM Tris-HCl pH 8
- 2  $\mu$ M kallikrein stock solution prepared in H<sub>2</sub>O (diluted from 50  $\mu$ M prepared in water)
- 50 mM Tris-HCl pH 8.7
- 10 mM BAEE in 50 mM Tris-HCl pH 8.7

### Method

Enzymatic activity measurements were done spectrophotometrically on a CARY60 UV-vis spectrophotometer. Molecular weights of trypsin and kallikrein taken to prepare the stock solutions were 23.8 kDa and 33 kDa respectively. The calibration curves for trypsin (procedures 1-3) and kallikrein (procedures 4-6) were constructed as follows:

1. Pipet 50  $\mu$ L of 10 mM TAME (final concentration: 500  $\mu$ M, final volume of assay: 1 mL) into a quartz cuvette containing 50 mM Tris-HCl, pH 8.
2. Add 10 to 100  $\mu$ L of 1  $\mu$ M trypsin solution (final concentration: 10 to 100 nM) into the cuvette.

3. Mix by inverting the cuvette upside-down rapidly and insert the cuvette immediately into the cell holder, and monitor the hydrolysis of TAME by measuring the change in absorbance at 247 nm for 1.5 min. The calibration curve for trypsin is shown in Fig. 8A.

4. Pipet 50  $\mu\text{L}$  of 10 mM BAEE (final concentration: 500  $\mu\text{M}$ , final volume of assay: 1 mL) into a quartz cuvette containing 50 mM Tris-HCl, pH 8.7.

5. Add 10 to 100  $\mu\text{L}$  of 2  $\mu\text{M}$  kallikrein (final concentration: 20 to 200 nM, final volume of assay: 1 mL)

6. Mix by inverting the cuvette upside-down rapidly and put the cuvette immediately into the cell holder, and monitor the hydrolysis of BAEE by measuring the change in absorbance at 253 nm for 5 min. The calibration curve for kallikrein is shown in Fig. 8B.

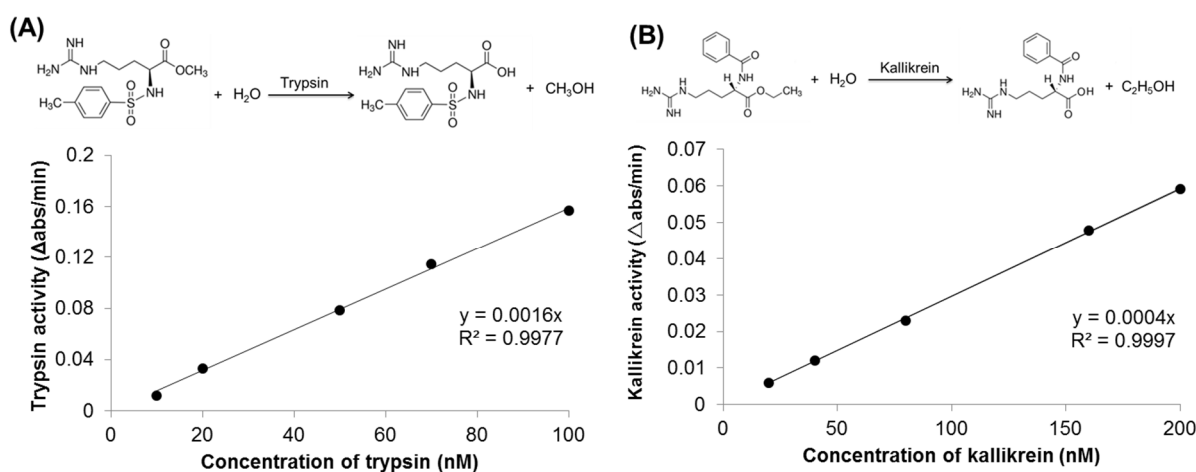


**Figure 9** Representative calibration curves of activity of (A) trypsin and (B) kallikrein.

### 3. Determination of apparent dissociation constants ( $K_{\text{dapp}}$ )

In order to determine the  $K_{\text{dapp}}$  (Fig. 6), first the apparent concentrations in (M) of the MIP-

NPs must be determined using the following equation (Hoshino et al, 2008; Guerreiro et al, 2014):

$$[\text{NPs}] = (6 / \pi N_A d^3 \rho) X$$

where  $N_A$  is the Avogadro's constant,  $d$  is the hydrodynamic diameter of the particles found by DLS (cm),  $\rho$  is the density of the particles ( $\text{g}/\text{cm}^3$ ) and  $X$  is the polymer weight concentration ( $\text{mg}/\text{mL}$ ). The polymer density was taken to be  $0.36 \pm 0.03 \text{ g}/\text{cm}^3$  ( $\rho$  values for NIPAM-based polymers in the collapsed state) (Meewes, Ricka, De Silva, Nyffenegger & Binkert, 1991).

## **ACKNOWLEDGMENTS**

J. Xu thanks the China Scholarship Council for financial support. We thank the European Regional Development Fund and the Regional Council of Picardie (co-funding of equipment under CPER 2007–2013), as well as Frederic Nadaud and Caroline Boulnois for the SEM/TEM images.

## **REFERENCES**

Ambrosini, S., Beyazit, S., Haupt, K., & Tse Sum Bui, B. (2013). Solid-phase synthesis of molecularly imprinted nanoparticles for protein recognition.

*Chemical Communications*, 49(60), 6746–6748.

Beyazit, B., Tse Sum Bui, B., Haupt, K., & Gonzato, C. (2016). Molecularly imprinted polymer nanomaterials and nanocomposites by controlled/living radical polymerization.

*Progress in Polymer Science*, 62, 1–21.

Canfarotta, F., Poma, A., Guerreiro, A., & Piletsky, S. (2016). Solid-phase synthesis of molecularly imprinted nanoparticles.

*Nature Protocols*, 11(3), 443–455.

Chao, J., Shen, B., Gao, L., Xia, C. F., Bledsoe, G., & Chao, L. (2010). Tissue kallikrein in cardiovascular, cerebrovascular and renal diseases and skin wound healing.

*Biological Chemistry*, 391(4), 345–355.

Cutivet, A., Schembri, C., Kovensky, J., & Haupt, K. (2009). Molecularly imprinted microgels as enzyme inhibitors.

*Journal of the American Chemical Society*, 131(41), 14699–14702.

Guerreiro, A., Poma, A., Karim, K., Moczko, E., Takarada, J., Vargas-Sansalvador, I. P., et al. (2014). Influence of surface-imprinted nanoparticles on trypsin activity.

*Advanced Healthcare Materials*, 3(9), 1426–1429.

Haupt, K., Linares, A. V., Bompert, M., & Tse Sum Bui, B. (2012) Molecularly imprinted polymers.

*Topics in Current Chemistry*, 325, 1–28.

Hoshino, Y., Kodama, T., Okahata, Y., & Shea, K. J. (2008). Peptide imprinted polymer nanoparticles: a plastic antibody.

*Journal of the American Chemical Society*, 130(46), 15242–15243.

Lei, W., Xue, M., Zhong, X., Meng, Z. H., Zhang, W. B., & Zhang, L. Y. (2013). Preparation of surface-imprinted silica using metal coordination for the separation of proteins.

*Journal of Liquid Chromatography & Related Technologies*, 36(15), 2196–2207.

Li, S., Cao, S., Whitcombe, M. J., & Piletsky, S. A. (2014). Size matters: Challenges in imprinting macromolecules.

*Progress in Polymer Science*, 39, 145–163.

Li, X., Xiong, H., Yang, K., Peng, D., Peng, H., & Zhao, Q. (2012). Optimization of the biological processing of rice dregs into nutritional peptides with the aid of trypsin.

*Journal of Food Science and Technology*, 49, 537–546.

Liu, Y., Zhai, J., Dong, J., & Zhao, M. (2015). Magnetic surface imprinted hydrogel nanoparticles for specific and reversible stabilization of proteins.

*Molecular Imprinting*, 2, 75–82.

Marchyk, N., Maximilien, J., Beyazit, S., Haupt, K., & Tse Sum Bui, B. (2014). One-pot synthesis of iniferter-bound polystyrene core nanoparticles for the controlled grafting of multilayer shells. *Nanoscale*, 6(5), 2872–2878.

Meewes, M., Ricka, J., De Silva, M., Nyffenegger, R., & Binkert, T. (1991). Coil-globule transition of poly (N-isopropylacrylamide): a study of surfactant effects by light scattering.

*Macromolecules*, 24(21), 5811–5816.

Overlack, A., Stumpe, K. O., Kolloch, R., Ressel, C., & Krueck, F. (1981). Antihypertensive effect of orally administered glandular kallikrein in essential hypertension. Results of double blind study. *Hypertension*, 3, 118–121.

Poma, A., Guerreiro, A., Caygill, S., Moczko, E., & Piletsky, S. (2014). Automatic reactor for solid-phase synthesis of molecularly imprinted polymeric nanoparticles (MIP NPs) in water.

*RSC Advances*, 4(8), 4203–4206.

Raspi, G. (1996). Kallikrein and kallikrein-like proteinases: purification and determination by chromatographic and electrophoretic methods.

*Journal of Chromatography B: Biomedical Sciences and Applications*, 684(1), 265–287.

Schild, H. G. (1992). Poly (N-isopropylacrylamide): experiment, theory and application.

*Progress in Polymer Science*, 17(2), 163–249.

Šebela, M., Štosová, T. Á., Havliš, J., Wielsch, N., Thomas, H., Zdráhal, Z., et al. (2006).

Thermostable trypsin conjugates for high-throughput proteomics: synthesis and performance evaluation.

*Proteomics*, 6(10), 2959–2963.

Takeuchi, T., & Hishiya, T. (2008). Molecular imprinting of proteins emerging as a tool for protein recognition.

*Organic & Biomolecular Chemistry*, 6(14), 2459–2467.

Vandermarliere, E., Mueller, M., & Martens, L. (2013). Getting intimate with trypsin, the leading protease in proteomics.

*Mass Spectrometry Reviews*, 32, 453–465.

Verheyen, E., Schillemans, J. P., van Wijk, M., Demeniex, M. A., Hennink, W. E., & van Nostrum, C. F. (2011). Challenges for the effective molecular imprinting of proteins.

*Biomaterials*, 32(11), 3008–3020.

Xu, J., Ambrosini, S., Tamahkar, E., Rossi, C., Haupt, K., & Tse Sum Bui, B. (2016). Toward a universal method for preparing molecularly imprinted polymer nanoparticles with antibody-like affinity for proteins.

*Biomacromolecules*, 17(1), 345–353.

Ye, L. (2015) Synthetic strategies in molecular imprinting.

*Advances in Biochemical Engineering Biotechnology*, 150, 1–24.

Zuber, M., & Säche, E. (1972). Isolation and characterization of porcine pancreatic kallikrein.

*Biochemistry*, 13, 3098–3110.

# Chapter 3

---

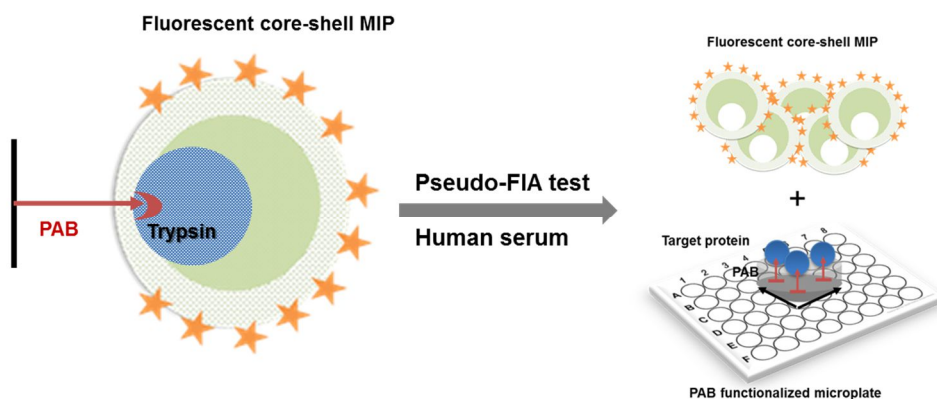
Application of a molecularly imprinted polymer  
as plastic antibody in bioassays

## Summary

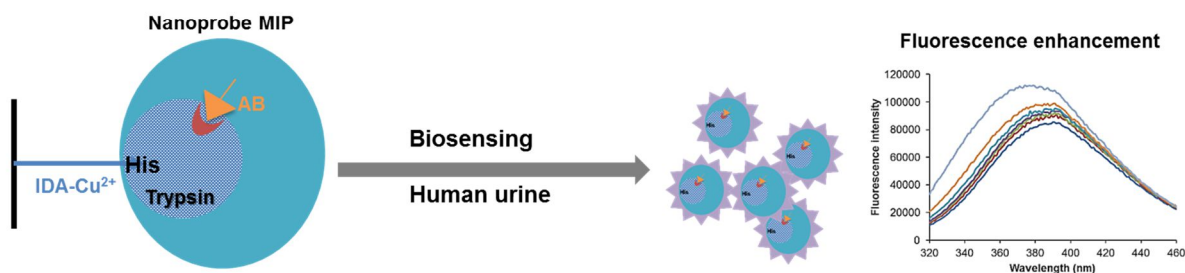
In this chapter, we show two real-life applications of the water soluble MIP-NPs obtained by solid-phase synthesis, described in Chapter 2. Some modifications have been brought to make this solid-phase synthesis method more user-friendly and rapid. Herein, the polymers are prepared by UV polymerization using a water-soluble iniferter, synthesized in-house. The solid-phase synthesis was not done in a thermostated column, as described earlier, but in a petri dish where the GBs cover only a few mm on its bottom, hence allowing the UV light to penetrate easily the pre-polymerization solution.

In the first example, fluorescent core-shell MIP-NPs, prepared on PAB-functionalized GBs are applied as a soluble antibody in a pseudo-fluorescence immunoassay (FIA) format, for the recognition and detection of trypsin in human serum. In the second example, fluorescent MIP-NPs, prepared on IDA-  $\text{Cu}^{2+}$  GBs are applied as a selective fluorescent nanoprobe for the sensing of trypsin in human urine. The two examples are illustrated in the following figure.

### Application of the MIP obtained on PAB functionalized GBs



### Application of the MIP obtained on IDA- $\text{Cu}^{2+}$ functionalized GBs



More in detail, for example 1, our objective was to replace natural antibodies by MIPs in a

direct FIA format. Generally, immunoassays are performed in direct, indirect, sandwich or competitive formats by immobilizing either antigens or antibodies. In an enzyme-linked immunoassay (ELISA), the detection (colorimetric or others) is usually carried out by measuring the activity of an enzyme like horseradish peroxidase (HRP), conjugated with antibodies or antigens. Water-soluble MIP is a promising candidate to replace natural antibody in an immunoassay. Recently, a soluble MIP, synthesized with HRP as functional monomer has been applied as recognition and signaling antibody in an ELISA format for the detection of immobilized antigen (vancomycin and ampicillin). The yield of polymerization was very low (2  $\mu\text{g}$  MIP/g GBs), with a limit of quantification (LOQ) in the mM range [Czulak et al, 2016]. However, most of the examples showing the performance of MIP-based ELISA, employ MIPs, even when they are obtained in their soluble forms, in an immobilized format. The immobilization is achieved by passive adsorption [Chianella et al., 2013; Cáceres et al., 2016], risking the loss of binding site orientation and the introduction of non-specific binding.

To avoid these risks, our strategy is to use a water-soluble MIP labeled with a fluorescence tag to detect immobilized antigen, which is trypsin, used as model, in a FIA type format. Via immobilized PAB, trypsin could be immobilized in an oriented configuration so as to maintain its active conformation in the wells plate; the direct binding of the fluorescent MIP generates the analytical signal. Our MIP-based pseudo-immunoassay system was successfully applied to detect low trypsin level in non-diluted human serum with an LOQ of 50 pM, which indicates the significant potential of this assay for analytical and biomedical diagnosis applications. We believe that this system can compete with the actual ELISA kit commercially available for the detection of trypsin.

In example 2, the study aims at developing a MIP as a biosensor for the detection of trypsin in aqueous media and in human urine. Literature reports only two examples of MIP-based sensors for trypsin, one is based on a quartz crystal microbalance [Hayden et al., 2006] and the other on a modified capacitive electrode [Ertürk et al., 2016] but both make use of immobilized MIPs and sophisticated instruments. In our study, using the fluorescence enhancement generated by the specific binding of trypsin to a PAB-derived monomer incorporated in a MIP, we show that

with a small amount of this water soluble fluorescent polymer (100 µg/mL), very sensitive detection (LOQ: 50 nM) can be obtained in solution. MIP in this format can be considered a cheap and reproducible method to detect trypsin rapidly (5 min incubation).

## References

Cáceres, C., Canfarotta, F., Chianella, I., Pereira, E., Moczko, E., Esen, C., et al. (2016). Does size matter? Study of performance of pseudo-ELISAs based on molecularly imprinted polymer nanoparticles prepared for analytes of different sizes. *Analyst*, 141(4), 1405-1412.

Chianella, I., Guerreiro, A., Moczko, E., Caygill, J. S., Piletska, E. V., De Vargas Sansalvador, I. M. P., et al. (2013). Direct replacement of antibodies with molecularly imprinted polymer nanoparticles in ELISA - Development of a novel assay for vancomycin. *Analytical Chemistry*, 85(17), 8462-8468.

Czulak, J., Guerreiro, A., Metran, K., Canfarotta, F., Goddard, A., Cowan, R., et al. (2016). Formation of target-specific binding sites in enzymes: solid-phase molecular imprinting of HRP. *Nanoscale*, 8(21), 11060-11066.

Ertürk, G., Hedström, M., & Mattiasson, B. (2016). A sensitive and real-time assay of trypsin by using molecular imprinting-based capacitive biosensor. *Biosensors and Bioelectronics*, 86, 557-565.

Hayden, O., Haderspöck, C., Krassnig, S., Chen, X., & Dickert, F. L. (2006). Surface imprinting strategies for the detection of trypsin. *Analyst*, 131(9), 1044-1050.

# **Fluorescent core-shell MIP nanoparticle as a plastic antibody for the pseudo-immunoassay of trypsin in human serum**

## **I. Introduction**

Antibodies are natural receptors that are widely used in immunoassays for analytical and clinical diagnosis purpose. In an immunoassay, antibodies conjugated with a variety of highly sensitive detection labels such as enzymes, radioactive isotopes, fluorescence or chemiluminescence probes, are used to detect an analyte. Coming in many different variations, the enzyme-linked immunosorbent assay (ELISA) based on an enzyme-linked antibody associated with a color change, is probably the most popular as many are commercially available as a kit. The shelf time of an ELISA kit is about 6 months at 4 °C, and its specificity and sensitivity are very high. However, the use of natural antibodies always brings some shortcomings, like the issue of stability and high cost, as well as the concern of batch-to-batch reproducibility. Thus, it has been a long-term goal for researchers to find more stable artificial antibody-like receptors for the replacement of natural antibodies. One of the most promising strategies, which has been increasingly adopted for the synthesis of artificial antibodies, is molecular imprinting [Haupt et al., 2012; Ye, 2015].

Molecularly imprinted polymers (MIPs), are synthetic receptors, prepared by creating 3D polymeric matrices around a template molecule by the co-polymerization of functional and cross-linking monomers. After extraction of the template, cavities with complementary size, shape and functional orientation will remain, resulting in MIPs able to recognize and rebind the template with high specificity and affinity [Beyazit et al., 2016]. These tailor-made synthetic receptors have considerable advantages over biological receptors due to their greater chemical and physical stability, their easy synthesis and their low fabrication cost. MIP-based ELISA was first introduced by Haupt's group for the detection of a herbicide 2,4-dichlorophenoxyacetic acid [Surugiu et al., 2000]. Since the obtention of selective MIP for proteins is still challenged by a lot of difficulties mostly related to the type of polymeric matrix used [Li et al., 2014], MIP-based ELISA to detect proteins has not been widely reported so far.

To overcome the aforementioned difficulties, a variety of strategies for protein imprinting has been developed [Bossi et al., 2007], such as surface imprinting [Yang et al., 2016; Kartal et

al., 2014], epitope approach [Yang et al., 2013; Qin et al., 2016], and solid-phase synthesis [Ambrosini et al., 2013; Poma et al., 2014]. Among these, the solid-phase synthesis approach using specific affinity ligands to orientate the immobilization of proteins has emerged as the most promising method because MIP nanoparticles obtained by this method are endowed with homogeneous binding sites with very high affinity ( $K_{dapp} = 0.02\text{-}2\text{ nM}$ ) [Xu et al., 2017]. Moreover, their water-compatibility and non-cytotoxicity [Panagiotopoulou et al., 2017] should enable a direct replacement of natural antibodies in immunoassay or in *in vivo* applications.

Controlled/living radical polymerization has drawn great attention due to its advantage in the generation of homogeneous MIP structure and well-defined properties [Zhang, 2015]. The ATRP system uses  $\text{CuCl}/\text{CuCl}_2/\text{Bpy}$  as catalyst, which may introduce impurities into the polymer network [Jiang et al., 2016]. In contrast to ATRP, no biological-unfriendly metal catalyst is employed for conducting RAFT. However, high temperatures ( $50 - 60\text{ }^\circ\text{C}$ ) and long reaction time ( $24 - 48\text{h}$ ) are needed for RAFT [Yang et al., 2011]. Recently, with the successful development of water soluble iniferters, iniferter-induced polymerization has drawn more and more interest [Bonomi et al., 2016; Sunayama et al., 2014] due to its advantage of mild conditions and easy-to-operate properties. Herein, a solid-phase synthesis approach using a water-soluble iniferter-induced polymerization for the fabrication of tailor-made synthetic core-shell receptors of proteins will be described.

Solid-phase synthesis of MIP nanoparticles with high affinity and selectivity for target proteins has already made some progress [Guerreiro et al., 2014; Cáceres et al., 2016; Xu et al., 2016].-Nanosized MIP offers significant surface to volume ratio, which leads to increased binding capacity per gram material when using the solid-phase approach. However, the sole recognition (or binding) of protein by MIP nanoparticles is not enough for applications to real-world situations. Thus, many efforts have been devoted to introduce additional function to the high-affinity polymers obtained by solid-phase synthesis approach, for instance, by developing core-shell MIP nanoparticles [Moczko et al., 2013].

In the present work, a water soluble core-shell MIP imprinted with trypsin and post-functionalized with a high content of fluorescent groups on its surface was prepared. Trypsin is one of the most important proteases found in the digestive system of vertebrates, where it hydrolyses proteins. It is produced in the pancreas, as its inactive precursor trypsinogen. Under normal conditions, some trypsinogen is converted to active trypsin, itself inactivated by the pancreatic secretory trypsin inhibitor (PSTI). This process self-regulates trypsin so that

it is never in excess so as to prevent autodigestion of the pancreas, which would cause some types of pancreatic disease such as chronic or acute pancreatitis and cystic fibrosis. Under these conditions, trypsin is released into the blood and hence the level of trypsin can serve as a reliable and specific diagnostic biomarker for alteration in the pancreatic function [Hirota et al., 2006; Ionescu et al., 2006]. Healthy individuals have a mean serum trypsin concentration of 6 - 17 nM, whereas chronic and acute pancreatitis patients exhibit respectively concentrations < 6 nM or higher concentrations of 25 - 273 nM [Cisbio Bioassays, OCFE07-TRYPS]. These values were determined by an immunological assay because in blood, all tryptic activity is blocked by three specific inhibitors,  $\alpha_1$ -antitrypsin,  $\alpha_2$ -macroglobulin and inter- $\alpha$ -trypsin inhibitor. Thus, enzyme activity measurements cannot be used to determine blood levels of trypsin. Consequently, new convenient assays for trypsin are highly desired for the development of efficient diagnostic and therapeutic methods toward these pancreatic diseases.

Herein, molecular imprinting of trypsin was performed by a multi-step solid-phase approach (Figure 1). Glass beads (GBs), functionalized with *p*-aminobenzamidine (PAB), a competitive inhibitor of trypsin, were used as a solid support. The core-MIP was composed of *N*-isopropylacrylamide (NIPAm) as functional monomer and *N,N'*-methylenebis(acrylamide) (Bis) as cross-linker. After polymerization and removal of low-affinity core-polymers and non-reacted monomers, the generated cavities on the remaining high-affinity core-MIP, were still blocked by immobilized trypsin. To introduce the shell on the core MIP, still attached to the support, an *in situ* grafting using a mixture of allylamine and Bis was used. The shell was composed of 98% allylamine so as to introduce a high percentage of primary amines for post-conjugation with fluorescein isothiocyanate (FITC). The core-shell MIP was released from the solid support by a simple temperature change. FITC was then conjugated on the core-shell MIP. Here, the solid phase not only plays the role of a reactor and a separation column, but also a protector of high-affinity binding sites by blocking them during shell formation. In order to avoid the interaction between FITC and PAB functionalized GBs, allylamine composed shell was introduced and FITC conjugation was performed with core-shell MIP in the absence of GBs.

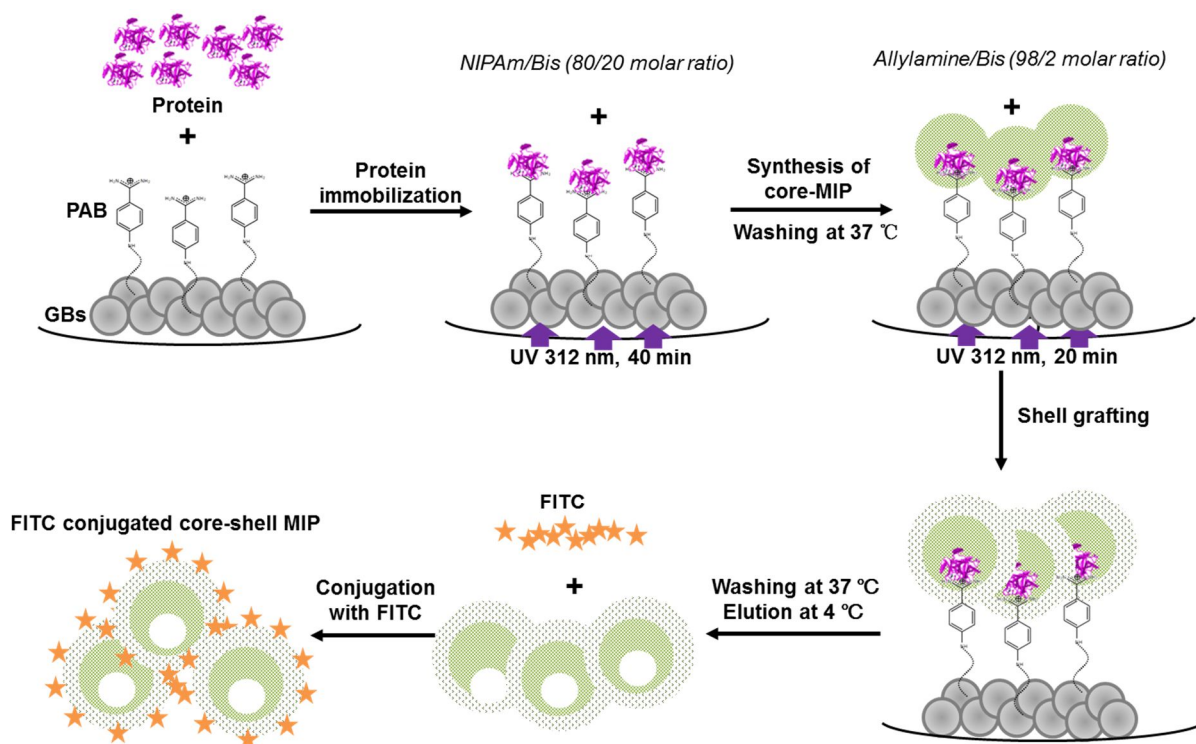


**Figure 1:** Representation of the solid-phase synthesis of core-shell MIP with post-functionalization of FITC on the surface of the shell.

With these fluorescent core-shell MIPs in our hands, we further proceeded to demonstrate their feasibility as soluble antibody mimics in a pseudo-immunoassay format for the label-free, easy-to-operate determination of trypsin in human serum. Figure 2 shows the procedure leading to a highly sensitive bioassay of trypsin. A 48-well microplate was functionalized with PAB so as to capture the trypsin in an oriented configuration. This controlled orientation, as compared to random orientation (physical adsorption) on the support, avoids the denaturation of the enzyme, increases its loading capacity and decreases non-specific interactions [Liu & Yu, 2016]. This highly sensitive bioassay is also due to a high coverage of PAB in the wells allowing a high amount of trypsin to be captured. After washing the excess trypsin, fluorescent core-shell MIPs are added as detection/quantification antibody. The core-shell MIP has been rendered highly fluorescent by post-functionalization on its surface so that little amounts of antibody (LOQ: 0.2 nM) can be used and detected by simple fluorescence intensity measurements. The results showed high specificity and selectivity of the MIP and demonstrated its ability to detect trypsin level in human serum in the low nM range.

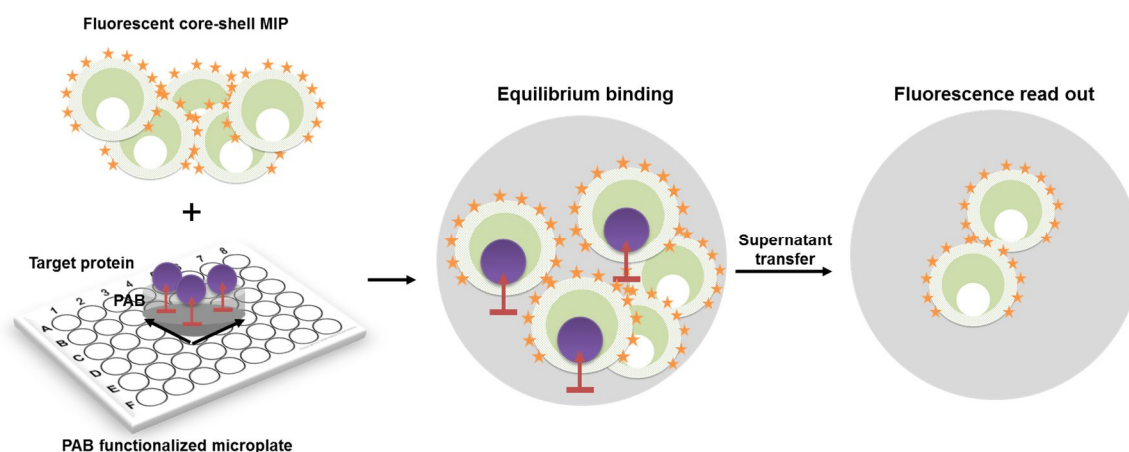


**Figure 2.** Illustration of fluorescent core-shell MIP nanoparticles as soluble plastic antibodies for the detection of proteins in a pseudo-immunoassay format.

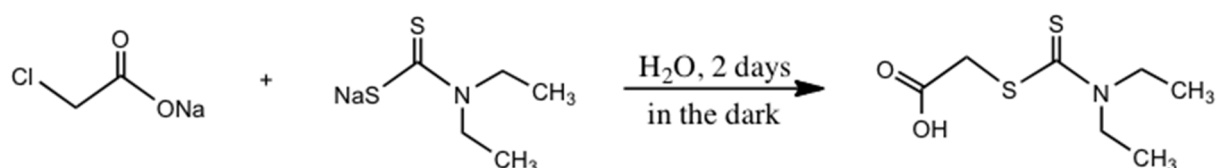
## II. Experimental section

### Materials and Methods

All chemicals and solvents were of analytical grade and purchased from VWR International (Fontenay sous Bois, France) or Sigma-Aldrich (St Quentin Fallavier, France), unless otherwise stated. The proteins: trypsin from bovine pancreas (MW: 23.8 kDa, specific activity: > 10 000 units/mg protein), thrombin from bovine plasma (MW: 37 kDa), kallikrein from porcine pancreas (MW: 25.6 kDa), cytochrome c from horse heart (MW: 11.7 kDa) and human serum albumin (MW: 66.4 kDa) were purchased from Sigma-Aldrich. Glass beads (GBs) of diameter 0.1 mm and dialysis membrane (MWCO 6-8 kDa) were obtained from Roth Sochiel E.U.R.L (Lauterbourg, France). Buffers were prepared with Milli-Q water, purified using a Milli-Q system (Millipore, Molsheim, France). The chemicals for the quantification of trypsin: 3, 3', 5, 5'-tetramethylbenzidine (TMB) one component horse radish peroxidase (HRP) substrate and ELISA stop solution, were purchased from Bethyl Labs. (Montgomery, USA). Human serum (from human male AB plasma, sterile filtered) was purchased from Sigma-Aldrich. Polystyrene 48-well microplates from Becton Dickinson (Le Pont De Claix, France) were used for all experiments. All fluorescence measurements were done on a FluoroLog-3 spectrofluorimeter (Horiba Jobin Yvon, Longjumeau, France). UV-Vis absorbance was measured on a Cary 60 UV-vis spectrophotometer (Agilent Technologies). Polymerization was carried out at 312 nm using a UV lamp (6 x 8 W) (Fisher Bioblock Scientific, France). The hydrodynamic size, conductivity and zeta potential measurements were recorded in a disposable capillary cell (DTS1061), using a Zetasizer NanoZS (Malvern

Instruments Ltd., Orsay, France) at 25 °C. Scanning electron microscopy (SEM) imaging was carried out on a Quanta FEG 250 scanning electron microscope (FEI Europe, Netherlands). Transmission electron microscopy (TEM) images were captured using a JEM-2100F (JEOL, Japan). The TEM grid was a 300 mesh carbon-coated copper grid from AGAR Scientific (Stansted, UK). <sup>1</sup>H NMR spectra were recorded on a Bruker 400 MHz spectrometer.

## II.1 Synthesis of the water-soluble iniferter, diethylthiocarbamoylsulfanyl acetic acid (DCAA)



DCAA was synthesized as previously reported [Tsuji et al., 2006] with some modifications which led to a higher yield. First, 1801.2 mg (8 mmol) of sodium diethylthiocarbamate trihydrate was dissolved in 10 mL of water (referred as solution 1). Second, 932 mg (8 mmol) of sodium chloroacetate was dissolved in 10 mL of water (referred as solution 2). Solution 2 was added to solution 1 dropwise and the reaction was left to proceed for 2 days under magnetic stirring. The mixture was shielded from light with aluminum foil. HCl (38%) was then added to the solution to precipitate the product until pH 1.5 – 2.0 (monitored on a pH meter). The final product was recrystallized from acetone at 8 °C and then filtered, yielding the water-soluble iniferter, which is a white powder. The yield was 67.1%. <sup>1</sup>H NMR (400 MHz, CDCl<sub>3</sub>) spectrum is shown in Figure 3. <sup>1</sup>H NMR: δ (ppm) 4.19 (s, 2H, CH<sub>2</sub>), 4.02 (q, 2H, CH<sub>2</sub>-CH<sub>3</sub>), 3.77 (q, 2H, CH<sub>2</sub>-CH<sub>3</sub>), 1.34 (t, 3H, CH<sub>2</sub>-CH<sub>3</sub>), 1.29 (t, 3H, CH<sub>2</sub>-CH<sub>3</sub>).

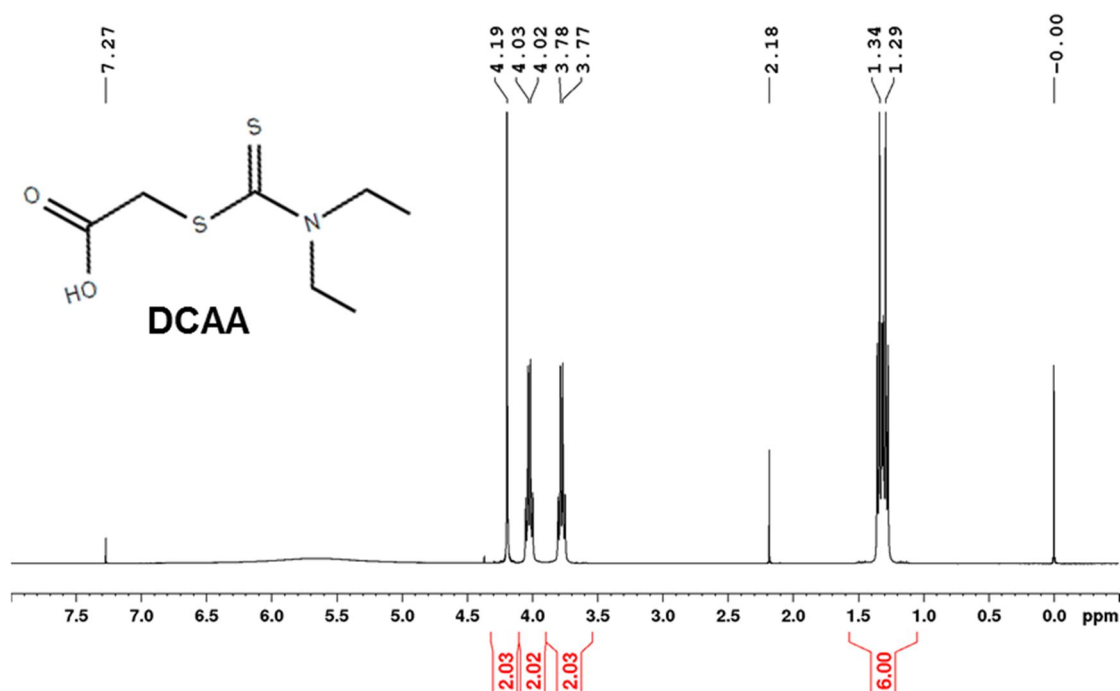


**Figure 3.**  $^1\text{H}$  NMR spectrum of DCAA in  $\text{CDCl}_3$

## II.2. Solid-phase synthesis of core-shell MIP nanoparticles

*Functionalization of GBs with PAB.* Glass beads (GBs) functionalized with PAB was synthesized as previously reported [Xu et al., 2016] and chapter 2. Briefly, 100 g glass beads were boiled for 10 min in 100 mL of 4 M NaOH solution at 100 °C. After intensive washing with water, the GBs were dried in an oven at 50 °C. The activated GBs were then incubated in a solution of 2% (v/v) (3-aminopropyl)triethoxysilane (APTES) in toluene, with shaking overnight at room temperature. Afterward, the silanized GBs were incubated in a 5% (v/v) glutaraldehyde solution in 0.1 M sodium phosphate buffer + 0.15 M NaCl pH 7.4 (PBS buffer). After shaking at 30 °C for 12h, the GBs were washed with water. The glutaraldehyde-activated glass beads were dispersed in a 0.1 M PAB solution in PBS buffer. The mixture was incubated at room temperature for 5h. Then the PAB-GBs were washed with PBS buffer and immersed in 1 mg/mL solution of  $\text{NaBH}_4$  in PBS buffer for 30 min at room temperature. The unreacted carbonyl groups were blocked by incubation in 40 mM ethanolamine for 30 min. Finally, the obtained PAB-GBs were washed with PBS buffer, water and stored at 8 °C in 1 M NaCl containing 20% ethanol until use.

*Synthesis of MIP-NPs.* 30 g of PAB-GBs were placed in a glass petri dish (d x h: 14 x 2 cm) fitted with a cover lid, followed by washing 5 times with 40 mL 25 mM sodium phosphate buffer pH 7.0 (buffer A). Then the GBs were incubated with 40 mL of 0.5 mg/mL trypsin

(prepared in buffer A) for 1 h, and washed with 5 x 40 mL buffer A. The pre-polymerization mixture for the core polymers was prepared by mixing 181.1 mg (1.6 mmol) of NIPAm and 61.6 mg (0.4 mmol) of Bis in 48.6 mL of buffer A so that the total monomer concentration is 0.5% (w/w). After purging with N<sub>2</sub> for 20 min, 17.1 mg (0.0826 mmol, 3.5% of double bonds) of DCAA was added, and the mixture was poured into the petri dish. The polymerization was done under UV light at 312 nm at ambient temperature for 40 min. The temperature inside the polymerization mixture reached 37 °C in the end. At this temperature, the growing polymeric nanoparticles, which are in the collapsed state, encapsulate the immobilized protein during polymerization. The GBs were then washed twice with 50 mL buffer A preheated at 37 °C so as to remove unreacted monomers and low-affinity polymers. The shell pre-polymerization mixture, composed of 98% allylamine (0.98 mmol, 147 μL) and 2% Bis (0.02 mmol, 6.2 mg), prepared in 23.6 mL of buffer A so that the total monomer concentration is 0.5% (w/w), was incubated in a water-bath at 37 °C. After purging with N<sub>2</sub> for 20 min, 7.5 mg (0.036 mmol, 3.5% of double bonds) of DCAA was added and the mixture was poured in the petri dish and polymerized under UV light for 20 min. Afterward, the GBs were washed with 50 mL of 50 mM sodium carbonate buffer, pH 9.2 at 37 °C. The high-affinity core-shell MIP was eluted with 20 mL of 50 mM sodium carbonate buffer, pH 9.2 at 5 °C. The core-shell MIP was then conjugated with 1 mL of FITC (FITC was prepared in dimethyl sulfoxide: 10 mg/mL) in the same buffer for 2h. To ensure the removal of excess unreacted FITC in both water and buffer A, the MIP solution was dialysed 5 times in 1 L water and 5 times in 1 L buffer A, by changing the dialysis solution once every day. The non-imprinted polymer (NIP) was synthesized in the same way but in the absence of trypsin. The dialyzed MIP or NIP solution in buffer A constituted the stock working polymers.

### **II-3. Characterization of fluorescent core-shell polymers**

*Yield of synthesis.* 10 mL of MIP or NIP stock solution was dialyzed overnight in 2 L of water. Their concentration was calculated after lyophilization and weighing of the dialyzed aliquots on a precision balance.

*Physicochemical characterization.* The polymer size in buffer A and the zeta potential in water (the sample was desalted so as to have a conductivity < 0.4 mS/cm, a requirement to obtain zeta potential values of good quality, as recommended by the manufacturer) were measured by dynamic light scattering (DLS) analysis on a Zetasizer NanoZS at 25 °C.

*Fluorescence calibration of MIP and NIP.* The stock solution of MIP or NIP (0.2 mg/mL in buffer A) was diluted with buffer A so as to obtain concentrations between 0.1 – 10 µg/mL. Fluorescence measurements were done on a spectrofluorimeter, with excitation/emission wavelengths set at 490/515 nm with slit of 3 nm.

*Molecular weight determination.* The molecular weight of MIP in buffer A was obtained by analysis of the intensity of light scattered from the particle at different concentrations, in the dilute regime. This is done by applying the Rayleigh equation [George & Wilson, 1994]:

$$KC/R_0 = 1/M + 2A_2C$$

$R_0$  is the Rayleigh ratio: ratio of scattering of the sample compared to the scattering of a standard (toluene),  $K$  is an optical constant,  $C$  is the sample concentration,  $M$  is the molecular weight and  $A_2$  is the second virial coefficient (representing the magnitude of particle - solvent interactions). To determine the molecular weight, the Rayleigh equation is represented graphically in the form of a Debye plot showing the concentration ( $C$ ) dependence of intensity of scattered light ( $KC/R_0$ ).  $M$  is determined from the intercept on the y-axis and  $A_2$  from the slope of the Debye plot.

The stock solution of MIP (0.2 mg/mL in buffer A) was concentrated on Amicon Ultra centrifugal filters (30 kDa, Merck Chimie SAS, France) or diluted with buffer A to prepare concentrations varying between 0.05 to 0.8 mg/mL for measurements. The molecular weight was determined on a Zetasizer NanoZS at 25 °C. The Debye plot is shown in Figure 4, which indicates a molecular weight of  $500 \pm 55$  kDa ( $R^2 = 0.895$ ) and a second virial coefficient of  $-0.00045$  mL mol/g<sup>2</sup>; a negative  $A_2$  indicates that the polymer-polymer interaction is stronger than polymer-solvent interaction, and at high concentrations the polymers may aggregate.

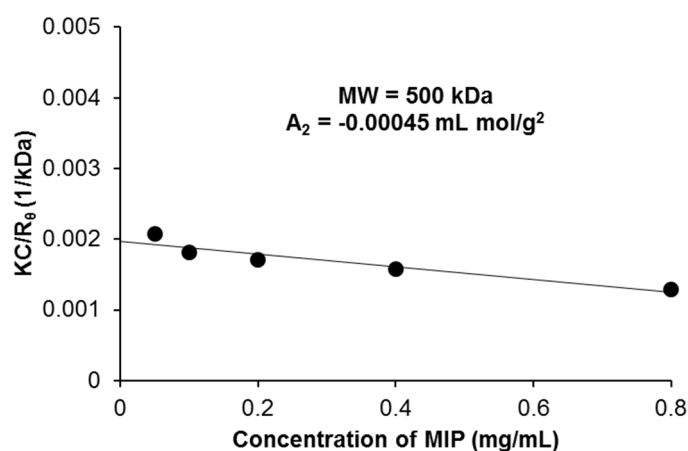


**Figure 4.** Debye plot for the determination of the absolute molecular weight of MIP.

#### **II-4. Activation and functionalization of 48-well microplates.**

The activation of the microplate was performed according to Bi and Liu, 2013. PAB functionalization was done by following a similar protocol as used for the PAB-functionalized glass beads. First, each well was filled with 0.5 mL of H<sub>2</sub>SO<sub>4</sub> (95%)/HNO<sub>3</sub> (63%) mixture (3:1, v/v) and left at room temperature for 30 min. Then the activated microplate was washed intensively with water until the pH became neutral. Afterward, 0.5 mL of 5% (v/v) APTES in methanol was added into the well, shaken at room temperature overnight, and dried at 60 °C for 2h. Later, each well was washed 5 times with 1 mL methanol. The silanized wells were then incubated in a 5% (v/v) glutaraldehyde solution in buffer A. After shaking at 30 °C overnight, the wells were washed with buffer A. The glutaraldehyde-activated wells were filled with a 0.1 M PAB solution in buffer A and incubated at room temperature for 5h. Then the wells were washed with buffer A and 1 mg/mL solution of NaBH<sub>4</sub> in buffer A was added for 30 min at room temperature. The unreacted carbonyl groups were blocked by incubation in 40 mM ethanolamine for 30 min. Finally, the obtained PAB functionalized microplate was washed with buffer A containing 0.05% tween 20 and stored in buffer A at 8 °C until use.

#### **II-5. Characterization of functionalized microplate**

*Determination of amino groups.* After silanization with APTES, the amino groups available on the silanized well surface were determined using a colorimetric assay with the anionic dye Orange II [Ambrosini et al., 2013]. Briefly, the silanized wells were filled with 0.5 mL of 40 mM Orange II acidic solution (water adjusted to pH 3.0 with 1 M HCl) and shaken for 30 min at 40 °C. The sample was then intensively washed with the acidic solution to remove unbound dye. Once air-dried, 0.5 mL of alkaline solution (water adjusted to pH 12 with 1 M NaOH) was added, so as to release the adsorbed dye. The desorbed dye solution was adjusted to pH 3.0 by adding 15 µL of 1 M HCl. The concentration of the desorbed dye was determined by measuring the absorbance at 485 nm.

*Determination of PAB.* PAB was quantified by measuring its absorbance at 285 nm on a UV-vis spectrophotometer. Each well was incubated with 0.6 mL of 100 mM PAB in buffer A. This corresponds to an excess of PAB with respect to the amount of amino groups determined in each well. Bound PAB was calculated by subtracting the amount of the unbound ligand from the total amount of ligand added, after dilution so as to fall within the calibration curve (Figure 5).

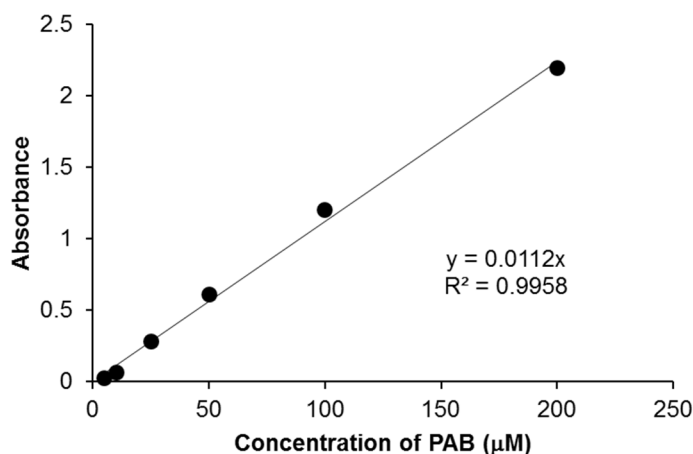


**Figure 5.** Calibration curve of PAB in buffer A, absorbance was read at 285 nm.

*Determination of trypsin.* The amount of trypsin immobilized on PAB-functionalized plate was determined by a colorimetric method using cytochrome c as substrate (Zhang et al., 2016). The method relies on the digestion of cytochrome c by trypsin to generate heme-peptide fragments which catalyse the oxidation of TMB with  $H_2O_2$  giving an intense blue color. The absorbance at 450 nm was proportional to the concentration of trypsin (see section II.6).

*SEM analysis.* The surface of the wells after activation and the different derivatization processes was characterized by scanning electron microscopy.

## **II-6. Quantification of trypsin using cytochrome c immobilized on glass beads.**

*Immobilization of cytochrome c on GBs.* Glass beads functionalized with iminodiacetic acid (IDA) was synthesized as previously reported [Xu et al., 2016]. Briefly, 50 g of GBs were boiled for 10 min in 50 mL of 4 M NaOH solution at 100 °C. After intensive washing with water, the GBs were dried in an oven at 50 °C. The activated GBs were then added to a 200 mL mixture of anhydrous toluene and (3-glycidyloxypropyl)trimethoxysilane (Glymo) (1/1, v/v) in a round bottom flask and refluxed at 110 °C for 17h. The Glymo-coupled glass beads (Glymo-GBs) were collected and washed three times with toluene and acetone. After drying, the Glymo-GBs were immersed into 500 mL of a 0.75 M IDA solution (containing 0.34 M NaCl and 2.0 M  $Na_2CO_3$ , pH 11.0) and stirred at 70 °C for 17h. The final GBs were obtained after washing five times with water.

The maximum binding capacity was obtained by incubating 1 g of IDA-GBs with 1 mL of 5

mg/mL cytochrome c in buffer A (Figure 6B), followed by washing 5 times with buffer A. 1 M HCl was added to desorb the bound cytochrome c which was determined by measuring its absorbance at 408 nm on a UV-vis spectrophotometer, using the calibration curve in Figure 6A.

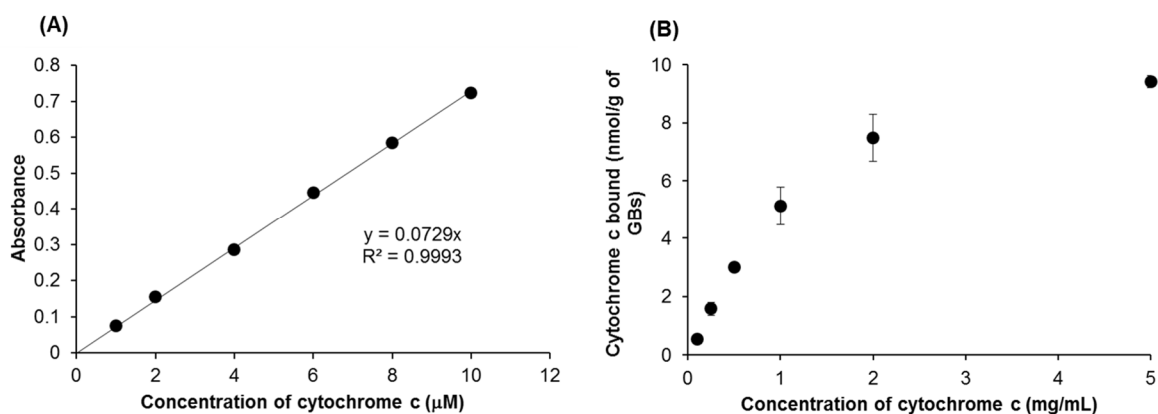


**Figure 6.** (A) Calibration curve of cytochrome c, absorbance was read at 408 nm; (B) Binding capacity of 1 g of IDA-GBs with 1 mL of varying concentrations of cytochrome c, in 25 mM sodium phosphate buffer pH 7.

*Quantification of trypsin.* A calibration curve was prepared with concentrations of free trypsin, representing the level of trypsin in healthy patients's blood (6-17 nM) or lower for patients suffering from chronic pancreatitis. A stock solution of trypsin (50  $\mu\text{M}$ ) was prepared in 1 mM HCl + 10 mM  $\text{CaCl}_2$  (pH  $\sim$  5) and stored in ice. Trypsin concentrations ranging from 1 to 50 nM were prepared in buffer A and 0.5 mL of each concentration was added to a microplate containing 150 mg GBs functionalized with cytochrome c, corresponding to 1.4 nmol of immobilized cytochrome c, in each well. The tryptic hydrolysis was performed for 1h at room temperature, and then 0.4 mL of supernatant was transferred to empty wells for oxidation reaction. 200  $\mu\text{L}$  of TMB one component HRP substrate was added and left at room temperature for 30 min (solution turned yellow), and stopped by an equal volume of ELISA stopping solution (final solution became blue). After 5 min, the microplate was read at 450 nm (Figure 7) on a DYNEX microplate reader (Magellan Bioscience, USA).

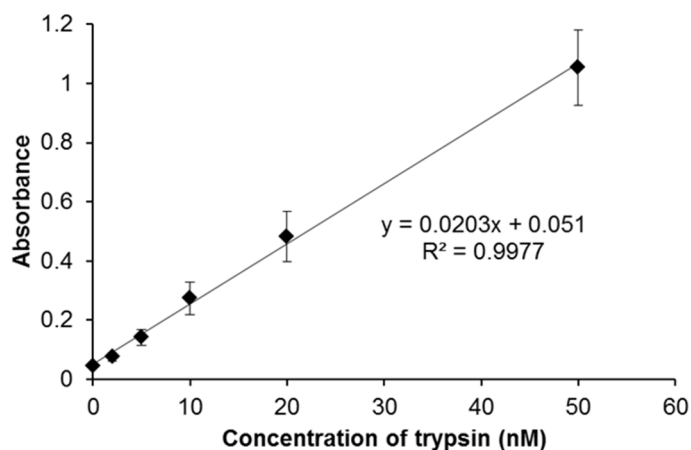


**Figure 7.** Calibration curve of trypsin using a fixed amount of cytochrome c as substrate and H<sub>2</sub>O<sub>2</sub>-mediated TMB oxidation as chromogenic agents. Absorbance was read at 450 nm.

The tryptic cleavage of cytochrome c (UniProtKB number: P00004) was analyzed by “PeptideMass” ([http://web.expasy.org/peptide\\_mass/](http://web.expasy.org/peptide_mass/)). Trypsin cleaves peptide chains after the amino acids lysine (K) and arginine (R) generating peptide fragments of cytochrome c, as marked in Figure 8. The fragments containing the heme should include peptides CAQCHTVEK and MIFAGIK.

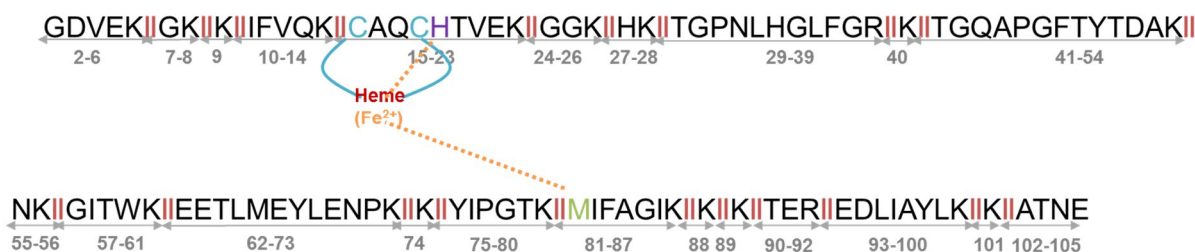


**Figure 8.** Peptide sequences obtained by tryptic cleavage of horse heart cytochrome c.

## II-7. Binding assay with MIP and NIP with saturated trypsin immobilized on PAB-functionalized well plate

In order to determine the amount of trypsin that is needed to saturate all the PAB (2 μmole per well) in the wells, PAB-functionalized microplate was incubated with 0.6 mL of 1 mg/mL (42 μM) trypsin, prepared in buffer A, for 1h, and the supernatant was withdrawn and diluted with buffer A, so as to fall within the calibration curve in Figure 7. After washing 5 times with

buffer A, another round of 0.6 mL of 1 mg/mL trypsin was added for incubation, and immobilized trypsin was determined in the same way. This procedure was repeated one more time until no more adsorption of trypsin was observed. The first, second and third rounds respectively showed that  $1.57 \pm 0.18$ ,  $0.47 \pm 0.08$  and  $0.01 \pm 0$  nmol of trypsin was bound.

After saturating the PAB functionalized microplate with trypsin (2 nmol per well), 0.5 mL of MIP or NIP with concentrations ranging from 0.2 – 200  $\mu\text{g/mL}$  was added for equilibration binding assay. After 2h incubation, the supernatant was withdrawn for fluorescence measurement. The polymer adsorbed was determined by subtracting the amount of the unbound from the total amount of MIP added in PAB-functionalized well, without trypsin, i.e. with only buffer A (Figure 13).

#### **II-8. Competitive binding assay- selectivity test.**

In order to investigate the selectivity of the MIP toward saturated trypsin immobilized on PAB-functionalized well, various competitors such as free trypsin, kallikrein, thrombin, cytochrome c and human serum albumin (HSA) with concentrations between 0.5 nM – 50  $\mu\text{M}$ , were added to 0.5 mL of 10  $\mu\text{g/mL}$  of MIP. After incubation for 2h, the amount of MIP adsorbed was calculated by measuring the unabsorbed MIP in the supernatant, as described above (Figure 14).

#### **II-9. Application of fluorescent core-shell MIP as ‘plastic antibody’ in a pseudo-immunoassay format for the detection of low concentrations of trypsin in human serum.**

A stock solution of trypsin (50  $\mu\text{M}$ ) was prepared in 1 mM HCl + 10 mM  $\text{CaCl}_2$  (pH  $\sim$  5) and stored in ice. Human serum was centrifuged at 7,500g for 10 min at room temperature, and the supernatant was used for subsequent experiments. Trypsin concentrations ranging from 50 pM to 5 nM was spiked in human serum, and 0.6 mL of each concentration (including blank) was added into the microplate for incubation. After 1h, the microplate was intensively washed with 5 times of 1 mL buffer A each well. Then 0.5 mL of 10  $\mu\text{g/mL}$  MIP or NIP was added, and incubated for 2h with shaking. Afterward, the supernatant was withdrawn for fluorescence measurement. The amount of adsorbed polymers was determined by subtracting the amount of the unbound from the total amount of MIP or NIP added in PAB

functionalized well without trypsin (blank) (Figure 15).

### **III. Results and discussion**

The solid-phase synthesis of the polymers was carried out in a petri dish, instead of a thermostated column (chapter 2). This time, the polymerization was initiated by UV light using a water soluble iniferter (instead of KPS/TEMED initiated by heat, chapter 2); therefore the GBs were disposed at the bottom of a petri dish so that they constituted only a thickness of 2.5 – 3.0 mm to allow the penetration of the UV light from the bottom. This novel set-up presents some advantages as it is more easy to manipulate (than in a column), is cheaper (thermostated column and height adapters are fragile and expensive), compact and space-saving (no pump and no circulating water-bath are needed). However the yield was lower: 0.13 g of MIP/g GBs as compared to previous reports for MIPs obtained by overnight thermal polymerization in a column (0.3 g/g GBs). For this set-up, an optimized polymerization time of 40 min was used so as to obtain small homogeneous nanoparticles; longer polymerization time led to micrometer sized particles that agglomerated.

#### **III-1. Characterization of fluorescent core-shell MIP and NIP**

The yield of synthesis was found to be 0.13 mg/g of GBs for both MIP and NIP. This was deduced from the concentration of polymer particles collected after synthesis. An aliquot of known volume (10 mL) was dialysed in water, lyophilized and weighed on a precision balance. The concentration was found to be 0.2 mg/mL. Knowing the mass of GBs and the total volume of polymer eluted, the yield of synthesis as mg per g of GBs was calculated.

The physicochemical characterization (size and zeta potential) of the polymers, as determined by dynamic light scattering (DLS) is summarized in table 1. The transmission electron microscope (TEM) image of MIP is shown in Figure 9; the core and the shell can be clearly distinguished. The presence of FITC on the polymers is revealed by the fluorescence calibration curves (Figure 10). The polymers were highly fluorescent since a LOQ of 0.1 µg/mL corresponding to 0.2 nM, taking the molecular mass of the MIP to be 500 kDa (Figure 4), was detected.

**Table 1.** Physicochemical characterization of MIP and NIP.

	MIP	NIP
Diameter (nm)	104.0 ± 5.8	91.0 ± 9.0
Polydispersity index (PDI)	0.404	0.592
Zeta potential (mV)	-34.0	-30.2
Conductivity (mS/cm)	0.0274	0.043

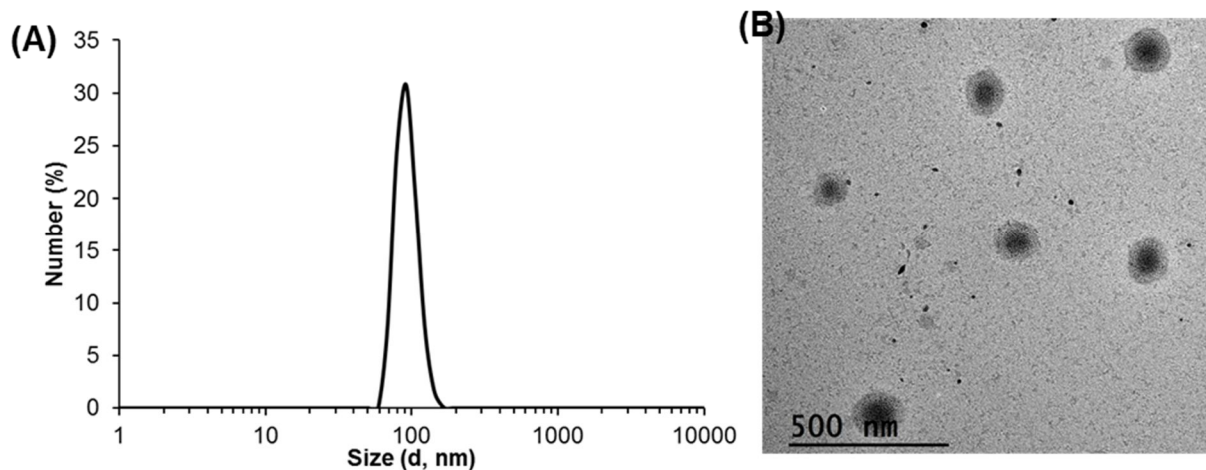


**Figure 9.** (A) Size distribution in 25 mM sodium phosphate buffer pH 7 and (B) TEM image of fluorescent core-shell MIP.

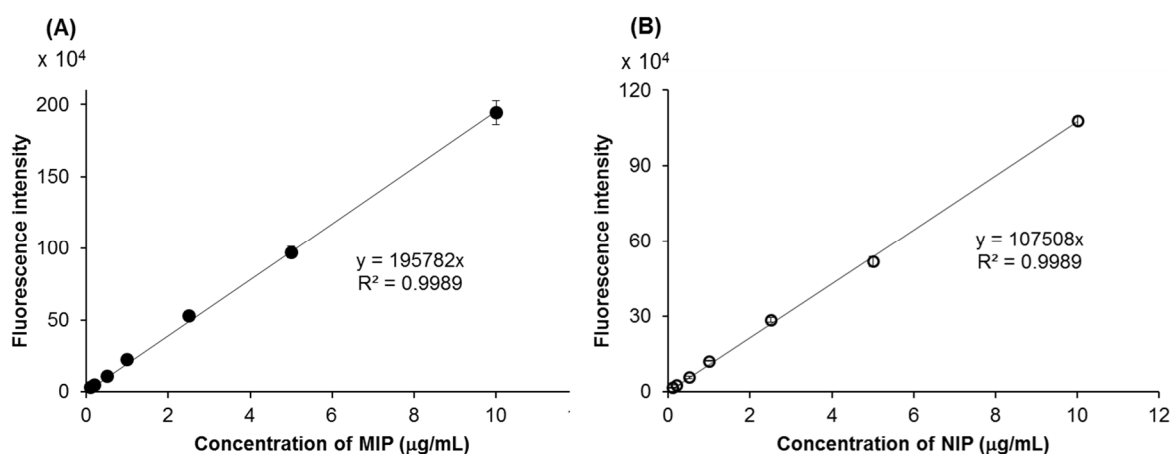


**Figure 10.** Calibration curves of core-shell MIP (A) and NIP (B) in 25 mM sodium phosphate buffer pH 7.0. Fluorescence measurements were done at  $\lambda_{ex}/em = 490/515$  nm, slit 3 nm.

### III-2. Characterization of functionalized microplate.

In ELISA-based applications, proteins are often immobilized on the polystyrene surface of the well plate by physical adsorption through hydrophobic interaction. It has been reported that not only this method is inefficient for hydrophilic or small-sized proteins [Suzuki et al., 1997], but they can also be denatured. Therefore, for our work, in order to have a high coverage of active trypsin, it was immobilized as follows. The hydrophobic polystyrene microplate was first rendered hydrophilic by treating with  $H_2SO_4/HNO_3$ . Amino groups were then introduced by reacting with APTES (Figure 11) [Kaur et al., 2004].

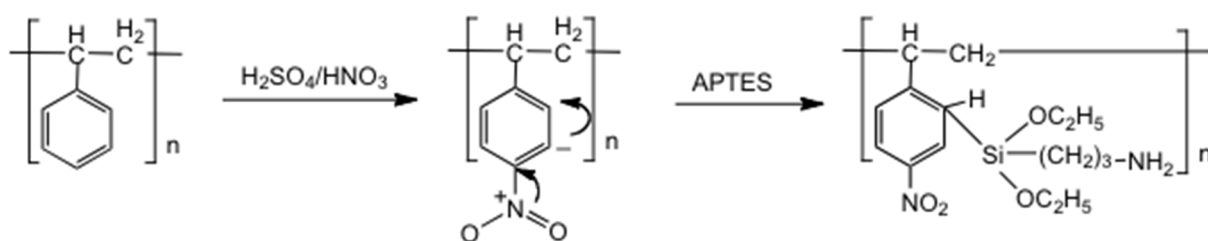


**Figure 11.** Activation and functionalization of polystyrene well plates

This procedure allowed further functionalization with glutaraldehyde and PAB. The successful activation is shown by determining the density of APTES and PAB on the surface of each well (Table 2).  $\sim 2 \mu\text{mol/well}$  for both is observed; thus 100% of the introduced  $-NH_2$  is covered by PAB, which indicates the absence of free  $-NH_2$ .

The SEM images of the wells are presented in Figure 12. After activation with  $H_2SO_4/HNO_3$ , small seeds with a diameter of  $\sim 40 \text{ nm}$  were observed. The silanization with APTES produced particles with diameters of  $\sim 200 \text{ nm}$ . After functionalization with glutaraldehyde and PAB, bigger particles with diameter  $\sim 2.5 \mu\text{m}$  could be seen (Figure 12D). The homogeneity of particles distribution on the surface looks promising to give reproducible and reliable immobilization of trypsin.

**Table 2.** Characterization of functional groups on well-plate

Chemical groups	Amount per well
APTES	$2.08 \pm 0.03 \mu\text{mol}$
PAB	$2.06 \pm 0.08 \mu\text{mol}$
Trypsin	$2.05 \pm 0.03 \text{ nmol}$

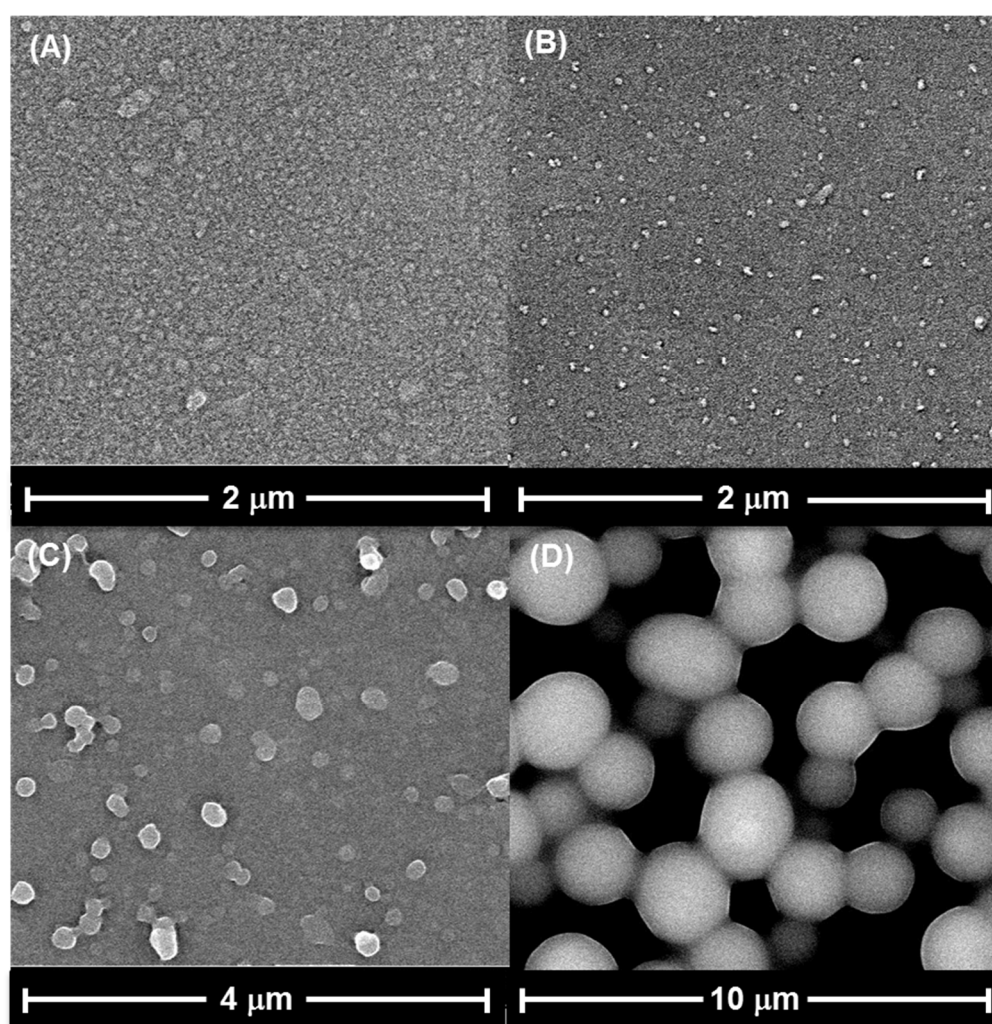


**Figure 12.** SEM images of the well surface after different derivatization processes. (A) Non-treated; (B) Activated with H<sub>2</sub>SO<sub>4</sub>/HNO<sub>3</sub>; (C) Silanized with APTES; (D) functionalized with glutaraldehyde followed by PAB.

The next step was to determine the maximum amount of trypsin that will saturate the PAB moieties. This was done by successive trypsin incubation/washing until the amount of bound trypsin remains constant. The total amount of trypsin to saturate PAB was found to be  $2.05 \pm 0.03$  nmol/well, which is 1000 times less than the amount of PAB present in the wells, and can be due to steric hindrance. As compared to our previous report (chapter 2), where trypsin was determined by Bradford or enzymatic activity assay, here trypsin was determined by making use of cytochrome c as substrate. This very sensitive method enabled the determination of trypsin in the low nM range, so as to coincide with the level of trypsin in healthy patients's blood (6-17 nM), or lower for people suffering from chronic pancreatitis. With the other assays using Bradford or enzymatic activity, the limit of quantification (LOQ) was respectively 4  $\mu$ M and 10 nM. Moreover, enzymatic activity assays for determining trypsin in blood is non-valid because of the presence of trypsin inhibitors [Kandregula et al., 2016]. In this method, cytochrome c is digested by trypsin into heme-peptide fragments, which display very high catalytic effect on the H<sub>2</sub>O<sub>2</sub>-mediated 3,3',5,5'-tetramethylbenzidine (TMB) oxidation [Zhang et al., 2016]. In order to separate the digested heme-peptide fragments from the non-digested cytochrome c, which is not catalytic, cytochrome c-coated GBs were used as substrates. Cytochrome c (pI : 10.3) was bound to IDA-functionalized GBs by electrostatic interactions in buffer A; the amount of cytochrome c grafted on 1 g of GBs was determined to be 0.11 mg. In the presence of active trypsin, peptides containing heme were released, which had an intense catalytic effect on TMB oxidation. The reaction made the color of the solution turn to blue, which could be read at 450 nm. The absorbance was proportional to the concentration of trypsin whose calibration curve is shown in Figure 7. The limit of quantification was 2 nM.

### **III-3. Binding assay of MIP and NIP with saturated trypsin immobilized on PAB-functionalized plate**

Each PAB-functionalized well was saturated with  $\sim 2$  nmol of trypsin. Concentrations of polymers varying from 0.2 – 200  $\mu$ g/mL were added to the wells for equilibrium binding assay in buffer A. After incubation, the supernatant (diluted if needed to fall within the calibration curves of figure 10) was read by fluorescence measurements. The binding isotherms show that the adsorption of the polymers behaves linearly, with almost 100% binding for the concentrations of MIP tested. On the other hand, there is very low binding of the NIP (Figure 13). The NIP was prepared without trypsin, that is on PAB alone and should

have bound to the excess PAB present in the wells, but it seems that they are not accessible probably due to steric hindrance caused by the trypsin coverage .

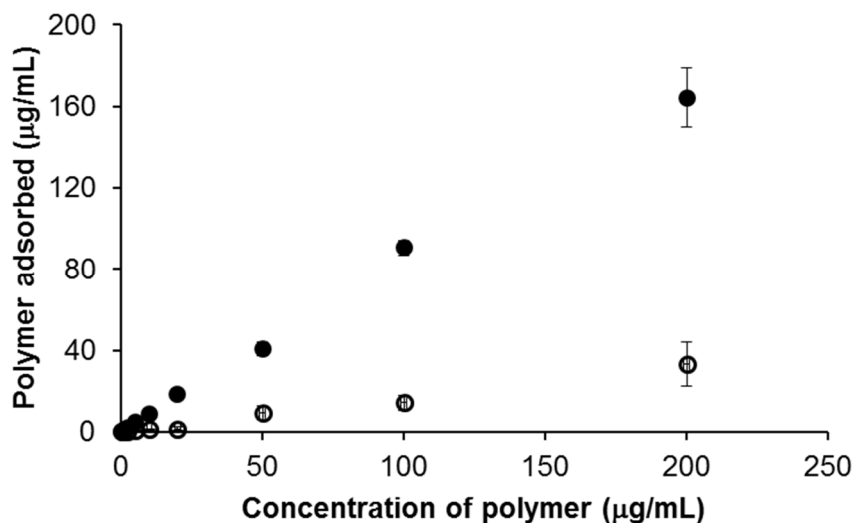


**Figure 13.** Binding isotherms of MIP (filled circles) and NIP (open circles) on immobilized-PAB saturated with trypsin. Adsorbed polymer was determined by measuring the fluorescence of the unbound polymer, using the calibration curves of Figure 10.

#### III-4. Selectivity test

In order to investigate the selectivity of the MIP toward immobilized trypsin, various competitors were tested. PAB is a competitive inhibitor of serine proteases, including trypsin, kallikrein and thrombin. Thus, all three serine proteases were selected to compete with a saturated amount of trypsin immobilized on PAB-functionalized well. In human serum, there is usually a high content of albumin (HSA) (57 – 71%, w/w), and a certain amount of cytochrome c (under 0.1 ng/ml) [Adachi et al., 2004]. For the purpose of future serum diagnosis, cytochrome c and HSA were also investigated. Therefore these five enzymes with concentrations between 0.5 nM – 50 µM, were added to 0.5 mL of 10 µg/mL of MIP. Figure 14 shows that the MIP has less affinity for immobilized trypsin in the presence of competing free trypsin, indicating that the MIP was very selective toward trypsin with an  $IC_{50}$  (the concentration of competing ligand required to displace 50% of the MIP) of 8.7 µM. The  $IC_{50}$  of all competitors, determined from a nonlinear regression fit, are shown in Table 3. Very low cross-reactivities were observed with the other proteins.

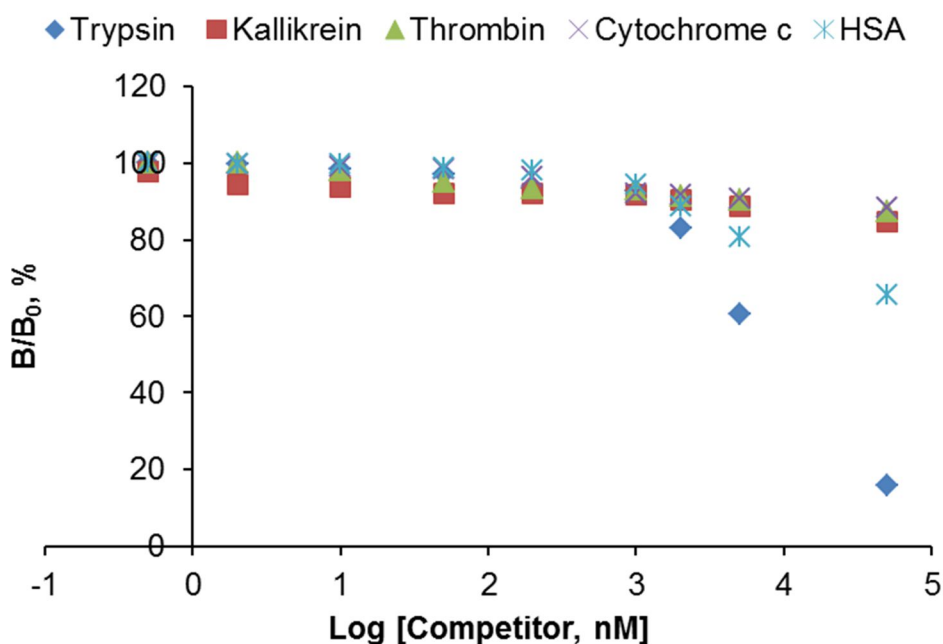


**Figure 14.** Displacement of 10 µg/mL MIP from immobilized trypsin (2 nmol) by free trypsin, kallikrein, thrombin, cytochrome c and HSA, in 25 mM sodium phosphate buffer pH 7. B/B<sub>0</sub> is the ratio of the amounts of MIP bound in the presence and absence of displacing ligand. Values represent the mean from two independent experiments.

**Table 3.** IC<sub>50</sub> of competitive proteins.

	Trypsin	Kallikrein	Thrombin	Cytochrome c	HSA
IC <sub>50</sub> (nM)	8.7 x 10 <sup>3</sup>	5.9 x 10 <sup>10</sup>	5.5 x 10 <sup>8</sup>	2.3 x 10 <sup>8</sup>	1.8 x 10 <sup>5</sup>
Cross reactivity, %	100	< 0.1	< 0.1	< 0.1	4.8

### III-5. Application of fluorescent core-shell MIP nanoparticles as plastic antibody in a pseudo-immunoassay format for the detection of trypsin in human serum

Trypsin concentrations ranging from 50 pM to 5 nM was spiked in human serum and applied to the PAB-functionalized well plate. A fixed amount of MIP (10 µg/mL = 20 nM) was used as detection plastic antibody for the quantification of trypsin.

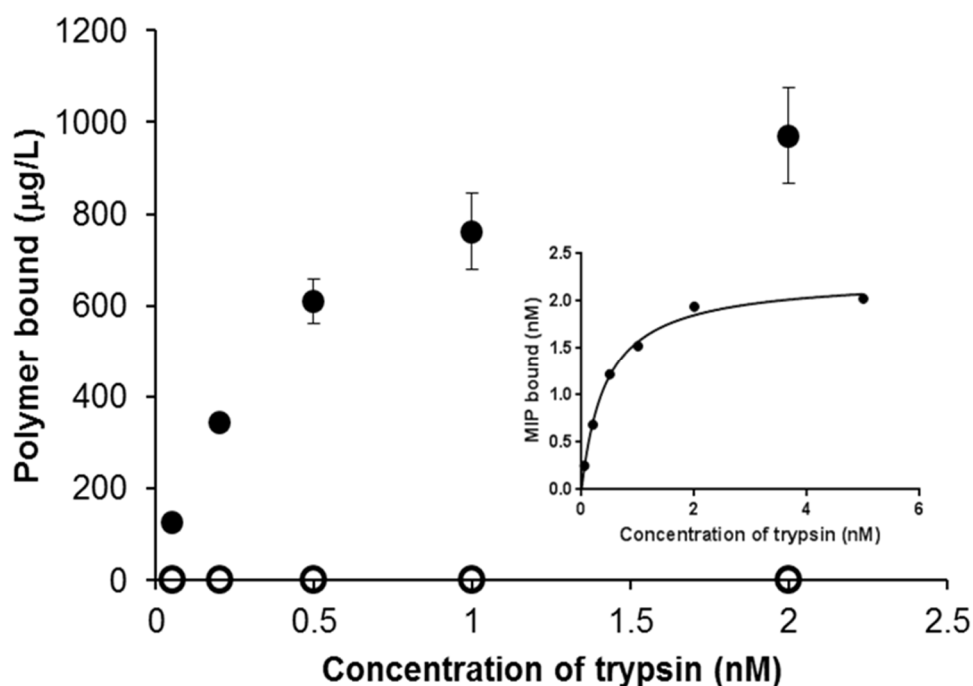


**Figure 15.** Application of fluorescent core-shell MIP (full circles) and NIP (empty circles) in a pseudo-ELISA format for the direct quantification of trypsin in human serum. Inset: Non-linear fitting of the data to a single site Langmuir binding isotherm. The molecular mass of the MIP was taken to be 500 kDa.

According to Figure 15, MIP specifically bound to immobilized trypsin in human serum, as no binding was observed with the NIP. The NIP was prepared without trypsin, that is in the presence of PAB alone and should have bound the large excess of PAB present in the wells. Apparently, these PAB are not accessible and might be due to steric hindrance due to the high coverage of trypsin or they are saturated by components present in the serum. The working region of the MIP covers 50 pM to 2 nM of trypsin. ~1000 µg/L of MIP which corresponds to ~2 nM, taking its molecular weight to be 500 kDa (Figure 4), was adsorbed by 2 nM trypsin. After fitting with Langmuir isotherm equation, the dissociation constant ( $K_d$ ) was found to be 0.34 nM (Figure 15, inset).

These results show that our assay is sensitive enough to detect low concentrations of trypsin directly in human serum. Other assays generally use diluted serum to dilute high background signals that interfere with the fluorescence measurements. Compared with traditional antibody-based ELISA kits for trypsin detection, this promising PAB-functionalized immunoassay would prove to be more rapid and straightforward, more stable, cheaper and

easier to operate. One limitation of the current format, however, is the possible presence in the serum of other proteins with affinity for PAB, for example other serine proteases like kallikrein or thrombin. It would therefore be interesting to develop a similar assay format where the capture of the analyte is also by a MIP (MIP sandwich format). Another alternative is to use the above-demonstrated competitive immunoassay format, where the selectivity is brought in by the detection MIP.

#### **IV. Conclusion**

Our main objective was to synthesize a sensitive ‘plastic antibody’ to detect trypsin, based on a water-soluble fluorescent MIP in a pseudo immunoassay-based format. Nowadays, commercially-available ELISA kits for the determination of trypsin are mainly based on a sandwich enzyme immunoassay where two antibodies are employed. Indeed, the kit usually comprises a microtiter plate pre-coated with an antibody specific to trypsin. Standards or samples are then added to the appropriate microtiter plate wells with a biotin-conjugated antibody specific to trypsin. Next, avidin conjugated to horseradish peroxidase is added to each microplate well and incubated. After TMB substrate solution is added, only those wells that contain trypsin, biotin-conjugated antibody and enzyme-conjugated avidin will exhibit a change in color, read spectrophotometrically at a wavelength of 450 nm. The concentration of trypsin in the samples is then determined by comparing the absorbance of the samples to the standard curve.

In this work, the fluorescent core-shell MIP acted as both the recognition and detection antibody. The MIP was stable during 4 months at room temperature (no aggregation and no loss of fluorescence were observed). With the assistance of a PAB-functionalized microtiter plate, the MIP can detect trypsin at very low concentrations in human serum (LOQ: 50 pM), comparable to the commercially available ELISA kits. The detection of trypsin in real samples with MIP has proven its great potential for its further application in clinical diagnosis. Noteworthy is the high stability of the PAB-functionalized well plate (more than 2 months) and together with the MIP could constitute an ELISA kit with high sensitivity, stability and cost-effectiveness.

## Acknowledgments

J. Xu thanks the China Scholarship Council (CSC). The authors acknowledge financial support from the Region of Picardy (cofunding of equipment under CPER 2007-2013). We thank Frederic Nadaud for the SEM images and Caroline Boulnois for TEM measurements.

## References

- Adachi, N., Hirota, M., Hamaguchi, M., Okamoto, K., Watanabe, K., & Endo, F. (2004). Serum cytochrome c level as a prognostic indicator in patients with systemic inflammatory response syndrome. *Clinica Chimica Acta*, 342(1), 127-136.
- Ambrosini, S., Beyazit, S., Haupt, K., & Tse Sum Bui, B. (2013). Solid-phase synthesis of molecularly imprinted nanoparticles for protein recognition. *Chemical Communications*, 49(60), 6746-6748.
- Beyazit, S., Tse Sum Bui, B., Haupt, K., & Gonzato, C. (2016). Molecularly imprinted polymer nanomaterials and nanocomposites by controlled/living radical polymerization. *Progress in Polymer Science*, 62, 1-21.
- Bi, X., & Liu, Z. (2013). Facile preparation of glycoprotein-imprinted 96-well microplates for enzyme-linked immunosorbent assay by boronate affinity-based oriented surface imprinting. *Analytical Chemistry*, 86(1), 959-966.
- Bonomi, P., Attieh, M. D., Gonzato, C., & Haupt, K. (2016). A new versatile water - soluble iniferter platform for the preparation of molecularly imprinted nanoparticles by photopolymerisation in aqueous media. *Chemistry-A European Journal*, 22(29), 10150-10154.
- Bossi, A., Bonini, F., Turner, A. P. F., & Piletsky, S. A. (2007). Molecularly imprinted polymers for the recognition of proteins: the state of the art. *Biosensors and Bioelectronics*, 22(6), 1131-1137.
- Cáceres, C., Canfarotta, F., Chianella, I., Pereira, E., Moczko, E., Esen, C., et al. (2016). Does size matter? Study of performance of pseudo-ELISAs based on molecularly imprinted polymer nanoparticles prepared for analytes of different sizes. *Analyst*, 141(4), 1405-1412.
- George, A., & Wilson, W. W. (1994). Predicting protein crystallization from a dilute solution property. *Acta Crystallographica Section D: Biological Crystallography*, 50(4), 361-365.

- Guerreiro, A., Poma, A., Karim, K., Moczko, E., Takarada, J., de Vargas - Sansalvador, I. P., et al. (2014). Influence of surface - imprinted nanoparticles on trypsin activity. *Advanced Healthcare Materials*, 3(9), 1426-1429.
- Haupt, K., Linares, A. V., Bompert, M., & Tse Sum Bui, B. (2012). Molecularly imprinted polymers. *Molecular Imprinting* (pp. 1-28). Springer Berlin Heidelberg.
- Hirota, M., Ohmuraya, M., & Baba, H. (2006). The role of trypsin, trypsin inhibitor, and trypsin receptor in the onset and aggravation of pancreatitis. *Journal of Gastroenterology*, 41(9), 832-836.
- Ionescu, R. E., Cosnier, S., & Marks, R. S. (2006). Protease amperometric sensor. *Analytical Chemistry*, 78(18), 6327-6331.
- Jiang, L., Bagán, H., Kamra, T., Zhou, T., & Ye, L. (2016). Nanohybrid polymer brushes on silica for bioseparation. *Journal of Materials Chemistry B*, 4(19), 3247-3256.
- Kandregula, C. A. B., Aseervatham, G. S. B., Bentley, G. T., & Kandasamy, R. (2016). Alpha-1 antitrypsin: Associated diseases and therapeutic uses. *Clinica Chimica Acta*, 459, 109-116.
- Kartal, F., & Denizli, A. (2014). Surface molecularly imprinted magnetic microspheres for the recognition of albumin. *Journal of Separation Science*, 37(15), 2077-2086.
- Kaur, J., Singh, K. V., Raje, M., Varshney, G. C., & Suri, C. R. (2004). Strategies for direct attachment of hapten to a polystyrene support for applications in enzyme-linked immunosorbent assay (ELISA). *Analytica Chimica Acta*, 506(2), 133-135.
- Li, S., Cao, S., Whitcombe, M. J., & Piletsky, S. A. (2014). Size matters: challenges in imprinting macromolecules. *Progress in Polymer Science*, 39(1), 145-163.
- Liu, Y., & Yu, J. (2016). Oriented immobilization of proteins on solid supports for use in biosensors and biochips: a review. *Microchimica Acta*, 183(1), 1-19.
- Moczko, E., Poma, A., Guerreiro, A., de Vargas Sansalvador, I. P., Caygill, S., Canfarotta, F. et al. (2013). Surface-modified multifunctional MIP nanoparticles. *Nanoscale*, 5(9), 3733-3741.
- Panagiotopoulou, M., Kunath, S., Medina-Rangel, P. X., Haupt, K., & Bui, B. T. S. (2017). Fluorescent molecularly imprinted polymers as plastic antibodies for selective labeling and imaging of hyaluronan and sialic acid on fixed and living cells. *Biosensors and Bioelectronics*, 88, 85-93.

- Poma, A., Guerreiro, A., Caygill, S., Moczko, E., & Piletsky, S. (2014). Automatic reactor for solid-phase synthesis of molecularly imprinted polymeric nanoparticles (MIP NPs) in water. *RSC Advances*, 4(8), 4203-4206.
- Qin, Y. P., Li, D. Y., He, X. W., Li, W. Y., & Zhang, Y. K. (2016). Preparation of high-efficiency cytochrome c-imprinted polymer on the surface of magnetic carbon nanotubes by epitope approach via metal chelation and six-membered ring. *ACS Applied Materials & Interfaces*, 8(16), 10155-10163.
- Sunayama, H., Ooya, T., & Takeuchi, T. (2014). Fluorescent protein-imprinted polymers capable of signal transduction of specific binding events prepared by a site-directed two-step post-imprinting modification. *Chemical Communications*, 50(11), 1347-1349.
- Surugiu, I., Ye, L., Yilmaz, E., Dzgoev, A., Danielsson, B., Mosbach, K., & Haupt, K. (2000). An enzyme-linked molecularly imprinted sorbent assay. *Analyst*, 125(1), 13-16.
- Suzuki, N., Quesenberry, M. S., Wang, J. K., Lee, R. T., Kobayashi, K., & Lee, Y. C. (1997). Efficient immobilization of proteins by modification of plate surface with polystyrene derivatives. *Analytical Biochemistry*, 247(2), 412-416.
- Xu, J., Ambrosini, S., Tamahkar, E., Rossi, C., Haupt, K., & Tse Sum Bui, B. (2016). Toward a universal method for preparing molecularly imprinted polymer nanoparticles with antibody-like affinity for proteins. *Biomacromolecules*, 17(1), 345-353.
- Xu, J., Medina-Rangel, P. X., Haupt, K., Tse Sum Bui, B. (2017). Guide to the preparation of molecularly imprinted polymer nanoparticles for protein recognition, by solid-phase synthesis. *Methods in Enzymology*, 590, in press.
- Yang, C., Yan, X., Guo, H., & Fu, G. (2016). Synthesis of surface protein-imprinted nanoparticles endowed with reversible physical cross-links. *Biosensors and Bioelectronics*, 75, 129-135.
- Yang, H. H., Lu, K. H., Lin, Y. F., Tsai, S. H., Chakraborty, S., Zhai, W. J., & Tai, D. F. (2013). Depletion of albumin and immunoglobulin G from human serum using epitope - imprinted polymers as artificial antibodies. *Journal of Biomedical Materials Research Part A*, 101(7), 1935-1942.
- Yang, H., Guo, T. Y., & Zhou, D. (2011). Surface hydrophilic modification with well-defined glycopolymer for protein imprinting matrix. *International Journal of Biological Macromolecules*, 48(3), 432-438.

Ye, L. (2015). Synthetic strategies in molecular imprinting. *Molecularly Imprinted Polymers in Biotechnology* (pp. 1-24). Springer International Publishing.

Zhang, H. (2015). Recent advances in macromolecularly imprinted polymers by controlled radical polymerization techniques. *Molecular Imprinting*, 3(1), 35-46.

Zhang, L., & Du, J. (2016). A sensitive and label-free trypsin colorimetric sensor with cytochrome c as a substrate. *Biosensors and Bioelectronics*, 79, 347-352.

# **Rapid detection of trypsin with a molecularly imprinted polymer as a selective fluorescence nanoprobe**

## **I. Introduction**

Trypsin, a member of the serine proteases family, is widely used for the fragmentation of proteins into peptides and is the most-frequently used protease in mass spectrometry-based proteomics. Due to this proteolytic property, trypsin is also used in many biochemical and biomedical domains like for instance in the production of hydrolyzed cow milk formula for newborns who are allergic to cow milk [von Berg et al., 2003], in the isolation and culture of mesenchymal stem cells from bone marrow, where trypsin is used to separate the different cell types [Soleimani & Nadri, 2009] or in the isolation of retinal endothelial cells, where it is used to remove pericyte contamination [Banumathi et al., 2009]. In humans, trypsin is a digestive enzyme, produced in the pancreas, as its inactive precursor trypsinogen. It plays an essential role in controlling the exocrine pancreas function, thus the level of trypsin serves as a reliable and specific diagnostic biomarker for alteration in the pancreatic function [Hirota et al., 2006]. Although there is no trypsin in healthy people's urine, the level of trypsin in pancreas transplant patients is very high, for whom an average concentration of 84.4  $\mu\text{g/mL}$  (3.6  $\mu\text{M}$ ) was found [See & Smith, 1991]. Thus, developing simple, selective and sensitive assays for trypsin is useful for a wide number of biotechnological and diagnostic applications.

Traditional methods for trypsin detection include colorimetric [Zhang & Du, 2016], amperometric [Ionescu et al., 2006], ELISA [Antibodies-online, ABIN1116730; Boster Biological Technology, EK1531; MyBioSource, MBS701760] and fluorescence analysis [Gao et al., 2012]. Of these, the latter method was reported to process advantages like high sensitivity and simplicity. Therefore, the development of highly sensitive fluorescent sensors has been largely reported. In particular, molecularly imprinted polymers (MIPs) have been widely used as artificial receptors for fluorescence sensing, [Wackerlig & Lieberzeit, 2015; Ton et al., 2013]. Target binding can be monitored by directly measuring a fluorescent analyte, or, if the analyte is not fluorescent, by a competitive assay

with a fluorescent analog as a probe. Alternatively, non-fluorescent analytes can be monitored if a fluorescent monomer is incorporated into the MIP that shows a change in its fluorescence properties when analyte binding occurs [Haupt & Mosbach, 2000], namely fluorescence quenching [Takeuchi et al., 2005; Wagner et al., 2013], fluorescence shift [Matsui et al., 2000] or fluorescence enhancement [Leung et al., 2001; Kubo et al., 2003; Ton et al., 2013]. Among all these techniques, detection by fluorescence enhancements is preferred because quenching can be due to non-specific interactions, resulting in false-positive responses [Ton et al., 2015] and fluorescence shift can sometimes not be sensitive enough.

MIPs are biomimetic synthetic receptors possessing specific cavities designed for a target molecule. Produced by a templating process at the molecular level, MIPs are capable of recognizing and binding their targets with specificities and affinities comparable to those of natural receptors. These tailor-made synthetic receptors have considerable advantages over biological receptors due to their greater chemical and physical stability, and have become an interesting alternative as recognition elements for biosensors. Currently, literature reports two MIP-based biosensors for trypsin detection; one is based on a quartz crystal microbalance [Hayden et al., 2006] and the other on capacitive electrodes [Ertürk et al., 2016]. These MIP-based biosensors, though sensitive, are not easy to set up and require sophisticated laboratory equipment and trained personnel.

Herein, we describe the development of a cheap and user-friendly water-soluble fluorescent MIP-based nanoprobe for the rapid sensing and quantification of trypsin. *p*-aminobenzamidine (PAB), a competitive inhibitor of serine proteases has been reported to undergo a 50-fold and 230-fold fluorescence enhancement, while binding to either trypsin or thrombin respectively. Fluorescence titration of PAB with the latter proteins showed that the PAB-protein complex had a 1:1 stoichiometry and the enhancement was due to interaction at the enzyme's active center [Evans et al., 1982]. Thus PAB can be considered a specific sensitive fluorescent probe for serine proteases. On the other hand, we previously reported the use of a polymerizable PAB monomer, (4-acrylamidophenyl)(amino) methaniminium chloride (AB), to orientate trypsin in a fixed position during the preparation of a MIP [Cutivet et al., 2009]. This strategy confined the polymerization to the close proximity of the recognition site of the protein and in turn generates highly selective MIPs for trypsin. This MIP was synthesized in a nanoparticle format with soluble trypsin as template, and

may therefore suffer from difficult or incomplete template elimination and a certain binding site heterogeneity. In order to improve the binding properties and binding site heterogeneity, as well as the access to the sites for rapid detection, the binding site must be rapidly accessible and one possibility would be to create them at the surface of the MIP.

Therefore, a solid-phase synthesis approach is proposed here for the preparation of MIP nanoparticles with binding sites on their surface, for trypsin detection. Trypsin was immobilized on  $\text{Cu}^{2+}$ -iminodiacetic acid (IDA) functionalized glass beads (GBs), via its surface histidine residue. The functional monomer, AB, which proved to be fluorescent (like PAB), was next added so as to act as a signaling reporter group and at the same time, to interact with the active site of trypsin. A thermoresponsive MIP was synthesized with *N*-isopropylacrylamide (NIPAm), *N,N'*-methylenebis(acrylamide) (Bis) and a water-soluble iniferter, diethylthiocarbamoylsulfanyl acetic acid (DCAA) by UV polymerization around trypsin. After washing the unreacted monomers and low-affinity polymers, the high-affinity MIP nanoparticles were eluted from the solid phase by decreasing the temperature (Figure 1).

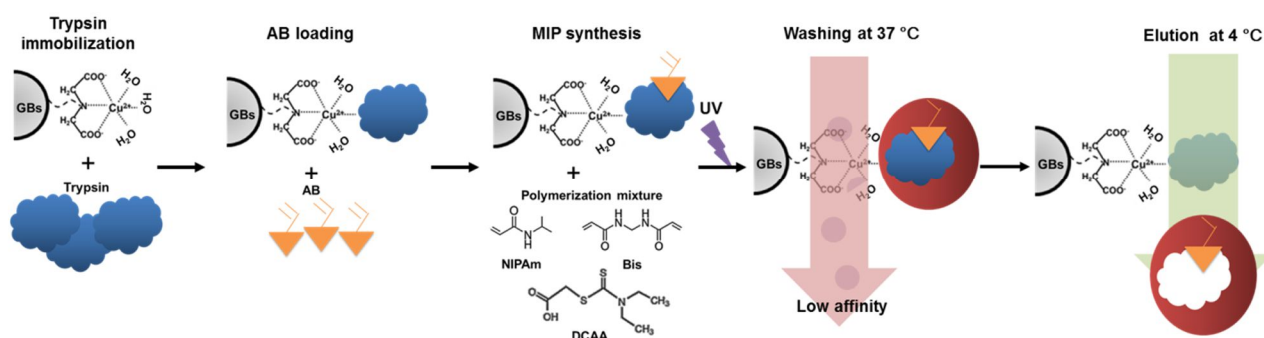


**Figure 1.** Solid-phase synthesis of trypsin MIP nanoparticles containing the fluorescent signaling monomer, AB.

The resulting MIP nanoparticles were water soluble and contained the fluorescent monomer AB, for sensing. When AB is excited at 280 nm, fluorescence enhancement occurs upon trypsin binding to the MIP, the fluorescence intensity being proportional to the trypsin concentration (Figure 2). The MIP proved to be specific and selective towards trypsin, as little cross-reactivity was observed during competitive binding assay with thrombin, human serum albumin (HSA) and cytochrome c. The MIP sensor was then applied to measure trypsin in human urine.

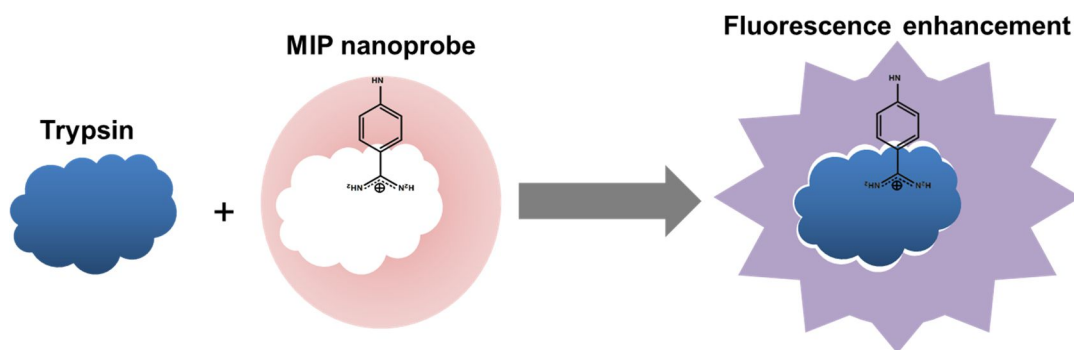


**Figure 2.** Schematic representation of fluorescence enhancement of MIP nanoprobe upon binding with trypsin. Binding of trypsin also results in a blue shift.

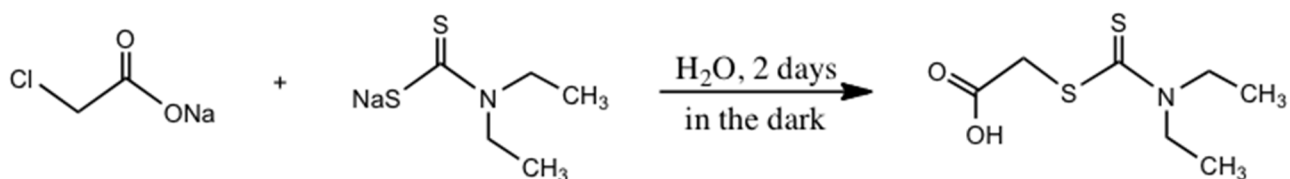
## II. Experimental section

### Materials and Methods

All chemicals and solvents were of analytical grade and purchased from VWR International (Fontenay sous Bois, France) or Sigma-Aldrich (St Quentin Fallavier, France), unless otherwise stated. The proteins: trypsin from bovine pancreas (specific activity: > 10 000 units/mg protein), thrombin from bovine plasma, cytochrome c from horse heart, and human serum albumin were purchased from Sigma-Aldrich. Glass beads (GBs) of diameter 0.1 mm, were obtained from Roth Sochiel E.U.R.L (Lauterbourg, France). Polystyrene 48-well microplates, used for competitive experiments, were purchased from BECTON DICKINSON (Le Pont De Claix, France). Buffers were prepared with Milli-Q water, purified using a Milli-Q system (Millipore, Molsheim, France). Human urine was collected from two healthy female and two healthy male volunteers, aged 25 years old.

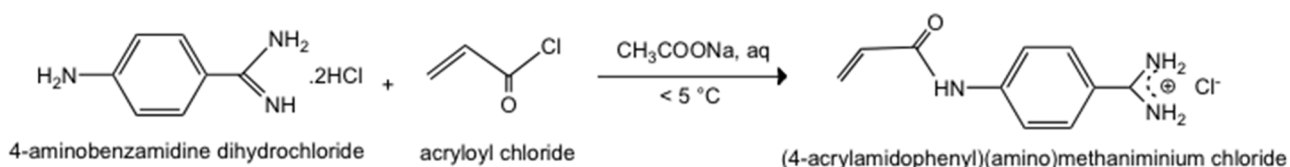
All fluorescence measurements were performed on a FluoroLog-3 spectrofluorimeter (Horiba Jobin Yvon, Longjumeau, France). Polymerization was carried out at 312 nm on a UV lamp (6 x 8 W) (Fisher Bioblock Scientific, France). Polymer size analysis was carried out by nanoparticle tracking analysis (NTA) on Nanosight NS500 (Malvern, France) at 25 °C. For scanning electron microscopy (SEM) imaging, polymer particles were sputter coated with gold prior to the analysis, and images were taken by a Quanta FEG 250 scanning electron microscope (FEI Europe, Netherlands).

### Synthesis of the water-soluble iniferter, diethylthiocarbamoylsulfanyl acetic acid (DCAA)



The synthesis of DCAA was prepared as previously reported [Tsuji & Kawaguchi, 2006] with some modification to have a higher yield. First, 1801.2 mg (8 mmol) of sodium diethylthiocarbamate trihydrate was dissolved in 10 mL of water (referred as solution 1). Second, 932 mg (8 mmol) of sodium chloroacetate was dissolved in 10 mL of water (referred as solution 2). Solution 2 was then added to solution 1 dropwise and the reaction was left to proceed for 2 days under magnetic stirring. The mixture was shielded from light with aluminum foil. HCl (38%) was then added to the solution to precipitate the product until pH 1.5 – 2.0 (monitored by pH meter). The final product was recrystallized from acetone in the fridge and then filtered, yielding the water-soluble iniferter, which is a white powder. Yield was 67.1%.  $^1\text{H NMR}$  (400 MHz,  $\text{CDCl}_3$ ):  $\delta$  (ppm) 4.19 (s, 2H,  $\text{CH}_2$ ), 4.02 (q, 2H,  $\text{CH}_2\text{-CH}_3$ ), 3.77 (q, 2H,  $\text{CH}_2\text{-CH}_3$ ), 1.34 (t, 3H,  $\text{CH}_2\text{-CH}_3$ ), 1.29 (t, 3H,  $\text{CH}_2\text{-CH}_3$ ).

### Synthesis of (4-acrylamidophenyl)(amino)methaniminium chloride (AB)



AB was prepared as previously reported [Beyazit et al., 2014]. 34 g (0.41 mol) of sodium acetate trihydrate was dissolved in 200 mL of water and 2 g (9.6 mmole) of 4-aminobenzamidine dihydrochloride (PAB) was added. The solution was cooled to  $< 5\text{ }^\circ\text{C}$  in an ice bath and 4 mL (49 mmole) of acryloyl chloride was added dropwise. The reaction was left to proceed for 1h. The pH was then adjusted to 4.0 with hydrochloric acid (37%) and precipitation was observed. After filtration, the precipitate was redissolved in 100 mL of water at  $40\text{ }^\circ\text{C}$ . Hydrochloric acid was again added this time to pH 1.0 and the product was left overnight to crystallize at  $4\text{ }^\circ\text{C}$ . The crystals were collected by filtration and dried in an oven maintained at  $50\text{ }^\circ\text{C}$ . The yield of (4-acrylamidophenyl)(amino)methaniminium chloride was 86.9%.  $^1\text{H NMR}$ :  $\delta$  (ppm) 11.01 (s, 1H,

NH), 9.31 (s, 2H, NH<sub>2</sub>), 9.10 (s, 2H, HN<sub>2</sub>), 7.93 (d, 2H, H<sub>aromatic</sub>), 7.86 (d, 2H, H<sub>aromatic</sub>), 6.59 (dd, 1H, CH=), 6.31 (dd, 1H, CH=), 5.81 (dd, 1H, CH=).

### Synthesis of FITC-trypsin

FITC-trypsin was synthesized as previously reported [Ambrosini et al., 2013]. Trypsin (2 mg/mL) was dissolved in 100 mM sodium bicarbonate buffer pH 9.2 and mixed with 78.5  $\mu$ L of FITC solution (10 mg/mL in DMSO). The reaction mixture was incubated for 2h at room temperature and the labeled protein was separated by gel filtration on a PD-10 column (GE Healthcare) equilibrated with 0.1 M Tris-HCl buffer + 0.15 M NaCl pH 7.2. To avoid trypsin autoproteolysis, the pH of the fraction containing FITC-trypsin was brought to 3.0 by adding a solution of 2 M HCl. The fraction was divided into aliquots of 3.5 mL which were then stored at -20 °C. To determine the fluorescein-trypsin ratio, trypsin concentration was measured with the Bradford method, whereas the bound fluorescein was determined via its absorption at 495 nm using a molar extinction coefficient of FITC  $\epsilon_{495\text{ nm}} = 68000\text{ M}^{-1}\text{ cm}^{-1}$ . FITC-trypsin was found to have a ratio of fluorescein/trypsin of 1.5. A calibration curve of FITC-trypsin over the concentration range of 10 – 1000 nM is shown in Figure 3. The fluorescence intensity was read on a spectrofluorimeter using  $\lambda_{\text{ex}} = 285\text{ nm}$  (excitation wavelength of trypsin),  $\lambda_{\text{em}} = 515\text{ nm}$  (emission wavelength of FITC-trypsin complex), with slit 3 nm.

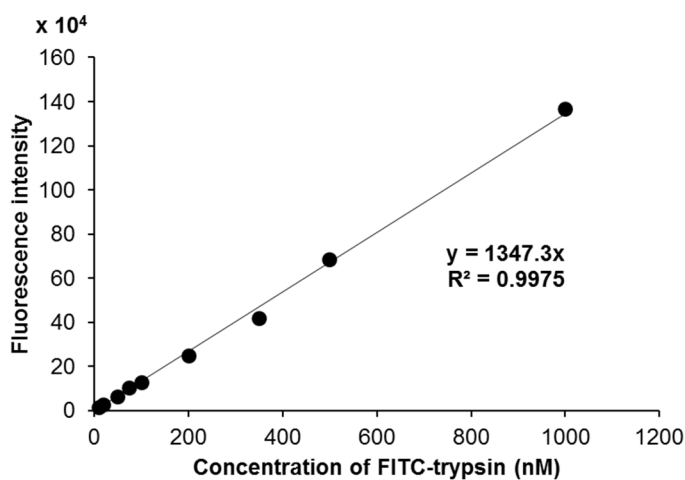


**Figure 3.** Calibration curve of FITC-trypsin over the concentration range of 10 – 1000 nM in 25 mM sodium phosphate buffer pH 7 ( $\lambda_{\text{ex}} = 285\text{ nm}$ ,  $\lambda_{\text{em}} = 515\text{ nm}$ , slit 3 nm).

## II-1. Solid-phase synthesis of protein-imprinted polymer nanoparticles

*Functionalization of GBs with IDA-Cu<sup>2+</sup>*. Glass beads (GBs) functionalized with IDA-Cu<sup>2+</sup> was synthesized as previously reported [Xu et al., 2016] and chapter 2. Briefly, 100 g glass beads were boiled for 10 min in 100 mL of 4 M NaOH solution at 100 °C. After intensive washing with water, the GBs were dried in an oven at 50 °C. Then, 50 g of activated GBs were added to a mixture of 100 mL anhydrous toluene and 100 mL (3-Glycidyloxypropyl)trimethoxysilane (Glymo) in a round-bottom flask and refluxed at 110 °C for 17h. The Glymo-coupled glass beads (Glymo-GBs) were collected and washed three times with toluene and acetone. After drying in an oven at 50 °C, the Glymo-GBs were immersed into 500 mL of a 0.75 M iminodiacetic acid (IDA) solution (containing 0.34 M NaCl and 2.0 M Na<sub>2</sub>CO<sub>3</sub>, pH 11.0) and stirred at 70 °C for 17 h. The final GBs were obtained after washing five times with water.

*Synthesis of MIP-NPs*. 20 g IDA-GBs were placed in a glass petri dish fitted with a cover lid (d x h: 14 x 2 cm), and incubated with 50 mL of 50 mM CuSO<sub>4</sub> with shaking overnight. Then the GBs were washed with 5 x 40 mL water, followed by equilibration with 5 x 40 mL of 25 mM sodium phosphate buffer, pH 7.0 (buffer A). 40 mL of 1 mg/mL trypsin was then added to the metal chelate-GBs and incubated for 1h, followed by washing with 5 x 40 mL buffer A. The fluorescent monomer, AB, (a stock solution of 5 mg/mL AB was first prepared in dimethyl sulfoxide, then 3 x 40 mL AB at a concentration of 6.25 µg/mL equivalent to 27.7 µM, which is 3 times the K<sub>d</sub> value of the complex PAB-trypsin, [Evans et al., 1982]) was put into the petri dish and incubated with GBs, with shaking for 15 min each volume, followed by washing with 40 mL buffer A. After purging with N<sub>2</sub> for 20 min, 48.6 mL of a pre-polymerization mixture in buffer A, containing 181.1 mg (1.6 mmol) of *N*-isopropylacrylamide (NIPAm), 61.6 mg (0.4 mmol) of *N,N'*-methylenebis(acrylamide) (Bis) and 17.1 mg (0.063 mmol) of diethylthiocarbamoylsulfanyl acetic acid (DCAA, 3.5% of double bonds, added at the end), was poured onto the GBs. The polymerization was carried out under UV 312 nm at room temperature for 40 min. The GBs were washed twice with 40 mL buffer A at 37 °C to remove the low-affinity nanoparticles and unreacted monomers, and the high-affinity MIPs were eluted at 4 °C with 20 mL of buffer A (Figure 1). The same procedure was followed in the absence of the template, for the synthesis of the non-imprinted polymers (NIPs).

## II-2. Characterization of polymers

*Yield of synthesis.* 10 mL of MIP and NIP solution was dialyzed (dialysis membrane MWCO 3500 Da, Interchim, France) overnight in 5 L of water. Their concentration was calculated after lyophilization of the dialyzed aliquots and weighing on a precision balance. The concentrations of both MIP and NIP were found to be 0.2 mg/mL, which means the yield of polymerization was 0.2 mg/g of GBs.

*Physicochemical characterization.* The hydrodynamic size of the dialyzed nanoparticles (diluted 10 times with water to a concentration of approximately  $10^8$  particles/mL prior to injection) was measured on a NanoSight NS500 (Malvern Instruments, France), using nanoparticles tracking analysis. Three independent analyses were performed recording 60 seconds videos at 25 °C. The zeta potential analysis was done on the same sample under 24.0 voltage (average current: 0.66 – 1.22  $\mu$ A). Two independent analyses were performed recording 90 seconds videos at 25 °C.

*Fluorescence calibration of MIP and NIP.* The stock solution of MIP or NIP (0.2 mg/mL in buffer A) was concentrated on Amicon Ultra centrifugal filters (30 kDa, Merck Chimie SAS, France) or diluted with buffer A to prepare concentrations varying between 0.1 to 2 mg/mL for measurements. Fluorescence measurements were done on a spectrofluorimeter, with  $\lambda_{\text{ex}} = 280$  nm,  $\lambda_{\text{em}} = 360$  nm, and slit of 3 nm.

*Molecular weight determination.* The molecular weight of MIP in buffer A was obtained by analysis of the intensity of light scattered from the particle at different concentrations, in the dilute regime. This is done by applying the Rayleigh equation [George & Wilson, 1994]:

$$KC/R_{\theta} = 1/M + 2A_2C$$

$R_{\theta}$  is the Rayleigh ratio: ratio of scattering of the sample compared to the scattering of a standard (toluene),  $K$  is an optical constant,  $C$  is the sample concentration,  $M$  is the molecular weight and  $A_2$  is the second virial coefficient (representing the magnitude of particle - solvent interactions). To determine the molecular weight, the Rayleigh equation is represented graphically in the form of a Debye plot showing the concentration ( $C$ ) dependence of intensity of scattered light ( $KC/R_{\theta}$ ).  $M$  is determined from the intercept on the y-axis and  $A_2$  from the slope of the Debye plot.

The stock solution of MIP (0.2 mg/mL in buffer A) was concentrated on Amicon Ultra centrifugal filters (30 kDa) or diluted with buffer A to prepare concentrations varying between 0.05 to 0.8 mg/mL for measurements. The molecular weight was determined on a Zetasizer NanoZS (Malvern Instruments Ltd., France) at 25 °C. The Debye plot is shown in Figure 4, which indicates a molecular weight of  $475 \pm 33$  kDa ( $R^2 = 0.94$ ) and a second virial coefficient of  $-0.00035$  mL mol/g<sup>2</sup>. A negative  $A_2$  indicates that the polymer-polymer interaction is stronger than polymer-solvent interaction, and at high concentrations the polymers may aggregate.

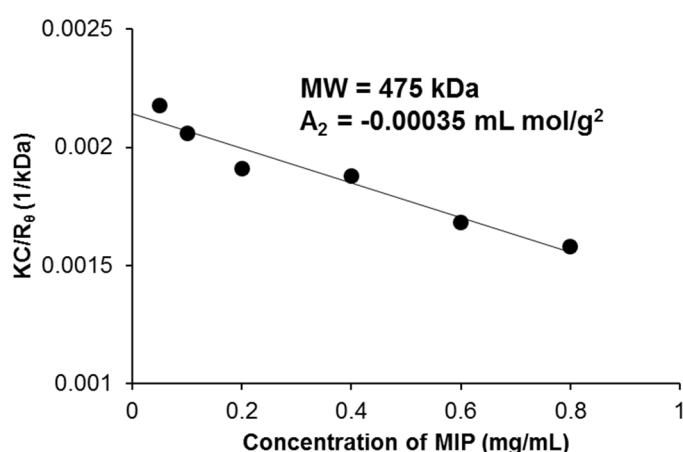


**Figure 4.** Debye plot for the determination of the absolute molecular weight of MIP

### II-3. Binding test of polymers based on fluorescence enhancement

The effect of different concentrations of trypsin (50 nM – 1000 nM), prepared in buffer A on the fluorescence enhancement of the polymers was evaluated. 0.5 mL of each concentration of trypsin was mixed with a fixed amount (0.5 mL from a stock solution: 0.2 mg/mL) MIP or NIP. After 5 min, the mixture was directly measured on the spectrofluorimeter ( $\lambda_{ex}$ : 280nm,  $\lambda_{em}$ : 360 nm, Slit: 3 nm). Fluorescence enhancement was calculated by subtracting the fluorescence intensity of 0.1 mg/mL MIP or NIP alone.

To test if the enhancement was selective towards trypsin, other proteins such as thrombin, HSA and cytochrome c, at the same concentration range (50 nM – 1000 nM), were incubated with 0.1 mg/mL of MIP. Fluorescence enhancement was calculated by subtracting the fluorescence intensity of 0.1 mg/mL MIP alone.

The binding was also evaluated by incubating a fixed amount of trypsin (250 nM) with varying MIP

or NIP concentrations (0.1 – 2 mg/mL) for 1 h. The fluorescence enhancement was calculated by subtracting the fluorescence intensity of the corresponding concentration of MIP or NIP.

#### **II-4. Competitive binding experiments of MIP with FITC-trypsin in presence of unlabeled trypsin, thrombin, HSA and cytochrome c**

Competitive binding experiments were done on MIP immobilized in a 48-well microtiter plate. The plate was first activated, as previously described [Bi & Liu, 2013]. Briefly, each well was filled with 0.5 mL of H<sub>2</sub>SO<sub>4</sub> (95%)/HNO<sub>3</sub> (63%) mixture (3:1, v/v), and left at room temperature for 30 min. Then, 0.5 mL of MIP (stock solution: 0.2 mg/mL) was added to each well, and physically coated on the plate by drying at 37 °C overnight. The activated microplate was intensively washed with water until the pH became neutral, followed by drying in air. The microplate was blocked with 0.5% tween 20 in buffer A, and washed three times with buffer A (1 mL each well). Afterward, 0.5 mL trypsin conjugated with FITC, concentrations ranging from 10 – 1000 nM, was added into each well. After incubation for 2h, the supernatant was withdrawn for fluorescence measurements. The trypsin-FITC bound to MIP was determined by subtracting the amount of unbound from the amount incubated in wells containing no MIP.

For the selectivity test, either free trypsin, thrombin, HSA, cytochrome c, or a mixture of thrombin, BSA and cytochrome were made to compete with trypsin-FITC. The MIP was immobilized as described above. After blocking with 0.5% tween 20, each well was washed 5 times with 1 mL buffer A. 0.5 mL of 200 nM trypsin-FITC was mixed with 0.5 mL of 200 nM of trypsin, thrombin, BSA, or cytochrome c, or their mixture. The amount of bound protein was calculated by measuring the amount of trypsin-FITC displaced.

#### **II-5. Application of MIP sensor for detection of trypsin in urine**

Urine samples were collected from two healthy female and two healthy male volunteers. The urine was centrifuged at 7,500g for 10 min, and the supernatant used for further application. 0.1 mL of each urine sample (or buffer A) was mixed with 0.9 mL of 0.11 mg/mL MIP and their fluorescence spectra was recorded ( $\lambda_{\text{ex}}$ : 280nm, Slit: 2 nm). The final concentration in the assay was 0.1 mg/mL of MIP and the urine was diluted 10-fold in buffer A. A stock solution of trypsin (50  $\mu$ M) was

prepared in 1 mM HCl + 10 mM CaCl<sub>2</sub> (pH ~ 5) and stored in ice. The urine samples were spiked with trypsin at concentrations ranging from 0 to 1000 µg/mL. Then 0.1 mL of trypsin spiked urine sample was added into 0.9 mL of 0.11 mg/mL MIP. After 5 min, the samples were directly measured on the spectrofluorimeter ( $\lambda_{\text{ex}}$ : 280nm,  $\lambda_{\text{em}}$ : 380 nm, Slit: 2 nm).

### III. Results and discussion

#### III-1. Fluorescence characterization of AB monomer

Prior to the preparation of the fluorescent imprinted polymers, the signaling monomer AB, was characterized and titrated with increasing concentrations of trypsin (50 – 500 nM) to verify whether fluorescence enhancement and thus the interaction was taking place. The maximum excitation and emission wavelengths of AB were 285 nm and 365 nm, respectively. Binding to trypsin results in a blue shift of the emission peak to 340 nm. The fluorescence enhancement of AB was observed to be concentration-dependent and increased with increasing concentrations of trypsin (Figure 5B), confirming that AB could be used as a fluorescent probe. Here, the contribution of trypsin alone, to the fluorescence of AB is negligible.

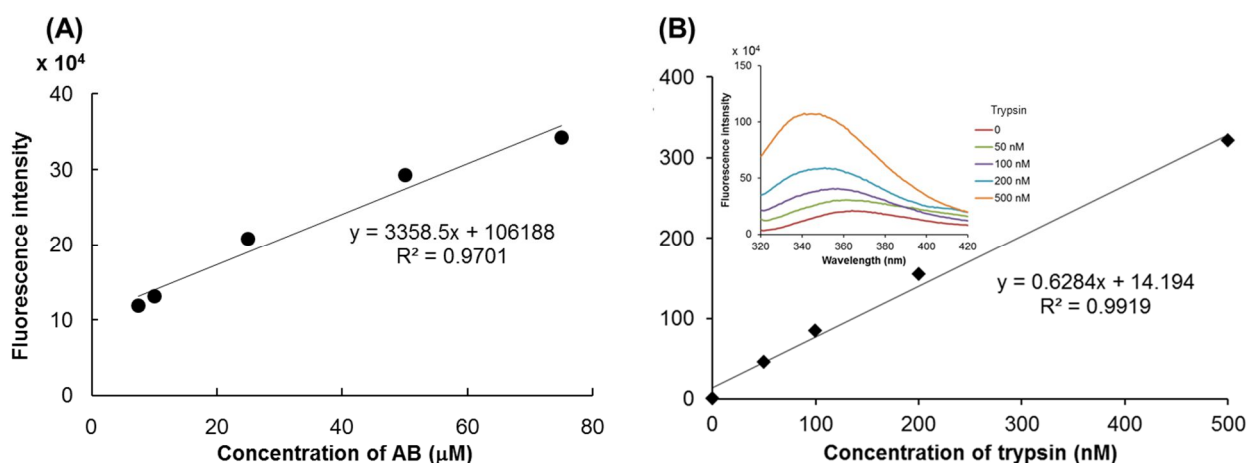


**Figure 5.** (A) Calibration curve of AB; (B) Fluorescence response of AB (25 µM) with increasing concentrations of trypsin (50, 100, 200, 500 nM), in 25 mM sodium phosphate buffer pH 7. Inset: Corresponding fluorescence spectra of AB with increasing concentrations of trypsin with  $\lambda_{\text{ex}} = 285$ ,  $\lambda_{\text{em}} = 365$  nm, slit 4 nm.

### III-2. Synthesis of polymers

The solid-phase synthesis of the polymers is represented in Figure 1 and was done as previously reported [Xu et al., 2016], with some modifications. Briefly, activated GBs obtained by boiling in NaOH so as to introduce –OH groups, were silanized with Glymo, followed by coupling with the chelating agent IDA. The latter was saturated by coordinate bonds with  $\text{Cu}^{2+}$  which in turn can bind proteins containing surface exposed histidines. Trypsin has two surface histidines, as deduced from the Swiss-Pdb viewer program by selecting 10% surface accessibility of the 3D structure of bovine pancreas trypsin (1s0q). One histidine is implicated in the Ser/His/Asp triad responsible for the catalysis of the enzyme and it is the other His residue which is implicated in the immobilization of trypsin to  $\text{Cu}^{2+}$  [Ma et al., 2011]. The amount of trypsin bound per gram of IDA- $\text{Cu}^{2+}$  GBs was  $15.9 \pm 0.8$  nmol. After the formation of IDA- $\text{Cu}^{2+}$ -trypsin complex, the fluorescent monomer AB was added and since the active site of trypsin was left free, AB got anchored to it. This configuration is highly advantageous because it will give rise to oriented MIP with high affinity binding sites.

The polymerization mixture was composed of NIPAm and Bis (80/20 molar ratio) and the water soluble iniferter DCAA, in buffer A. NIPAm was used as the major component in this polymer recipe in order to obtain thermoresponsive MIPs. PolyNIPAm undergoes a volume-phase transition at the lower critical solution temperature (LCST = 32 °C), which means it changes from a swollen hydrated state to a shrunken dehydrated state when heated above 32 °C. The imprinted polymer was synthesized in a petri dish, by iniferter-induced polymerization for 40 min, initiated by UV light at 312 nm. The temperature inside the polymerization mixture reached 37 °C. After polymerization, the GBs were washed with buffer A at 37 °C to remove unreacted monomers and low-affinity polymers. The high affinity MIPs were eluted at 5 °C, temperature at which they swell and are detached from the protein. The eluted fraction was analyzed for the presence of active trypsin by measuring the enzymatic activity, and of denatured trypsin by using the Bradford assay. No trypsin was detected, indicating that the MIPs were template-free.

### III-3. Characterization of MIPs

The yield of polymerization was 0.2 mg/g GBs. This was deduced from the concentration of polymer

particles collected after synthesis. An aliquot of known volume (10 mL) was dialysed in water, lyophilized and weighed on a precision balance. The concentration was found to be 0.2 mg/mL. Knowing the mass of GBs and the total volume of polymer eluted, the yield of synthesis as mg per g of GBs was calculated.

The morphology of the MIP nanoparticles was analysed by SEM. Figure 6 shows that the particles were fairly homogeneous, with a maximum size of 70 nm. Figure 7 presents the size and zeta potential of the MIP, analyzed by nanoparticle tracking analysis on Nanosight NS500. The hydrodynamic diameter of MIP was  $109.3 \pm 6.3$  nm with zeta potential of  $-11.4 \pm 0.1$  mV, and NIP particles was  $150.3 \pm 27.3$  nm with zeta potential of  $-11.7 \pm 4.4$  mV.

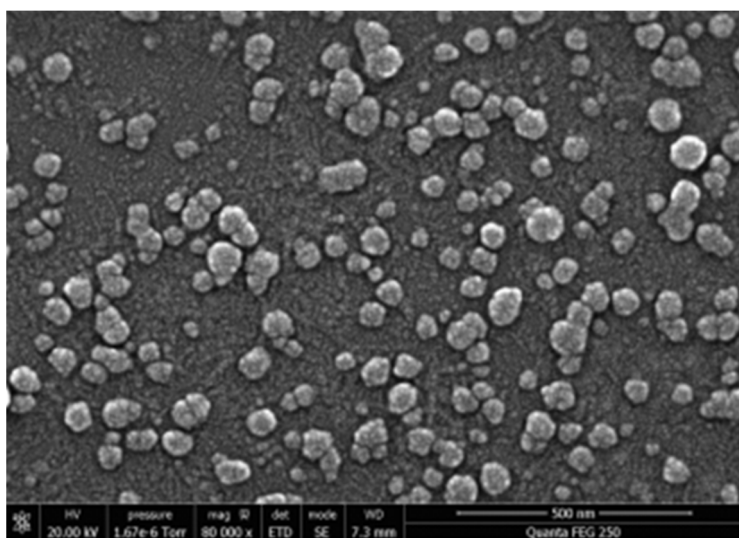


**Figure 6.** SEM image of MIP nanoparticles.

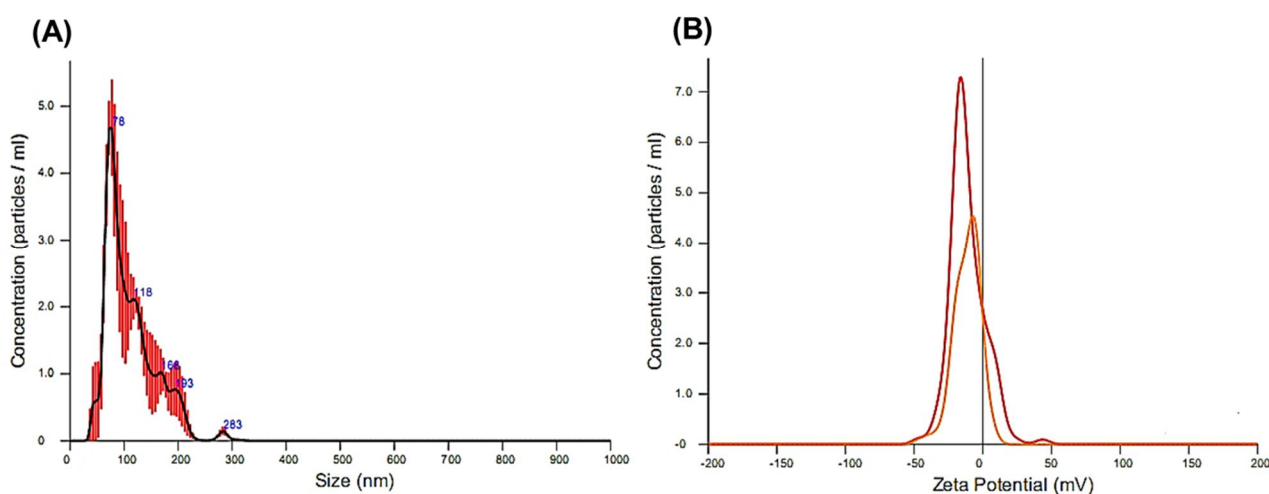


**Figure 7.** Representative results of MIP in water at 25 °C analyzed by Nanosight, (A) Size graph for

three times capture with averaged concentration/size; (B) Zeta potential for two times capture with concentration/zeta potential.

### III-4. Binding test based on fluorescence enhancement

In order to verify whether AB has been incorporated in the polymers during polymerization, fluorescence intensities of MIP and NIP were measured and their calibration curves are presented in Figure 8.

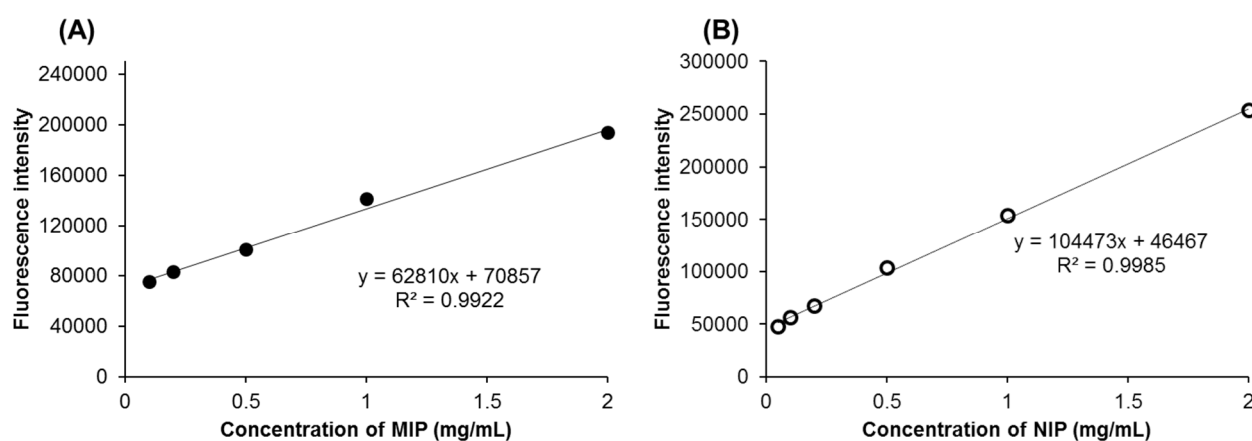


**Figure 8.** Fluorescence calibration curves of MIP (A) and NIP (B), using  $\lambda_{\text{ex}} = 280$ ,  $\lambda_{\text{em}} = 360$  nm and slit = 3 nm.

The binding properties of the polymers were then evaluated by spectrofluorimetric titrations with trypsin. Solutions of 0.1 mg/mL of MIP and NIP were incubated with 50–1000 nM of trypsin in buffer A. As shown in Figure 9A, the fluorescence response of the MIP increased with increasing concentrations of trypsin; the fluorescence enhancement of MIP reached more than 100% in the presence of 1000 nM trypsin. The LOQ was 50 nM.

To test if the enhancement was selective towards trypsin, other proteins such as thrombin, HSA and cytochrome c were tested. Solutions of 0.1 mg/mL of MIP were incubated with varying concentrations of each protein. For the three proteins, no or little fluorescence enhancement (20%) was observed (Figure 9B), much less than with trypsin. Kallikrein, another serine protease which is inhibited by PAB was also tested but surprisingly negligible fluorescence enhancement effect was observed on AB fluorescence. On the other hand, thrombin, the other serine protease inhibited by PAB produced more enhancement on AB than HSA and cytochrome c. Still, the selectivity of MIP

for trypsin was high, considering that binding of thrombin to PAB, produced 4.6-fold more enhancement than binding of trypsin to PAB [Evans et al., 1982]. These results clearly indicate that specific imprinted sites have been created in the MIP.

The binding specificity of the polymers was evaluated using concentrations ranging from 0.1 to 2 mg/mL with 250 nM trypsin in buffer A. Figure 9C shows that the MIP exhibited a stronger fluorescence response than the NIP. After fitting with Langmuir isotherm equation, the calculated  $K_d$  value of MIP was found to be 237 nM.

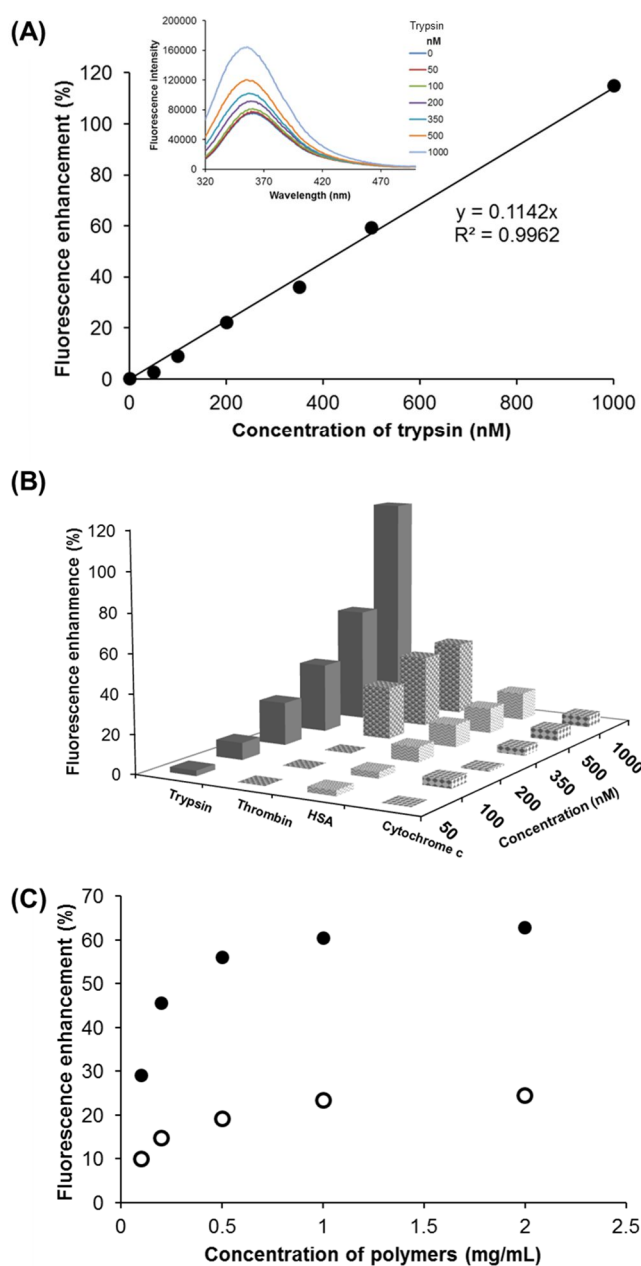


**Figure 9.** Fluorescence responses of (A) MIP (0.1 mg/mL) after incubation with increasing concentrations of trypsin. Inset: corresponding fluorescence spectra; (B) MIP (0.1 mg /mL) after

incubation with trypsin, thrombin, HSA and cytochrome c; (C) Varying concentrations of MIP (full circles) and NIP (empty circles) for 250 nM trypsin, normalized according to AB content. Experiments done in 25 mM sodium phosphate buffer pH 7 at 25 °C.

### III-5. Selectivity and cross-reactivity test of MIP

MIP selectivity was further studied by competitive binding assays between trypsin-FITC and either trypsin, thrombin, HSA or cytochrome c, for MIP immobilized on the wells of microtiter plates. Prior to MIP immobilization, the plates were activated with a mixture of H<sub>2</sub>SO<sub>4</sub>/HNO<sub>3</sub> to render them hydrophilic so that the MIPs, composed mainly of hydrophilic monomers, could tightly adhere to them. Before doing the selectivity test, the capacity of immobilized MIP for FITC-trypsin was investigated (Figure 10A). MIP binding was saturated with 500 nM of trypsin-FITC. After fitting with the Langmuir isotherm equation, the dissociation constant ( $K_d$ ) was found to be 225 nM, which is similar to the  $K_d$  of 237 nM found with free MIP and free trypsin.

For the selectivity studies, 200 nM trypsin-FITC was mixed with either 200 nM of trypsin, thrombin, HSA, or cytochrome c, or their mixture. The amount of bound protein was calculated by measuring the amount of trypsin-FITC displaced (Figure 10B). In the mixture of 200 nM thrombin, BSA, cytochrome c each, there was still 60% trypsin bound, which shows the high selectivity of MIP.

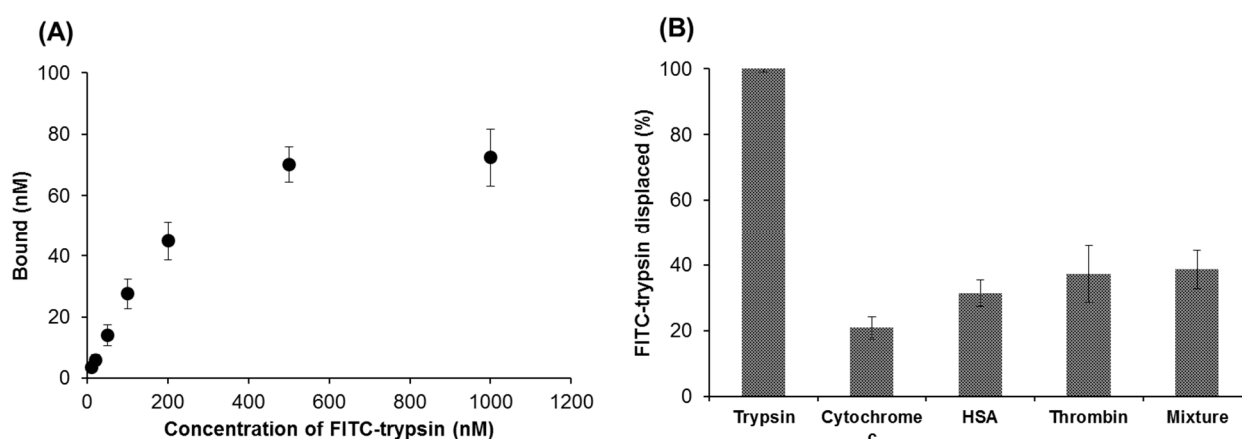


**Figure 10.** (A) Binding capacity of immobilized MIP (0.1 mg) for trypsin-FITC in 25 mM sodium phosphate buffer pH 7 at 25 °C. (B) Cross-reactivity test of MIP toward thrombin, HSA and cytochrome c and a mixture of them.

### III-6. Application of MIP for detection of trypsin in human urine

Trypsin plays a key role in controlling pancreatic exocrine function and its level is increased in pancreas transplant patients [See and Smith, 1991]. In order to demonstrate the potential application of the proposed method for trypsin assays in clinical diagnosis, various concentrations of trypsin were spiked into human urine taken from two male and two female healthy volunteers, collected either in the morning or in the afternoon. The urine samples were centrifuged and the supernatants were either used immediately or frozen as aliquots. Human urine is a complex biological fluid, containing 91 – 96% water, a variety of metabolites, inorganic salts, and organic compounds (including proteins, hormones, etc.). The normal pH values of urine range from pH 4.6 to pH 8.0. It was found that, urine samples collected in the morning were ~ pH 6.0, because no food or beverages were consumed while sleeping, whereas during the day the body buffers the pH of consumed food, thus samples collected in the afternoon were ~ pH 7.4. The 4 urine samples were diluted 10 times and mixed with 0.1 mg/mL MIP, in buffer A. The fluorescence spectra of each urine/MIP sample are shown in Figure 11A. As urine contains many intrinsic fluorophores that can be excited in the UV region, autofluorescence occurs [Zvarik, et al., 2013]; this is reflected in the spectra of all MIP samples containing urine whose fluorescence intensities were ~ 4 to 10 times higher than the MIP sample containing only buffer, used as control. Moreover, each sample's spectrum was different as this depends on different dietary habits and metabolism levels [Adamko et al., 2007]. In order to determine whether MIP can sense trypsin in urine samples, the latter was spiked with trypsin concentrations ranging from 2 – 40  $\mu\text{M}$ , followed by addition of 0.1 mg/mL of MIP. Figure 11B shows that the fluorescence enhancement due to the interaction of trypsin (final concentrations in assay: 0.2 - 4  $\mu\text{M}$ ) with MIP was similar and linear (Figure 11C) for all samples. The emission of the intrinsic fluorophores present in urine did not seem to interfere with the enhancement, indicating that the interaction of trypsin with the MIP is selective. The imprinted polymer probe shows lower sensitivity in urine (detected range: 0.2 – 4  $\mu\text{M}$ ) as compared to that in buffer A (50 – 1000 nM). The method provides a convenient detection of trypsin in high concentrations from 2 – 40  $\mu\text{M}$  (50 – 1000  $\mu\text{g/mL}$ ) in urine.

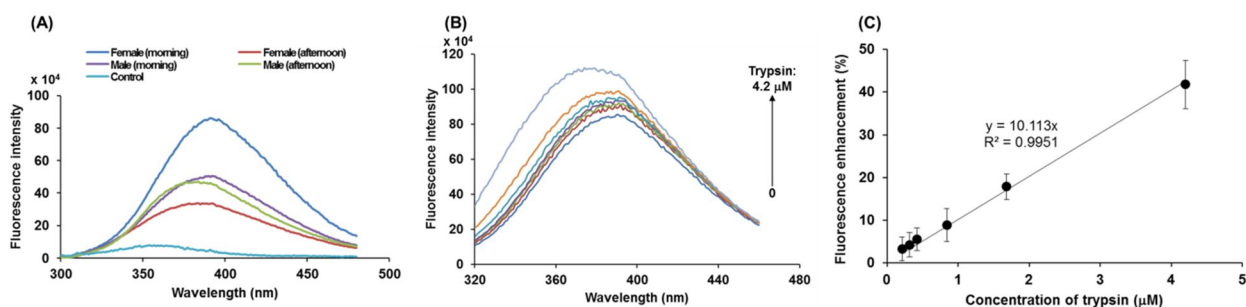


**Figure 11.** (A) Fluorescence spectra of 0.1 mg/mL MIP added to 25 mM sodium phosphate buffer pH 7 (control) and to urine obtained at different time of the day as indicated, from 4 volunteers; (B) Fluorescence spectra of 0.1 mg/mL of MIP when binding trypsin (0.21 – 4.2  $\mu$ M), in female urine (morning); (C) Corresponding fluorescence response of 0.1 mg/mL of MIP when binding trypsin in urine ( $\lambda_{\text{ex}}$ : 280 nm,  $\lambda_{\text{em}}$ : 380 nm). Experiment done at 25  $^{\circ}$ C.

## IV. Conclusions

We have developed a water-soluble fluorescent MIP nanoprobe for the determination of trypsin in both phosphate buffer and in human urine. Sensing within the MIP was achieved by incorporating a benzamidine-based monomer, which exhibits fluorescence enhancement when interacting with trypsin. Thus trypsin could be selectively determined in the nM and  $\mu$ M range respectively in buffer and urine. This cheap, rapid and simple assay is very convenient for screening the level of trypsin (3.6  $\mu$ M) in pancreas transplant patients. For this study, human trypsin was not employed for economic reasons. Since bovine trypsin possesses respectively 72.5% and 95.1% identity and similarity with human trypsin, as deduced from alignment of bovine trypsin (UniprotKB P00760) and human trypsin (UniprotKB P07477) by Clustal Omega program, the results obtained here can well be transposed to the detection of human trypsin. We believe that this assay has great potential for diagnostic purpose.

## Acknowledgments

J. Xu thanks the China Scholarship Council (CSC). The authors acknowledge financial support from the Region of Picardy (cofunding of equipment under CPER 2007-2013). We thank Frederic Nadaud for the SEM images.

## References

- Adamko, D., Rowe, B. H., Marrie, T., & Sykes, B. D. (2007). Variation of metabolites in normal human urine. *Metabolomics*, 3(4), 439-451.
- Ambrosini, S., Beyazit, S., Haupt, K., & Bui, B. T. S. (2013). Solid-phase synthesis of molecularly imprinted nanoparticles for protein recognition. *Chemical Communications*, 49(60), 6746-6748.
- Banumathi, E., Haribalaganesh, R., Babu, S. S. P., Kumar, N. S., & Sangiliyandi, G. (2009). High-yielding enzymatic method for isolation and culture of microvascular endothelial cells from bovine retinal blood vessels. *Microvascular Research*, 77(3), 377-381.
- Beyazit, S., Ambrosini, S., Marchyk, N., Palo, E., Kale, V., Soukka, T., et al. (2014). Versatile synthetic strategy for coating upconverting nanoparticles with polymer shells through localized photopolymerization by using the particles as internal light sources. *Angewandte Chemie International Edition*, 53(34), 8919-8923.
- Bi, X., & Liu, Z. (2013). Facile preparation of glycoprotein-imprinted 96-well microplates for enzyme-linked immunosorbent assay by boronate affinity-based oriented surface imprinting. *Analytical Chemistry*, 86(1), 959-966.
- Cutivet, A., Schembri, C., Kovensky, J., & Haupt, K. (2009). Molecularly imprinted microgels as enzyme inhibitors. *Journal of the American Chemical Society*, 131(41), 14699-14702.
- Ertürk, G., Hedström, M., & Mattiasson, B. (2016). A sensitive and real-time assay of trypsin by using molecular imprinting-based capacitive biosensor. *Biosensors and Bioelectronics*, 86, 557-565.
- Evans, S. A., Olson, S. T., & Shore, J. D. (1982). *p*-Aminobenzamidine as a fluorescent probe for the active site of serine proteases. *Journal of Biological Chemistry*, 257(6), 3014-3017.
- Gao, X., Tang, G., Li, Y., & Su, X. (2012). A novel optical nanoprobe for trypsin detection and inhibitor screening based on Mn-doped ZnSe quantum dots. *Analytica chimica acta*, 743, 131-136.
- George, A., & Wilson, W. W. (1994). Predicting protein crystallization from a dilute solution property. *Acta Crystallographica Section D: Biological Crystallography*, 50(4), 361-365.

- Haupt, K., & Mosbach, K. (2000). Molecularly imprinted polymers and their use in biomimetic sensors. *Chemical Reviews*, 100(7), 2495-2504.
- Hayden, O., Haderspöck, C., Krassnig, S., Chen, X., & Dickert, F. L. (2006). Surface imprinting strategies for the detection of trypsin. *Analyst*, 131(9), 1044-1050.
- Hirota, M., Ohmuraya, M., & Baba, H. (2006). The role of trypsin, trypsin inhibitor, and trypsin receptor in the onset and aggravation of pancreatitis. *Journal of Gastroenterology*, 41(9), 832-836.
- Ionescu, R. E., Cosnier, S., & Marks, R. S. (2006). Protease amperometric sensor. *Analytical Chemistry*, 78(18), 6327-6331.
- Kubo, H., Nariai, H., & Takeuchi, T. (2003). Multiple hydrogen bonding-based fluorescent imprinted polymers for cyclobarbitol prepared with 2, 6-bis (acrylamido) pyridine. *Chemical Communications*, (22), 2792-2793.
- Leung, M. K. P., Chow, C. F., & Lam, M. H. W. (2001). A sol-gel derived molecular imprinted luminescent PET sensing material for 2, 4-dichlorophenoxyacetic acid. *Journal of Materials Chemistry*, 11(12), 2985-2991.
- Ma, J., Hou, C., Liang, Y., Wang, T., Liang, Z., Zhang, L., & Zhang, Y. (2011). Efficient proteolysis using a regenerable metal - ion chelate immobilized enzyme reactor supported on organic-inorganic hybrid silica monolith. *Proteomics*, 11(5), 991-995.
- Matsui, J., Kubo, H., & Takeuchi, T. (2000). Molecularly imprinted fluorescent-shift receptors prepared with 2-(trifluoromethyl) acrylic acid. *Analytical chemistry*, 72(14), 3286-3290.
- See, W. A., & Smith, J. L. (1991). Urinary levels of activated trypsin in whole-organ pancreas transplant patients with duodenocystostomies. *Transplantation*, 52(4), 630-633.
- Soleimani, M., & Nadri, S. (2009). A protocol for isolation and culture of mesenchymal stem cells from mouse bone marrow. *Nature protocols*, 4(1), 102-106.
- Takeuchi, T., Mukawa, T., & Shinmori, H. (2005). Signaling molecularly imprinted polymers: molecular recognition - based sensing materials. *The Chemical Record*, 5(5), 263-275.

Ton, X. A., Acha, V., Bonomi, P., Tse Sum Bui, B., & Haupt, K. (2015). A disposable evanescent wave fiber optic sensor coated with a molecularly imprinted polymer as a selective fluorescence probe. *Biosensors and Bioelectronics*, 64, 359-366.

Ton, X. A., Tse Sum Bui, B., Resmini, M., Bonomi, P., Dika, I., Soppera, O., & Haupt, K. (2013). A Versatile Fiber - Optic Fluorescence Sensor Based on Molecularly Imprinted Microstructures Polymerized in Situ. *Angewandte Chemie International Edition*, 52(32), 8317-8321.

Tsuji, S., & Kawaguchi, H. (2006). Effect of graft chain length and structure design on temperature-sensitive hairy particles. *Macromolecules*, 39(13), 4338-4344.

von Berg, A., Koletzko, S., Grübl, A., Filipiak-Pittroff, B., Wichmann, H. E., Bauer, C. P., et al. (2003). The effect of hydrolyzed cow's milk formula for allergy prevention in the first year of life: the German infant nutritional intervention study, a randomized double-blind trial. *Journal of Allergy and Clinical Immunology*, 111(3), 533-540.

Wackerlig, J., & Lieberzeit, P. A. (2015). Molecularly imprinted polymer nanoparticles in chemical sensing—Synthesis, characterisation and application. *Sensors and Actuators B: Chemical*, 207, 144-157.

Wagner, R., Wan, W., Biyikal, M., Benito-Peña, E., Moreno-Bondi, M. C., Lazraq, I., et al. (2013). Synthesis, spectroscopic, and analyte-responsive behavior of a polymerizable naphthalimide-based carboxylate probe and molecularly imprinted polymers prepared thereof. *The Journal of Organic Chemistry*, 78(4), 1377-1389.

Xu, J., Ambrosini, S., Tamahkar, E., Rossi, C., Haupt, K., & Tse Sum Bui, B. (2016). Toward a universal method for preparing molecularly imprinted polymer nanoparticles with antibody-like affinity for proteins. *Biomacromolecules*, 17(1), 345-353.

Zhang, L., & Du, J. (2016). A sensitive and label-free trypsin colorimetric sensor with cytochrome c as a substrate. *Biosensors and Bioelectronics*, 79, 347-352.

Zvarik, M., Martinicky, D., Hunakova, L., Lajdova, I., & Sikurova, L. (2013). Fluorescence characteristics of human urine from normal individuals and ovarian cancer patients. *Neoplasma*,

60(5), 533-537.

# Chapter 4

---

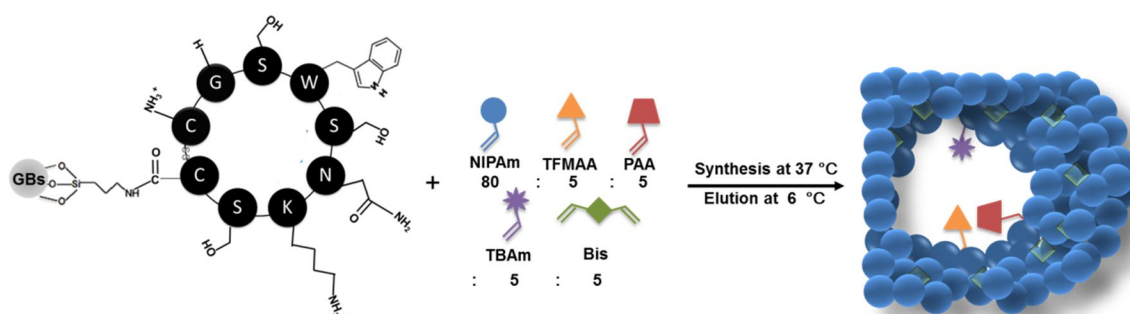
Peptide epitope molecular imprinting by  
solid-phase synthesis

## Summary

In this chapter, we show the versatility of our solid-phase synthesis approach by extending the method to prepare antibody-like MIP-NPs for a peptide motif with the sequence SWSNKS (referred as 3S peptide), present as an epitope on a transmembrane glycoprotein gp41 on the HIV virus. This peptide is implicated in the decline of CD4<sup>+</sup> T cells during HIV infection. Therefore the obtention of a MIP which would block this peptide is of high interest.

Traditionally, epitope imprinting is performed toward a well-defined specific linear, often terminal, peptide on the surface of a protein [Qin et al., 2016; Mujahid et al., 2013] because of its easy definition and acquirement. However, most antibodies recognize a conformational epitope (3-D structure) or a structural epitope (internal sequence) of a protein rather than its linear terminal structure [Zhang et al., 2015], and it was pointed out that more attention should be paid to the internal peptide of the protein target, due to its more conserved feature and relation with immune response [Bossi et al., 2012]. Following this aspect, to mimic the conformation of an internal peptide in a protein, the structure of the template peptide has been designed to be cyclic by adding two cysteine residues to form a disulfide bridge [Cenci et al., 2016; Zhang et al., 2015].

Herein, we have also designed the 3S peptide to be cyclic by adding two cysteine residues. A glycine is also added to stabilize the cyclic structure. The final cyclic peptide presents the following sequence: CGSWSNKSC (C-C cyclic). Its immobilization was done through the carboxyl group on amino-functionalized glass-beads, so as to orientate the SWSNKS motif in a fixed non-hindered position, as shown in the figure.



In order to improve the selectivity of the MIP toward this 3S peptide, multiple functional monomers with hydrogen bond forming, negatively-charged,  $\Pi$ - $\Pi$  and hydrophobic functionalities were selected to build up the three-dimensional binding sites. The results show that one MIP has high affinity (in the nM range) for the 3S peptide. This MIP shows great potential to block the function of 3S peptide and looks promising for *in vivo* applications.

## References

- Bossi, A. M., Sharma, P. S., Montana, L., Zoccatelli, G., Laub, O., & Levi, R. (2012). Fingerprint-imprinted polymer: rational selection of peptide epitope templates for the determination of proteins by molecularly imprinted polymers. *Analytical Chemistry*, 84(9), 4036-4041.
- Cenci, L., Guella, G., Andreetto, E., Ambrosi, E., Anesi, A., & Bossi, A. M. (2016). Guided folding takes a start from the molecular imprinting of structured epitopes. *Nanoscale*, 8(34), 15665-15670.
- Mujahid, A., Iqbal, N., & Afzal, A. (2013). Bioimprinting strategies: From soft lithography to biomimetic sensors and beyond. *Biotechnology Advances*, 31(8), 1435-1447.
- Qin, Y. P., Li, D. Y., He, X. W., Li, W. Y., & Zhang, Y. K. (2016). Preparation of high-efficiency cytochrome c-imprinted polymer on the surface of magnetic carbon nanotubes by epitope approach via metal chelation and six-membered ring. *ACS Applied Materials & Interfaces*, 8(16), 10155-10163.
- Zhang, Y., Deng, C., Liu, S., Wu, J., Chen, Z., Li, C., & Lu, W. (2015). Active targeting of tumors through conformational epitope imprinting. *Angewandte Chemie International Edition*, 54(17), 5157-5160.

# Antibody-like molecularly imprinted polymer nanoparticles for the recognition of the HIV-gp41 epitope peptide

## I. Introduction

According to a report of the Joint United Nations Program on HIV/AIDS (UNAIDS), at the end of 2015, 37 million people were globally living with the human immunodeficiency virus (HIV), the infectious agent that brings acquired immune deficiency syndrome (AIDS) [http://www.unaids.org/en/resources/fact-sheet, accessed on March 07, 2017]. Approximately, 1.1 million people died in 2015 from AIDS-related causes worldwide, which makes HIV infection a serious global concern worth billions US\$ investment.

Infection by HIV type 1 leads to the progressive deterioration of the immune system due to the progressive depletion of CD4<sup>+</sup> T cells. Research from the group of Prof. Debré (Vieillard et al., 2015) has shown that natural killer (NK) cells from infected patients were activated, and expressed the natural cytotoxicity receptor NKp44. The expression of the ligand for NKp44 (NKp44L) is induced by a highly conserved peptide motif SWSNKS (3S) of the HIV gp41 transmembrane protein (Figure 1).

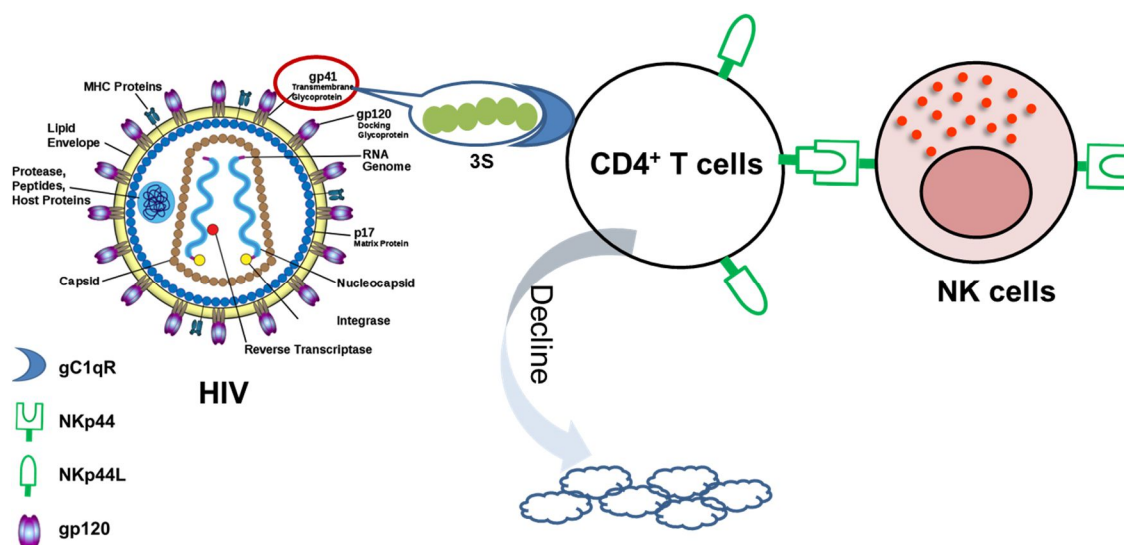


**Figure 1.** Illustration of the 3S-activated expression of NKp44L on CD4<sup>+</sup> T cells, resulting in the destruction of CD4<sup>+</sup> T cells by NK cells. Adapted from [http://hivinthesouth.blogspot.fr/2013\\_11\\_01\\_archive.html](http://hivinthesouth.blogspot.fr/2013_11_01_archive.html), accessed March 07, 2017

This 3S peptide is an internal sequence of gp41 and is exposed only during the interaction of the surface protein gp120 of the virus with the host cell. During this process, conformational changes in the gp120-gp41 complex make several gp41 motifs become accessible to the surface, including the 3S peptide located between residues 618 – 623 [Sattentau & Moore, 1991]. The receptor of the 3S motif on CD4<sup>+</sup> T cells is gC1qR [Fausther-Bovendo et al., 2010] and its interaction with the 3S peptide activates the signaling pathway, leading to NKp44L surface expression.

Following the identification of the 3S peptide, further studies by the same group [Vieillard et al., 2008], have shown that anti-3S antibodies inhibited the expression of NKp44L and the activation and cytotoxicity of NK cells *in vivo*, thus preventing CD4<sup>+</sup> T cell depletion. The synthetic peptide used to generate the anti-3S antibodies was a linear peptide with the following sequence NH<sub>2</sub>-PWNASWSNKSLDDIW-COOH. Consequently, a vaccine project against this HIV-gp41 epitope peptide has been launched since 2008, and some progress on monoclonal antibody generation has been made. To date, an effective vaccine VAC-3S targeting a “3S” peptide of gp41 seems to show great potential to cure HIV infection, and is now under phase II clinical study by the company InnaVirVax. [<http://www.france-biotech.org/innavirvax-la-fda-autorise-un-essai-clinique-de-phase-2-de-vacc-3s-dans-la-guerison-fonctionnelle-du-vih-aux-usa/>, accessed March 07. 2017].

However, biological antibodies have a few shortcomings such as low stability outside their natural environment, thus they require careful storage at low temperatures, and animals are needed for their production, thus high cost. Herein, we propose a strategy to synthesize a “plastic antibody” based on a molecularly imprinted polymer (MIP) to target the 3S peptide, so as to block the function of this peptide and stop NKp44L overexpression. MIPs are tailor-made receptor materials (Haupt et al., 2012; Mattiasson and Ye, 2015), synthesized by a templating process at the molecular level. Monomers carrying functional groups self-assemble around a template molecule (the target or a derivative), followed by copolymerization with cross-linking monomers, which results in the formation of a polymeric mold around the template. Subsequent removal of the template reveals 3D-binding sites in the polymer that are

complementary to the template in size, shape and position of the functional groups. Consequently, MIPs exhibit binding affinities and specificities comparable to those of antibodies but in contrast to the latter, their production is reproducible, relatively fast and economic, and no animals are necessary. Moreover, they are physically and chemically stable and are not degraded by proteases and nucleases.

Recently, we applied an innovative solid-phase synthesis approach to prepare water-soluble ‘monoclonal’-type MIPs, which exhibit antibody-like affinities (apparent dissociation constants in the nM range) [Ambrosini et al., 2013; Xu et al., 2016]. Glass-beads were used as solid support to immobilize the template via an affinity ligand. The latter orientates the template in a fixed position so that the resulting MIP has improved binding site homogeneity since its binding site has the same orientation. Inspired by the fact that most antibodies recognize their protein antigen via a conformational or an internal structural epitope [Zhang et al., 2015], our 3S peptide template, with the motif SWSNKS, was designed in a cyclic conformation by adding two cysteine (C) residues to the two sides of the linear 3S peptide, so as to form a disulfide bond and generate a cyclic structure. This will allow a better display of the 3S peptide antigen during molecular imprinting. A glycine (G) residue was added between the N-terminal serine and cysteine to make this cyclic structure more stable (Figure 2A). This strategy of designing the structure of a template peptide in a cyclic configuration which is a closer mimic to the conformation of a peptide in a protein has been recently applied to the synthesis of MIPs for assisting protein refolding [Cenci et al., 2016] and recognizing tumor cells *in vivo* [Zhang et al., 2015].

The cyclic 3S peptide was immobilized on (3-aminopropyl)triethoxysilane (APTES)-functionalized glass beads via its –COOH group so as to present the motif SWSNKS in a fixed orientation for targeting by the MIP (Figure 2B). The monomers were carefully chosen to interact specifically with the motif (Figure 2C). Three MIPs were synthesized and their binding performance for the cyclic 3S peptide were compared. The ‘best’ MIP seems very promising for *in vivo* application.

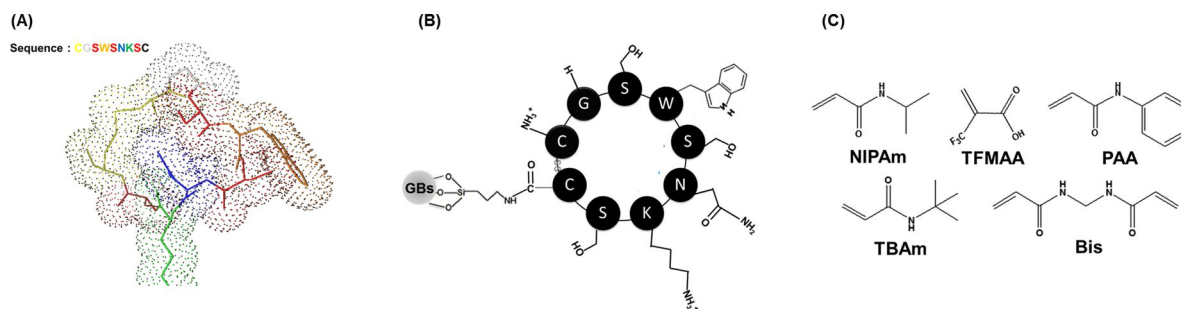


**Figure 2.** (A) Schematic representation of cyclic 3S peptide (designed by Prof. Bérangeère Bihan-Avalle); (B) cyclic 3S peptide immobilized on APTES-GBs; (C) monomers used to target the peptide.

## II. Experimental section

### Materials and Methods

All chemicals and solvents were of analytical grade and purchased from VWR International (Fontenay sous Bois, France) or Sigma-Aldrich (St Quentin Fallavier, France), unless otherwise stated. Buffers were prepared with Milli-Q water, purified using a Milli-Q system (Millipore, Molsheim, France). Glass beads (GBs) of diameter 0.1 mm, were obtained from Roth Sochiel E.U.R.L (Lauterbourg, France). Cyclic 3S peptide (purity 95%, ESI-MS (m/z):  $[M+H]^+$  969.3558 g/mol) was designed by Prof. Bérangeère Bihan-Avalle using SwissPDB viewer [<http://spdbv.vital-it.ch/>, accessed March 07, 2017] and custom-synthesized by GL Biochem (Shanghai, China). Polystyrene 48-well microplates were purchased from BECTON DICKINSON (Le Pont De Claix, France). Fluorescence measurements were performed on a FluoroLog-3 spectrofluorimeter (Horiba Jobin Yvon, Longjumeau, France).

#### II-1. Boc protection of primary amines on the 3S peptide

In order to synthesize a MIP specific toward the SWSNKSC sequence, the immobilization of the cyclic 3S peptide was done via its  $-COOH$ , so as to expose the SWSNKSC motif (Figure 2A). The carboxyl group is activated with 1-ethyl-3-(3-dimethylaminopropyl)carbodiimide/N-hydroxysuccinimide (EDC/NHS) followed by covalent attachment of the (3-aminopropyl)triethoxysilane (APTES)-functionalized glass beads, by its primary amine.

Since the 3S peptide also contains primary amines, to prevent coupling between themselves, the amino groups of the peptide were protected by *tert*-butyloxycarbonyl (BOC). *tert*-butoxycarbonylation of amino groups was done as previously described [Shendage et al., 2004]. Briefly, to a solution of 100 mg (103  $\mu$ mol) cyclic 3S peptide dissolved in 20 mL of a mixture of tetrahydrofuran /water (1/1), 840 mg (10 mmol) of NaHCO<sub>3</sub> and 100 mg (458  $\mu$ mol) of di-*tert*-butyl dicarbonate (Boc<sub>2</sub>O) was added at 0 °C. The mixture was stirred in an ice bath for 30 min and the reaction left to proceed overnight at room temperature. The reaction mixture was extracted twice with 20 mL of diethyl ether (Et<sub>2</sub>O). Because of the high water solubility of the 3S peptide (hydropathy index < 0) [Kyte & Doolittle, 1982], the Boc-3S peptide was unexpectedly found in the aqueous phase. The aqueous layer was adjusted to pH 5-6 by addition of 2-(N-morpholino)ethanesulfonic acid (MES) at 0 °C. This Boc-3S peptide in MES solution constituted our stock working solution. It was kept in small aliquots at -20 °C until use. The Boc-3S peptide product was analyzed by liquid chromatography-high resolution mass spectrometry (LC-HRMS).

The HPLC system (Infinity 1290, Agilent Technologies, France) was equipped with a diode array detector coupled to a Q-TOF micro hybrid quadrupole time of flight mass spectrometer (Agilent 6538, Agilent Technologies, France). The chromatographic column was a Hypersyl GOLD C18 reversed phase (RP) (150  $\times$  2.1 mm, 3  $\mu$ m, 100 Å) (Thermo Scientific, France). The mobile phase consisted of water containing 0.1% formic acid (eluent A) and acetonitrile (eluent B). The gradient program began with 5% B, ramped to 95% B at 20 min, was held at 95% for 5 min, increased to 100% B at 30 min and was kept constant at 100% B until 35 min. The flow rate was set at 0.4 mL/min. Detection was monitored at 280 nm. An aliquot of 10  $\mu$ L of Boc-3S peptide was injected. Positive ion electrospray (ESI) mass spectra was acquired by scan mode in the range *m/z* 100 to *m/z* 2000 at electrospray voltage of 3800 V and fragmentor voltage of 180 V. Nitrogen was used as the dry gas at a flow rate of 10.0 L/min and a pressure of 30.0 psi. The nebulizer temperature was set to 300 °C.

## II-2. Solid-phase synthesis of molecularly imprinted polymers

*Immobilization of peptide on APTES-functionalized GBs.* 100 g of glass beads (GBs) were activated by boiling in 100 mL of 4 M NaOH for 10 min. After washing with water and drying in an oven at 50 °C, the activated GBs were incubated with 100 mL of 2% (v/v) APTES in toluene overnight, washed with acetone and dried at 50 °C. Hereafter, APTES- functionalized GBs were coupled with Boc-3S peptide via the free carboxyl group by EDC/NHS coupling procedure. Briefly, 10 mL of Boc-3S peptide stock was activated by adding 191.7 mg (1 mmol) EDC and 287.5 mg (2.5 mmol) NHS for 15 min, then this solution was diluted to 100 mL with 25 mM sodium phosphate buffer pH 7 (referred as buffer A) and incubated with APTES-functionalized GBs, with shaking overnight at room temperature [Poma et al., 2015]. After the immobilization of Boc-3S peptide, Boc deprotection was done by immersing the GBs in 120 mL of 1 M HCl in 100 mL of Et<sub>2</sub>O for 5 h at room temperature [Albrecht et al., 2006].

APTES-functionalized GBs, GBs immobilized with Boc-3S peptide and GBs immobilized with deprotected-3S peptide, were analyzed by Fourier Transform Infrared Spectroscopy (FT-IR). FT-IR spectra (4000-800 cm<sup>-1</sup>, 4 cm<sup>-1</sup> resolution, 500 scans) were measured on a Thermo Nicolet 6700 spectrometer equipped with a ZnSe ATR (attenuated total reflectance) system and MCT-B detector.

*Solid-phase synthesis of polymers.* The solid-phase synthesis of molecularly imprinted polymer nanoparticles (MIP-NPs) was carried out in a glass column equipped with a thermostated jacket (XK 26/40, GE Healthcare, France), connected to a circulating thermostated water-bath (Bioblock Scientific Polystat 5, Fischer Scientific, France). The solvents were pumped through the column using a peristaltic pump (ISMATEC Rotary Piston Pumps, REGLO-CPF Analog, Germany) at a flow rate of 2.5 mL/min. The column was packed with 33 g of APTES-functionalized GBs with the immobilized 3S peptide, corresponding to a bed height of 4.2 cm. The GBs were washed with 100 mL water, and then equilibrated with 100 mL of buffer A. MIP 1, MIP 2, and MIP 3 were prepared with polymer composition, as described in Table 2. The polymerization mixture was prepared in 48 mL of

buffer A so that the total monomer concentration is 0.5% (w/w). The solution was purged with nitrogen for 30 min. Afterwards, the initiation couple composed of KPS (18 mg in 500  $\mu$ L buffer A) and TEMED (1.3  $\mu$ L) (7.5/1 molar ratio, where the amount of KPS was 3% mol/mol with respect to polymerizable double bonds) were added to the reaction mixture. After overnight polymerization at 37  $^{\circ}$ C, the column was washed with 50 mL buffer A at 37  $^{\circ}$ C, and then cooled down to 6  $^{\circ}$ C. Polymers were eluted by 2 or 3 aliquots of 5 mL buffer A (i.e. until there are no longer particles detected by DLS). Non-imprinted polymer (NIP 1-3) were prepared using the same protocol on 33 g of APTES-GBs but coupled with 35 mL of 1 mM acetyl chloride (prepared in buffer A). The solid-phase synthesis procedure is presented in Figure 3.

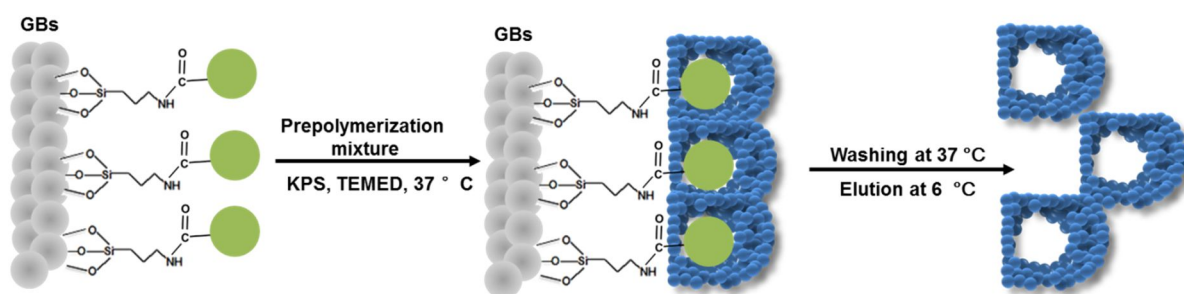


**Figure 3.** Schematic illustration of solid-phase synthesis process, including polymerization at 37  $^{\circ}$ C and elution at 6  $^{\circ}$ C after a washing step.

### II-3. Characterization of polymers

*Physicochemical characterization.* The eluted fractions in buffer A were analyzed by dynamic light scattering (DLS) on a Zetasizer NanoZS (Malvern Instruments Ltd., Worcestershire, UK). Fractions with similar sizes and polydispersity index (PDI) were mixed together to constitute a working stock solution. Zeta potential determination was carried out with a desalted sample of the stock solution. The desalting was performed by washing 1 mL of the stock solution 5 times with 3 mL of water on an Amicon Ultra centrifugal filter with centrifugation at 5,000 g for 5 min each washing (30 kDa, Merck Chimie SAS, France).

*Determination of polymer yield.* In order to facilitate the precipitation of polymers during centrifugation, the repulsive forces within the negatively charged polymers, caused by the

presence of TFMAA, had to be suppressed. To 3 mL of each polymer, was added 1 M HCl until the pH reaches 1 – 2. The polymers were centrifuged at 40,000 g for 1h at 37 °C so that they precipitate. After discarding the supernatant, the precipitate was re-suspended in 4 mL water and lyophilized so as to calculate their concentration in mg/mL and the yield of synthesis per g of GBs.

*LCST analysis of MIP 1 – 3.* In order to determine the lower critical solution temperature (LCST) of each MIP, 1 mL of MIP solution was put in a glass cuvette, and then 100  $\mu$ L of 1 M HCl was added to adjust the pH to 1 – 2. The absorbance of each sample was read at 600 nm [Maynard et al., 2007] at temperatures varying from 25 to 50 °C on a Cary 60 UV-vis spectrophotometer, connected to a circulation thermostated Cary Single Cell Peltier Accessory (Agilent Technologies, France). To demonstrate that polymer transition is reversible, repeated heating/cooling cycles were applied until no change of absorbance values was observed [Medel et al., 2011]. LCST was determined according to the solution turbidity.

#### **II-4. Evaluation of the binding characteristics of the polymers by piezoelectric microgravimetry**

A quartz crystal microbalance (QCM) was employed to evaluate the recognition properties of the MIP-NPs. All measurements were performed with a Q-Sense E1 instrument (Biolin Scientific, Sweden) in a flow-through mode using a peristaltic pump (flow rate: 40  $\mu$ L/min). The functionalization of the QCM crystal with APTES was carried out at 25 °C, whereas the binding experiments with the MIP-NPs were performed at 37 °C.

*Cleaning and activation of QCM crystals:* 5 silicon dioxide-coated crystals (QSX 303) (Lot Quantum Design, France) were immersed in a glass beaker containing 80 mL of NH<sub>4</sub>OH (28%)/H<sub>2</sub>O<sub>2</sub> (35%)/H<sub>2</sub>O (1/1/6, v/v/v). The beaker was placed in a water-bath maintained at 70 °C for 10 min. Afterward, the QCM crystals were washed 5 times with 5 mL water, and dried under nitrogen gas. Further cleaning of QCM crystals was carried out under UV/ozone irradiation (ProCleaner™ 220, BioForce Nanoscience, USA) for 10 min, followed by washing

with water and drying under nitrogen.

*Immobilization of peptide:* 5 cleaned QCM crystals were functionalized with APTES (5 mL APTES in 5 mL toluene) by incubation on a laboratory shaker overnight at room temperature. Then the APTES-functionalized QCM crystals were rinsed with toluene and acetone and dried under nitrogen. 1 mL of Boc-3S peptide solution in MES buffer was activated by adding 19.2 mg (0.1 mmol) EDC, followed by 28.8 mg (0.25 mmol) NHS, and incubated for 15 min at room temperature. The mixture was added to 9 mL of buffer A, and the immobilization of Boc-3S peptide was done by incubating with APTES-functionalized QCM crystals, overnight. Then each chip was washed with 0.1 M HCl in Et<sub>2</sub>O for Boc deprotection, dried under nitrogen and stored at 6 °C until use.

*Comparison of binding between MIP 1 – 3.* The experiments were carried out on the same QCM sensor at 37 °C using a flow rate of 40 µL/min. 200 µg/mL of MIP 1 – 3 was prepared and pre-heated in a water-bath at 37 °C. Then each sample was injected through the system for 30 min, followed by 15 min washing with buffer A. Between each sample, buffer A at 5 °C was used to wash and desorb the polymers.

*Binding specificity of MIP 1 – 3.* Due to the low binding of MIP 2 and MIP 3, higher concentrations were employed to compare the binding effects with their corresponding NIPs. 200 µg/mL of MIP and NIP 1, 400 µg/mL of MIP and NIP 2, and 600 µg/mL of MIP and NIP 3 were tested. The polymers were pre-heated in a water-bath at 37 °C. Then the measurement of each pair of MIP and NIP was performed as aforementioned on one QCM sensor, consuming three QCM crystals in total. The imprinting factor ( $IF = \frac{MIP_{bound}}{NIP_{bound}}$ ) was calculated by using the saturated amount of MIP and NIP bound on the same chip.

## **II-5. Binding characteristics of MIP 1 immobilized on microplate wells**

*Preparation of rhodamine 123-conjugated peptide.* 5 mL of Boc-3S peptide stock was activated by adding 95.8 mg (0.5 mmol) EDC and 143.8 mg (1.25 mmol) NHS and incubated for 15 min

at room temperature. The mixture was then added to 45 mL of buffer A containing 19.1 mg (0.05 mmol) rhodamine 123 and incubated overnight (Bai et al., 2009). The Boc deprotection was performed by adding 37% HCl to reach 1 M final concentration, followed by extraction with 50 mL Et<sub>2</sub>O. The sample was purified on PD Mditrap G-10 columns (Exclusion limit: 700 Da) by injecting portions of 1 mL. Fractions of 1.2 mL were collected, pooled together to form 12 mL-aliquots and stocked at -20 °C until use. The concentration of rhodamine 123 in the pep-rho complex was determined via its absorption at 495 nm using a molar extinction coefficient of 75,000 M<sup>-1</sup>cm<sup>-1</sup> [Wang & Taylor, 1989], and this measurement was performed on each pooled 12-mL aliquot before use so as to know the concentration of pep-rho in each aliquot. Concentrations from 15 – 22 μM were obtained. The fluorescence of pep-rho was verified by constructing a calibration curve using concentrations ranging from 2 – 225 nM (Figure 4). Fluorescence measurements were done on a spectrofluorimeter, using λ<sub>ex</sub> = 290 nm and λ<sub>em</sub> = 520 nm with slit 3 nm. No presence of unconjugated 3S peptide was observed; there was no emission peak around 360 nm when the peptide was excited at 290 nm.

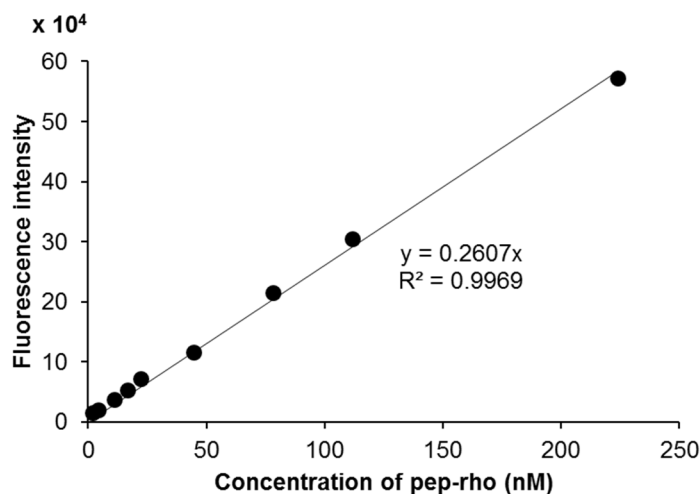


**Figure 4.** Fluorescence calibration curve of pep-rho in 25 mM sodium phosphate buffer pH 7 (λ<sub>ex</sub> = 290 nm and λ<sub>em</sub> = 520 nm, slit 3 nm).

*Binding isotherm of MIP 1 toward pep-rho.* 0.5 mL of MIP 1 over the concentration range of 0 – 400 μg/mL was added into a 48 wells microplate. The polymers were immobilized by physical adsorption after overnight solvent evaporation at 37 °C. Each well was first

conditioned by washing three times with 0.5 mL of buffer A, and then blocked with 0.5 mL of buffer A containing 0.1% of bovine serum albumin (BSA) and 1% of Tween 20 [Chianella et al., 2013], followed by washing again with buffer A. Afterward, 0.5 mL of 1.5  $\mu$ M pep-rho was added into the wells and incubated with immobilized MIP 1 overnight at 37 °C. For the measurements, the supernatant was withdrawn and diluted to fall within the calibration curve, then read on the spectrofluorimeter using  $\lambda_{\text{ex}} = 290$  nm and  $\lambda_{\text{em}} = 520$  nm with slit 3 nm. The amount of pep-rho bound was calculated by subtracting the unbound from the amount added to the well.

To investigate the binding capacity of MIP 1 toward pep-rho, 0.2 mL of 0.5 mg/mL (100  $\mu$ g in total) was taken as a constant amount of MIP 1 immobilized on the microplate. After washing, blocking and washing steps as described above, 0.5 mL of pep-rho concentrations ranging from 5 – 1500 nM was added. After overnight incubation at 37 °C, the supernatant was withdrawn and read on the spectrofluorimeter using  $\lambda_{\text{ex}} = 290$  nm and  $\lambda_{\text{em}} = 520$  nm with slit 3 nm. The amount of pep-rho bound was calculated in the same way as mentioned above.

*Competitive assay.* 100  $\mu$ g of MIP1 was immobilized on 48-wells microplate. After washing, blocking and washing steps as described above, 100 nM of pep-rho was added together with other peptides with concentrations ranging from 1 to 100 nM. Cyclic 3S peptide, linear wild type 3S peptide, two different peptides referred as competitor 1 and competitor 2, and a mixture of competitor 1 and 2 were used to compete with pep-rho. The amount of pep-rho displaced by the other peptides is reflected by the increase of the fluorescence intensity in the supernatants.

### **III. Results and discussion**

#### **III-1. Analysis of Boc-3S peptide**

Boc-3S peptide was analyzed by LC-ESI/HRMS. The chromatograms are presented in Figure 5. Three major peaks, corresponding to three kinds of Boc-3S peptide, were observed. The assignments of peaks are given in Table 1. Peptide coupled with either 1 Boc, 2 Bocs or 3

Bocs were present but there was no free peptide seen, which indicates the 100% *N*-*tert*-butoxycarbonylation of 3S peptide. Although, there were some fragments of 3S peptide or Boc-3S peptide, ~92% of 3S peptide was coupled with Boc. In this experiment, we expected to obtain 2 Boc peptides because the 3S peptide contains two primary amines, the N-terminal amino group and the lysine. However, 36% of 3 Boc peptide was also observed; though unusual, the only possibility would be the  $-\text{CONH}_2$  group of asparagine (N) or the indole of tryptophan (W).

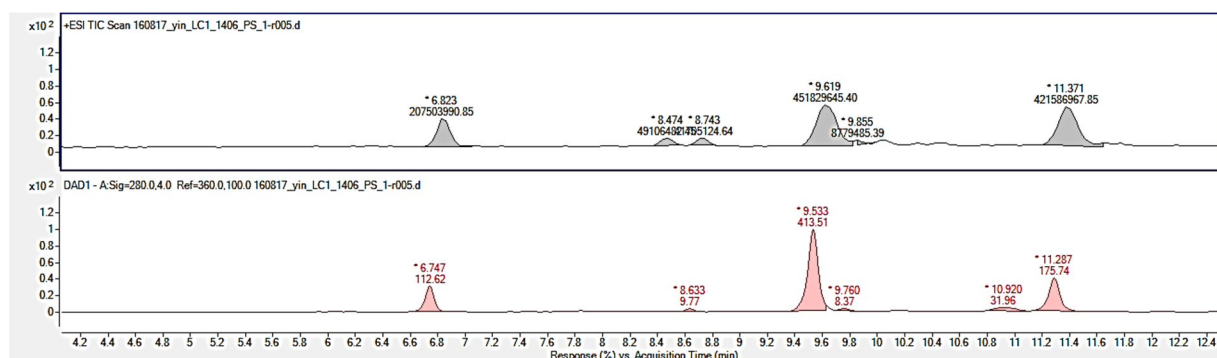


**Figure 5.** Chromatograms of Boc-3S peptide. The identification of peaks was performed by LC-ESI/HRMS in positive mode: (A)  $[\text{M}+\text{Na}]^+$  and (B)  $[\text{M}+\text{H}]^+$ . Detection with UV at 280 nm. Assignment of peaks in Table 1.

**Table 1.** Assignments of peaks from LC-ESI/HRMS spectra of Boc-3S peptide

Boc groups	Relative amount (%)	Proposed Boc-3S peptide	$[\text{M}+\text{Na}]^+$		$[\text{M}+\text{H}]^+$	
			$t_R$	$m/z$	$t_R$	$m/z$
1 Boc	17.6	$\text{C}_{\text{Boc}}\text{GSWSNKSC}$ or $\text{CGSWSNK}_{\text{Boc}}\text{SC}$	6.823 min	1091.3896	6.747 min	1069.4077
2 Boc	38.3	$\text{C}_{\text{Boc}}\text{GSWSNK}_{\text{Boc}}\text{SC}$	9.619 min	1191.4421	9.533 min	1169.4602
3 Boc	35.7	$\text{C}_{\text{Boc}}\text{GSWSN}_{\text{Boc}}\text{K}_{\text{Boc}}\text{SC}$	11.371 min	1291.4945	11.287 min	1269.5126

### **III-2. Characterization of APTES-functionalized GBs alone, coupled with immobilized Boc-3S peptide, and after Boc deprotection, by FT-IR**

To bring an additional proof that protection and deprotection of the peptide occurred, FT-IR measurements were done on the GBs. Figure 6A clearly shows the peaks representing the amino groups of APTES, at  $875.8\text{ cm}^{-1}$ ,  $746.8\text{ cm}^{-1}$  and  $668.5\text{ cm}^{-1}$ . Not much free  $\text{-OH}$ , present on activated GBs before APTES functionalization was observed, since the peak representing  $\text{-OH}$  at  $1409.7\text{ cm}^{-1}$  was negligible as compared with that of the  $\text{-NH}_2$  groups. Compared with APTES-functionalized GBs, the amount of free  $\text{-OH}$  groups corresponding to serine residues of the 3S peptide has dramatically increased (Figure 6B) as seen by the peak at  $3273\text{ cm}^{-1}$ , which indicates the successful coupling of APTES-GBs with Boc-3S peptide. Moreover, the peak of the tert-butyl group is clearly present at  $1412\text{ cm}^{-1}$  in Figure 6B. This peak is no longer seen in Figure 6C, indicating the successful deprotection of Boc.

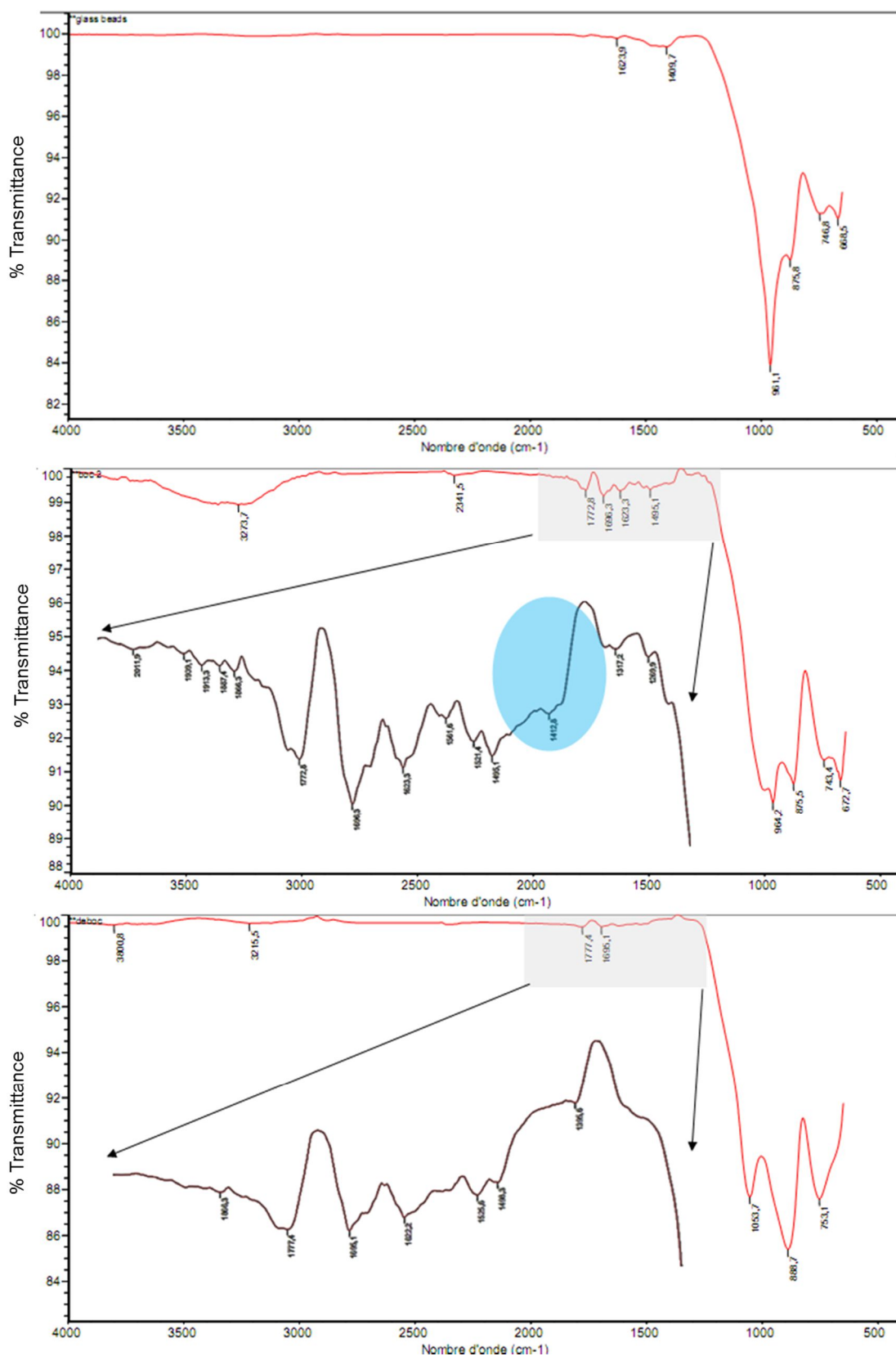


**Figure 6.** FT-IR spectra of (A) APTES-GBs; (B) APTES-GBs with Boc-3S peptide, where the peak corresponding to tert-butyl is highlighted in blue; and (C) APTES-GBs after Boc deprotection.

### III-3. Synthesis of MIPs for selective recognition of cyclic 3S peptide – choice of monomers

In order to provide the MIPs with high biocompatibility, acrylamide-based monomers were selected. The monomers chosen, except 2-(trifluoromethyl)acrylic acid (TFMAA), and their relative molar ratios were inspired from previous work targeting peptides [Weisman et al., 2014; Hoshino et al., 2008], namely *N*-phenylacrylamide (PAA) and *N*-*tert*-butylacrylamide (TBAm), as a  $\Pi$ - $\Pi$  donor and hydrophobicfunctional monomers, respectively and *N,N'*-methylenebis(acrylamide) (Bis) as cross-linker. Additionally, *N*-isopropylacrylamide (NIPAm) was added at a high molar ratio, to endow the polymers with thermoresponsiveness and facilitate their elution from the solid support. Due to the flexible property of the 3S peptide conformation *in vivo*, a low cross-linking degree of 5% (molar ratio) was used, so as to obtain a flexible MIP. Three MIPs, MIP 1, MIP 2 and MIP 3, with their corresponding NIPs were synthesized, using the following polymerization composition: NIPAm:TFMAA:PAA:TBAm:Bis with molar ratio 80:5:5:5:5, 75:5:5:10:5, and 70:5:5:15:5, respectively (Table 2).

**Table 2.** Composition of MIP or NIP 1-3

Monomers	MIP 1		MIP 2		MIP 3	
NIPAm	181.1 mg	1.6 mmol	169.7 mg	1.5 mmol	158.4 mg	1.4 mmol
TFMAA	14 mg	0.1 mmol	14 mg	0.1 mmol	14 mg	0.1 mmol
PAA	14.7 mg	0.1 mmol	14.7 mg	0.1 mmol	14.7 mg	0.1 mmol
TBAm	12.7 mg	0.1 mmol	25.4 mg	0.2 mmol	38.2 mg	0.3 mmol
Bis	15.4 mg	0.1 mmol	15.4 mg	0.1 mmol	15.4 mg	0.1 mmol
KPS	18 mg (0.0315 mmol)					
TEMED	1.3 $\mu$ L (0.0042 mmol)					
Buffer A	48 mL					

TFMAA is a highly acidic monomer ( $pK_a = 2.3$ ) and can act as a proton donor [Matsui et al.,

2000], thus generating a protonated indole on tryptophan, resulting in fluorescence quenching of the 3S peptide. In order to determine if TFMAA has any interaction with our 3S peptide, a fixed amount, 5  $\mu\text{M}$ , of 3S peptide was titrated with TFMAA concentrations ranging from 0.5 – 100  $\mu\text{M}$ . The quenching response is shown in Figure 7. After fitting with the Langmuir isotherm equation, the dissociation constant  $K_d$  was found to be  $2.1 \pm 0.3 \mu\text{M}$ .

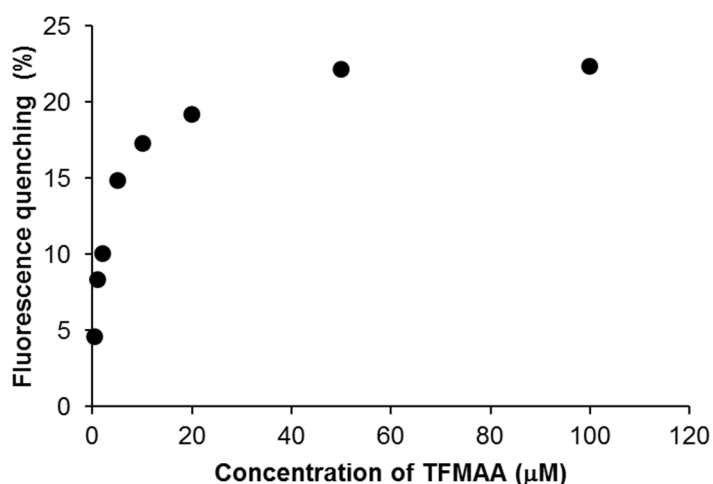


**Figure 7.** Fluorescence response of 5  $\mu\text{M}$  3S peptide after titration with increasing concentrations of TFMAA (0.5 – 100  $\mu\text{M}$ ) in 25 mM sodium phosphate buffer pH 7 ( $\lambda_{\text{ex}} = 280 \text{ nm}$ ,  $\lambda_{\text{em}} = 360 \text{ nm}$ , slit 3 nm). Data are mean of 2 independent experiments.

### III-4. Characterization of polymers

#### III-4-1. Physicochemical characterization

The size distribution of the polymers in buffer A were determined by DLS analysis. The diameters of MIP 1 – 3 were 65 nm, 57 nm and 49 nm, respectively (Table 3). Since all three MIPs contain the same amount of TFMAA, the zeta potentials were similar, with a value of -11.6 mV and conductivity of 0.365 mS/cm. A representative example of size and zeta potential analysis of MIP 1 is shown in Figure 8.

The yield of synthesis was found to be  $\sim 0.17 \text{ mg/g}$  of GBs for both MIP and NIP (Table 3). This was deduced from the concentration of polymer particles collected after synthesis. Knowing the mass of GBs and the total volume of polymer eluted, the yield of synthesis, as

mg per g of GBs, was calculated.

**Table 3.** Physicochemical characterization (n = 3) and yield of polymers

Polymer	Diameter (nm)	PDI	Concentration (mg/mL)	Yield (mg/g)
MIP 1	65	0.384	0.5	0.15
MIP 2	57	0.215	0.4	0.18
MIP 3	49	0.418	0.6	0.18
NIP 1	450	0.559	0.475	0.14
NIP 2	397	0.457	0.6	0.18
NIP 3	312	0.359	0.5	0.15

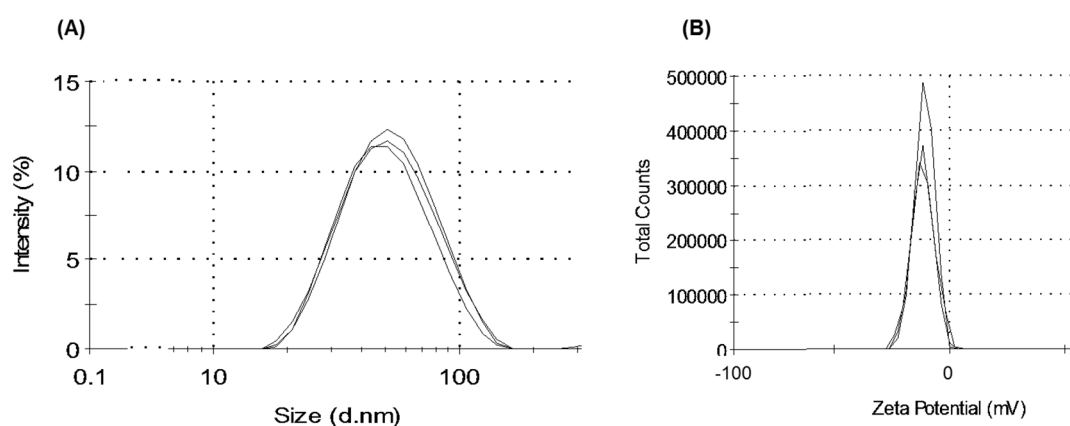


**Figure 8.** (A) Size distribution as measured by DLS and (B) zeta potential measurements, of MIP 1 (n=3).

#### III-4-2. LCST analysis of MIP 1 – 3

The LCST of the polymers were determined via turbidity measurement (cloud point determination) by measuring the absorbance versus temperature using a UV-vis spectrophotometer. With temperature increase, NIPAm-based polymers change from a hydrated hydrophilic conformation (< LCST) to a collapsed hydrophobic state (> LCST), accompanied

by an increase of turbidity. Therefore, the thermoresponsive behavior of the non-charged MIP 1 – 3 at pH 1 – 2 was analyzed by recording changes in absorbance at 600 nm at different temperatures.

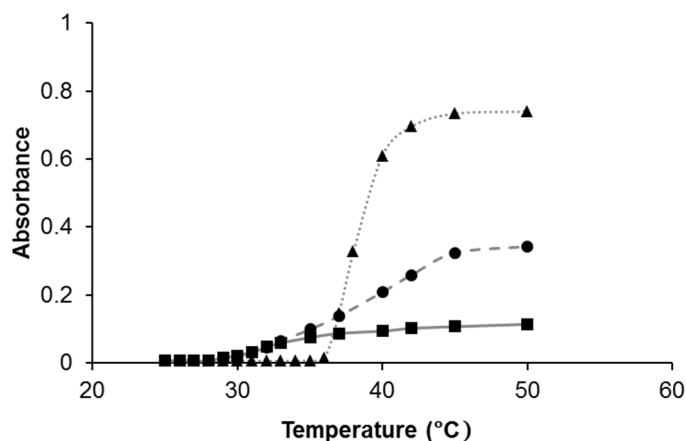


**Figure 9.** Turbidity measurement curves of 0.5 mg/mL of MIP 1 (▲), MIP 2 (●) and MIP 3 (■) at temperatures from 25 °C to 50 °C. Absorbance was measured at 600 nm.

The LCST value was determined by “tangent plot” [Heppner et al., 2013; Hu et al., 2015] of the results shown in Figure 9. The LCST values of MIP 1 – 3 were found to be 37 °C, 37 °C, and 32.5 °C. In general, incorporation of more hydrophobic co-monomers decreases the LCST [Huber & Jordan, 2008], which explains the lower LCST of MIP 3 compared with MIP 1 and 2. Although the LCST of MIP 1 and 2 are similar, the sharpness of the transitions are different. With more TBAm incorporated in MIP 2, that is less NIPAm, the polymer exhibited a slower transition rate and less turbidity. Adjustment of the LCST of thermosensitive MIP is important for biomedical applications; for our applications, MIPs that bind 3S peptide at 37°C are required.

### **III-5. Evaluation of the binding characteristics of the polymers by piezoelectric microgravimetry**

The binding assay of MIP 1 – 3 was performed with the 3S peptide immobilized on an

APTES- functionalized QCM sensor (in the same way as it was immobilized on APTES-GBs), at 37 °C. If binding occurs between MIP and the immobilized peptide, the frequency of the oscillating quartz crystal sensor should decrease. To compare the binding capacity of MIP 1 – 3, the same concentration (200  $\mu\text{g/mL}$ ) of MIP 1 – 3 was injected onto the same sensor, successively (with desorption in between). As shown in Figure 10A, among the three MIPs, MIP 1 exhibits the highest binding toward 3S peptide. To investigate the contribution of non-specific binding, NIP 1 – 3 were injected onto the 3S peptide immobilized QCM sensors as well. Here, the imprinting factor (IF) was calculated when saturated binding was reached. Thus, three experiments were carried out with 200  $\mu\text{g/mL}$  of MIP 1 and NIP 1, 400  $\mu\text{g/mL}$  of MIP 2 and NIP 2, and 600  $\mu\text{g/mL}$  of MIP 3 and NIP 3 on three different sensors. The IF values of MIP 1 – 3 were found to be 1.7, 1.1, 2.2, respectively. Although the IF of MIP 3 is slightly higher than those of MIP 1 and 2, MIP 1 exhibits the highest binding toward the 3S peptide when used at the same concentration with respect to MIP 2 and 3. Moreover, MIP 1 displays the highest structural flexibility to fit with the changable conformation of the 3S peptide occurring during membrane fusion, according to LCST study. Thus this MIP was chosen for further studies.

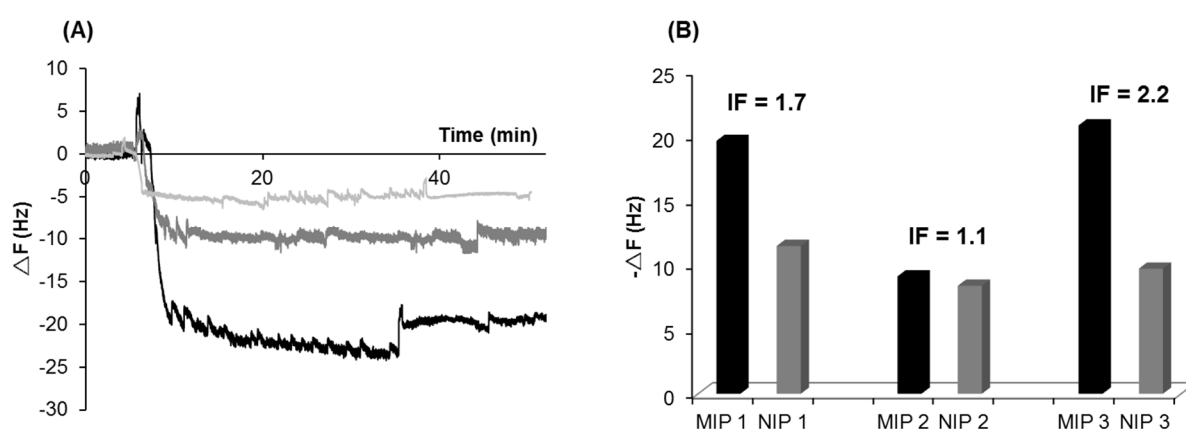


**Figure 10.** (A) Time course of the frequency change ( $\Delta F$ ) on 3S peptide-immobilized QCM sensor following injection of 200  $\mu\text{g/mL}$  of MIP 1 (black), MIP 2 (dark gray) and MIP 3 (light gray) in 25 mM sodium phosphate buffer pH 7.0 at 37 °C; (B)  $\Delta F$  response toward 200  $\mu\text{g/mL}$  of MIP and NIP 1, 400  $\mu\text{g/mL}$  of MIP and NIP 2, and 600  $\mu\text{g/mL}$  of MIP and NIP 3.

### III-6. Binding studies of MIP 1 on microplate wells

Since MIP 1 shows a better binding performance compared with others two MIPs, it appears to be the most promising candidate for biomedical applications, further experiments to investigate its binding properties were pursued.

*Equilibrium binding assay.* MIP 1, with concentrations ranging from 5 – 400  $\mu\text{g/mL}$ , corresponding to final amounts of 2.5 – 200  $\mu\text{g}$ , was immobilized in the wells of a microtiter plate. Figure 11A shows that the binding of MIP 1 with 1.5  $\mu\text{M}$  (final amount: 750 pmol) pep-rho, saturates at 200  $\mu\text{g/mL}$  (final amount: 100  $\mu\text{g}$ ), with a maximum binding of 300 pmol.

*Binding capacity.* A fixed amount of MIP 1, 100  $\mu\text{g}$ , was immobilized on the well and pep-rho concentrations ranging from 5 – 1500 nM, corresponding to 2.5 – 750 pmol was added. After fitting with the Langmuir equation, the  $K_d$  value was found to be 79.6 nM.

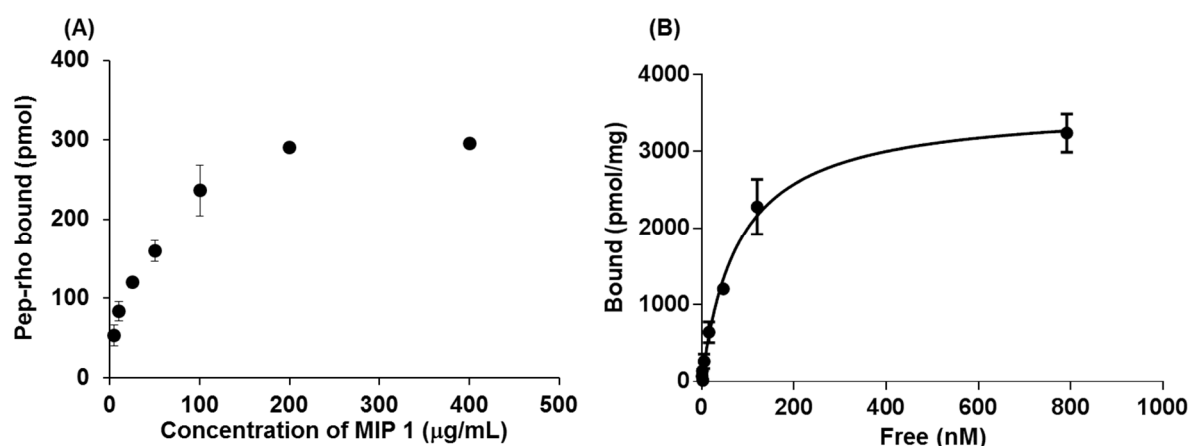


**Figure 11.** (A) Equilibrium binding isotherms of MIP 1 for 1.5  $\mu\text{M}$  pep-rho; (B) binding capacity of 100  $\mu\text{g}$  MIP 1 immobilized on microplate with pep-rho concentrations varying from 5 – 1500 nM. All experiments were done in 25 mM sodium phosphate buffer pH 7. Data are mean from 3 independent experiments with 3 different batches of polymers. The error bars represent standard deviations.

For competitive binding assays, various peptides donated by Prof. Patrice Debré of Pitié-Salpêtrière hospital were tested; a linear 3S peptide: CPWNASWSNKSLLDIW, competitor 1: CQKYNTQGSDVC (C-C cyclic) and competitor 2: CWDALNDWSPSKIAS. The assay was carried out with 100  $\mu\text{g}$  of immobilized MIP 1. 100 nM of pep-rho was added

with non-labeled cyclic 3S peptide, linear 3S peptide, competitor 1, competitor 2 and a mixture of competitor 1 and 2 at concentrations ranging from 1 – 100 nM. The results are shown in Figure 12. The  $IC_{50}$  (the concentration of competing ligand required to displace 50% of pep-rho from the MIP), as determined from a nonlinear regression fit, is summarized in Table 4. The affinity of MIP 1 toward non labeled cyclic 3S peptide is 18.7 nM and almost 100% displacement was observed.  $IC_{50}$  value of linear 3S peptide was found to be 69 nM, which indicates this amount of linear 3S peptide can replace 50% of pep-rho bound. About 27% cross-reactivity was found for linear 3S peptide because the linear form is more flexible, thus dynamic conformation change may render this linear 3S peptide fit to the binding sites in MIP 1. As shown in Table 4, 1525 nM of competitor 1, or 136.3 nM of competitor 2, or 292.6 nM of their mixture was needed to replace 50% of pep-rho bound. By analyzing cross-reactivity of competitor 1, whose sequence has nothing in common with cyclic 3S peptide, its competitive ability was almost zero with only 1.2% cross-reactivity. However, the cross-reactivity of competitor 2 was found to be 13.7%, relatively high ( $> 10\%$ ), probably because of the closer similarity in amino acids. Multi-targets by mixing competitor 1 and 2 were applied for competitive test as well. It was found that the binding of competitor 2 was inhibited by competitor 1; multi-targets exhibited cross reactivity of 6.4% ( $<10\%$ ). This result indicates that in a more complex environment, the cross-reactivity of competitor 2 might be lower than 10%.

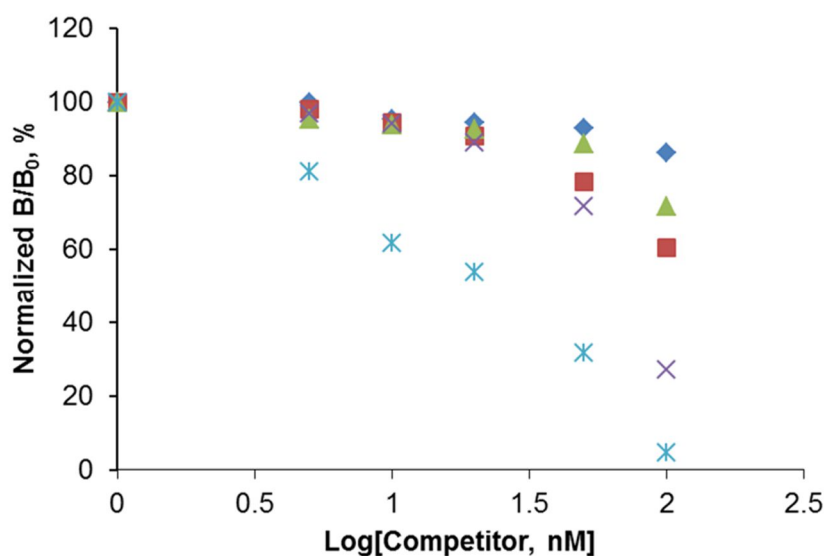


**Figure 12.** Inhibition of pep-rho (100 nM) binding to 100 µg MIP by (◆) competitor 1, (■) competitor 2, (▲) a mixture of competitor 1 and 2, (×) linear 3S peptide and (\*) cyclic 3S peptide. B/B<sub>0</sub> is the ratio of the amounts of pep-rho bound in the presence and absence of displacing competitors.

**Table 4.** Calculated IC<sub>50</sub> and cross-reactivity of MIP 1

Competing peptides	IC <sub>50</sub> (nM)	Cross-reactivity, %
Cyclic 3S peptide: CGSWSNKSC (C-C cyclic)	18.7	100
Linear 3S peptide: CPWNASWSNKSLDDIW	69.0	27.1
Competitor 1: CQKYNTQGSDVC (C-C cyclic)	1525	1.2
Competitor 2: CWDALNDWSPSKIAS	136.3	13.7
Mixture of competitor 1 and 2	292.6	6.4

#### IV. Conclusion and perspectives

We have synthesized 65 nm-sized water-soluble MIP particles using a solid-phase synthesis approach. These particles bind to the 3S peptide with high affinity (IC<sub>50</sub>:18.7 nM) and selectivity, as determined from a competitive binding assay with fluorescent-labeled 3S peptide, performed on immobilized MIPs on a microplate. However, the polymer yield is

lower (as compared to the yield in chapter 2), due to the low amount of peptide immobilized on the GBs. The problem probably arises from the coupling method with EDC/NHS, combined with the Boc/deBoc procedures that the 3S peptide has to undergo. A more straightforward method using click chemistry will be attempted in the future. The novel cyclic 3S peptide contains an additional lysine residue bearing an azide group which will be conjugated by click reaction to an alkyne moiety present on functionalized GBs (Figure 13). The yield of this reaction is generally 100%, hence a higher coverage of the peptide would be expected. Nevertheless, our results show the great potential of this MIP to block the function of 3S peptide and offer a low cost alternative to natural antibody in *in vivo* applications. On-going studies, examining the cytotoxicity and activity of the MIP toward CD4<sup>+</sup> T cells, in the presence of HIV, are under way in Prof. Debré's group.

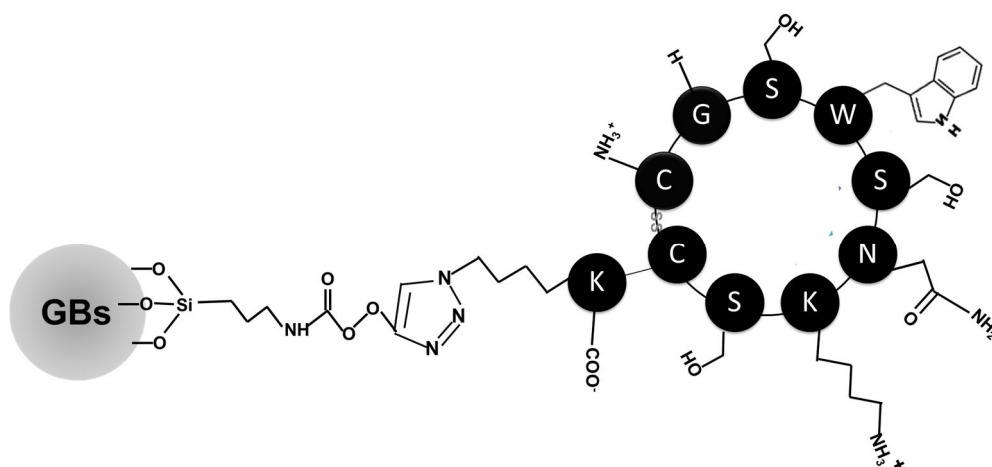


**Figure 13.** Illustration of immobilized template after click reaction of N<sub>3</sub>-cyclic 3S peptide with GBs functionalized with o-(propargyloxy)-n-(triethoxysilylpropyl) urethane.

## References

Albrecht, S., Defoin, A., & Tarnus, C. (2006). Simple preparation of O-substituted hydroxylamines from alcohols. *Synthesis*, (10), 1635-1638.

Ambrosini, S., Beyazit, S., Haupt, K., & Tse Sum Bui, B. (2013). Solid-phase synthesis of molecularly imprinted nanoparticles for protein recognition. *Chemical*

*Communications*, 49(60), 6746-6748.

Bai, J., Mak, W. C., Chang, X. Y., & Trau, D. (2009). Organic Phase Coating of Polymers onto Agarose Microcapsules for Encapsulation of Biomolecules with High Efficiency. In *13th International Conference on Biomedical Engineering* (pp. 821-824). Springer Berlin Heidelberg.

Cenci, L., Guella, G., Andretto, E., Ambrosi, E., Anesi, A., & Bossi, A. M. (2016). Guided folding takes a start from the molecular imprinting of structured epitopes. *Nanoscale*, 8(34), 15665-15670.

Chianella, I., Guerreiro, A., Moczko, E., Caygill, J. S., Piletska, E. V., De Vargas Sansalvador, I. M. P., et al. (2013). Direct replacement of antibodies with molecularly imprinted polymer nanoparticles in ELISA-development of a novel assay for vancomycin. *Analytical Chemistry*, 85(17), 8462-8468.

Fausther-Bovendo H, Vieillard V, Sagan S, Bismuth G, Debré P. (2010). HIV gp41 engages gC1qR on CD4+ T cells to induce the expression of an NK ligand through the PIP<sub>3</sub>/H<sub>2</sub>O<sub>2</sub> pathway. *PLoS Pathog*, 6(7): e1000975.

Haupt, K., Linares, A. V., Bompart, M., & Tse Sum Bui, B. (2012). Molecularly imprinted polymers. *Molecular Imprinting* (pp. 1-28). Springer Berlin Heidelberg.

Heppner, I. N., Islam, M. R., & Serpe, M. J. (2013). Unexpected cononsolvency behavior of poly (N - isopropylacrylamide) - Based Microgels. *Macromolecular Rapid Communications*, 34(21), 1708-1713.

Hoshino, Y., Kodama, T., Okahata, Y., & Shea, K. J. (2008). Peptide imprinted polymer nanoparticles: a plastic antibody. *Journal of the American Chemical Society*, 130(46), 15242-15243.

Hu, L., Gao, S., Ding, X., Wang, D., Jiang, J., Jin, J., & Jiang, L. (2015). Photothermal-responsive single-walled carbon nanotube-based ultrathin membranes for on/off switchable separation of oil-in-water nanoemulsions. *ACS Nano*, 9(5), 4835-4842.

Huber, S., & Jordan, R. (2008). Modulation of the lower critical solution temperature of 2-alkyl-2-oxazoline copolymers. *Colloid and Polymer Science*, 286(4), 395-402.

Kyte, J., & Doolittle, R. F. (1982). A simple method for displaying the hydropathic character of a protein. *Journal of Molecular Biology*, 157(1), 105-132.

Matsui, J., Kubo, H., & Takeuchi, T. (2000). Molecularly imprinted fluorescent-shift receptors prepared with 2-(trifluoromethyl) acrylic acid. *Analytical Chemistry*, 72 (14), 3286-3290.

Mattiasson, B., & Ye, L. (Eds.). (2015). *Molecularly Imprinted Polymers in Biotechnology* (Vol. 150). Springer.

Maynard, H. D., Heredia, K. L., Li, R. C., Parra, D. P., & Vázquez-Dorbatt, V. (2007). Thermoresponsive biohybrid materials synthesized by ATRP. *Journal of Materials Chemistry*, 17(38), 4015-4017.

Medel, S., Manuel García, J., Garrido, L., Quijada - Garrido, I., & París, R. (2011). Thermo - and pH - responsive gradient and block copolymers based on 2-(2-methoxyethoxy) ethyl methacrylate synthesized via atom transfer radical polymerization and the formation of thermoresponsive surfaces. *Journal of Polymer Science Part A: Polymer Chemistry*, 49(3), 690-700.

Poma, A., Brahmabhatt, H., Pendergraff, H. M., Watts, J. K., & Turner, N. W. (2015). Generation of novel hybrid aptamer–molecularly imprinted polymeric nanoparticles. *Advanced Materials*, 27(4), 750-758.

Sattentau, Q. J., & Moore, J. P. (1991). Conformational changes induced in the human immunodeficiency virus envelope glycoprotein by soluble CD4 binding. *The Journal of Experimental Medicine*, 174(2), 407-415.

Shendage, D. M., Fröhlich, R., & Haufe, G. (2004). Highly efficient stereoconservative amidation and deamidation of  $\alpha$ -amino acids. *Organic Letters*, 6(21), 3675-3678.

Vieillard V., Le Grand R., Dausset J., and Debré P. (2008). A vaccine strategy against AIDS:

an HIV gp41 peptide immunization prevents NKp44L expression and CD4+ T cell depletion in SHIV-infected macaques. *Proceedings of the National Academy of Sciences*, 105(6): 2100-2104.

Vieillard, V., Strominger, J. L., & Debré, P. (2005). NK cytotoxicity against CD4+ T cells during HIV-1 infection: a gp41 peptide induces the expression of an NKp44 ligand. *Proceedings of the National Academy of Sciences of the United States of America*, 102(31), 10981-10986.

Wang, Y. L., & Taylor, D. L. (1989). *Fluorescence Microscopy of Living Cells in Culture, Part A: Fluorescent Analogs, Labeling Cells and Basic Microscopy* (Vol. 29). Academic Press.

Weisman, A., Chen, Y. A., Hoshino, Y., Zhang, H., & Shea, K. (2014). Engineering nanoparticle antitoxins utilizing aromatic interactions. *Biomacromolecules*, 15(9), 3290-3295.

Xu, J., Ambrosini, S., Tamahkar, E., Rossi, C., Haupt, K., & Tse Sum Bui, B. (2016). Toward a universal method for preparing molecularly imprinted polymer nanoparticles with antibody-like affinity for proteins. *Biomacromolecules*, 17(1), 345-353.

Zhang, Y., Deng, C., Liu, S., Wu, J., Chen, Z., Li, C., & Lu, W. (2015). Active targeting of tumors through conformational epitope imprinting. *Angewandte Chemie International Edition*, 54(17), 5157-5160.

## General conclusion and perspectives

In this thesis, we propose a solid-phase synthesis approach to obtain water-soluble molecularly imprinted polymer nanoparticles (MIP-NPs) as antibody mimics for the recognition of proteins. Advantages are that the template proteins are immobilized in one fixed orientation for molecular imprinting, thus the MIP-NPs exhibit high affinity and are endowed with homogeneously oriented binding sites.

We first developed a universal technique of solid-phase synthesis in a column reactor by using a polymerization recipe with *N*-isopropylacrylamide cross-linked with ethylene bisacrylamide, resulting in thermoresponsible polymer nanogels. This can be used for any protein, and has been demonstrated on three examples, the serine proteases trypsin and kallikrein, and RNase A. These were immobilized on the solid support by using an affinity ligand, either a specific inhibitor (benzamidine), or a metal chelate targeting surface histidine residues.

In order to be able to post-functionalize the MIP-NPs, an iniferter-induced living polymerization protocol was developed, using solid-phase synthesis in batch mode. This method is more rapid and easy to operate compared with the synthesis in a column reactor, and better adapted to photopolymerization. The resulting MIP-NPs were successfully applied to detect trypsin in human fluids, and show great potential for clinical analysis.

In the last part, a peptide epitope of the HIV gp41 protein (3S peptide) was chosen as imprinting template for the purpose of developing a MIP able to recognize this protein during HIV membrane fusion. In order to recognize the internal peptide epitope, a cyclic peptide was designed as the imprinting template. For the first time in this thesis, multiple functional monomers were selected, and their ratio fine-tuned using a small polymer library to create specific binding sites for the 3S peptide. The optimized MIP exhibits antibody-like affinity ( $K_d = 18.7$  nM) toward the 3S peptide. *In vivo* studies are currently on-going at the Paris Pitié Salpêtrière hospital.

Future work may focus on the application of MIP-NPs obtained by solid-phase, in

immunoassay for other proteins, for example recombinant proteins carrying His-tags, and their combination with different labels such as quantum dots or HRP for immunoassay-like applications or bioimaging.

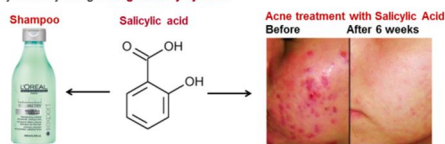
## Water Compatible Silica Sol-Gel Molecularly Imprinted Polymer as a Potential Delivery System for the Controlled Release of Salicylic Acid

Jingjing Xu, Bin Li, Karsten Haupt and Bernadette Tse Sum Bui\*

Compiègne University of Technology, CNRS Enzyme and Cell Engineering Laboratory, Rue Roger Couvrot, CS 60319, 60203 Compiègne Cedex, France

### Introduction

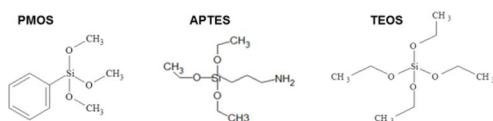
Salicylic acid (SA) is an **anti-inflammatory** drug, known for its efficacy to ease pains and reduce fevers. It is used as a hair-conditioning agent and skin-conditioning agent miscellaneous in a wide range of **cosmetic products** at concentrations ranging from **0.0008% to 3%**. Moderate doses of SA have been shown to be effective in topical skin applications for the treatment of seborrheic dermatitis, acne and psoriasis. The main side effects caused by SA treatment at high concentrations are **acute skin irritation, stinging and inflammation**, together with **moderate chemical burns** [1]. Therefore, to maximize the efficacy and safety of the drug during treatment, it could be advantageous to control the delivery of SA by using a **drug delivery system**.



In this study, we were interested in obtaining molecularly imprinted polymers (MIPs) specific for SA in **solvents compatible with drug formulation** for the skin (water and ethanol) and of **size >300 nm**, which would not penetrate the skin barrier so as to avoid potential toxic effects *in vivo* [2]. After optimisation, we found that the most suitable MIP was a sol-gel MIP based on silane monomers [3].

### Formulation of the polymer

**Sol-gel MIP (MSG).** The sol-gel MIP was synthesized using a mixture of (3-aminopropyl)triethoxysilane (APTES), trimethoxyphenylsilane (PMOS) and tetraethyl orthosilicate (TEOS) in ethanol/water (4/1) for 3 days at 60 °C. Non-imprinted sol-gel (NSG) polymer was synthesized using the same protocol but without the template.

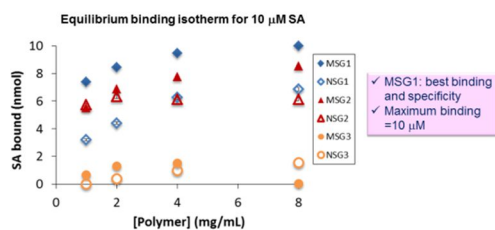


Polymer	Composition of sol-gel imprinted polymers				
	SA (mmol)	APTES (mmol)	PMOS (mmol)	TEOS (mmol)	HCl (mmol)
MSG1	0.5	0.5	0.5	5	0.1
NSG1	-	0.5	0.5	5	0.1
MSG2	0.5	0.5	-	5	0.1
NSG2	-	0.5	-	5	0.1
MSG3	0.5	-	0.5	5	0.1
NSG3	-	-	0.5	5	0.1

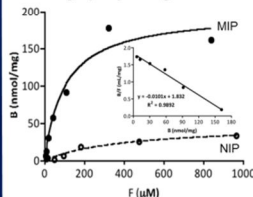
### Results

#### Binding characteristics in ethanol at room temperature

Bound SA was determined by fluorescence measurement ( $\lambda_{exc} = 306/400\text{nm}$ )



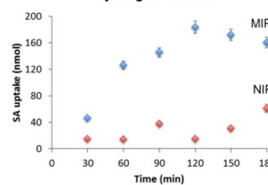
#### Binding capacity of 1 mg MIP and NIP



SA was varied from 10 µM to 1 mM.

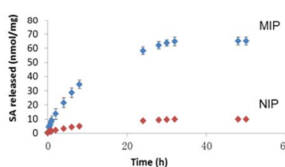
B and F represent bound and free SA respectively.

#### Time-dependent uptake of 1 mM SA by 1 mg MIP and NIP

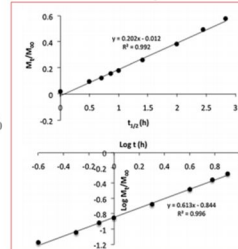


#### Release studies in water at room temperature

After uptake, MSG1 and NSG1 were washed 3 times with ethanol and the SA left for release in water. MIP was  $84 \pm 0.9$  nmol and in NSG1 was  $10 \pm 0.6$  nmol.



#### Mathematical modelling of the release



$M_t$ : amount of drug released at time 't'

$M_{\infty}$ : total amount of drug released

K: constant of diffusivity of SA

n: indicative of the mechanism of transport of the drug through the polymer

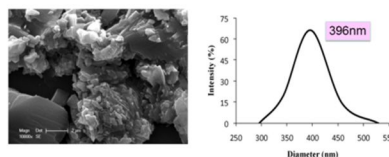
For the range  $M_t/M_{\infty} \leq 0.60$

✓ Fick's law of diffusion [4]:  $M_t/M_{\infty} = k't^{1/2}$

✓ Power law [5]:  $M_t/M_{\infty} = kt^n$

$k' = 0.20$ ,  $k = 0.14$  and  $n = 0.61$  (for 'n' values between 0.45 and 0.60, the release is Fickian), indicating that the release was predominantly diffusion-controlled

#### SEM images and DLS measurements of MSG1 in ethanol



#### References

- [1] Tsai JC *et al* (1999), *Int. J. Pharm.* 188: 145-153
- [2] Schneider M *et al* (2009), *Dermatoendocrinol.* 1:197-206
- [3] Li B *et al* (2014), *J. Mol. Recognit.* 27: 559-565
- [4] Siepmann J *et al* (2001), *Adv. Drug Deliv. Rev.* 48: 139-157
- [5] Duarte ARC *et al* (2006), *Int. J. Pharm.* 308: 168-174

#### CONCLUSION

We developed a water-compatible molecularly imprinted sol-gel polymer specific for salicylic acid, for its application as a drug delivery carrier. The sol-gel MIP has a high specificity (IF=9) and can bind 11.6 µg of SA per mg of polymer. This corresponds to an encapsulation of 1.2%, compatible with commercial cosmetic formulation. The MIP sol-gel was subsequently used for release studies. Mathematical modelling of the release by Fick's law of diffusion and the power law indicates that SA release from the sol-gel polymers was diffusion-controlled. The application of MIPs as drug delivery systems is still in its beginnings, mostly due to the poor compatibility of these polymers with polar environments. We have shown with this example that MIPs prepared by the sol-gel approach could be a very promising alternative in this field.

\* Corresponding author: [jeanne.tse-sum-bui@utc.fr](mailto:jeanne.tse-sum-bui@utc.fr)

We thank the European Regional Development Fund and the Regional Council of Picardie for co-funding of equipment under CPER 2007-2013. Jingjing Xu and Bin Li acknowledge the China Scholarship Council (CSC) for financial support



### Publication 3

**Water compatible silica sol–gel molecularly imprinted polymer as a potential delivery system for the controlled release of salicylic acid.**

Bin Li<sup>a†</sup>, Jingjing Xu<sup>a†</sup>, Andrew J. Hall<sup>b</sup>, Karsten Haupt<sup>a\*</sup> and Bernadette Tse Sum Bui<sup>a\*</sup>.

\* Correspondence to: K. Haupt and B. Tse Sum Bui, Compiègne University of Technology, CNRS Enzyme and Cell Engineering Laboratory, Rue Roger Couitolenc, CS 60319, 60203 Compiègne Cedex, France.

E-mail: [karsten.haupt@utc.fr](mailto:karsten.haupt@utc.fr); [jeanne.tse-sum-bui@utc.fr](mailto:jeanne.tse-sum-bui@utc.fr)

† Both contributed equally to the work.

a B. Li, J. Xu, K. Haupt, B. Tse Sum Bui

CNRS Enzyme and Cell Engineering Laboratory, Compiègne University of Technology, Rue Roger Couitolenc, CS 60319, 60203 Compiègne, Cedex, France

b A. J. Hall

Medway School of Pharmacy, Universities of Greenwich and Kent at Medway, Chatham, UK

# Water-compatible silica sol–gel molecularly imprinted polymer as a potential delivery system for the controlled release of salicylic acid

Bin Li<sup>a†</sup>, Jingjing Xu<sup>a†</sup>, Andrew J. Hall<sup>b</sup>, Karsten Haupt<sup>a\*</sup> and Bernadette Tse Sum Bui<sup>a\*</sup>



Molecularly imprinted polymers (MIPs) for salicylic acid were synthesized and evaluated in aqueous environments in the aim to apply them as drug delivery carriers. One organic MIP and one inorganic MIP based on the sol–gel process were synthesized. The organic MIP was prepared by radical polymerization using the stoichiometric functional monomer, 1-(4-vinylphenyl)-3-(3,5-bis(trifluoromethyl)phenyl)urea, which can establish strong electrostatic interactions with the –COOH of salicylic acid. The sol–gel MIP was prepared with 3-(aminopropyl)triethoxysilane and trimethoxyphenylsilane, as functional monomers and tetraethyl orthosilicate as the crosslinker. While the organic MIPs bound the target specifically in acetonitrile, they exhibited lower binding in the presence of water, although the imprinting factor increased under these conditions, due to reduced non-specific binding. The sol–gel MIP has a high specificity and capacity for the drug in ethanol, a solvent compatible with drug formulation and biomedical applications. *In vitro* release profiles of the polymers in water were evaluated, and the results were modelled by Fick's law of diffusion and the power law. Analysis shows that the release mechanism was predominantly diffusion-controlled. Copyright © 2014 John Wiley & Sons, Ltd.

Additional supporting information may be found in the online version of this article at the publisher's web site.

**Keywords:** water compatible; drug release; molecularly imprinted polymer; sol–gel imprinting; salicylic acid

## INTRODUCTION

Salicylic acid (SA), a beta-hydroxy acid (Figure 1), is an anti-inflammatory drug, known for its efficacy to ease pains and reduce fevers. It is used as a hair-conditioning agent and skin-conditioning agent miscellaneous in a wide range of cosmetic products at concentrations ranging from 0.0008% to 3% (Cosmetic Ingredient Review Expert Panel, 2003). Moderate doses of SA have been shown to be effective in topical skin applications for the treatment of seborrheic dermatitis, acne and psoriasis. SA is used in some countries in 1–3% alcoholic solutions for the treatment of acne (Gollnick and Schramm, 1998), whereas the maximum strength of SA permitted on over-the-counter acne products in the US is 2% as it is likely to cause local skin peeling when used at higher concentrations (Bowe and Shalita, 2008). The main side effects caused by SA treatment are acute skin irritation, stinging and inflammation, together with moderate chemical burns (Tsai *et al.*, 1999). Therefore, to maximize the efficacy and safety of the drug during treatment, it could be advantageous to control the delivery of SA by using a drug delivery system (Rhein *et al.*, 2004; Niamlang and Sirivat, 2009).

Molecularly imprinted polymers are tailor-made synthetic receptors, synthesized by co-polymerization of functional and crosslinking monomers in the presence of a molecular template. After removal of the template, binding sites are revealed that allow binding of the target molecule with a very high specificity and affinity, comparable to that of biological antibodies (Vlatakis

*et al.*, 1993; Alexander *et al.*, 2006; Haupt *et al.*, 2012). MIPs display considerable advantages over biological recognition elements, as they possess greater chemical, thermal and mechanical stability and thus have been successfully applied in several domains, such as separation (Pichon and Haupt, 2006), sensing (Henry *et al.*, 2005), catalysis (Wulff and Sarhan, 1972) and more recently, drug delivery (Lago *et al.*, 2011; Puoci *et al.*, 2011; Salian and Byrne, 2013).

In this study, we were interested in obtaining MIPs specific for salicylic acid in solvents compatible with drug formulation for the skin [water and ethanol (EtOH)] and of sizes >300 nm, which would not penetrate the skin barrier so as to avoid potential toxic effects *in vivo* (Schneider *et al.*, 2009). The vast majority of MIPs is synthesized by the non-covalent approach, exploiting

\* Correspondence to: K. Haupt and B. Tse Sum Bui, Compiègne University of Technology, CNRS Enzyme and Cell Engineering Laboratory, Rue Roger Couttolenc, CS 60319, 60203 Compiègne Cedex, France.  
E-mail: karsten.haupt@utc.fr; jeanne.tse-sum-bui@utc.fr

† Both contributed equally to the work.

a B. Li, J. Xu, K. Haupt, B. Tse Sum Bui  
CNRS Enzyme and Cell Engineering Laboratory, Compiègne University of Technology, Rue Roger Couttolenc, CS 60319, 60203 Compiègne, Cedex, France

b A. J. Hall  
Medway School of Pharmacy, Universities of Greenwich and Kent at Medway, Chatham, UK

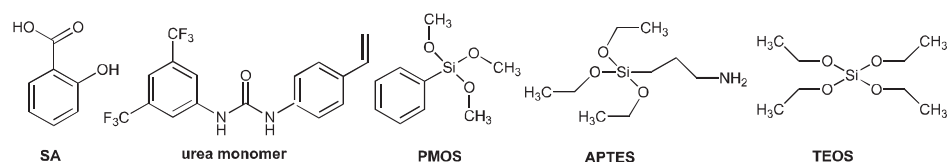


Figure 1. Chemical structures of compounds used in the study.

weak molecular interactions (hydrogen bonding, electrostatic and van der Waals interactions) between template and functional monomers. Non-polar aprotic organic solvents [chloroform, toluene and acetonitrile (ACN)] are usually employed during synthesis in order not to disrupt these weak interactions. During the subsequent use of the MIP, usually in the same solvents, specific interactions occur. If the material is used in aqueous-based environments, non-specific interactions often predominate (Pichon and Haupt, 2006). However, examples reporting specific binding in water do exist (Tse Sum Bui and Haupt, 2010). For instance, selective recognition in aqueous media has been achieved through the use of monomers that form a strong, and in the ideal case, stoichiometric (1:1) complex with the template (association constant,  $K_a \geq 10^3 \text{ M}^{-1}$ ) (Wulff and Knorr, 2002). A series of urea-based functional monomers was synthesized by Hall *et al.* (Hall *et al.*, 2005), of which the 1-(4-vinylphenyl)-3-(3,5-bis(trifluoromethyl)phenyl)urea (Figure 1) proved to have the highest association constant ( $K_a = 8820 \text{ M}^{-1}$ ) with tetrabutylammonium benzoate in dimethyl sulfoxide (DMSO). Stoichiometric imprinted polymers templated with penicillin G (Urraca *et al.*, 2006) or enrofloxacin (Benito-Pena *et al.*, 2008) were prepared in the presence of 1-(4-vinylphenyl)-3-(3,5-bis(trifluoromethyl)phenyl)urea. This monomer formed strong electrostatic interactions with the carboxylate group of the templates, hence enabling their direct extraction in aqueous samples.

Another alternative to obtain water-compatible MIPs is to perform molecular imprinting in silica-based matrices by using the sol-gel technique. Sol-gel MIPs are formed by the acid or base-catalysed hydrolysis and condensation of several silane-based monomers around the template (Díaz-García and Lainño, 2005). The synthesis has the advantage of taking place in aqueous media, and, moreover, silica-based materials are biocompatible and non-toxic (Ciriminna *et al.*, 2011). Most sol-gel MIPs have been used in analytical applications such as solid-phase extraction materials (Lordel *et al.*, 2011; Raof *et al.*, 2013) and sensors (Mujahid *et al.*, 2010). Although sol-gel-based materials have been widely used and even commercialized for the encapsulation/entrapment of drugs for drug delivery (Radin *et al.*, 2009; Ciriminna *et al.*, 2011), the potential of sol-gel MIPs as a drug delivery device has not been exploited. The drug's improved interaction with the memory cavities bearing the functional groups organized within the polymer network should slow its release, as compared to non-imprinted polymers (NIPs).

Several groups have previously reported the synthesis of non-water-compatible MIPs for SA, and in different formats, such as bulk polymers (Park *et al.*, 2007; Jafari *et al.*, 2012), spherical nanoparticles (Li *et al.*, 2008) and as films (Wang *et al.*, 2012). In this report, we describe the development of MIPs specific for SA in aqueous samples for their potential application in drug delivery. One organic MIP, based on 1-(4-vinylphenyl)-3-(3,5-bis(trifluoromethyl)phenyl)urea as the functional monomer, together with one sol-gel MIP, based on a mixture of (3-aminopropyl)triethoxysilane (APTES), trimethoxyphenylsilane (PMOS) and tetraethyl orthosilicate (TEOS) were synthesized. The sol-gel MIP proved to have the

highest capacity and specificity for SA in an aqueous environment and was subsequently used for release studies.

## EXPERIMENTAL SECTION

### Materials and methods

#### Materials

All solvents were of analytical grade and purchased from VWR International (Strasbourg, France) or Sigma-Aldrich (St-Quentin Fallavier, France). SA, APTES, PMOS, TEOS, ethylene glycol dimethacrylate, benzyl methacrylate and triethylamine (TEA) were purchased from Sigma-Aldrich. Azo-bis-dimethylvaleronitrile was from DuPont Chemicals (Wilmington, USA). 1-(3,5-bis(trifluoromethyl)phenyl)-3-(4-vinylphenyl)urea was synthesized as previously described (Hall *et al.*, 2005). Water was purified using a Milli-Q system (Millipore, Molsheim, France). Visking dialysis membrane (Molecular weight cut-off 14 kDa) was purchased from Roth Sochiel EURL (Lauterbourg, France). Fluorescence measurements were performed on a FluoroLog-3 spectrofluorimeter (Horiba Jobin Yvon, Longjumeau, France). Scanning electron microscopy (SEM) imaging was carried out on a Philips XL30 Field Emission Gun Scanning Electron Microscope (Amsterdam, Netherlands). Polymer particles were sputter coated with gold prior to the SEM measurement.

#### Preparation of molecularly imprinted polymers

**Urea polymers.** The polymers were prepared by bulk polymerization in a glass vial fitted with an air-tight septum. 0.125 mmol of SA and 0.5 mmol of TEA were first dissolved in 1.4 ml of ACN/DMSO (2/1) mixture and incubated for 30 min. Then, 0.125 mmol of urea monomer, 2.5 mmol of ethylene glycol dimethacrylate and 0.026 mmol azo-bis-dimethylvaleronitrile were added. The mixture was purged with nitrogen for 5 min, and polymerization was performed overnight at 40°C in a water bath. The bulk polymers were ground manually with a mortar and pestle, transferred to 2-ml microcentrifuge tubes and milled with 2.8-mm ceramic beads in the presence of methanol in a Precellys 24 homogenizer (Bertin Technologies, Montigny-le-Bretonneux, France). The polymers were transferred to 50-ml centrifuge tubes and washed at room temperature on a tube rotator (SB2, Stuart Scientific) with three rounds of methanol/acetic acid (9/1), three rounds of methanol/0.1 M  $\text{NH}_4\text{OH}$ , two rounds of water and two rounds of methanol. They were then dried overnight under vacuum. NIPs were synthesized in the same way but without the addition of the imprinting template.

**Sol-gel polymers.** The composition of the sol-gel polymers is described in Table 1. All components were added together in a solvent mixture consisting of 4 ml EtOH and 1 ml  $\text{H}_2\text{O}$ . The vial was capped, and the mixture was stirred for 3 days at 60°C. The

**Table 1.** Composition of sol-gel imprinted polymers

Polymer	SA (mmol)	APTES (mmol)	PMOS (mmol)	TEOS (mmol)	HCl (mmol)
<sup>a</sup> MSG1	0.5	0.5	0.5	5	0.1
<sup>b</sup> NSG1	—	0.5	0.5	5	0.1
MSG2	0.5	0.5	—	5	0.1
NSG2	—	0.5	—	5	0.1
MSG3	0.5	—	0.5	5	0.1
NSG3	—	—	0.5	5	0.1

SA, salicylic acid; APTES, (3-aminopropyl)triethoxysilane; PMOS, trimethoxyphenylsilane; TEOS, tetraethyl orthosilicate.  
<sup>a</sup>MSG: molecularly imprinted polymer (MIP) sol-gel.  
<sup>b</sup>NSG: non-imprinted polymer (NIP) sol-gel.

polymers were dried overnight in an oven maintained at 100°C. They were ground manually with a mortar and pestle, transferred to 2-ml microcentrifuge tubes and milled with 2.8-mm ceramic beads in the presence of methanol in a Precellys 24 homogenizer. The polymers were then transferred to 50-ml centrifuge tubes and washed under agitation at 60°C with three rounds of methanol/0.1 M HCl, three rounds of methanol/0.1 M NH<sub>4</sub>OH, two rounds of water and two rounds of methanol. They were then dried overnight under vacuum. NIPs were synthesized in the same way but without the addition of the template.

#### Equilibrium binding studies

The binding properties of the polymers with SA were evaluated by equilibrium binding experiments. SA was determined by fluorescence measurements. The excitation/emission wavelengths were set at 306/400 nm with 1.5 nm band pass slits. All manipulations with SA were performed in the dark. A calibration curve (Figure S1) was constructed with concentrations of SA between 0.2 μM and 5 μM. Higher concentrations of SA employed in the course of the work were diluted with EtOH so as to fall in this range.

**Urea polymers.** A stock solution of SA (4 mM) was prepared in ACN. For the assays, an aliquot of the stock solution was freshly diluted to 100 μM in ACN. The polymers were suspended by sonication in the incubation solvent (ACN or ACN + 1% TEA). From this stock suspension, polymer concentrations (0.5–10 mg/ml) were pipetted in 1.5-ml polypropylene microcentrifuge tubes, and 100 μl of SA solution was added. The final volume was adjusted to 1 ml with solvent. The tubes were incubated at room temperature overnight on a tube rotator. They were then centrifuged at 30 000 g for 30 min, and the amount of free SA in the supernatant was quantified by fluorescence measurements. The amount of SA bound to the polymers was calculated by subtracting the amount of free analyte from the initial amount of SA added to the mixture.

**Sol-gel polymers.** Binding tests with sol-gel materials were performed using similar procedures as for organic polymers except that the amount of polymers used varied from 1 to 8 mg/ml and the solvent used was EtOH.

#### Determination of the binding capacity of sol-gel polymers

Stock suspensions of MIP sol-gel 1 (MSG1) and NIP sol-gel 1 (NSG1) (Table 1) (2 mg/ml) were prepared in EtOH. In 1.5-ml microcentrifuge tubes were added 0.5 ml of polymer and various concentrations of SA (0.01–1 mM) in a total volume of 1 ml of EtOH. Tubes containing polymers alone in EtOH, without SA, were also prepared so as to test for any eventual template bleeding from MSG1. The tubes were incubated at ambient temperature overnight on a tube rotator. Then, the polymers were centrifuged at 30 000 g for 30 min, and the fluorescence of the supernatant was read. The amount of SA bound to the polymers (B) was calculated by subtracting the amount of free analyte (F) from the initial amount of SA added to the mixture. The data were plotted in B versus F format, and the corresponding Scatchard plot was derived to determine the association constant.

#### Time-dependent uptake of salicylic acid by sol-gel polymers

Stock suspensions of 2 mg/ml of polymers and a stock solution of 10 mM SA were prepared in EtOH. A series of 1.5 ml microcentrifuge tubes each containing 1 mg of MSG1 or NSG1 were incubated with 1 mM SA in a total volume of 1 ml of EtOH. The tubes were incubated at ambient temperature on a tube rotator. At definite time points (30–180 min), the polymers were centrifuged at 30 000 g for 30 min, and the fluorescence of the supernatant was read. The uptake of SA by the polymers was calculated by subtracting the amount of free SA found in the supernatant, from the initial amount of SA added to the mixture.

#### Release studies of salicylic acid and analysis of release

In 1.5 ml polypropylene tubes were added MSG1 or NSG1 (1 mg final amount) and SA (1 mM final concentration) in a total volume of 1 ml of EtOH. The tubes were incubated at room temperature on a tube rotator. After 4 h, the tubes were centrifuged for 30 min at 30 000 g, and the supernatant was first removed with a pipet and then by turning the tube upside-down. The amount of SA bound to the polymers was determined by measuring the fluorescence in the supernatant. The precipitated polymers were washed three times successively, with 1 ml of EtOH to remove non-specifically adsorbed SA. Finally, the polymer pellet was left to dry overnight, suspended in 1 ml of Milli-Q water and transferred to a dialysis membrane. Dialysis was performed in 10 ml of water, under constant stirring at room temperature. At predetermined time intervals, 1 ml aliquots was withdrawn and replaced with 1 ml of fresh Milli-Q water. The amount of released salicylic acid was analysed by fluorescence spectroscopy. A calibration curve (Figure S2) was constructed with concentrations of SA between 0.2 μM and 6 μM in water. Higher concentrations of SA employed in the course of the work were diluted with water so as to fall in this range.

## RESULTS AND DISCUSSION

### Synthesis and binding characterization of organic polymers

A MIP for SA using the urea functional monomer, (1-(4-vinylphenyl)-3-(3,5-bis(trifluoromethyl)phenyl)urea (Figure 1) was synthesized, with the expectation that the interaction between SA and the monomer would be so strong that it will induce specific binding in water, as previously described (Urraca *et al.*, 2006; Benito-Pena *et al.*, 2008). Figure 2(A) represents the binding behaviour of the

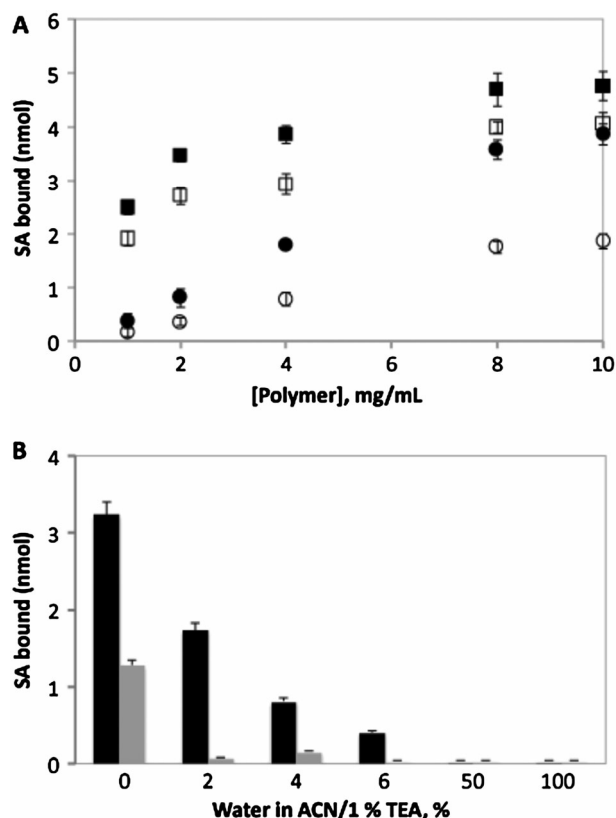


**Figure 2.** (A) Equilibrium binding isotherms for salicylic acid (SA) (10 nmol) on molecularly imprinted polymer (MIP)-urea (black squares) and non-imprinted polymers (NIP)-urea (white squares) in acetonitrile (ACN) and MIP-urea (black circles) and NIP-urea (white circles) in ACN + 1% triethylamine (TEA). (B) Influence of water on the binding behaviour of SA (10 nmol) to 10 mg MIP-urea (black bars) and NIP-urea (grey bars) polymers in ACN + 1% TEA. Data are means from three independent experiments from two different batches of polymers. The error bars represent standard deviations.

urea-based polymers in ACN with and without 1% TEA. TEA serves as a base to deprotonate SA (Hall *et al.*, 2003, 2005), and as seen in Figure 2(A), its presence is essential to induce specific binding, in accord with previous reports of MIPs imprinted with N-Z-L-glutamic acid and a urea-based monomer (Hall *et al.*, 2003). A maximum imprinting factor of 2.3 was obtained.

The binding in aqueous conditions was also assessed. Both MIP and NIP bind to the same extent but without any specificity in 100-mM HEPES buffer, pH 7.5, or in ACN/100-mM HEPES buffer, pH 7.5 (50/50), the conditions used for the recognition of other carboxyl anions, namely, enrofloxacin and penicillin G (Urraca *et al.*, 2006; Benito-Pena *et al.*, 2008). Other aqueous conditions were also tested (Figure 2(B)). In 100% water, there was no binding at all for both MIP and NIP; the addition of water to the ACN + 1% TEA mixture seems to hamper the binding of SA. Although the best specificity can be achieved by the addition of 2% water, which suppresses non-specific binding, the binding capacity unfortunately was lower.

### Synthesis and characterization of sol-gel polymers

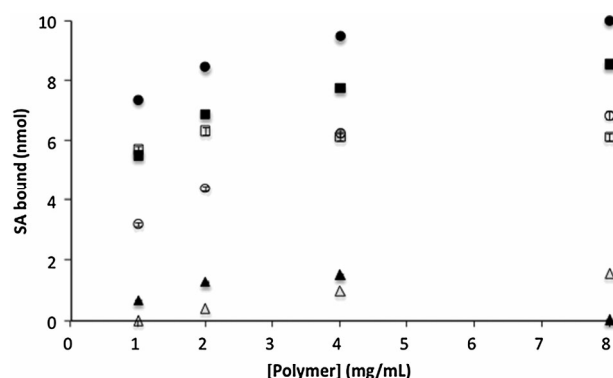
We then turned towards the sol-gel process for generating MIPs for SA. Imprinting in sol-gel materials has the advantage that the imprinting takes place in non-toxic polar environments, usually

EtOH and water (Díaz-García and Lainño, 2005; Radin *et al.*, 2009). An MIP sol-gel for SA was prepared by acid hydrolysis and condensation of APTES, PMOS and TEOS (Figure 1). APTES with its amino group can interact with the -COOH of SA and PMOS can form  $\pi$ - $\pi$  interactions with the aromatic functionality on the template. TEOS was used as crosslinker. After some optimization, we found that the ratio SA:APTES:PMOS:TEOS of 1:1:1:10 corresponding to MSG1 in Table 1 gave the best binding and specificity in EtOH, specially for low polymer concentrations where 1 mg of MSG1 can bind ~8 nmol of SA, resulting in an imprinting factor of 2.3 (Figure 3). This imprinting factor however seemed to improve when higher SA concentrations were used (Figure 5(A)). It should be noted that APTES is essential for recognition, because its omission (MSG3) results in no binding at all. In the presence of only APTES, (MSG2) in Figure 3, there was binding but no specificity. These results show that both APTES and PMOS are required to induce specific recognition.

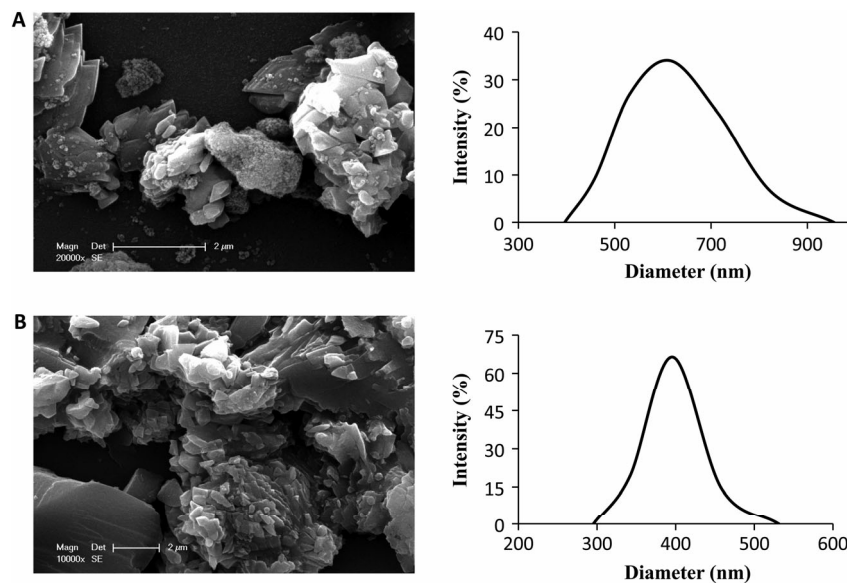
The hydrodynamic size of MSG1 and NSG1 polymers was measured by dynamic light scattering on a Zeta-sizer NanoZS (Malvern Instruments Ltd., Worcestershire, UK) and was found to be 396 and 615 nm, respectively. The corresponding SEM images are also shown (Figure 4).

### Determination of the binding capacity and loading time of sol-gel polymers

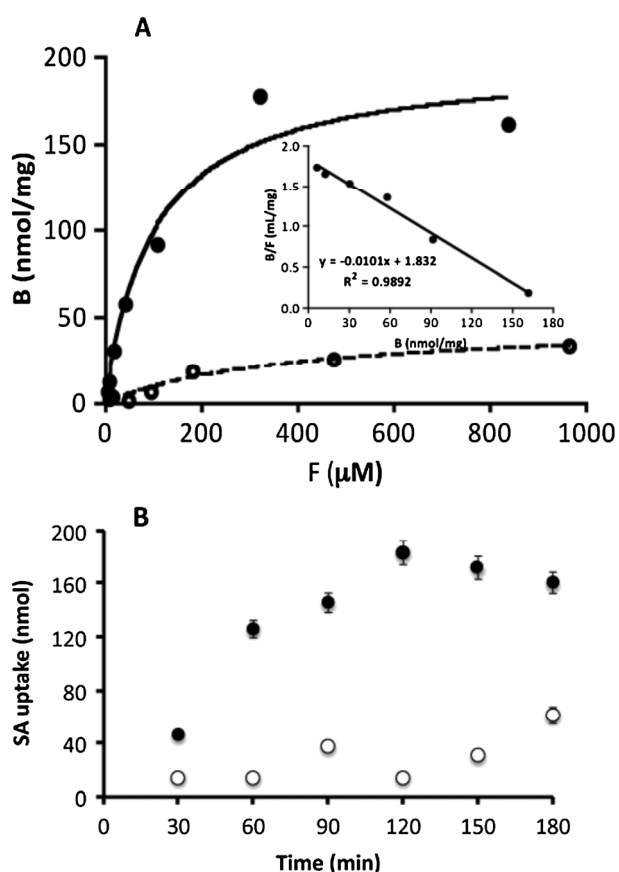
To determine the binding capacity of the sol-gel polymers, MSG1 and NSG1 (1 mg) were incubated overnight with concentrations of SA varying from 10  $\mu$ M to 1 mM in 1 ml EtOH. Polymers alone were incubated in parallel so as to check for any eventual template bleeding from MSG1. Fluorescence measurements indicated no presence of SA, at least <0.2  $\mu$ M, the limit of quantification of SA (Figure S1). Langmuir-type isotherms were generated when plotted in B versus F format (Figure 5(A)), where B and F are the concentrations of bound and free analyte. Low binding was observed for NSG1. MSG1 reached saturation at 1 mM of SA. The corresponding Scatchard plot, B/F versus B is represented by a straight line, indicating a homogeneous MIP (Figure 5(A), inset). The variables N and  $K_a$  in the Scatchard equation  $B/F = K_a N - K_a B$  correspond to the total number of binding sites and the association constant, respectively (Shimizu, 2005).  $K_a$  and N for MSG1 were found to be  $10^4 \text{ M}^{-1}$  and 183 nmol/mg, respectively.



**Figure 3.** Equilibrium binding isotherms for salicylic acid (SA) (10 nmol) on sol-gel polymers: MSG1 (black circles) and NSG1 (white circles), MSG2 (black squares) and NSG2 (white squares) and MSG3 (black triangles) and NSG3 (white triangles), in EtOH. Data are means from three independent experiments from three different batches of polymers. The error bars represent standard deviations.



**Figure 4.** Scanning electron microscopy images and dynamic light scattering measurements of (A) NSG1 and (B) MSG1. The samples were prepared in EtOH.



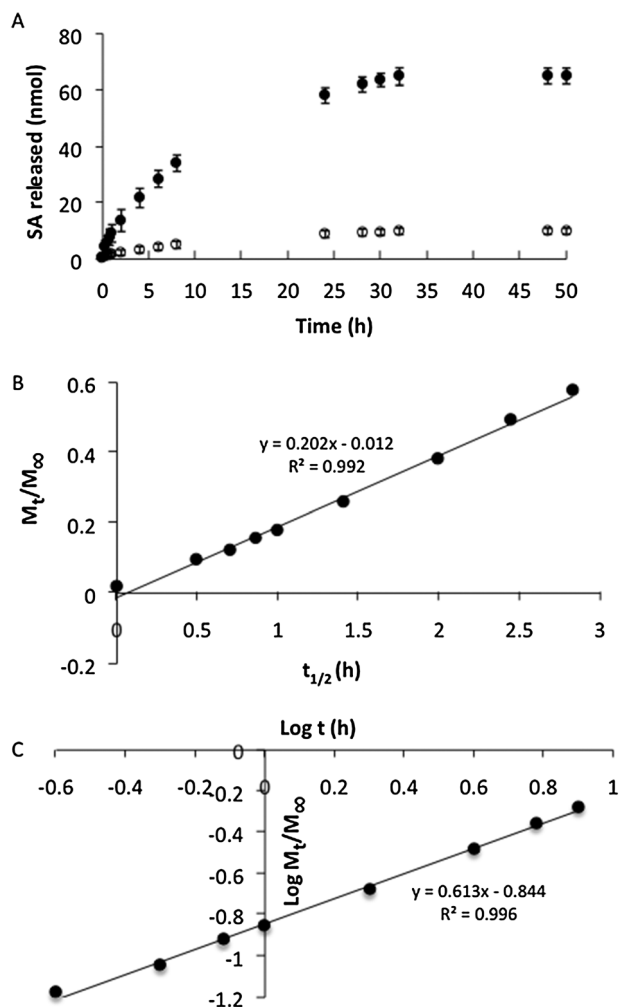
**Figure 5.** (A) Determination of the binding capacity of MSG1 and NSG1 (1 mg) in EtOH. Salicylic acid (SA) was varied from  $10\ \mu\text{M}$  to 1 mM. B and F represent bound and free SA, respectively. Data are means of two independent experiments. Inset: corresponding Scatchard plot of MSG1. (B) Time-dependent uptake of SA by 1 mg of MSG1 (black circles) and NSG1 (white circles) in EtOH containing 1 mM SA. Data are means from three independent experiments. The error bars represent standard deviations.

Figure 5(B) shows that 150 min was sufficient for 1 mg of MSG1 to bind a maximum ( $\sim 180\ \text{nmol}$ ) of SA, when incubated with 1 mM SA in 1 ml EtOH. No significant uptake by NSG1 was observed.

#### Release studies of sol-gel polymers

After incubating 1 mg of MSG1 and NSG1 with 1 mM SA for 4 h, the polymers were precipitated and the supernatant was separated for fluorescence analysis in order to determine the amount of SA bound to the polymers. The precipitate was then washed with EtOH to remove the non-specifically adsorbed SA from the polymers. This was performed three times consecutively, until the SA detected in the supernatant of NSG1 was constant. The SA washed away was monitored by fluorescence measurement of the supernatants. The final amount of SA left in the polymers for release studies amounted to  $84 \pm 0.9$  and  $10 \pm 0.8\ \text{nmol}$  for MSG1 and NSG1, respectively, that is, practically nothing was bound to NSG1, implying the remarkable specificity of the sol-gel polymers. The value corresponds to a loading of 11.6 mg of SA per grammes of MSG1 polymer, that is, 1.2% of SA, complying with dermatological formulations (Gollnick and Schramm, 1998; Cosmetic Ingredient Review Expert Panel, 2003; Bowe and Shalita, 2008; Niamlang and Sirivat, 2009). The polymers were then dried and subjected to release studies in water at room temperature ( $\sim 20^\circ\text{C}$ ) (Figure 6(A)). Fick's law of diffusion (Siepmann and Peppas, 2001) and the power law (Ritger and Peppas, 1987; Duarte et al., 2006) were applied to better understand the drug release mechanism of the system. The amount of drug released at time  $t$  ( $M_t$ ) with respect to the total amount of drug released ( $M_\infty$ ) can be expressed, according to Fick's law of diffusion, as  $M_t/M_\infty = k't^{1/2}$  for  $M_t/M_\infty < 0.60$ .  $M_t/M_\infty$  hence corresponds to the fraction of drug released, and  $k'$  is a constant reflecting the diffusivity of the drug. Figure 6(B) (see Figure S3A, for NSG1) shows that Fick's law fitted well the experimental data of our release studies, indicating that SA release from MSG1 was diffusion-controlled.

In the power equation written as  $M_t/M_\infty = kt^n$ , ' $k$ ' is a constant incorporating structural and geometric characteristics of the



**Figure 6.** (A) Release profile of salicylic acid (SA)-loaded MSG1 (black circles) and NSG1 (white circles) in water at room temperature ( $\sim 20^\circ\text{C}$ ). Data are means from three independent experiments. The error bars represent standard deviations. Application of (B) Fick's law of diffusion and (C) power law, to experimental data obtained with MSG1 (1 mg).

device and 'n' is the release exponent, indicative of the mechanism of transport of the drug through the polymer. For 'n' values ranging between 0.45 and 0.59, the release is considered as Fickian (diffusion-controlled), and for 'n' values above, the kinetics is considered to be non-Fickian (anomalous) release (Ritger and Peppas, 1987). The kinetic constants calculated from our release studies, for the range  $M_t/M_\infty < 0.60$ , were found to be 0.14 for 'k' and 0.61 for 'n' for MSG1, indicating that the release was predominantly diffusion-controlled (Figure 6(C)), consistent with the precedent results.

## CONCLUSIONS

We developed a water-compatible molecularly imprinted sol-gel polymer specific for salicylic acid, for its application as a drug delivery carrier. The sol-gel MIP was prepared using APTES and PMOS as the functional monomers and TEOS as the crosslinker. It has a high specificity (imprinting factor of 9) and can bind  $11.6 \mu\text{g}$  of SA per milligrammes of polymer. This corresponds to an encapsulation of 1.2%, compatible with commercial cosmetic formulations. The MIP sol-gel was subsequently used for release studies. Mathematical modelling of the release by Fick's law of diffusion and the power law indicates that SA release from the sol-gel polymers was diffusion-controlled. The application of MIPs as drug delivery systems is still in its beginnings, mostly due to the poor compatibility of these polymers with polar environments. We have shown with this example that MIPs prepared by the sol-gel approach could be a very promising alternative in this field.

## Acknowledgements

B. Li and J. Xu thank the China Scholarship Council for financial support. Part of the equipment used was funded by the European Regional Development Fund (ERDF) under CPER 2007–2013.

## REFERENCES

- Alexander C, Andersson HS, Andersson LI, Ansell RJ, Kirsch N, Nicholls IA, O' Mahony J, Whitcombe MJ. 2006. Molecular imprinting science and technology: a survey of the literature for the years up to and including 2003. *J. Mol. Recognit.* **19**: 106–180.
- Benito-Pena E, Urraca JL, Sellergren B, Moreno-Bondi MC. 2008. Solid-phase extraction of fluoroquinolones from aqueous samples using a water-compatible stoichiometrically imprinted polymer. *J. Chromatogr. A* **1208**: 62–70.
- Bowe WP, Shalita AR. 2008. Effective over-the-counter acne treatments. *Semin. Cutan. Med. Surg.* **27**: 170–176.
- Ciriminna R, Sciortino M, Alonzo G, de Schrijver A, Pagliaro M. 2011. From molecules to systems: sol-gel microencapsulation in silica-based materials. *Chem. Rev.* **111**: 765–789.
- Cosmetic Ingredient Review Expert Panel. 2003. Safety assessment of salicylic acid, butyloctyl salicylate, calcium salicylate, C12-15 alkyl salicylate, capryloyl salicylic acid, hexyldodecyl salicylate, isocetyl salicylate, isodecyl salicylate, magnesium salicylate, MEA-salicylate, ethylhexyl salicylate, potassium salicylate, methyl salicylate, myristyl salicylate, sodium salicylate, TEA-salicylate, and tridecyl salicylate. *Int. J. Toxicol.* **22**: 1–108.
- Díaz-García ME, Laíño RB. 2005. Molecular imprinting in sol-gel materials: recent developments and applications. *Microchim. Acta* **149**: 19–36.
- Duarte ARC, Costa MS, Simplicio AL, Cardoso MM, Duarte CMM. 2006. Preparation of controlled release microspheres using supercritical fluid technology for delivery of anti-inflammatory drugs. *Int. J. Pharm.* **308**: 168–174.
- Gollnick H, Schramm M. 1998. Topical drug treatment in acne. *Dermatology* **196**: 119–125.
- Hall AJ, Achilli L, Manesiotes P, Quaglia M, De Lorenzi E, Sellergren B. 2003. A substructure approach toward polymeric receptors targeting dihydrofolate reductase inhibitors. 2. Molecularly imprinted polymers against Z-L-glutamic acid showing affinity for larger molecules. *J. Org. Chem.* **68**: 9132–9135.
- Hall AJ, Manesiotes P, Emgenbroich M, Quaglia M, Lorenzi ED, Sellergren B. 2005. Urea host monomers for stoichiometric molecular imprinting of oxyanions. *J. Org. Chem.* **70**: 1732–1736.
- Haupt K, Linares AV, Bompert M, Tse Sum Bui B. 2012. Molecularly imprinted polymers. In *Topics in current chemistry*, Haupt K (ed). Springer: Berlin/Heidelberg; 1–28.
- Henry OYF, Cullen DC, Piletsky SA. 2005. Optical interrogation of molecularly imprinted polymers and development of MIP sensors: a review. *Anal. Bioanal. Chem.* **382**: 947–956.
- Jafari MT, Badihi Z, Jazan E. 2012. A new approach to determine salicylic acid in human urine and blood plasma based on negative electrospray ion mobility spectrometry after selective separation using a molecular imprinted polymer. *Talanta* **99**: 520–526.
- Lago MA, Grinberg VY, Burova TV, Concheiro A, Alvarez-Lorenzo C. 2011. Ionic and polyampholyte N-isopropylacrylamide-based hydrogels

- prepared in the presence of imprinting ligands: stimuli-responsiveness and adsorption/release properties. *J. Funct. Biomater.* **2**: 373–390.
- Li Q, Zhang W, Li X. 2008. Preparation and properties of salicylic acid-imprinted polymers from emulsions. *Macromol. Symp.* **261**: 91–96.
- Lordel S, Chapuis-Hugon F, Eudes V, Pichon V. 2011. Selective extraction of nitroaromatic explosives by using molecularly imprinted silica sorbents. *Anal. Bioanal. Chem.* **399**: 449–458.
- Mujahid A, Lieberzeit PA, Dickert FL. 2010. Chemical sensors based on molecularly imprinted sol–gel materials. *Materials* **3**: 2196–2217.
- Niamlang S, Sirivat A. 2009. Electric field assisted transdermal drug delivery from salicylic acid-loaded polyacrylamide hydrogels. *Drug Deliv.* **16**: 378–388.
- Park HR, Yoon SD, Lee JC, Chough SH. 2007. Separation of hydroxybenzoic acid isomers using the molecular imprinting technique. *J. Appl. Polym. Sci.* **105**: 2824–2829.
- Pichon V, Haupt K. 2006. Affinity separations on molecularly imprinted polymers with special emphasis on solid-phase extraction. *J. Liq. Chromatogr. Relat. Technol.* **29**: 989–1023.
- Puoci F, Cirillo G, Curcio M, Parisi OI, Iemma F, Picci N. 2011. Molecularly imprinted polymers in drug delivery: state of art and future perspectives. *Expert Opin. Drug Deliv.* **8**: 1379–1393.
- Radin S, Chen T, Ducheyne P. 2009. The controlled release of drugs from emulsified, sol gel processed silica microspheres. *Biomaterials* **30**: 850–858.
- Raof SFA, Mohamad S, Abas MR. 2013. Synthesis and evaluation of molecularly imprinted silica gel for 2-hydroxybenzoic acid in aqueous solution. *Int. J. Mol. Sci.* **14**: 5952–5965.
- Rhein L, Chaudhuri B, Jivani N, Fares H and Davis A. 2004. Targeted delivery of salicylic acid from acne treatment products into and through skin: role of solution and ingredient properties and relationships to irritation. *J. Cosmet. Sci.* **55**: 65–80.
- Ritger PL, Peppas NA. 1987. A simple equation for description of solute release II. Fickian and anomalous release from swellable devices. *J. Control. Release* **5**: 37–42.
- Salian VD, Byrne ME. 2013. Controlled drug release from weakly crosslinked molecularly imprinted networks: the benefit of living radical polymerization. *Macromol. Chem. Phys.* **214**: 2355–2366.
- Schneider M, Stracke F, Hansen S, Schaefer UF. 2009. Nanoparticles and their interactions with the dermal barrier. *Dermatoendocrinol.* **1**: 197–206.
- Siepmann J, Peppas NA. 2001. Modeling of drug release from delivery systems based on hydroxypropyl methylcellulose (HPMC). *Adv. Drug Deliv. Rev.* **48**: 139–157.
- Shimizu KD. 2005. Binding isotherms. In *Molecularly imprinted materials: science and technology*, Yan M, Ramström O (eds.). CRC Press: New York; 419–434.
- Tsai JC, Chuang SA, Hsu MY, Sheu HM. 1999. Distribution of salicylic acid in human stratum corneum following topical application in vivo: a comparison of six different formulations. *Int. J. Pharm.* **188**: 145–153.
- Tse Sum Bui B, Haupt K. 2010. Molecularly imprinted polymers: synthetic receptors in bioanalysis. *Anal. Bioanal. Chem.* **398**: 2481–2492.
- Urraca JL, Hall AJ, Moreno-Bondi MC, Sellergren B. 2006. A stoichiometric molecularly imprinted polymer for the class-selective recognition of antibiotics in aqueous media. *Angew. Chem. Int. Ed.* **118**: 5282–5285.
- Vlatakis G, Andersson LI, Müller R, Mosbach K. 1993. Drug assay using antibody mimics made by molecular imprinting. *Nature* **361**: 645–647.
- Wang Z, Liu X, Wu B, Wang F, Lu X. 2012. Voltammetric determination of salicylic acid by molecularly imprinted film modified electrodes. *Int. J. Polym. Anal. Ch.* **17**: 122–132.
- Wulff G, Knorr K. 2002. Stoichiometric noncovalent interaction in molecular imprinting. *Bioseparation* **10**: 257–276.
- Wulff G, Sarhan A. 1972. The use of polymers with enzyme-analogous structures for the resolution of racemates. *Angew. Chem. Int. Ed.* **11**: 341–342.

## SUPPORTING INFORMATION

Additional supporting information may be found in the online version of this article at the publisher's web site.

---

## Achievements

### Publications:

Li, B., Xu, J., Hall, A. J., Haupt, K., & Tse Sum Bui, B. (2014). Water compatible silica sol-gel molecularly imprinted polymer as a potential delivery system for the controlled release of salicylic acid. *Journal of Molecular Recognition*, 27(9), 559-565.

Xu, J., Ambrosini, S., Tamahkar, E., Rossi, C., Haupt, K., & Tse Sum Bui, B. (2016). Toward a universal method for preparing molecularly imprinted polymer nanoparticles with antibody-like affinity for proteins. *Biomacromolecules*, 17(1), 345-353.

Xu, J., Medina-Rangel, P. X., Haupt, K., Tse Sum Bui, B. (2017). Guide to the preparation of molecularly imprinted polymer nanoparticles for protein recognition, by solid-phase synthesis. *Methods in Enzymology*, 590, in press.

### Manuscripts ready to be submitted:

“Rapid detection of trypsin with a molecularly imprinted polymer as a selective fluorescence nanoprobe”.

“Fluorescent core-shell MIP nanoparticle as a plastic antibody for the pseudo-immunoassay of trypsin in human serum.”

### Oral presentations:

E-MRS 2015 spring meeting, Lille, France, 11<sup>th</sup> May 2015

Graduate student symposium on molecular imprinting, Kent, UK, 27 – 28<sup>th</sup> August 2015

SAMOSS summer school, Vienna, Austria, 5 – 11<sup>th</sup> June 2016

9<sup>th</sup> international conference on molecular imprinting (MIP2016), Lund, Sweden, 26 – 30<sup>th</sup> June 2016

### Poster presentation:

8<sup>th</sup> international conference on molecular imprinting (MIP 2014), Zhengjiang, China, 18-21 Sept 2014

**Supervising** engineer student Paulina Ximena Medina Rangel to perform her internship during September 2015 – February 2016, subject entitled “preparation of molecularly imprinted polymer nanoparticles by solid-phase approach for the application of protein protection and inhibition”.